

## STATUS OF THESIS

Title of thesis

LANDSLIDE SUSCEPTIBILITY MODELLING UNDER ENVIRONMENTAL CHANGES: A CASE STUDY OF CAMERON HIGHLANDS, MALAYSIA
---

I, ABDUL BASITH

hereby allow my thesis to be placed at the Information Resource Center (IRC) of Universiti Teknologi PETRONAS (UTP) with the following conditions:

1. The thesis becomes the property of UTP
2. The IRC of UTP may make copies of the thesis for academic purposes only.
3. This thesis is classified as

☐ Confidential

☒ Non-confidential

If this thesis is confidential, please state the reason:

---

---

---

---

The contents of the thesis will remain confidential for \_\_\_\_\_ years.

Remarks on disclosure:

---

---

---

---

Endorsed by

\_\_\_\_\_  
Signature of Author

\_\_\_\_\_  
Signature of Supervisor

Permanent address:  
Dept. of Geodesy Engineering  
Gadjah Mada University  
Jln. Grafika No. 2 Yogyakarta,  
Indonesia.

Name of Supervisor  
Assoc. Prof. Dr. Abd Nasir Matori

Date : \_\_\_\_\_

Date : \_\_\_\_\_

UNIVERSITI TEKNOLOGI PETRONAS

LANDSLIDE SUSCEPTIBILITY MODELLING UNDER ENVIRONMENTAL  
CHANGES: A CASE STUDY OF CAMERON HIGHLANDS, MALAYSIA

by  
ABDUL BASITH

The undersigned certify that they have read, and recommend to the Postgraduate Studies Programme for acceptance this thesis for the fulfilment of the requirements for the degree stated.

Signature: \_\_\_\_\_

Main Supervisor: Assoc. Prof. Dr. Abd Nasir Matori

Signature: \_\_\_\_\_

Co-Supervisor: Assoc. Prof. Dr. Indra Sati H Harahap

Signature: \_\_\_\_\_

Head of Department: Assoc. Prof. Ir. Dr. Mohd Shahir Liew

Date: \_\_\_\_\_

LANDSLIDE SUSCEPTIBILITY MODELLING UNDER ENVIRONMENTAL  
CHANGES: A CASE STUDY OF CAMERON HIGHLANDS, MALAYSIA

by

ABDUL BASITH

A Thesis

Submitted to the Postgraduate Studies Programme

as a Requirement for the Degree of

DOCTOR OF PHILOSOPHY

CIVIL ENGINEERING DEPARTMENT

UNIVERSITI TEKNOLOGI PETRONAS

BANDAR SERI ISKANDAR,

PERAK

SEPTEMBER 2011

## DECLARATION OF THESIS

Title of thesis

LANDSLIDE SUSCEPTIBILITY MODELLING UNDER ENVIRONMENTAL CHANGES: A CASE STUDY OF CAMERON HIGHLANDS, MALAYSIA
---

I, ABDUL BASITH

hereby declare that the thesis is based on my original work except for quotations and citations which have been duly acknowledged. I also declare that it has not been previously or concurrently submitted for any other degree at UTP or other institutions.

Witnessed by

\_\_\_\_\_  
Signature of Author

\_\_\_\_\_  
Signature of Supervisor

Permanent address:  
Dept. of Geodesy Engineering  
Gadjah Mada University  
Jln. Grafika No. 2 Yogyakarta,  
Indonesia.

Assoc. Prof. Dr. Abd Nasir Matori

Date : \_\_\_\_\_

Date : \_\_\_\_\_



## DEDICATION

*Quran, Ash-Sarh*

*But lo! with hardship goeth ease, (5) Lo! with hardship goeth ease(6)*

To my parents whose prayers never stop:

*Mustofa Adnan (Allah yarham) and Kastini*

To my beloved wife for her patient and support:

*Diah Harmastuti*

And to my lovely children for being the joy of my eyes:

*Muhammad, Abdurrahman Arrayyan,*

*Sarah Nur Sajidah and Muadz Abdul Aziz*

## ACKNOWLEDGEMENT

In the name of Allah, the Beneficent, the Merciful. All thanks and praises are due to Allah, Most High. May peace and blessings be upon the Prophet Muhammad, his family, his Companions, and those who followed his tradition. This dissertation would not have been possible without the support of UTP graduate assistantship scheme and kindness/guidance of several individuals for completion of this study.

First and foremost, I would like to thank to Datuk Dr. Zainal Abidin Hj Kasim, the Vice Chancellor, who invited me to conduct the research at Universiti Teknologi PETRONAS. I would also like to express my gratitude to my supervisor Assoc. Prof. Dr. Abd Nasir Matori for the continuous support for my research, his advice, guidance, and motivation; Assoc. Prof. Dr. Indra Sati H Harahap, my co-supervisor, for his criticism to my research. I would like to thank to Malaysian Remote Sensing Agency (ARSM) and NASA-USGS, for providing satellite images; JUPEM (Department of Survey and Mapping Malaysia), for providing topographical data, and Malaysian Meteorological Department (MMD) for providing rainfall data.

I would like also to thank everyone who has directly or indirectly contributed towards this research work: Indonesian community at UTP, V5C, Bandar University, and Bandar Seri Iskandar, Civil Engineering staff members/technicians/colleagues, my colleagues at Department of Geodesy Engineering Gadjah Mada University, Postgraduate Study Programme staff members, and colleagues at Universiti Teknologi PETRONAS.

## ABSTRACT

Modeling landslide susceptibility usually does not include multi temporal factors, e.g. rainfall, especially for medium scale. Landslide occurrences in Cameron Highlands, in particular, and in Peninsular Malaysia, in general, tend to increase during the peak times of monsoonal rainfall. Due to the lack of high spatial resolution of rainfall data, Normalized Different Vegetation Index (NDVI), soil wetness, and LST (Land Surface Temperature) were selected as replacement of multi temporal rainfall data. This research investigated their roles in landslide susceptibility modeling.

In doing so, four Landsat 7 Enhanced Multi Temporal Plus (ETM+) images acquired during two peak times of rainy and dry seasons were used to derive multi temporal NDVI, soil wetness, and LST. Topographic, geology, and soil maps were used to derive 'static' factors namely slope, slope aspect, curvature, elevation, road network, river/lake, lithology, soil geology lineament maps. Landslide map was used to derive weighting system based on spatial relationship between landslide occurrences and landslide factor using bivariate statistical method. A non-statistical weighting system was also used for comparison purpose. Different scenarios of data processing were applied to allow evaluation on the roles of multi temporal factors in landslide susceptibility modeling in terms of the accuracy of the landslide susceptibility maps (LSMs), the appropriate weighting system of the models, the applicability of the model, the ability to confirm the relation between landslide occurrences and rainfall.

The results show that the average accuracy of LSMs produced by the developed models with inclusion of multi temporal factors is 49.1% on the overall. Addition of LST tends to improve the accuracy of LSMs. NDVI can be a suitable replacement for rainfall data since it can explain the relation between landslides occurrences and rainfall cycle. Statistical-based weighting system produced more accurate LSMs than non-statistical-based one and is applicable for landslide susceptibility modeling elsewhere. Significant causative factors were proven to produce more accurate LSMs.

## ABSTRAK

Model kecenderungan tanah runtuh biasanya tidak melibatkan faktor-faktor multi temporal, contohnya hujan, terutamanya untuk skala pertengahan. Kejadian tanah runtuh terutamanya di Cameron Highlands dan amnya di Semenanjung Malaysia lebih cenderung meningkat semasa kemuncak musim tengkujuh. Disebabkan ketiadaan data hujan dengan resolusi spasial tinggi, data Normalized Different Vegetation Index (NDVI), kebasahan tanah, dan suhu permukaan tanah (LST) telah dipilih sebagai pengganti data hujan. Kajian ini menyiasat peranan data multi temporal dalam pemodelan kecenderungan tanah runtuh.

Untuk melakukan kajian ini, empat imej satelit Landsat 7 Enhanced Multi Temporal Plus (ETM+) yang telah diperolehi dalam dua masa kemuncak musim hujan dan kemarau digunakan untuk menjana multi temporal NDVI, kebasahan tanah, dan LST. Peta-peta topografi, geologi, dan tanah telah digunakan untuk faktor-faktor tanah runtuh 'statik' iaitu peta cerun, aspek cerun, kelengkungan, ketinggian, jaringan jalan raya, sungai/tasik, jenis batuan, tanah, dan lineamen geologi. Peta tanah runtuh digunakan untuk menerbitkan perhubungan spasial antara kejadian tanah runtuh dan faktor tanah runtuh menggunakan kaedah bivariate statistik. Satu sistem pemberat bukan statistik juga digunakan untuk tujuan perbandingan. Senario pemprosesan data berbeza-beza diaplikasikan untuk membolehkan penilain terhadap peranan faktor multi temporal dalam pemodelan kecenderungan tanah runtuh dari segi ketepatan peta, system pemberat yang sesuai untuk model, kebolegunaan model, keupayaan model untuk mengesahkan perhubungan antara kejadian tanah runtuh dan hujan.

Keputusan menunjukkan bahawa purata ketepatan peta yang dihasilkan oleh model dengan penyertaan faktor multi temporal adalah 49.1% pada keseluruhan. Penambahan LST cenderung untuk meningkatkan ketepatan peta. NDVI boleh menjadi pengganti yang sesuai bagi data hujan kerana ianya dapat menjelaskan

hubungan antara kejadian tanah runtuh dan kitaran hujan. Sistem pemberat berasaskan statistik menghasilkan peta lebih tepat daripada system pemberat berasaskan bukan statistik dan boleh digunakan untuk pemodelan kerentanan tanah runtuh di tempat lain. Faktor-faktor ketara penyebab tanah runtuh telah terbukti menghasilkan peta yang lebih tepat.

In compliance with the terms of the Copyright Act 1987 and the IP Policy of the university, the copyright of this thesis has been reassigned by the author to the legal entity of the university,

Institute of Technology PETRONAS Sdn Bhd.

Due acknowledgement shall always be made of the use of any material contained in, or derived from, this thesis.

© Abdul Basith, 2011

Institute of Technology PETRONAS Sdn Bhd

ALL RIGHTS RESERVED

## TABLE OF CONTENTS

STATUS OF THESIS .....	i
APPROVAL PAGE .....	ii
TITLE PAGE .....	iii
DECLARATION OF THESIS .....	iv
DEDICATION .....	v
ACKNOWLEDGEMENT.....	vi
ABSTRACT .....	vii
ABSTRAK .....	viii
COPYRIGHT PAGE.....	x
TABLE OF CONTENTS .....	xi
LIST OF TABLES .....	xv
LIST OF FIGURES .....	xvii
ABBREVIATIONS.....	xx
NOMENCLATURES.....	xxi
 CHAPTER 1 INTRODUCTION.....	 1
1.0 Background of Study.....	1
1.1 Problem Statements .....	6
1.2 Research Objectives and Expected Outcomes .....	6
1.3 Scope of Study.....	7
1.4 Contributions of Research .....	8
1.5 Thesis Organization.....	9
 CHAPTER 2 LITERATURE REVIEW.....	 11
2.0 Overview .....	11
2.1 Landslide Hazard Studies: Terminologies and Associated Concepts .....	11
2.2 Landslide Triggering and Causative Factors .....	15
2.2.1. Geology.....	16
2.2.2. Geomorphology .....	18
2.2.2.1 Slope gradient .....	19
2.2.2.2 Slope Aspect .....	20
2.2.2.3 Curvature.....	21
2.2.2.4 Elevation .....	21
2.2.3. Hydrology conditions and Climate .....	22
2.2.3.1 Soil Moisture.....	23
2.2.3.2 Factor related to river.....	23
2.2.4. Vegetation and Land Use Land Cover .....	24
2.2.4.1 Land use land cover (LULC) .....	25
2.2.4.2 Vegetation Index .....	25
2.2.5. Human activities .....	26
2.2.5.1 Factors related to deforestation.....	26
2.2.5.2 Factors related to road network development .....	27

2.2.6.	Number of Causative Factors Used for LHA .....	28
2.2.7.	Multi Temporal Environmental Factors .....	29
2.2.7.1	Change in vegetation index .....	29
2.2.7.2	Change in soil moisture .....	29
2.2.7.3	Change in LST.....	30
2.3	Scales of LHZ Maps .....	30
2.4	Methods for Landslide Hazard Assessment.....	31
2.4.1.	Qualitative Methods .....	33
2.4.1.1	Field Geomorphology Analysis.....	33
2.4.1.2	Overlay or Combination of Index Maps or Parameter Maps ....	34
2.4.2.	Quantitative Methods .....	38
2.4.2.1	Bivariate statistical method .....	39
2.4.2.2	Multivariate statistical methods.....	42
2.4.3.	Production of Final Landslide Susceptibility Map.....	44
2.5	Landslide Events in Malaysia and Cameron Highlands .....	44
2.6	The Efforts on Reducing Landslides Hazards .....	49
2.6.1	Efforts by the Government and Individuals .....	49
2.6.2	Previous Works of LHA in Cameron Highlands.....	49
2.6.2.1	LHA in Cameron Highlands using Qualitative Methods .....	50
2.6.2.2	LHA in Cameron Highlands using Quantitative Methods .....	51
2.7	Remote Sensing and Its Roles in Landslide Hazard Assessment .....	52
2.7.1	Remote Sensing: The Concepts.....	52
2.7.2	Spectral Signatures and Multi Spectral Sensors.....	53
2.7.3	Landsat 7 ETM+ Satellite Mission.....	54
2.7.4	SPOT 5 Satellite Mission .....	57
2.7.5	Image Pre-processing .....	58
2.7.5.1	Geometric Corrections .....	59
2.7.5.2	Atmospheric Correction .....	63
2.7.6	Image Enhancement .....	65
2.7.6.1	Band Combination.....	66
2.7.6.2	Linear stretch .....	67
2.7.7	Image Classification for derivation of Land Use and Land Cover.....	69
2.7.7.1	Unsupervised Classification .....	69
2.7.7.2	Supervised Classification .....	70
2.7.7.3	LULC Classification Scheme .....	72
2.7.8	Land Surface Temperature .....	74
2.7.9	Vegetation Indices .....	76
2.7.10	Tasseled Cap Transformation for Landsat ETM 7 data .....	77
2.7.11	The Roles of Remote Sensing in Landslide Hazard Assessment.....	78
2.8	GIS and Its Roles in Landslide Hazard Assessment.....	80
2.8.1.	GIS roles in Landslide Hazard Assessment .....	80
2.8.2.	Concept of GIS .....	81
2.8.3.	GIS Software .....	84
2.9	Chapter Summary .....	85
CHAPTER 3 DATA AND METHODOLOGY .....		87
3.0	Overview.....	87
3.1	Characteristics of Study Area .....	87



3.2.1	Limits of Study Area.....	87
3.2.2	Topography, LULC and Soil of Cameron Highlands .....	88
3.2.3	Climate of Cameron Highlands .....	89
3.2.4	Geology of Cameron Highlands .....	91
3.2.5	Landslide Occurrences in Cameron Highlands.....	91
3.2	Hardwares and Softwares .....	93
3.3	Source of Spatial Data .....	93
3.3.1	Topographic Map-Derived Spatial Data .....	94
3.3.2	SPOT 5 Satellites Data.....	95
3.3.3	Landsat 7 ETM+ Satellite Data and Strategy of Data Selection.....	97
3.3.4	Soil Map.....	99
3.3.5	Geology Map-Derived Spatial Data.....	101
3.3.6	Rainfall Data .....	102
3.3.7	Landslide Inventory map .....	103
3.4	Data Processing and Derivation .....	104
3.4.1	RSO Reference System.....	104
3.4.2	Digital Elevation Model (DEM) .....	106
3.4.3	Elevation .....	107
3.4.4	Slope .....	109
3.4.5	Slope Aspect .....	110
3.4.6	Curvature.....	114
3.4.7	Road Network and River-Lake .....	116
3.4.8	River and Lake .....	117
3.4.9	Geometric Correction of Topographic Map .....	119
3.4.10	Image Pre-Processing for SPOT and Landsat Images.....	121
3.4.10.1	Image Subsetting.....	121
3.4.10.2	Dealing with Atmospheric Effects.....	121
3.4.10.3	Geometric Correction of SPOT and Landsat Images .....	124
3.4.10.4	Image Enhancement.....	127
3.4.11	Land use land cover map.....	127
3.4.11.1	Image classification scheme .....	128
3.4.11.2	Ground Truthing, Training Sites and Signatures Generation .	130
3.4.11.3	Image Classification and Raster Generalization .....	133
3.4.12	Normalized Difference Vegetation Index (NDVI).....	136
3.4.13	Soil Wetness from Tasseled Cap Transformation .....	137
3.4.14	Land Surface Temperatures.....	138
3.4.15	Dealing with Cloud Cover Problem .....	140
3.4.16	Lithology and Lineament Maps.....	141
3.4.17	Soil Map .....	143
3.4.18	Landslide Inventory.....	145
3.5	Landslide Susceptibility Modeling.....	147
3.5.1	Extraction of Terrain Attributes of Landslide Sites .....	147
3.5.2	Landslide Attributes Reclassification .....	149
3.5.3	Weighting System.....	151
3.5.4	Final Landslide Susceptibility Maps and Scenarios .....	151
3.5.5	Validation of Final LSMs .....	154
3.5.6	Analysis of Relative Role of Causative Factor .....	155
3.5.7	Test of Applicability of the Developed Model .....	155
3.6	Chapter Summary .....	156

CHAPTER 4 RESULTS AND DISCUSSION.....	159
4.0 Overview.....	159
4.1 Weighting System and Construction of Thematic Maps .....	159
4.1.1 Weight Values and Thematic Map of Land Use Land Cover.....	160
4.1.2 Weight Values and Thematic Map of Lithology .....	164
4.1.3 Weight Values and Thematic Map of Elevation.....	168
4.1.4 Weight Values and Thematic Map of Slope Gradient.....	171
4.1.5 Weight Values and Thematic Map of Slope Aspect.....	172
4.1.6 Weight Valued and Thematic Map of Curvature.....	173
4.1.7 Weight Values and Thematic Map of Proximity to Road.....	177
4.1.8 Rating Weight and Thematic Map of Lineament .....	180
4.1.9 Weight Values and Thematic Map of River and Lake .....	182
4.1.10 Weight Values and Thematic Map of Soil .....	185
4.1.11 Weight Values and Thematic Maps of NDVI.....	185
4.1.12 Weight Values and Thematic Maps of Soil Wetness .....	189
4.1.13 Weight Values and Thematic Maps of LST .....	191
4.1.14 Anbalagan's LHEF Weighting System .....	193
4.2 Final Landslide Susceptibility Maps (LSMs) and Maps Validation.....	197
4.2.1 Final LSMs of Scenario 1 and Validation of the Maps .....	199
4.2.2 Final LSMs of Scenario 2 and Validation of the Maps .....	204
4.2.3 Final LSMs of Scenario 3 and Validation of the Maps .....	212
4.2.4 Final LSMs of Scenario 4 and Validation of the Maps .....	217
4.2.5 Static versus Multi Temporal Causative Factors-Based LSMs .....	224
4.3 Evaluation on Significance of Landslide Causative Factors.....	226
4.3.1 One by One Inclusion of Causative Factors .....	227
4.3.2 Accumulative Inclusion of Causative Factors .....	230
4.4 GIS-Based LSM Constructed Using Selected Causative Factors.....	231
4.5 Test of Applicability of The developed Landslide Model.....	233
4.6 Discussion.....	239
4.7 Chapter Summary .....	241
 CHAPTER 5 CONCLUSIONS AND RECOMMENDATIONS .....	 243
5.0 Overview.....	243
5.1 Conclusions.....	243
5.2 Recommendations for Future Works .....	246
 REFERENCES .....	 247
APPENDIX A Rainfall and Raindays Data.....	271
APPENDIX B RSO Projection Parameters .....	272
APPENDIX C RMS of Geometric Correction of Topographic Map .....	273
APPENDIX D RMS of Geometric Correction of SPOT 5, 19 April 2005.....	276
APPENDIX E NDVI Maps .....	281
APPENDIX F TCT Soil Wetness Maps .....	283
APPENDIX G LST Maps.....	285
APPENDIX H Cloud and shadow masks .....	287
LIST OF PUBLICATIONS .....	289

## LIST OF TABLES

Table 2.1 Category of terrain attributes associated with landslide.....	17
Table 2.2 LHEF rating for causative factors .....	36
Table 2.3 LHEF Rating System .....	37
Table 2.4 Land use changes in Bertam and Telom Catchment .....	48
Table 2.5 Characteristics of Landsat 7 ETM+ bands .....	56
Table 2.6 Characteristics of SPOT 5 bands.....	58
Table 2.7 Image classification scheme .....	73
Table 2.8 Tasseled Cap coefficients for use with Landsat 7 ETM+ imagery .....	78
Table 3.1 The Coordinates of the study area corners .....	88
Table 3.2 Number of landslide occurrences in Cameron Highlands (1961-2007).....	92
Table 3.3 Data source for deriving landslide causative factors .....	94
Table 3.4 Selected Landsat 7 ETM+ images.....	98
Table 3.5 The distribution of elevation at the study area .....	109
Table 3.6 The distribution of slope at the study area .....	110
Table 3.7 The distribution of slope aspect of the study area .....	113
Table 3.8 The distribution of curvature at the study area.....	116
Table 3.9 Offsets of Landsat and SPOT bands.....	122
Table 3.10 Geometric correction results of Landsat images .....	127
Table 3.11 Modified image classification scheme for LULC mapping .....	129
Table 3.12 Dendrogram of the Landsat image Signatures .....	133
Table 3.13 Statistic of LULC map derived from the Landsat image .....	135
Table 3.14 Scenario of data set for landslide susceptibility modeling.....	153
Table 4.1 Landslide attributes from land use, geology, elevation, slope maps, and weighting systems .....	163
Table 4.2 Landslide attributes from slope aspect, curvature, distance from road maps, and weighting systems.....	175
Table 4.3 Landslide attributes from distance from lineament, distance from river/lake, soil maps, and weighting systems .....	183
Table 4.4 Landslide attributes of NDVI and weighting system .....	187
Table 4.5 Landslide attributes of Soil Wetness and weighting system .....	190
Table 4.6 Landslide attributes of LST and weighting system.....	192
Table 4.7 Adaption of LHEF rating system for the current case study .....	195
Table 4.8 Statistics of LSM of scenario 1 .....	202
Table 4.9 Validation for GIS-based LSM of scenario 1.....	203
Table 4.10 Statistic of LSMs of scenario 2 .....	208
Table 4.11 Statistic of the training area for scenario 2.....	209
Table 4.12 Validation for GIS-based LSM of scenario 2.....	211
Table 4.13 Statistic of LSMs of scenario 3 .....	213
Table 4.14 Statistic of the training area for scenario 3.....	217
Table 4.15 Validation of LSMs of scenario 3 .....	217
Table 4.16 Statistic of LSMs of scenario 4 .....	219
Table 4.17 Statistic of the training area for scenario 4.....	219
Table 4.18 Validation of LSMs of scenario 4 .....	222

Table 4.19	Statistic of training areas and validated points of LSMs of scenario 1...	225
Table 4.20	The order of significance of causative factors .....	230
Table 4.21	Accumulative inclusions of causative factors and the order of significance factors .....	231
Table 4.22	LSI of Cameron Highlands applied to dataset of Penang Island .....	235
Table 4.23	Rating weight system of Penang Island .....	236
Table 4.24	Results of test of applicability of the landslide susceptibility model .....	239
Table 5.1	Summary of accuracy of LSMs (in %) .....	244
Table 5.2	Expansion and contraction of areas susceptible to landslide (in km <sup>2</sup> ).....	244

## LIST OF FIGURES

Fig. 1.1 Rainfall cycle and landslide occurrences in PM .....	2
Fig. 1.2 Weather stations in PM .....	3
Fig. 1.3 Rainfall cycle and landslide occurrences in Cameron Highlands .....	5
Fig. 2.1 Type of mass movement .....	12
Fig. 2.2 Landslide hazard assessment methods .....	32
Fig. 2.3 Schematic overview of bivariate statistical analysis .....	40
Fig. 2.4 Landslide events distribution in PM from JKR [13] database (1961-2007) ..	47
Fig. 2.5 Landslides a) along Kampung Raja-Ringlet road, b) at Pos Selim.....	47
Fig. 2.6 Spectral signatures of different objects and Landsat ETM+ bands .....	54
Fig. 2.7 Schematic of Landsat 7 ETM+ satellite .....	55
Fig. 2.8 SPOT 5 satellite and onboard instruments .....	58
Fig. 2.9 Geometric correction procedures .....	60
Fig. 2.10 Pattern of distortion due to the number and distribution of GCPs.....	63
Fig. 2.11 Histogram of band 1 and 5 and the respective offsets .....	64
Fig. 2.12 Band combinations: a) natural color and b) FCC.....	66
Fig. 2.13 Illustration of linear stretching .....	67
Fig. 2.14 A Landsat image in RGB 543 and the corresponding histogram adjustment: a) before and b) after linear stretching .....	68
Fig. 2.15 Illustrations of supervised classification classifiers .....	71
Fig. 2.16 Illustration of Tasseled Cap Transformation .....	77
Fig. 2.17 GIS roles in phases of LHA .....	82
Fig. 2.18 Vector and raster data model.....	83
Fig. 3.1 Location of the study area .....	88
Fig. 3.2 Monthly averaged rainfalls of Cameron Highlands (2000-2005) .....	90
Fig. 3.3 Different conditions of landslide at Pos Selim.....	96
Fig. 3.4 Handheld GPS device for data collection .....	96
Fig. 3.5 Preview of SPOT 5 image.....	96
Fig. 3.6 Identified peak time of rainy and dry seasons for Landsat data selection .....	98
Fig. 3.7 Selected Landsat 7 ETM+ satellite images .....	100
Fig. 3.8 Soil map of PM and CH .....	100
Fig. 3.9 Source of geology maps of the study area .....	101
Fig. 3.10 Rainfall data at Tanah Rata, Cameron Highlands.....	102
Fig. 3.11 Source of landslide map: a) site survey, b) the map from ARSM .....	103
Fig. 3.12 Derivation of spatial data for landslide susceptibility modeling.....	105
Fig. 3.13 RSO projection parameters defined in ArcGIS environment .....	106
Fig. 3.14 TINs surface .....	107
Fig. 3.15 Contour lines and TINs surface .....	108
Fig. 3.16 Raster surface of part of the study area.....	108
Fig. 3.17 a) A 3x3 neighborhood cells for slope computation, b) slope in degree and rise (Source: ESRI [63]) .....	109
Fig. 3.18 Slope map of the study area .....	111
Fig. 3.19 a) compass direction, b) elevation (input), c) slope aspect (output) .....	111
Fig. 3.20 Slope aspect map of the study area .....	113

Fig. 3.21 The concept of calculating curvature.....	115
Fig. 3.22 Curvature map of the study area.....	115
Fig. 3.23 Updated road network map.....	117
Fig. 3.24 Distance from road map of the study (in meter).....	118
Fig. 3.25 Distance from river map of the study area (in meter).....	118
Fig. 3.26 a) Scanned and cropped topographic map, b) the grid coordinates.....	120
Fig. 3.27 Geometrically corrected topographic map of Cameron Highland.....	120
Fig. 3.28 Subsetting a SPOT 5 and Landsat 7 satellite image .....	123
Fig. 3.29 a) Histogram of band 1 and 5 of Landsat image, b) histogram of band 1 of SPOT 5 image .....	123
Fig. 3.30 a) Inaccurate and b) accurate geometric correction.....	125
Fig. 3.31 Snapshot of image-to-image geometric correction.....	126
Fig. 3.32 Geometrically corrected SPOT 5 image .....	126
Fig. 3.33 Image classification procedures.....	128
Fig. 3.34 Various ground truth for LULC classification .....	131
Fig. 3.35 Training areas for image classification of the Landsat image .....	131
Fig. 3.36 Separability of urban with the surroundings seen on classified image and the corresponding image and topographic map .....	134
Fig. 3.37 Land Use Land Cover Map .....	134
Fig. 3.38 a) Illustration of generalization, b) before and after generalization .....	136
Fig. 3.39 NDVI (a) and RGB images (b) of Tanah Rata-Ringlelet.....	139
Fig. 3.40 Snapshot of soil wetness at Tanah Rata (center), topographic map (left), and the corresponding image (right) .....	139
Fig. 3.41 Snapshot of LST at Tanah Rata (center), topographic map (left), and the corresponding image (right).....	139
Fig. 3.42 A Landsat image with cloud and shadow (left); cloud mask and remaining cloud shadows (right).....	141
Fig. 3.43 (a) Cloud and shadow mask, (b) the satellite image, (c) the mask over the image, (d) cloud free image.....	142
Fig. 3.44 (a) a classified image with ‘holes’; (b) a classified image with ‘holes’ on top of another classified image; (c) ‘holes’ have been filled up.....	142
Fig. 3.45 Geology and lineament map .....	144
Fig. 3.46 Euclidean distances from geology lineament .....	144
Fig. 3.47 Soil map of the study area .....	146
Fig. 3.48 Landslide map of the study area .....	146
Fig. 3.49 Work flow of landslide susceptibility modeling.....	148
Fig. 3.50 Crossing landslide map and slope map.....	149
Fig. 3.51 Classification of slope attributes into five .....	150
Fig. 3.52 Landslide map of Penang Island on top of a Landsat image .....	156
Fig. 3.53 Flow chart of chapter 3 .....	157
Fig. 4.1 Landslide occurrences number and Landslide Susceptibility Index of land use land cover .....	161
Fig. 4.2 Landslide Susceptibility and Landslide Frequency Indices of LULC.....	165
Fig. 4.3 Thematic map of land use.....	165
Fig. 4.4 (a) LSI and LFI, (b) Landslide occurrences number and Landslide Susceptibility Index of lithology .....	167
Fig. 4.5 a) Thematic map of lithology, b) Overlay of lithology, land use and landslide maps.....	169

Fig. 4.6 Landslide occurrences number and Landslide Susceptibility Index of lithology .....	170
Fig. 4.7 Thematic map of elevation.....	170
Fig. 4.8 Landslide occurrences number and LSI of elevation.....	174
Fig. 4.9 Thematic map of slope .....	174
Fig. 4.10 Landslide occurrences number and LSI values of slope aspects .....	176
Fig. 4.11 Thematic map of slope aspect.....	176
Fig. 4.12 Landslide occurrences number and LSI values of curvature .....	178
Fig. 4.13 Thematic map of slope aspect.....	178
Fig. 4.14 LSI values and landslide occurrences number of distance from road.....	179
Fig. 4.15 Thematic map of distance from road .....	181
Fig. 4.16 LSI values and landslide occurrences number of distance from lineaments .....	181
Fig. 4.17 Thematic map of distance from lineaments .....	184
Fig. 4.18 Thematic map of distance from river/lake .....	184
Fig. 4.19 Thematic map of distance from river/lake .....	186
Fig. 4.20 Thematic map of soil.....	186
Fig. 4.21 Different NDVI conditions in Tanah Rata.....	189
Fig. 4.22 Monthly average rainfall and temperature in Cameron Highlands .....	194
Fig. 4.23 LST at Pos Selim landslide sites .....	194
Fig. 4.24 LHEF rating system-based LSM derived using: a) 6, and b) 7 factors.....	200
Fig. 4.25 LSI-based LSM derived using: a) 6, and b) all static factors.....	201
Fig. 4.26 LSMs of Scenario 2: all static factors and NDVI February and May .....	206
Fig. 4.27 LSMs of Scenario 2: all static factors and NDVI June and September .....	207
Fig. 4.28 Polygons used as training areas shown as dark areas .....	209
Fig. 4.29 The increase and decrease of areas fall in very high and high susceptibility status due to change of NDVI.....	210
Fig. 4.30 Average rainfall and the number of predicted landslide points falls in very high and high susceptibility status due to change of NDVI.....	211
Fig. 4.31 LSMs of Scenario 3: all static factors and soil wetness of February and May .....	214
Fig. 4.32 LSMs of Scenario 3: all static factors and soil wetness of June and September .....	215
Fig. 4.33 Average rainfall, areas of very high and high susceptibility statuses, and the number of validated points due to change of soil wetness.....	218
Fig. 4.34 LSMs of Scenario 4: all static factors and LST of February and June .....	220
Fig. 4.35 LSMs of Scenario 4: all static factors and LST of June and September....	221
Fig. 4.36 Average rainfall, areas of very high and high susceptibility statuses, and the number of validated points due to change of soil wetness.....	223
Fig. 4.37 Comparison of the percentage of validated points from LSMs of all scenarios.....	228
Fig. 4.38 a) clouds/shadows coverage on September and landslide sites .....	228
Fig. 4.39 The number of validated points from one by one inclusion of causative factors and the percentage of increase/decrease .....	229
Fig. 4.40 Comparison of GIS-based LSMs using selected significant factors with those of all scenarios.....	233
Fig. 4.41 Final LSM of Penang Island using: a) CH model, and b) Penang model ..	238
Fig. 4.42 a) Latest landslide location on topographic map, b) the corresponding LSM .....	240

## ABBREVIATIONS

ALOS	= Advanced Land Observation Satellite
CH	= Cameron Highlands
DEM	= Digital Elevation Model
ESRI	= Environmental System Research Institute
ETM	= Enhanced Thematic Mapper
GIS	= Geographic Information System
GPS	= Global Positioning System
LHZ	= Landslide Hazard Zonation
LHA	= Landslide Hazard Assessment
LHEF	= Landslide Hazard Evaluation Factor
LSMs	= Landslide Susceptibility Maps
LST	= Land Surface Temperature
LULC	= Land Use Land Cover
NDVIA	= Normalize Difference Vegetation Index
PM	= Peninsular Malaysia
RMSE	= Root Mean Square Error
RSO	= Rectified Skew Orthomorphic
SPOT	= Système Probatoire d'Observation de la Terre
TCT	= Tasseled Cap Transformation



## NOMENCLATURES

$A_L$	= landslide size, a proxy for magnitude
$dx$	= different in x coordinates
$dy$	= different in y coordinates
$dz$	= different in z coordinates
$D_{area}$	= area density per millage
$D_{number}$	= number density per millage
$DN$	= digital number
$\delta N_i, \delta E_i$	= different in northing and easting coordinates
$\varepsilon$	= emissivity
$H$	= height (m)
$H_L$	= landslide hazard
$I$	= information value of $X_i$
$K_1$	= free parameter ( $60.776 \text{ mWcm}^{-2}\text{sr}^{-1}\mu\text{m}^{-1}$ , )
$K_2$	= free parameter (1260.56 K.)
$L_R$	= spectral reflectance ( $\text{Wm}^{-2}\text{sr}^{-1}\mu\text{m}^{-1}$ )
$LS$	= landslide susceptibility, probability of spatial occurrence
$N$	= the total number of land units or pixels
$N_i$	= the number of land units or pixels with landslides
$N_L$	= temporal occurrence of a landslide
$R_S$	= landslide Risk
$S$	= the total number of land units or pixels with landslides
$S_i$	= the number of land units or pixels with landslides and the presence of variable $X_i$
$SX_i$	= pixels within variable class $X_i$
$T_a$	= near surface temperature ( $\text{K}^0$ )
$T_B$	= brightness temperature ( $\text{K}^0$ )
$T_S$	= surface temperature ( $\text{K}^0$ )
$\tau_0$	= atmospheric transmittance

$V_L$  = landslide Vulnerability

$X_i$  = pixels with mass movements within variable class  $X_i$

$W_i$  = weight values

## CHAPTER 1

### INTRODUCTION

#### **1.0 Background of Study**

Landslide is the movement of rock mass, debris or earth down a slope as defined by Cruden [1]. Intense or prolonged rainfall, earthquakes, and various human activities may cause landslides. Landslides cause damage to properties and loss of lives. One of efforts to reduce damages/casualties resulting from landslides is by providing a landslide susceptibility map (hereinafter referred to as LSM). Such a map shows likelihood of a landslide occurring in a particular area on the basis of local terrain conditions. Such a map ranks slope stability of a particular area into categories that range from very stable to very unstable based on the conditions of local terrain. To have such a map, susceptibility of an area should be modeled by considering all possible landslide contributing factors. By having good landslide susceptibility, hazard, and risk models, steps for mitigation and avoidance from unwanted consequences of mass movement can be optimized.

In providing LSM, researchers mostly incorporate landslide causative factors that can be called as ‘static contributing factors’, such as slope, slope aspect, soil, lithology, geology, etc. These factors are treated or assumed to be constant during the period of study. In fact, some factors change by time especially due to rainfall cycle. Examples of works for landslide susceptibility modeling using static factors can be found in Anbalagan [2] and Saha, et al. [3] for landslide cases in India; Peloquin and Gwyn [4] for landslide cases in Bolivia; Ayalew and Yamagishi [5] for the cases in Japan; Hervas, et al. [6] for the cases in Italy; and Lee and Pradhan [7], Talib [8], Omar, et al. [9], Lee and Pradhan [10], Pradhan and Lee [11], Pradhan and Lee [12] for the cases in Malaysia.

Most of landslide occurrences were reported to be induced by rainfall, e.g. either by intense or prolonged rainfall. Therefore, it is important to have rainfall data included in the modeling landslide susceptibility. Other important spatial data related to rainfall may be included in the modeling such as, pore pressure, ground water table, vegetation index in the form of Normalized Difference Vegetation Index (NDVI), surface soil wetness, and land surface temperature (LST). However, involving these data acquired from only one epoch of data acquisition means that these data are treated as static contributing factors. The fact that rainfall has a cycle in a year and some factors such as vegetation and soil are responsive to rainfall seasons makes the inclusion of such data acquired at different time of acquisition with respect to rainfall cycle in the modeling becomes important. In addition, the number of landslide occurrences tends to be more frequent during rainy seasons.

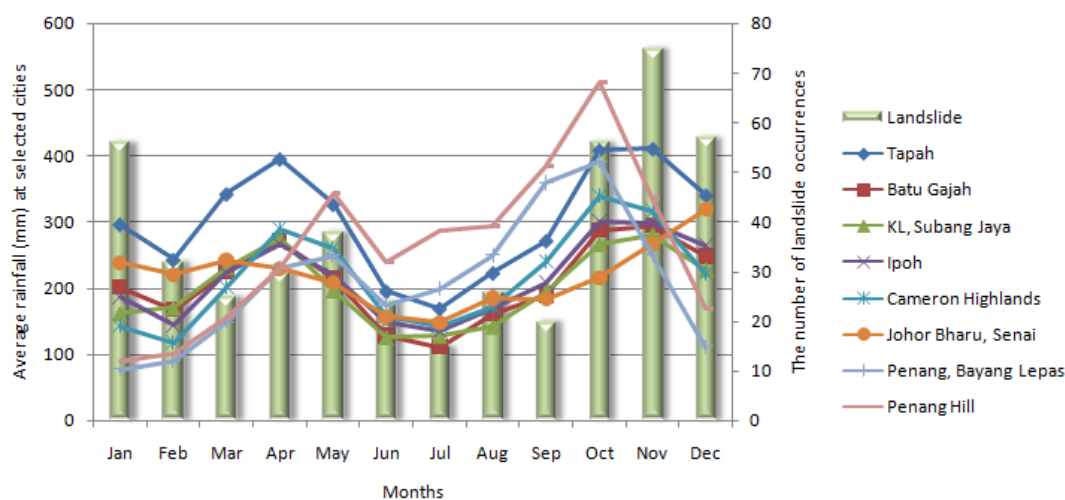


Fig. 1.1 Rainfall cycle and landslide occurrences in PM

Source: Rainfall data from [www.worldclimate.com](http://www.worldclimate.com); Landslides data from JKR [13]

In Peninsular Malaysia (hereinafter referred to as PM) where landslides are typically induced by rainfall, modeling landslide susceptibility taking into account the rainfall factor becomes a necessity. Moreover, the rainfall system acting on this area is governed by monsoonal system which brings two rainy and dry seasons. Fig. 1.1 shows average rainfall of selected cities in PM, for example Tapah, Batu Gajah, Ipoh (all located in Perak), Subang Jaya (Kuala Lumpur), Cameron Highlands (Pahang), Senai (Johor Bharu), Bayan Lepas, and Penang Hill (Penang), against landslide

occurrences number within PM. The relation between the number of landslide occurrences and rainfall intensity is apparent. During rainy seasons (April-May and October-January) the number of landslide occurrences is relatively greater than that of dry seasons (February-March and June-August).

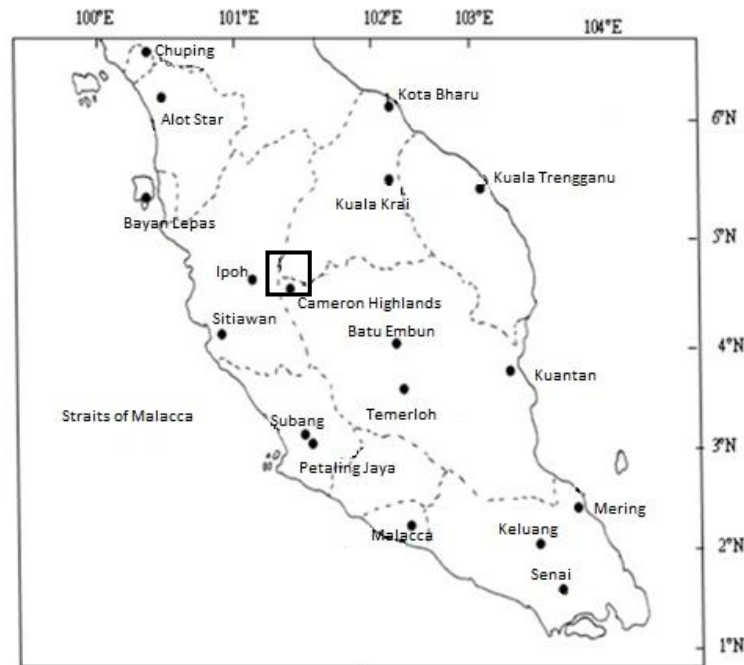


Fig. 1.2 Weather stations in PM

Source: Suhaila and Jemain [14]

Involving rainfall map in landslide susceptibility model of medium scale (1:25,000 to 1:50,000) requires such data to have sufficient spatial resolution especially when blended with remote sensing data such as Landsat 7 ETM+ (Enhanced Thematic Mapper Plus) satellite images spatial resolution of 30 m. The availability of rainfall map with adequate spatial resolution, e.g. 30 m, for medium scale, unfortunately, is doubted even though it is available in multi temporal version. Fig. 1.2 shows the distribution of weather stations in PM which is quite sparse. If the area in the box is used as a study area and rainfall data is interpolated from its surrounding rainfall stations, there will be no sufficient spatial resolution of rainfall data due to its sparse distribution. Rainfall data derived from TRMM (Tropical Rainfall Measuring Mission) satellite can be the solution of this problem. However, the spatial resolution of this data is low that is about 5 km with swath width of 247

km. Detail information regarding this satellite mission can be found in <http://trmm.gsfc.nasa.gov/>.

There are spatial data that may be used as alternative replacement for rainfall data. Pore pressure and ground water table level are considered to experience direct effect from rainfall. Prolonged and high rainfall tends to increase the level of ground water table level. However, these data are not appropriate for medium scale landslide susceptibility mapping. Another alternative is by using spatial data such as NDVI, soil wetness, and Land Surface Temperature derived from Landsat 7 ETM+ satellite mission. The relation between rainfall and these three factors is, indeed, complex or not straightforward. The investigation confirming the correlation of rainfall and NDVI can be found such as in Davenport and Nicholson [15] and Xia, et al. [16]; rainfall and soil moisture in Korres, et al. [17], Zribi, et al. [18], Kyoung-Wook, et al. [19], Nash, et al. [20], and Findell and Eltahir [21]; rainfall and LST in Iijima, et al. [22], Berg, et al. [23], Kulawardhana [24], and Hu and Feng [25]. These data experience changes due to seasonal rainfall. Furthermore, series of these spatial data that coincide with rainfall cycle can be extracted from the satellite mission whose repeat period is 16 days.

Previous works on Landslide susceptibility modeling abroad mostly involves only static factors as mentioned earlier. This is also the case of local studies in Malaysia. The number of publications on landslide susceptibility modeling taking into account multi temporal factors is quite rare as reported by Terlien [26]. Van Asch, et al. [27] emphasized that for the case of rainfall-induced landslides, the temporal activity/variation should be involved. However, investigation on the role of multi temporal factors, e.g. NDVI, soil wetness, and LST, on the modeling of landslide susceptibility has not been investigated yet. Agostoni, et al. [28], Guzzetti [29] and Guzzetti, et al. [30] incorporated multi temporal factors in order to improve the landslide hazard models. Van Asch and Van Steijn [31] and Van Beek and Van Asch [32] added that the actual landslide hazard is strongly linked to the temporal frequency of triggering events, meaning that multi temporal factors are important to take into account. By having multi temporal factors involved in landslide susceptibility modeling, the possible expansion and depreciation of susceptible areas

to landslide due to the changing environmental factors and the relation of the large number of landslide occurrences during rainy seasons can be explained.

There are two things highlighted from information mentioned previously: a research gap and, at the same time, an opportunity in modeling landslide susceptibility. Briefly, the gap is the absent of investigation on landslide susceptibility that takes multi temporal factors into account. Meanwhile, the opportunity is the application of rainfall related spatial data derived from Landsat images for use in landslide susceptibility modeling as the replacement of the rainfall data. This research accommodates these two factors.

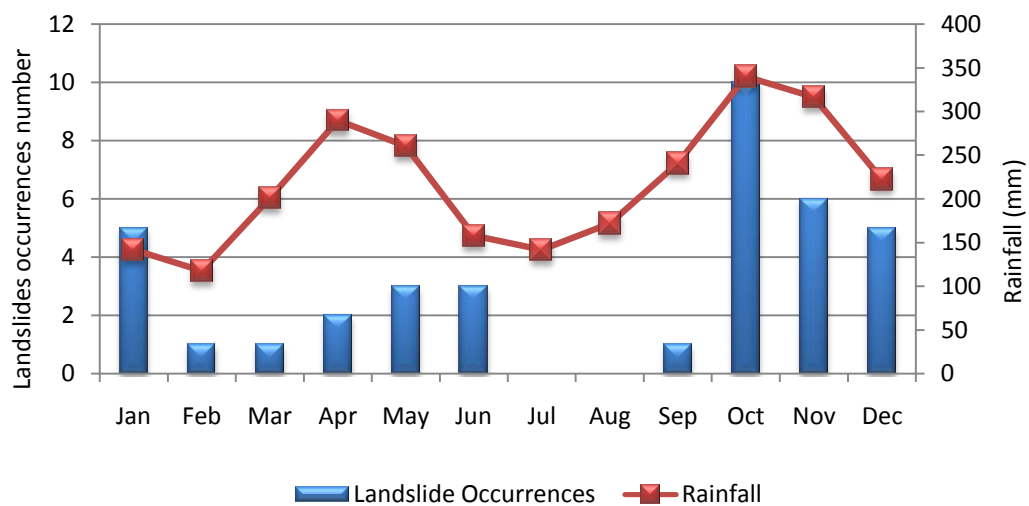


Fig. 1.3 Rainfall cycle and landslide occurrences in Cameron Highlands

Source: Landslides data from JKR [13]; Rainfall data from MMD [33]

Implementation of these two factors requires a case study. Cameron Highlands (CH), located in Pahang State, Malaysia, is selected for the case study for several reasons. This region is considered as a landslide prone area referring to the record of landslide occurrences compiled by JKR [13] from 1967-2007. The climate is characterized by two distinctive rainy seasons during which most of landslide occurrences took place. As shown in Fig. 1.3, two distinctive rainy seasons governed by monsoonal systems are associated with a number of landslide occurrences compiled from 1961-2007. Another reason is that the human activities e.g. land use conversion from forest to for example, infrastructures development and farming are

quite obvious so that it may worsen the stability of the hill slopes. In addition, the place is famous in term of plantation/farming activities and products. As a consequence, it increases the demand of expansion for plantation/farming area. This is how this place attracts many researches for studying landslides.

### **1.1 Problem Statements**

The main problem that motivates the author to conduct this research is the absence of multi temporal factors in landslide susceptibility modeling. In relation to this problem, there are two main issues that need to be resolved as follows:

1. Landslide susceptibility modeling rarely involves multi temporal factors. In fact, the trend of landslide occurrences either in PM or CH is apparently associated with multi temporal factor that is multi temporal rainfall.
2. The inclusion of multi temporal rainfall related factors derived from Landsat images, i.e. DVI, soil wetness, and LST, as replacement of rainfall map in landslide susceptibility model has not been investigated as far as they are concerned.

### **1.2 Research Objectives and Expected Outcomes**

The main objective of this research is to develop landslide susceptibility models of Cameron Highlands that incorporate environmental factor changes in form of different conditions of NDVI, soil wetness, and LST, due to monsoonal rainfall system.

By setting up the above main objective, the outcomes of the research are set to cover the following partial objectives:

1. To produce multi temporal landslide susceptibility maps showing different environmental factors, i.e. NDVI, soil moisture, and LST, and comparing maps.
2. To evaluate the developed landslide susceptibility maps including accuracy of the maps, appropriate weighting system, roles of multi temporal



environmental factors, identification of possible expansion or contraction of areas susceptible to landslides, and identification of significant and insignificant factors.

3. To evaluate the developed model and the approach the model developed by testing their applicability to another case study.
4. To draw recommendations on assessment of landslide susceptibility that incorporates environmental changes.

### **1.3 Scope of Study**

This research is focused on modeling landslide susceptibility of Cameron Highlands taking into account multi temporal environmental factors. To strictly focus on the objective of the research, the scope of the study was set as follows:

1. In regard to the outcome of the modeling, the medium scale, 1:25000 to 1:50000, is chosen to suit to the scale of topographic map and it is the appropriate scale used to accommodate remote sensing data with medium spatial resolution, e.g. Landsat images with 15-30 m resolution.
2. This research is emphasized on modeling landslide susceptibility rather than landslide hazard. The explanation regarding these two terms is given in section 2.1. To produce landslide Susceptibility maps (LSMs), geotechnical aspect was not involved. Otherwise, spatial relationship between landslide causative factors and landslide inventory map was used.
3. The term ‘environmental changes’ is limited to the change of NDVI, soil wetness, and LST derived from Landsat satellite images as response to rainfall cycle. The selection of multi temporal Landsat images was attempted to fit to the peak time of two rainy and dry seasons with the additional constraint that was, satellite image availability that meet the said requirements were collected for further data processing. Standard image processing procedures were applied during image processing.

4. The temporal factors, i.e. NDVI, soil wetness, and LST, derived from Landsat satellite images were not calibrated. In other words, ground truthing of these factors were not conducted.
5. The study area is set to fit to a sheet of topographic map with the size of 30 km x 30 km and scale of 1:25000. Besides CH, the study area also covers part of Kinta (Perak), Batang Padang (Perak), and Gua Musang (Kelantan).
6. The landslide data/map used for map validation is assumed to be the accurate one. The map was mainly prepared by Malaysian Remote Sensing Agency (ARSM).
7. For analysis using Geographic Information System (GIS) tool, weighted sum was chosen as the overlay method. There is no advance method applied for this study. In landslide hazard study, there is no single method proven to be superior applicable for any areas and for any types of landslides. Selection of methods appears less importance than the availability, quality, resolution and abundance of input data as suggested by Guzzetti [29].
8. Penang Island was selected as the test site of the applicability of the developed model. This place is categorized as a landslide prone area. The relevant data are available such as record of landslide or slope failure, required spatial, and the corresponding Landsat 7 ETM+ satellite images.
9. LST used in this study is in form of brightness temperature due to the absence of required parameters.

#### **1.4 Contributions of Research**

The research works have benefits for various stake holders dealing with landslide susceptibility modeling or slope stability studies in Malaysia. The contributions of this research are summarized as follows:

1. The developed landslide susceptibility maps.

This work is a manifestation of individual awareness and contribution to have a partnership with related stake holders, such as slope branch of Public Work Department and respective local authority in Cameron Highlands, in reducing risk and loss caused by landslide. A number of landslide susceptibility maps, either

constructed with or without multi temporal environmental factors, will be useful for a better land use planning.

2. The recommended procedures to model landslide susceptibility.

This research complements other's works and enriches the insight of landslide hazard studies. This research covers complete procedures for landslide susceptibility modeling beginning with site investigation, preparation of spatial data, treatments of remote sensing data to be used with other spatial data, derivation of weightage system, GIS analysis and verification of the results. The research shows the procedures to assess the significance of landslide contributing factors. This is important step in looking for efficient procedures in landslide hazard modeling. The research also shows the roles of additional multi temporal factors in the landslide susceptibility modeling and procedure to assess their significance on the accuracy of LSM. For Department of Civil Engineering, Universiti Teknologi PETRONAS, this research lays an important foundation for further study on landslide susceptibility modeling.

### **1.5 Thesis Organization**

The thesis is organized into five chapters. Chapter 1 describes reviews of background of the research and highlights the gaps, problems, and challenges that are compressed as the problem statement. This chapter also highlights objectives of the research, scope of the study, contributions of the research, and the thesis layout.

Chapter 2 provides a review of relevant literatures on landslide susceptibility modeling, and the methods; landslide causative factors; cases of landslide susceptibility modeling; landslide cases in Malaysia and Cameron Highlands in particular; basic of remote sensing and image processing; and GIS and its roles in landslide susceptibility studies.

Chapter 3 explains the research methodology that is the procedure of all stages to achieve the objectives. It consists of description of study area, hardware and software used, data preprocessing and GIS analysis. Data preprocessing includes preparation of all spatial data originated from topographic map, soil map, and geology map, so that

the data are in the same reference system. Image preprocessing of satellite image is meant to remove geometric and atmospheric errors of Landsat images. From the corrected images, land use land cover, multi temporal NDVI, soil wetness, and LST are derived. This chapter describes the procedures of selection of weighting system, designing scenarios for landslide susceptibility modeling, map validation and accuracy assessment, evaluation of significant role all causative factors, and test of the applicability of the developed model.

Chapter 4 contains the results and discussions of the work accomplished. It covers the discussion of developed rating weight systems selection, produced landslide susceptibility maps that incorporate multi temporal factors, validation of the models, significant role each causative factors including static and multi temporal factors and result of applicability test of the developed model. All results and discussions are focused to answer the objectives. Summary of this chapter is presented in the final section.

Chapter 5 provides conclusions of the research works that confirm and answer all objectives based on the findings during the research work. The chapter also suggests some recommendations for future works.

## CHAPTER 2

### LITERATURE REVIEW

#### 2.0 Overview

This chapter contains reviews of relevant literature on landslide hazard modeling including the terminologies, causative factors, and the methods of assessment. The review also covers previous works on this matter, either local or international case studies. The relevant literature on the basic theory of Geographic Information System (GIS), Remote Sensing, image processing, estimation of NDVI, soil wetness and LST, and the application of these disciplines in landslide studies area, are presented.

#### 2.1 Landslide Hazard Studies: Terminologies and Associated Concepts

As stated earlier, the term landslide means the movement of a mass of rock, debris or earth down a slope as defined by Cruden [1]. The term also includes slope failures as added by Highland and Bobrowsky [34]. The movement of a mass of rock can be a) falling, b) toppling, c) sliding, d) spreading, or e) flowing as shown in Fig. 2.1.

In studying landslide hazard, there are some terminologies and concepts associated with this matter. The terms used in this research are mainly taken from Gilbert, et al. [35] and Guzzetti [36]. Some importance definitions are given below:

1. **Landslide susceptibility** refers to the likelihood of a landslide occurring in an area on the basis of local terrain or environmental conditions. Susceptibility does not consider the temporal probability or time frame of failures. Most of approaches in assessing and mapping landslide susceptibility are based on accurate evaluation of the spatial distribution of both factors, i.e. geo-environmental factors and landslides.

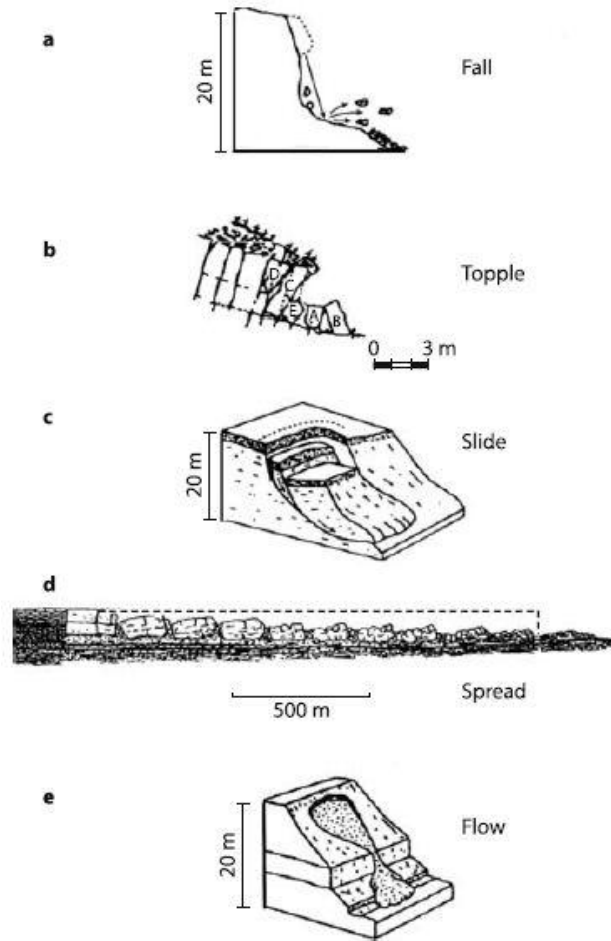


Fig. 2.1 Type of mass movement

Souce: Sassa [37]

2. **Landslide hazard** refers to the potential for occurrence of a damaging landslide within a given area and within a specified period of time. Such damage could include loss of life or injury, property damage, social and economic disruption, or environmental degradation. Guzzetti [36] extended the definition that includes ‘the magnitude of the event’. Thus, the definition incorporates the concepts of location, time, and magnitude of landslide hazard. Landslide hazard ( $H_L$ ) is formulated by International Association for Engineering Geology and the environment (IAEG) and Varnes [38] as multiplication of probability of landslide size ( $A_L$ ), probability of temporal occurrence ( $N_L$ ), and landslide susceptibility ( $LS$ ). The equation is as follows:

$$H_L = P(A_L) \times P(N_L) \times LS \quad (2.1)$$

Landslide susceptibility ( $LS$ ) is a component of landslide hazard ( $H_L$ ).

3. **Landslide risk** refers to the probability of harmful consequences, the expected number of lives lost, persons injured, extent of damage to property or ecologic systems, or disruption of economic activity, within a landslide prone area. The risk may be individual or societal in scope, resulting from the interaction between hazard and individual or societal vulnerability.
4. **Element at risk** refers to the population, public and private infrastructure, economic activities, ecologic values, etc., at risk in a given area.
5. **Specific landslide risk** means the expected degree of loss due to a particular landslide, based on risk estimation—the integration of frequency analysis and consequence analysis. Specific landslide risk ( $R_s$ ) is formulated by IAEG and Varnes [38] as follows:

$$R_s = H_L \times V_L \quad (2.2)$$

To determine risk, one needs to know landslide hazard ( $H_L$ ) and landslide vulnerability ( $V_L$ ).

6. **Landslide vulnerability** reflects the degree of loss to a given element (or set of elements) within the area affected by the hazard, expressed on a scale of 0 (no loss) to 1 (total loss); vulnerability is shaped by physical, social, economic, and environmental conditions.
7. **Slope instability hazard zonation** is defined by Varnes [38] as the mapping of areas with an equal probability of landslide occurrences within a specified period of time. Landslide instability hazard zonation is simply called as landslide hazard zonation (LHZ) as suggested by Gilbert, et al. [35] and most of relevant literature.

In term of mapping, there are various types of landslide hazard maps as the result of stage of landslide studies. The definitions of landslide hazard maps are adopted from AGS [39], UN [40], and Varnes [38]. Some important landslide map definitions are given below:

1. A **landslide inventory map** shows the locations and outlines of landslides. A landslide inventory is a map represents a single event or multiple events. Small-scale maps may show only landslide locations, whereas large-scale maps may distinguish landslide sources from deposits, classify different kinds of landslides, and show other relevant data.
2. A **landslide susceptibility map** ranks slope stability of an area into categories that range from stable to unstable. Many susceptibility maps use a color scheme that relates warm colors (red, orange, and yellow) to unstable and marginally unstable areas and cool colors (blue and green) to more stable areas.
3. A **landslide hazard map** indicates the annual probability of landslides occurring throughout an area. An ideal landslide hazard map shows not only the chances that a landslide may form at a particular place, but also the chances that a landslide from farther upslope may strike that place.
4. A **landslide risk map** shows the expected annual cost of landslide damage throughout an area. Risk maps combine the probability information from a landslide hazard map with an analysis of all possible consequences (property damage, casualties, and loss of service).

In most of literature the terms ‘susceptibility’ and ‘hazard’ are often used incorrectly as synonymous terms as explained by Guzzetti [36] whereas both terms have different meaning. ‘Landslide susceptibility’ is more in probability of ‘spatial’ occurrence of slope failures based on terrain parameter conditions or in other words it is an estimate of ‘where’ landslides likely to occur. Meanwhile, besides predicting ‘where’ a slope failure will occur, the term ‘landslide hazard’ forecasts ‘when’ or ‘how frequently’ it will occur, and ‘how large’ it will be. Thus, landslide hazard is more difficult to deal with than landslide susceptibility. Moreover, susceptibility is the spatial component of the hazard.

The reason that landslide hazard is more difficult to deal with than landslide susceptibility has made the number of publications on the study of landslide susceptibility abundance such as studies done by Agostoni, et al. [28], Ahmad, et al. [41], Anbalagan [2], Ayalew and Yamagishi [5], Chuanhua and Xueping [42],



Gahgah, et al. [43], Hong, et al. [44], Komac [45], Lee and Pradhan [10], Lee and Pradhan [7], Lee and Sambath [46], and Liao [47], even though these investigations are mostly entitled as landslide hazard study or assessment. This is what Brabb [48] found in most of literatures that landslide hazard (map) is often represented as landslide susceptibility (map). Guzzetti [36] added that literature on landslide hazard frequently discusses methods and techniques to model landslide susceptibility rather than landslide hazard. From this point of view, the author would like to emphasize that this research deals with landslide susceptibility mapping rather than landslide hazard mapping.

## **2.2 Landslide Triggering and Causative Factors**

A Combination of landslide causative factors and one single triggering factor may lead to a landslide occurrence. For every case of landslide event there will be causative factors and, at least, a triggering factor. Like ‘susceptibility’ and ‘hazard’ terms, the terms ‘landslide triggering’ and ‘landslide causative’ factors are often used as synonymous. In fact there is a subtle difference between both concepts. Landslide causative factors are the reason why a landslide occurs at a particular area. These factors are responsible to the vulnerability of the slope to failure. Landslide triggering factor is a single stimulus that initiates a landslide event. Storm, extreme rainfall or prolonged rainfall, earthquake/seismicity, snow melting, and human activity are well known as landslide triggering factors as described by Gilbert, et al. [35], Guzzetti [29], Van Westen, et al. [49] and Carrara, et al. [50]. As an example, the rainfall intensity and the migration of the center of the rainstorm were found as the triggering factor for landslide in Lantau Island, Hongkong, as reported by Zhou, et al. [51].

To assess landslide susceptibility, it is importance to understand the main conditions causing landsliding which are commonly known as landslide causative factors or simply written in this thesis as causative factors. A comprehensive review of causative factor can be found in Varnes [38]. The causative factors that cause slope instability are numerous and varied. The factors interact in complex and subtle ways. The basic causes of slope instability consist of inherent factors within the rock or soil, constant factors such as inclination, temporal factors such as ground water levels,

transient factors such as seismic vibration, and imposing factors such as construction or human activities. Beside inherent factors, there are factors producing unfavorable changes such as those that change stress in slope conditions (e.g. the stress vary due to erosion, fluctuation of ground water, change in land use, removal lateral support of slopes during cuts for roads, house sites, excavation, etc.) and those that change strength of materials in slopes (e.g. weathering and other physical and chemical actions). Varnes [38] further explained that inherent factors include geology, geomorphology, vegetation, hydrology conditions, and climate. Hutchinson [52] summarized terrain attributes (causative factors) associated with landslide shown in Table 2.1.

Even though the number of causative factors is quite large, only few causative factors are important ones as concluded by Hutchinson [52]. This is why the number of causative factors used by the investigators on landslide hazard assessment (LHA) varies. For examples, Liao [47] used six causative factors namely, soil moisture, land use land cover, geology, soil, and slope gradient, for LHA mapping in Washington County and Crawford county, United States. Pachauri and Pant [53] included eight causative factors namely geotechnical factor, distance from active fault, slope angle, relative relief, geological formation, land cover, distance from ridge top, and road density, for landslide hazard studies in Himalayas. A local study conducted by Lee and Pradhan [7] on landslide hazard mapping in Selangor, Malaysia, used ten causative factors i.e. slope, slope aspect, curvature, distance to drainage, geology, soil, distance to lineament, land use land cover, and NDVI. The underlying reasons in regard with the number of causative factors used/chosen were not clearly stated in these publications. In the following, the description of the importance of some causative factors is discussed.

### **2.2.1. Geology**

Many published literatures on LHA involve geology information as a causative factor for landslide hazard assessment such as the investigations done by Anbalagan [2], Chaco'n, et al. [54], Lee and Talib [55], Fell, et al. [56], Lee and Pradhan [7] and Suzen [57]. Jadda, et al. [58] found that the geology is the important landslide

causative factor during the investigation of LHA in Central Alborz, Iran. Varnes [38] explained that the simplest utilization of geology information is in form of a general geology map, showing geologic formations with accompanying tabular data stating the relative stability of the geology units.

Table 2.1 Category of terrain attributes associated with landslide

<b>Category/Causative Factors</b>	<b>Example</b>
Bedrock geology	Bedrock type
Quaternary geology	Glacial geology
Geomorphology	Slope gradient and aspect
Weathering	Physical, chemical, and biological weathering
Erosion	Surface erosion, gullying, and seepage erosion
Climate	Precipitation and freeze-thaw
Vegetation	Vegetation type and root strength
Hydrogeology	Runoff, snow melt and groundwater
Geotechnics	Geochemistry, shear strength, and swelling shrinkage
Volcanic activity	Ash accumulation and lava flows
Natural dams	Glaciers and ice sheets
Seismicity	Earthquake and shaking
Human activity	Land use

Source: Hutchinson [52]

Causative factors related to geology information are available as lithology and structure. Lithology includes the composition, fabric, texture or other attributes that affect the physical or chemical behavior of rocks and engineering soils as stated by Varnes [38]. Structure includes the features of inhomogeneity and discontinuity in rocks or soils at scale larger than a hand specimen including stratigraphic sequence, attitude of layering, gross changes in lithology, bedding planes, faults/geology lineaments, and folds. Slope stability is governed by the degree of fracturing and shearing. Geology fault/lineament also plays an important role in causing slope instability. For examples, areas with highly faulted zones in central Japan and southern Italy tend to have high occurrence of slope failures. Investigation conducted by Carrara, et al. [59] found that in the Umbria-Marche Apennines, the number of landslides is abundant along the major thrust. In constructing landslide hazard map in

Aglar River area, a tributary of the River Yamuna in Himalayas, Pachauri and Pant [53] considered the distance from active faults or geology lineament. The areas near active faults were classified into five groups and were given maximum weight values based on the closeness to the active faults. The closer the distance from active faults the higher the weight values.

Type of soil is also an important factor controlling slope stability. The progressive weakening of slope forming material due to natural processes such as weathering and tectonic uplift may cause slopes instable as reported by Zhou, et al. [51]. Soil is unconsolidated mineral matter and located on the earth surface. Soil is originated from underlying bedrock and characterized by the presence of layering that plays an important role in mass movement processes. Soil depth also plays a role in influencing the total mass of the over burden which induces landslides as described by Pande, et al. [60]. Soil information is therefore frequently involved in LHA. For examples, Anbalagan [2] involved soil and rock types as a group of lithology and soil depth map as well during construction of landslide hazard zonation map of the mountainous areas of Himalaya. Using the author's experience, the type of soils and rocks was ranked based on the degree of fracture and strength.

### **2.2.2. Geomorphology**

The presence or absence of former landslides is an important key if one would consider geomorphology factors in LHA as suggested by Varnes [38]. Past landslides would be the best guide to investigate the future behavior of the study area. Among the important aspects of geomorphology are slope and slope aspect. Carrara, et al. [61] added curvature factor as another aspect while DeGraff and Romesburg [62] included elevation factor in the landslide hazard model.

More practical and visual descriptions on slope, slope aspect, and curvature terms can be found in ESRI [63]. Slopes of a hill describe the steepness of hill slope. Slope aspect is defined as a compass direction a hill faces while curvature is used to explain the physical characteristics of drainage basin such as erosion and runoff process. Slope contributes the overall rate of movement downslope the hill. Slope aspect

shows the direction of flows. Curvature of terrain is shown as convex, concave, peaks, and flat surface. Sloping surfaces that are convex in the cross-sectional direction are called as ridges. Those having convex cross-section and convex longitudinal direction are called peaks. Meanwhile, pits are indicated by concave curvatures as described by Kumar, et al. [64]. Curvature affects the acceleration and deceleration of flow and, therefore, influences erosion and deposition. The curvature forms, i.e. convex or concave, influence the convergence and divergence of flow. This information is useful to identify the areas where the flow will accumulate and possible landslide or debris locations.

#### *2.2.2.1 Slope gradient*

Slope gradient is an important causative factor. The shape of slopes affects the direction of and the amount of surface runoff or subsurface drainage down the slopes. For hazard zoning purpose, Varnes [38] stated that the steepness of slopes is important to consider due to its relation with the strength of slope-forming material. Slope gradient is usually classified into ranges of degree or percent. However, the interrelation between slope gradient and slope instability is complex. The steepest slope gradients do not always mean as the most prone slopes to landslide. Steep slopes are usually occupied by very resistant/competent rock causing the slopes more stable than comparatively gentle slopes of weak material. Havenith, et al. [65] added that landslide body and scarp usually occur in areas with relatively small slope angles. The preferential location of landslides at small slope angles is not caused by the slope angle itself but related with complex interaction between slope angle and the environment.

The ranges of high risk slopes vary from one place to another. For examples, most of landslide cases in Lantau Island Hongkong occurred within a slope range of  $25^{\circ}$ - $35^{\circ}$  in the middle and western parts of the island and  $30^{\circ}$ - $35^{\circ}$  in the eastern part respectively from investigations conducted by Zhou, et al. [51]. Slopes above  $40^{\circ}$  and above  $45^{\circ}$  were set as the highest risk slopes referring to the works conducted by Anbalagan [2] and Pachauri and Pant [53] respectively. Meanwhile, Lee and Pradhan [7] found that slope range of  $16^{\circ}$ - $25^{\circ}$  occupied by most of landslide occurrences in

Selangor, Malaysia. Landslides may also occur at gentle slope e.g.  $9^{\circ}$ - $12^{\circ}$  as reported by Jäger and Wieczorek [66]. The different ranges of risky slope indicate that the typical risky slopes are different from place to place. Hence, the risky slope should be carefully recognized for LHA purpose.

#### *2.2.2.2 Slope Aspect*

Slope aspect and terrain curvature are frequently used as causative factors in LHA. Carrara, et al. [61] has conducted a study on analysis of digital terrain for slope stability. The study found that slope aspect and its curvature can be related to slope stability. However, researchers had different opinions about the importance role of slope aspect in causing slope instability. Greenbaum, et al. [67] concluded that slope aspects have no significant influence on landsliding. On the contrary, some authors such as Suzen [57] and Van Westen, et al. [68] agreed that there is a relationship between landslide and slope aspect. Dai and Lee [69] added that the condition of moisture retention and vegetation of slopes are affected by the orientation of slopes and in turn, these conditions can affect the soil strength. In spite of the existence of the relationship between slope aspect and landslides, researchers found that there is no single relationship between landslide and slope aspect. Moreover, the facts that some studies were carried in various places, e.g. some were in northern hemisphere countries, some were in the southern, and some were in equatorial belt, would surely produce different results considering the sun exposure (intensity).

Investigators found different relation between slope aspect and landslides. DeGraff and Romesburg [62] pointed out that slope aspect contains information about the structural and basic condition of a slope including fault planes and climatic factors respectively. The author further made assumptions that slopes which are facing the sun, particularly the afternoon sun, tend to have higher soil temperature, lower soil moisture, less vegetation, and therefore tend to have higher erosion rate. Further investigation carried out by Caiyan, et al. [70] in Gorges reservoir, China, found that landslides mostly occurred at slopes facing south, southwest and southeast. Lineback, et al. [71] found that the number of landslide occurrences is larger in the wetter north-facing slopes than in drier south facing slopes when assessing landslide potential

zones in Payette River, Idaho, United States. Marston, et al. [72] reported that soil exposed on south facing slopes tends to undergo wetting and drying cycle so that it contributes the increase of the number of landslides in Himalaya. Meanwhile, the investigation conducted by Lee and Pradhan [7] showed that high frequency of landslides in Selangor, Malaysia, took place in north and northwest facing slopes.

#### *2.2.2.3 Curvature*

Curvature also has a contribution to landsliding. The acceleration or deceleration of colluviums, the loose bodies of sediment, is affected by curvature. The shape of hill slope, i.e. concave or convex, will determine where colluviums will accumulate. Ahmad and McCalpin [73] stated that the abundance of colluvial slides was found in 'hollows' or concave terrain. Concave slopes behave as a channel. It contains and retains more water gained from rainfall for a longer period than convex slopes as described by Kumar, et al. [64] and Lee and Evangelista [74]. Investigation on the relation of curvature and landslides produced different results. Ohlmacher [75] found that planar plan curvature has the highest probability of landsliding in Appalachian Plateau and scattered regions within the Midcontinent of North America. In Pemalang, Indonesia, investigation on the landslide susceptibility conducted by Oh, et al. [76] showed that most of landslide occurrences took place in convex curvature areas. Similar results were reported by Lee and Talib [55] and Lee and Pradhan [7] that convex curvature areas were found to have more frequent landslides compared to concave and planar curvature areas in Penang and Selangor, Malaysia, respectively. Oh, et al. [77] also investigated landslide susceptibility in Pechabun area of Thailand. The landslide occurrences mostly occupied concave curvature areas.

#### *2.2.2.4 Elevation*

Elevation is one of geomorphology factors that affect slope instability. Authors are in different opinions about this. Asfaw [78] considered elevation as an important factor for a reason that precipitation and weathering are inherent factors of elevation. Chau and Chan [79] found that elevation as a causative factor is related to human

developments/activities that are concentrated at certain elevations belt. Dai and Lee [69] argued that at very high elevation, the terrain usually consists of weathered rocks whose shear strength is much higher. Meanwhile, at intermediate elevations, the terrain is covered by thin colluviums causing it more instable. At very low (gentle) elevations, the terrain is usually covered by thick colluviums or residual soils so that the frequency of landslides is low. Although landslides have been found to have a relationship with elevations, Gómez and Kavzoglu [80] argued that the relationship is still unclear. The author further described that the elevation influences the number of biophysical parameters and anthropogenic activities, and the soil characteristics are affected by the elevation. Gao and Lao [81] introduced an empirical formula relating possibility of landslide  $P(H)$  at a particular place with height factor as follows:

$$P(H) = (1.28229H^2 - 0.001847H^3) / 106 \quad (2.3)$$

### 2.2.3. Hydrology conditions and Climate

Water is the most important landslide causative factor as explained by Varnes [38]. As the consequence, it is important as well to identify the source, movement, amount of water, and water pressure. Slope failure types and severities vary from one region to another due to climatic patterns of temperature and precipitation, and also depend on the soils and weathering characteristic of each climatic region. In tropical region, such as Malaysia, the monsoon system plays important roles in causing landslides.

Spatial data associated with water, such as complete precipitation data as well as subsurface water level, pressures, and their seasonal fluctuation, area required for LHA purpose as suggested by Varnes [38]. Unfortunately, such data are generally unavailable or incomplete. Investigators then focused on gaining the information on how hydrology conditions are affected by lithology, structure, soils, topography, vegetation, climate, and by movement of landslide itself. Responding to this, investigators used remote sensing technology e.g. aerial photograph and satellite images, to detect ground surface temperatures, soil moisture, and vegetation condition. The latter can reflect the change of hydrologic conditions. For examples, Seker, et al. [82] used land surface temperature for locating landslide areas in



Sebinkarahisar township, Turkey. Landslides locations were characterized by having high thermal difference. Meanwhile, Mondini, et al. [83] made a hypothesis that the surface temperature between landslide and stable areas should be different. The preliminary result showed that the distribution of land surface temperature in landslide areas in Collozone, near Umbria, Italia, is lower than that in the non-landslide areas.

#### *2.2.3.1 Soil Moisture*

Soil moisture or soil wetness can be an important factor of areas prone to landslide. Theoretically, if the moisture of surface soil mass increases, the pore water pressure beneath the respective surface increases accordingly. In turn, it will decrease shear stress and shear strength, and can initiate landslides as described by Ray and Jacobs [84], Jotisankasa and Vathananukij [85] and Xu, et al. [86]. Ray and Jacobs [87] studied the relationship between soil moisture, precipitation and mass movements in three different places namely a district in Philippine, California and Nepal. The study found the strong relation between soil moisture, precipitation and landslide occurrences time. For areas with typical rainfall induced-landslides, like most places in Malaysia, as the amount of rainfall increases, the water content and pore water pressure increase as well. In turn, it will increase the water permeability and lateral water flux in the soil, causing the respective areas more inductive to landsliding.

#### *2.2.3.2 Factor related to river*

Hydrologic condition in river may be related to landsliding. Kallen, et al. [88], working on geotechnical mapping in Qingjiang River, China, found that there is a strong relation between lithology, slope angle, and texture, and landslide occurrences along the river. Most landslides take place on the rivers whose dip angle of bedding is nearly parallel to the slope, facilitating potential and effective side planes. Liu, et al. [89] found similar result that landslides mostly occur in close proximity the Yangtze River, Three Gorges, China. The fact that landslides frequently occur along the river is explained in the following. Landslides along the river are usually caused by the

changes in ground water level of river slope. If slopes are adjacent to a water body such as river or lake, and the water level of a water body suddenly falls, the ground water level cannot quickly escape. This condition may cause the slopes having shear stress higher than in normal condition, leading the slopes to unstable. Landslides along the river usually occur after flood eroding the river bank, causing the slope cut and unstable. The case of landslide along Shirayuki River represents this condition as reported by Shimazu and Oguchi [90].

In constructing landslide hazard map, investigators usually apply the distance to/from river/drainage as a landslide causative factor and make an assumption that the closer the distance to river the more unstable the slope. This principal is applied to a case of landslide in Shirinrood watershed, Iran, investigated by Kelarestaghi and Ahmadi [91]. The authors consider the closeness to the river as a causative factor for a reason that the river disturbs the stability of the slopes by eroding process or saturates the lower part of material until the ground water level increase. Other investigators applied similar principal were Lee and Talib [55], Jadda, et al. [58], Yilmaz [92], Lee and Evangelista [74]. Gómez and Kavzoglu [80] used buffered river channel of Jabonosa River Basin, Venezuela, as an input for landslide hazard modeling.

#### **2.2.4. Vegetation and Land Use Land Cover**

Vegetation is an importance landslide causative factor. It maintains the integrity of hill slopes by binding rocks and soils together against incessant torrential rains that last for days. Anbalagan [2] explained that different types of vegetation have different root strength and network. Hence, they contribute the stability of the slope. Well distributed root network system will increase shearing resistance of slope material because it acts as natural anchoring of slope material. In addition, slopes covered either by thick vegetation or grass experience less weathering and erosion and, as the consequence, it will strengthen the stability of the slopes. On the other hand, non-vegetated (or barren land) and sparsely vegetated slope are exposed to weathering and erosion process, causing the slopes prone to failure.

#### *2.2.4.1 Land use land cover (LULC)*

Land use is different from land cover even though these terms are frequently used interchangeably. Liao [47] described that land use express what human beings have done or developed on the land and its resources. Opening hilly areas for cultivation and irrigation can change the water budget on the slope and can lead to slopes instability. Land cover shows the physical state of the land surface such as, forest, grass, and lake, etc. Land cover can act as an indirect indicator of slope stability. In general, vegetated areas or slopes mean that these areas are more stable compared to non-vegetated ones because vegetation protects the sloping material from weathering and erosion.

In LHA, LULC has been a mandatory causative factor to include. Various land cover land use types are assigned different weight values referring to their contribution to slope instability such as in landslide hazard assessment works carried out by Anbalagan [2], Pachauri and Pant [53], Ramli, et al. [93], and Liao [47]. Forest land and thickly vegetated areas are usually assigned with low weight values while sparse vegetated areas and barren land are given relatively high weight values due to their vulnerability to slope failure. Zhou, et al. [51] studied the relationship between land use and landslide in Lantau Island, Hongkong, by overlaying landslide data overlaid with land cover. As the result, most of landslide occurrences took place in the bare/barren land, shrub-areas, and in the transition zones between different vegetation types.

#### *2.2.4.2 Vegetation Index*

Another expression of the condition of vegetation involved in LHA is in form of vegetation index. Gibson and Power [94] described that vegetation index is a measure of biomass and vegetation health. The higher the vegetation index value the denser and healthier the vegetation. Working on landslide hazard modeling in Namasigue and El Triunfo watersheds, Honduras, Perotto-Baldiviezo, et al. [95] found that areas with low vegetation index values such as on agriculture areas and removed-deep rooted permanent vegetation areas had high landslide occurrences. On the contrary,

areas with high vegetation index values such as shrub fallow and forest had relatively low landslide occurrences. Similar result was obtained by Jayaseelan and Sanjeevi [96] during the work on recognizing landslides locations using vegetation index values derived from remote sensing images in Nilgiris, South India. On satellite images, Vohora and Donoghue [97] explained that landslides areas can be identified based on tone, which indicated exposed surfaces, and feature shapes. Lin, et al. [98] found that the pre-quake vegetation, i.e. NDVI, condition at the Jou-Jou Mountain area is higher (0.4) than that after earthquake (0.08) where most of vegetated areas were covered by landslide debris. This fact suggests that the typical of vegetation index of landslide areas is low.

### **2.2.5. Human activities**

Human activities or frequently called as anthropogenic activities on hilly slopes are of important landslide causative factors. There are two anthropogenic activities namely deforestation and road network development.

#### *2.2.5.1 Factors related to deforestation*

Alexander [99] reported that deforestation has resulted in mudflow disaster in Calcianno, Southern Italia. Glade [100] reviewed history of landslide in New Zealand and found that extensive conversion of hill areas from native forest and bush to pasture had reduced the strength of the regolith, causing the slopes more susceptible to landslides. Erosion rate on clear slope or cut slope is 30 times higher than in forest as investigated by Sharma and Kumar [101] for case of H.J. Andrews Experimental Forest, United State. The rapid development of Penang Island, Malaysia, had negative consequences where urban expansion started to encroach hilly areas as reported by Chan [102]. Major development projects were mainly directed to hilly areas due to the limitation of land. As consequences, hilly areas experienced land use changes mainly from forest to open land such as for construction, housing and agriculture. These developments have made landslide as of major natural disaster to Penang Island. Lee and Pradhan [103] reported that there were 465 landslide sites identified

from aerial photograph and site investigation at this area. Anbalagan [2] added that watering the slope in case of agriculture field will add more water on the slope besides the water received from precipitation. This may affect the stability of the slopes. Housing and construction on the slopes will add load to natural weight of the slopes due to the weight of such structures.

#### *2.2.5.2 Factors related to road network development*

Road network development is another consequence of urban expansion. For hilly areas, development of new roads is frequently built traversing undulating areas. This inevitably employs works of clearing and cutting slopes. Liao [47] reported that extensive slope cutting for developing two new roads in Northern Arkansas, Washington, United State, had caused landslides occurred along these roads since the beginning of construction and continued to undergo slope failures years after the completion. Investigating landslide hazards in British Columbia, Canada, Jordan [104] found that approximately 95% of development relative landslides are related to road. A big landslide occurred in Pos Selim, Malaysia, during works for developing a road connecting Simpang Pulai and Kampung Raja and continued after its opening for public as reported by JKR [13] and Malone, et al. [105].

Given the fact that cut slope along the road poses a serious threat to the road passer and infrastructures along the road including the road itself, many investigators considered the road as an importance causative factor in landslide hazard analysis in term of the distance to/from the road. The closer the distance from the road the higher the slope failure threat and the greater the weight value as well. This concept has been applied in landslide hazard analysis by, for examples, Ahmad and McCalpin [73] for case study of Kingston Metropolitan areas, Jamaica; Kelarestaghi and Ahmadi [91] for case study of Northern Iran; and Yalcin [106] for case study of Ardesen, Turkey; and Sharma and Kumar [101] for case study of Parwanoo, Himalaya. As a practical example, Chung and Leclerc [107] classified the distance to the road into three classes: <25 meter (high hazard), 25-50 meter (medium hazard), and >50 meter (low hazard or safe).

### **2.2.6. Number of Causative Factors Used for LHA**

Reviewing a number of literatures on LHA, it can be concluded that there is no agreement among the authors about the number of landslide causative factors should be considered in LHA. Authors have different suggestion about this. Van Westen, et al. [68] suggested that all possible causative factors can be entered into a GIS-based landslide hazard analysis if a statistical method is selected. Van Westen [108] and Sarkar, et al. [109] agreed to use the available landslide causative factors to analyze landslide hazard. Dahal, et al. [110] recommended involving only relevant factors. In addition, Van Westen [111] highlighted an important suggestion that the factors acting to previous landslide events at a particular area should be chosen in landslide hazard assessment. Expert opinion on selection of causative factors was used for works on LHA carried out by Chung and Fabbri [112]. Anbalagan, et al. [113] used inherent causative factors responsible for slope instability when working on LHA in Himalaya terrain.

The following is examples of utilization of different number of causative factors applied to different landslide case studies. For examples, Neaupane and Piantanakulchai [114] involved the factors that were generally used in LHA such as slope, slope aspect, lithology, proximity to channel/stream, and land use land cover. Sharma and Kumar [101] incorporated the main contributory factors for landslide hazard assessment in Parwanoo, India. They were distance from fault, slope, slope aspect, lithology, land use land cover, flow accumulation, distance from road, and distance from drainage. In comparing between GIS-based landslide susceptibility assessment using multivariate and bivariate methods, Süzen and Doyuran [115] employed 13 factors that were believed to control the landslides in the study area of Asarsuyu catchment, Turkey. These factors were lithology, distance to fault, fault density, elevation, distance to drainage, drainage density, distance to ridge, slope aspect, slope, distance to settlement, distance to power and road, distance highway, and land use land cover.

### **2.2.7. Multi Temporal Environmental Factors**

The temporal component is important to involve in assessing landslide hazard under changing environmental condition. Most of published literatures on landslide hazard do not involve the impact of changing environmental condition. Guzzetti [29] recommended the addition of the temporal aspect (time component) of landslide into hazard models since actual landslide hazard has links with temporal factors. Temporal factor, as previously discussed, is directly linked to rainfall or ground water table. However, environmental factors such as vegetation condition, inform of NDVI, soil moisture/wetness, and LST are responsive to the main temporal factor that is rainfall. The publications investigating the responses (or changes) of such factors to rainfall are given below.

#### *2.2.7.1 Change in vegetation index*

Water is the most important factor for plant growth. In most of ecosystem, especially grassland and cropland, seasonal plant growth synch with the rain cycle. During drought season, vegetation grows poorly. Conversely, abundant rain increases the vigor and health of vegetation. Investigation carried out by Davenport and Nicholson [15] in East Africa showed that NDVI has been found as a sensitive indicator of inter-annual variability of rainfall. Xia, et al. [16] found that vegetation development is correlated with precipitation-derived moisture. The correlation is seasonal change.

#### *2.2.7.2 Change in soil moisture*

Change in rainfall amount and patterns can affect soil moisture/wetness. Korres, et al. [17] described that spatio-temporal patterns of soil wetness in agricultural areas are affected by multiple natural such as rainfall. Zribi, et al. [18] found that soil moisture estimated from ERS scatterometer estimators follow approximately the same variations as that in rainy season. Investigation carried out by Kyoung-Wook, et al. [19] showed that soil moisture experience significant change just after heavy rainfall events. Meanwhile, Nash, et al. [20] reported that there is a delay between change of

soil moisture and rainfall by a few lags. Findell and Eltahir [21] reported that the correlation of soil saturation condition and subsequent rainfall is linear and appears to be significant during summer months. These investigations show that rainfall has a role in determining soil moisture.

#### *2.2.7.3 Change in LST*

The Investigations carried out by several researches show that surface temperature changes due to variation of rainfall intensity. Iijima, et al. [22] investigated the relation between soil temperature and rainfall in Central Lena River Basin, Russia, and found that pre-winter rainfall in the following three years accelerated soil warming. Berg, et al. [23] found in his investigation in Europe domain that there was an exponential increase in the extreme precipitation with increasing surface temperatures in winter. In summer, the opposite occurred. Investigating spatio-temporal of land cover, LST, and rainfall relationship over Sri Lanka, Kulawardhana [24] found that rainfall and LST showed a significant correlation ( $r = 0.69$ ) during the second inter-monsoonal period from October to November. Hu and Feng [25] also found that surface air temperature and precipitation influenced soil temperature in the Eurasian continent. These studies show that the climate, more particularly, rainfall has a contribution in controlling soil temperature.

### **2.3 Scales of LHZ Maps**

To get appropriate LHZ maps, one should consider the appropriate scales and methods. Suzen [57] explained that the selection of the scales depends on the aim of the study, the required precession of the maps, and the availability of the resources e.g. finances, data, and manpower. For constructing LHZ maps using GIS, Van Westen [111] and Suzen [57] suggested the following scales:

1. National scale ( $< 1:1.000.000$ ). This scale is mainly used to outline the hazard type and hazard prone areas prepared for the entire country.
2. Regional/Synoptic scale ( $1:100.000$  to  $1:250.000$ ). This scale is suitable for regional planning in respond to landslide hazard threat. These maps cover area



of thousands of square kilometers. The suitable method for this scale is qualitative method such as geomorphologic field.

3. Medium scale (1:25.000 to 1:50.000). Medium scale is used for preliminary planning of infrastructural works, dealing with feasibility studies for large engineering works. The scope of these maps covers area of several hundreds of square kilometers. Quantitative method such as statistical analysis is suitable for this scale.
4. Large scale of 1:2000 to 10.000 is used at the level of the engineering geological site investigation. These hazard maps are intended to facilitate a detailed planning for infrastructure, housing or industrial projects. The maps cover very small area. Deterministic approach is suitable for this scale. A large portion

## **2.4 Methods for Landslide Hazard Assessment**

Risk and loss caused by landslide can be reduced either by modifying the hazard event itself which is related to engineering designs; or by reducing human vulnerability which is related to modification of human attitude and behavior towards hazards. Modification of human vulnerability includes preparedness, forecasting and warning, and land-use planning as mentioned by Chung and Leclerc [107]. Both modifications require the natural hazard to be zoned. As defined by Varnes [38], LHZ is the division of a land surface into homogenous areas according to the degree of actual or potential hazard due to landslides or other mass movements on slopes.

The principle “the past is the key to the future” has been used by landslide investigators for assessing landslide hazards. In order to have understanding of past landslide occurrences and to be able to predict future landslide hazards, one should begin with construction of landslide inventory map as suggested by Guzzetti [29], Van Westen [111] and most of the experts of this field. The next work is to have a good understanding about landslide causative factors and its relationship with landslide events as suggested by Varnes [38] and Liao [47]. This will allow the investigators to gather relevant causative factor maps. The next step is selection of the appropriate method(s). There are, of course, various methods for evaluating landslide

hazard. However, Guzzetti [29] and Aleotti and Chowdhury [116] emphasized that there is no method which is considered as the most suitable method for evaluation of landslide hazards effectively. This may be due to the wide spectrum of landslide phenomena so that there is no single method proven to be powerful to identify and map landslides, to ascertain landslide hazards, and to evaluate the associated risk. Hence, a combination of qualitative and quantitative methods is accommodated in especially in tweaking weighting system. Works of DeGraff and Romesburg [62], Ayele [117], and Baban and Sant [118] were examples of landslide hazard studies using combine methods.

There are several methods for landslide hazard analysis. The methods are mainly divided into qualitative and quantitative methods. The selection of methods determines the objectivity of the results. The first methods are subject to subjectivity of experts based on site experiment while the latter methods offer objectivity in result. Aleotti and Chowdhury [116] provided a comprehensive review on landslide hazard assessment methods along with the advantages and disadvantages. The methods are schematically shown in Fig. 2.2.

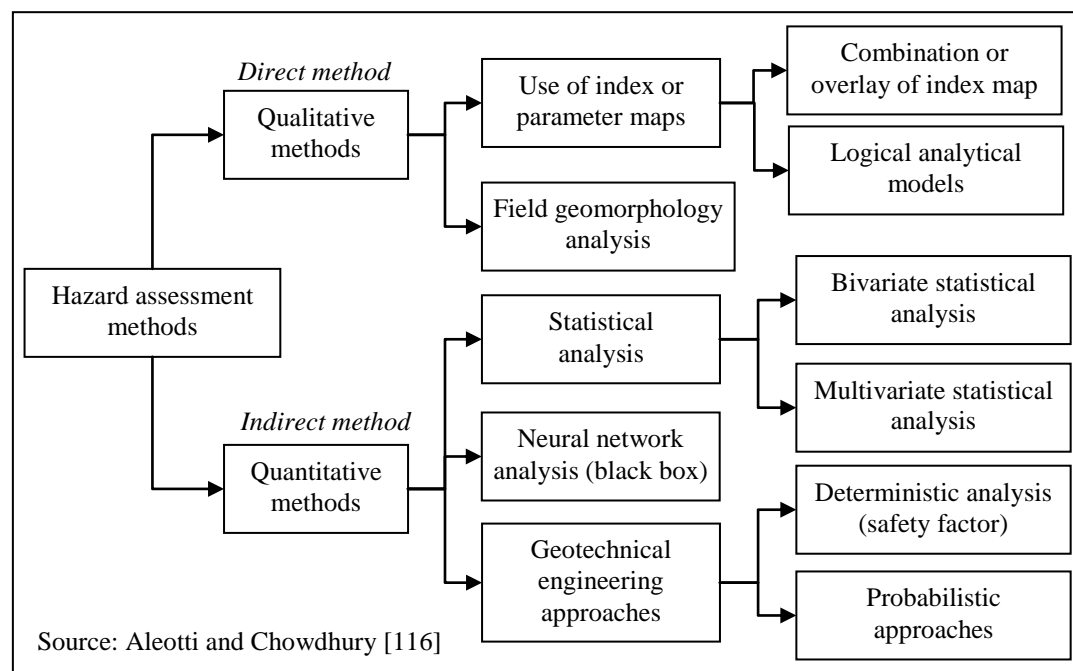


Fig. 2.2 Landslide hazard assessment methods

### **2.4.1. Qualitative Methods**

Qualitative methods are commonly known as direct methods. Qualitative methods include use of index or parameter maps and field geomorphology analysis approaches. Qualitative approaches are entirely based on the site specific-experience or judgment of experts. These approaches mainly require aerial photogrammetric images and field survey data as supporting data for image interpretation use. High resolution satellite images may complement required spatial data. More detail about qualitative methods can be found in Aleotti and Chowdhury [116], Suzen [57], Guzzetti [36], and Van Westen [108].

#### *2.4.1.1 Field Geomorphology Analysis*

This method is also called as heuristic method, landslide distribution mapping, and experience-based method. This method is considered as the most straight forward qualitative method to create LHZ map as stated by Wiecezorek [119]. Hazard assessment is carried out directly in the field by the experts of earth sciences based on their experience. Suzen [57] stated that this method requires identification of mass movements and assessment of the geomorphologic conditions for constructing LHZ map. The method also employs interpretation of aerial photo or high resolution satellite images. Another required data may come from database of historical landslide occurrences.

The advantage of this method is that the hazard map can be constructed directly after obtaining the required spatial data. The assessment of the stability at a particular area can be carried out quickly by involving a large number of causative factors. In Addition, this method can be applied to all scale as suggested by Aleotti and Chowdhury [116] and Suzen [57]. However, this method has disadvantages as reported by Aleotti and Chowdhury [116] as follow:

1. The spatial data selection to construct landslide hazard map and the rules that control slope stability are relied on the subjectivity of the investigators or experts. Hence, comparison between hazard maps produced by different

investigators is difficult to do due to the difference subjectivities of the investigators.

2. Subjectivity of the method. It means that there is no explicit rule so that critical analysis of the result is difficult to do. Another problem in assessment of the result may arise when new data become available.
3. This method is laborious because it requires lengthy field surveys.

Examples of mapping landslide hazard zones using geomorphology field analysis are mostly found in literatures of the 70s and 80s. Some recent investigations using this method can be found in Mantovani, et al. [120] who conducted geomorphologic survey at Olvera area, Spain; Hiramatsu, et al. [121] who carried out geomorphologic analysis using LiDAR (Light Detection And Ranging), Hearn [122] who worked on geomorphologic mapping of Ok Tedi copper mine, Papua New Guinea, and other investigations carried out by Canuti, et al. [123], Lee and Talib [55], and Mantovani, et al. [124]. The final product is a map showing spatial distribution of mass movement either shown as coverage (areas) or point symbols.

Suzen [57] stated that in most LHA methods, landslide distribution or inventory map is used as a base landslide map. By using this map, the relation between landslide and causative factors can be extracted. This relationship would provide useful information for applying statistical methods.

#### *2.4.1.2 Overlay or Combination of Index Maps or Parameter Maps*

To construct a landslide hazard map using this method, a set of landslide causative factors is selected by an expert based on his/her experiences. Each factor has classes. The expert assigns an appropriate weighted value to each factor; a value that is proportional to its relative contribution to cause slope stability. According to Soeters and van Westen [125], this method requires the following procedures to complete:

1. Division of each causative factor into a number of relevant classes.
2. Assignment of a weighted value to each class.
3. Assignment of a weighted value to each causative factor.

4. Overlay of the weighted thematic maps/causative factors.
5. Production of the landslide hazard map representing level of hazard.

Reviewed by Aleotti and Chowdhury [116], this method has advantages that the role in determining hazard level is explicit even though it still contains the subjectivity from the expert opinion in assigning weighted values. This method also enables automation using GIS and standardization of data management from data collection to analysis. In addition, it can be applied to various scales. However, this method is time consuming when applied for a large area. Another drawback of this method is that the subjectivity of the expert still exists in term of attributing weighted value for each causative factors and classes. Extrapolating a model built in a certain area to other areas faces difficulties.

Some examples of application of this method can be found in Anbalagan [2], Anbalagan and Singh [126], Abu-Zeid, et al. [127], Turrini and Visintainer [128], and Ramli, et al. [93]. The problem related to defining numerical weighted values has been overcome by Anbalagan [2] by introducing the first rating system called Landslide Hazard Evaluation Factor (LHEF) to evaluate the relative significance of each causative factor. Anbalagan [2] also developed a role to evaluate relative importance between classes /sub categories of a causative factor. To apply LHEF rating scheme, Liao [47] suggested the following procedures: 1) evaluating the relative importance between causative factors based on their influence to slope instability in the area of study; 2) evaluating the relative importance between classes of a particular causative factor according to their significance in contributing slope failure; 3) constructing a thematic for each causative factor showing weight values for pixels; 4) summing up all thematic map to produce the final LHZ map.

LHEF rating scheme was first applied to study landslide hazard in the mountainous terrain of Himalaya by Anbalagan [2]. The main causative factors included in this scheme were lithology, structure, slope gradient, relief, land use land cover, and ground water condition. The selection of these factors was based on field observation at the study area. Table 2.2 shows the maximum ratings/weight values of each factor. The rating was determined using empirical approach based on the author experience obtained from the field study about the relation between landslide

causative factors and their influence on landslide occurrences. The maximum LHEF value for lithology, structural discontinuities, slope gradient, land use land cover was set to 2.0 while the remaining factors were set to 1.0.

Table 2.2 LHEF rating for causative factors

Causative Factor	Maximum LHEF
Lithology	2.0
Structural discontinuities	2.0
Slope gradient	2.0
Relative relief	1.0
Land use and land cover	2.0
Ground water conditions	1.0

Source: Anbalagan [2]

For awarding weight values for causative factor classes, Anbalagan [2] applied an experience based subjective assignment. For example, land use land cover was subdivided into five classes: agriculture, thick forest, moderate forest, sparse forest, and barren land. Barren land was considered as the most unstable land cover and given a weight value of 2.0. Thickly vegetated forest areas were considered as the most stable areas and assigned a weight value of 0.8. The remaining classes were given weight values in this way, based on the experience of the investigator. The rating values of all causative factors along with their correspondence classes are presented in Table 2.3

The final landslide hazard map indicated the total estimated hazard (TEHD) which was the total summation of the weight values of all factors, i.e. lithology, structure, slope gradient, relief, land use land cover, and ground water condition. TEHD expressed the net probability of slope instability. Based on TEHD values, the final hazard zones map was presented in five categories namely very low hazard ( $TEHD < 3.5$ ), low hazard (3.5-5.0), moderate hazard (5.1-6.0), high hazard (6.1-7.5), and very high hazard ( $> 7.5$ ). The maximum of TEHD value may change as the number of factors involved in constructing final hazard map increases or decreases.

Table 2.3 LHEF Rating System

Factor	Subcategories/Classes	Rating
Lithology: rock type	Quartzite and limestone	0.2
	Granite and gabbro	0.3
	Gneiss	0.4
	Well-cemented terrigenous rocks	1
	Poorly-cemented terrigenous rocks	1.3
	Slate and phyllite	1.2
	Schist	1.3
	Shale with interbedded clayey rocks	1.8
	Highly weathered shale	2
Lithology: soil	Old well compacted fluvial fill material	0.8
	Clayey soil	1
	Sandy soil	1.4
	Debris	1.2
	Old well compacted young loose material	2
Structure: depth of soil cover	< 5 m	0.65
	6-10 m	0.85
	11-15 m	1.3
	16-20 m	2
	>20 m	1.2
Slope gradient	>45	2
	36-45	1.7
	26-35	1.2
	16-25	0.8
	<15	0.5
Relative relief	<100m	0.3
	101-300m	0.6
	>300	1
Land use land cover	Agriculture	0.65
	Thickly vegetated forest area	0.8
	Moderately vegetated forest area	1.2
	Sparsely vegetated forest area	1.5
	Barren land	2
Water conditions	Flowing	1
	Dropping	0.8
	Wet	0.5
	Damp	0.2
	Dry	0

Source: Anbalagan [2]

#### **2.4.2. Quantitative Methods**

Quantitative methods consist of statistical analysis, geotechnical engineering approach, and neural network analysis. Quantitative approaches are more rigorous than qualitative methods. These approaches offer objectivity in methodology so that the problem of hidden rule is reduced, total automation of steps for constructing landslide hazard map and standardization of data management. However, Aleotti and Chowdhury [116] highlighted the main drawbacks of the methods namely the difficulties in systematic data collection and impracticality in analysis of a large number of causative factors.

In the following, several methods such as landslide susceptibility analysis and information value method (both are of bivariate statistical analysis methods), and multiple regression method which is one of multivariate statistical methods, are explained. Detail explanation of the remaining methods such weight of evidence (another bivariate statistical analysis method), discriminant analysis (another multivariate statistical method), geotechnical engineering approaches such as deterministic analysis/safety factor, and neural network can be found in the literature such as Chuanhua and Xueping [129], Dahal, et al. [110], Glade [130] for weight of evidence method; Carrara [131], Agostoni, et al. [28], Komac [45], Dong, et al. [132], Ohlmacher and Davis [133] and Pradhan [134] for multivariate statistical methods; Jelínek and Wagner [135] and Terlien, et al. [136] for deterministic analysis which is of geotechnical engineering approaches; Gómez and Kavzoglu [80], Yilmaz [137], and Pradhan and Lee [138] for neural network application for LHZ.

As part of quantitative methods, statistical methods offer objectivity of the results and a better reproducibility of the hazard zonation. Statistical methods consist of bivariate and multivariate approaches. Using these methods, the relation between the causative factors and landslide occurrences in the past is determined. Analysis is usually based on the relationship between landslide densities per a particular class and landslide densities over the study area. Having found any relationship between both data, a quantitative prediction can be made for areas free of landslides but have the same conditions as suggested by Aleotti and Chowdhury [116]. To find any



relationship between landslide occurrences in the past and respective causative factors, Van Westen [139] and Suzen [57] suggested the following procedures:

1. Classification of each causative factor map into a number of relevant classes
2. Crossing causative factor maps with landslide map
3. Derivation of weight values based on crossing result
4. Assignment of weight values for involved causative factor maps together with their classes.

The final landslide hazard is constructed by summing up the weight values of causative factor classes. Overlay of thematic maps of causative factors and calculation of landslide densities are the core of statistical methods. Application of GIS for this method will be helpful especially when dealing with a medium scale hazard analysis and a large amount of spatial data.

#### *2.4.2.1 Bivariate statistical method*

There are many methods of bivariate statistical analysis for calculating weight values such as landslide susceptibility analysis, information value method, and weight of evidence modeling method. Landslide susceptibility analysis was selected for the current research work.

Suzen [57] explained that bivariate statistical method deals with one dependent variable that is landslide occurrence, and one independent variable, for examples, slope, elevation, and land use land cover. Each causative factor map is combined or crossed with the landslide distribution map. Weight values for each factor are computed on the basis of landslide densities. The final landslide hazard map is produced by combining all weighted maps into a single map. The remaining step is works of map validation. These procedures are schematically shown in Fig. 2.3.

Süzen and Doyuran [115] described that landslide susceptibility analysis is considered as a simple and useful statistical analysis method to determine the relationship between different variables (causative factor classes) and landslide occurrences by means of pair wise map crossing. Crossing between a landslide map

and individual causative factor map will result in a measure of the importance of individual factor class. There are two type of densities resulted from the crossing procedure namely area density and number density. The first is commonly known as Landslide Susceptibility Index (LSI) while the latter is known as Landslide Frequency Index (LFI) as explained Liao [47].

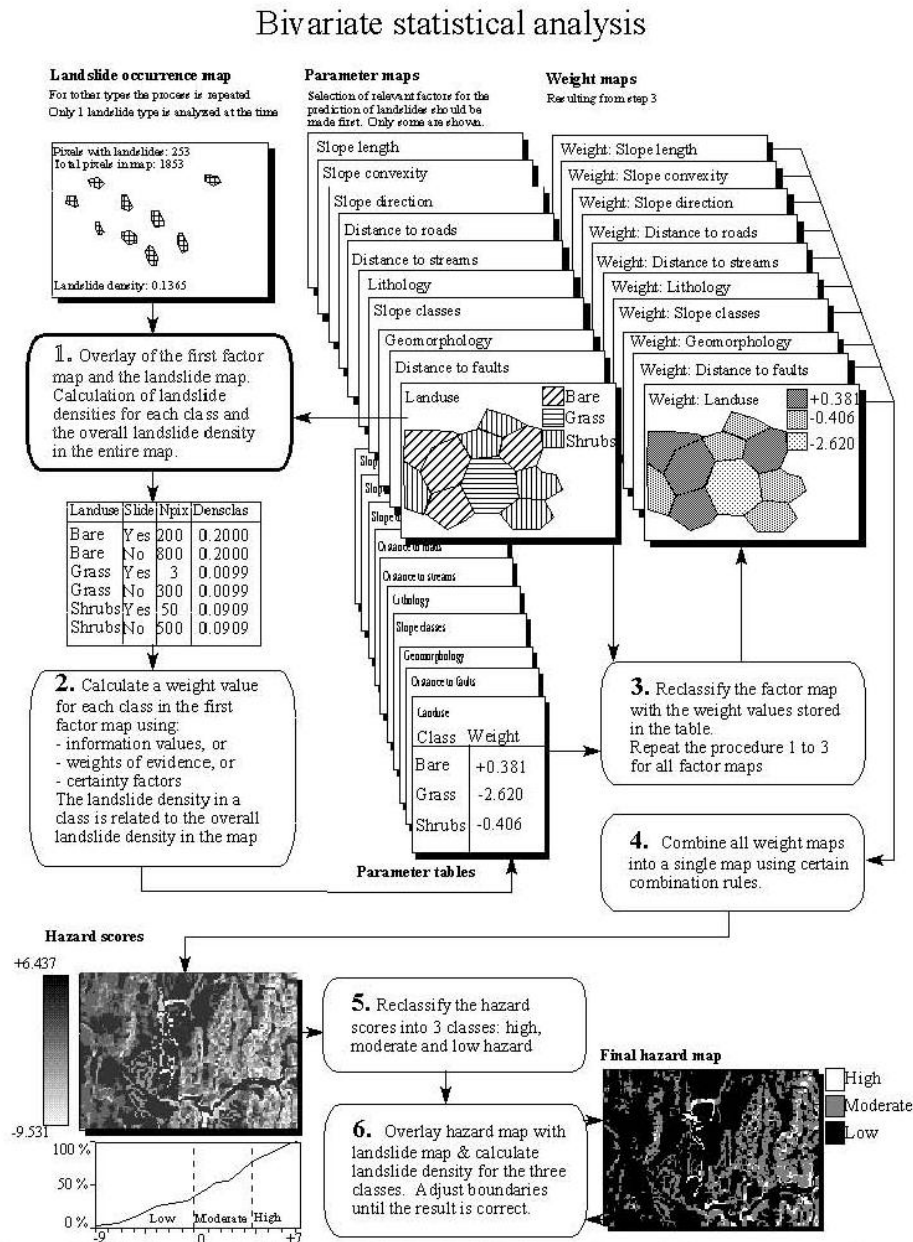


Fig. 2.3 Schematic overview of bivariate statistical analysis

Source: Van Westen [111]

1. Area density ( $D_{area}$ ). This density is obtained by dividing the number of pixels with landslides within factor class  $X_i$ , that is  $Npix(SX_i)$ , and the total number of pixels within factor class  $X_i$ , that is  $Npix(X_i)$ . This density is expressed as follows:

$$D_{area} = 1000 \frac{Npix(SX_i)}{Npix(X_i)} \quad (2.4)$$

2. Number density ( $D_{area}$ ). This density represents the number of landslide occurrences ( $Number(SX_i)$ ) per area ( $Area(X_i)$ ). The unit of area is usually in square kilometer. This density is expressed as follows:

$$D_{number} = \frac{1 * 10^6}{Area(X_i)} Number(SX_i) \quad (2.5)$$

Based on density values, weighting values can be derived for use of evaluation the influence of factor classes. Liao [47] demonstrated the derivation of weighting system based on the first density values by assigning a maximum value of 100 for a factor class with a maximum density value. The remaining classes are awarded weight values proportional to their influences within a causative factor. This method has been applied by researchers such as Van Westen [140], Liao [47], Süzen and Doyuran [115], Long [141], and Vergari, et al. [142].

Information value is another bivariate statistical method. This method is introduced to overcome the problem in combination of a causative factor with numerical value (such as elevation values) and alphanumeric values (such as soil types) by means of treating each causative factor class as a new map showing two conditions: present of landslide (1) or absence of landslide (0). This method can be applied for either land units or pixel basis. Yin and Yan [143] formulated information value method as shown in Equation 2.9. The information value  $I_i$  of variable  $i$  is:

$$I_i = \log \frac{S_i/N_i}{S/N} \quad (2.6)$$

In Equation 2.6,  $N$  represents the total number of data points (grid cells);  $S$  represents the total number of grid cells;  $S_i$  represents the number of grid cells involving the

parameter and containing landslide;  $N_i$  represents the number of grid cells involving the parameter.

The total information value of grid  $j$  is shown as Equation 2.7.  $M$  denotes the number of parameter involved.  $X_{ij}$  is the value of parameter.  $X_{ij} = 1$  if parameter  $i$  exists in grid cell  $j$  and  $X_{ij} = 0$  if parameter  $i$  is absence in grid cell  $j$ . The total of information value determines the hazard level of a particular grid cell. The higher the information value the higher the degree of landslide susceptibility. This method has been used by investigators such as Saha, et al. [3], Ayalew, et al. [144], Gao, et al. [145], and Caiyan, et al. [70].

$$I_j = \sum_{i=0}^M X_{ij} I_i \quad (2.7)$$

Although bivariate statistical analysis is considered as quantitative method widely used for assessing landslide hazard, this method still contains a certain degree of subjectivity. This subjectivity exists during classification of a causative factor map into a number of relevant and division of the final hazard map into hazard. These two problems limit bivariate statistical analysis as summarized by Suzen [57] and Aleotti and Chowdhury [116].

#### 2.4.2.2 Multivariate statistical methods

Multivariate statistical analysis was first applied in geology works petroleum exploration. Detail application of this method in LHA was began by Carrara [131]. This method utilizes training areas to get the relationship between causative factors and landslide occurrences. Should the relationships achieved and verified, they are extended to the entire of the study area. Aleotti and Chowdhury [116] recommended the following works on training areas:

1. Division of the study area into land units.
2. Selection of significant causative factors and preparation of input maps in form of numerical maps.
3. Preparation of landslide map.

4. Overlay of land unit map and landslide map in order to evaluate the percentage of landslide affected areas in every land unit and divide it unstable and stable units.
5. Overlay of the causative factor maps with the land unit map and building creation absence/presence matrix of a given class of a given class of a given parameter within each land unit.
6. Multivariate analysis carried out using either multiple regression or discriminant analysis.
7. Classification of the map into susceptibility classes referring to reclassified land units based on the results achieved in the previous phase.

Multiple regression is considered as the most well-known multivariate statistical method used in earth science. It examines the relationship between a dependent variable that is landslide occurrence map (denoted as  $Y_i$ ), and independent variables that are parameter maps, such slope classes and geology types (denoted as  $X_i$ ) using the following equation:

$$Y = b_0 + b_1X_1 + b_2X_2 + .....b_nX_n \quad (2.8)$$

The dependent variable  $Y$  represents the presence (1) or the absence (0) of a landslide of land units.  $X_1$ - $X_n$  are the independent variables. The notation of  $b_0$ - $b_n$  is the partial regression coefficient which can be estimated using least square adjustment method.

The methodology of bivariate and multivariate statistical analysis is typically data driven. Therefore, it offers high objectivity in developed LHZ map. However, the methods still contain some drawbacks as identified by Van Westen [111]. In general, the general problem is the collection data over a large area regarding landslide distribution and landslide causative factor maps. Data gathering could be costly. A difficulty may arise when applying multivariate statistical analysis due to the presence of extremely voluminous matrices required for solving the regression equation, especially when dealing with small size of grid cells. Another problem could also arise as the grid cells size increases. Meanwhile, Suzen [57] added that there is a little subjectivity in bivariate statistical method in the number of classes required for division of causative factor maps and the final hazard maps.

### 2.4.3. Production of Final Landslide Susceptibility Map

In this section, the term ‘susceptibility’ is re-used rather than ‘hazard’ for the final product map because the methods previously discussed for constructing landslide hazard map do not deal ‘when’ landslides might occur, otherwise the methods only discuss ‘where’ landslides might occur. This matter has been discussed in section 2.1.

As stated by Liao [47], Suzen [57], and most of relevant literature, the final landslide susceptibility map (LSM) was produced by summing up the pixel based weight values in GIS environment. Hence, the landslide susceptibility (LS) of grid cell  $j$ , expressed in Equation 2.9, is obtained by summing up weight values ( $W$ ) of causative factor  $i$  to  $M$  ( $M$  denotes the number of involved factors).

$$LS_j = \sum_{i=1}^M W_i \quad (2.9)$$

Another problem arises when deciding the optimal combination and number of causative factors should be involved in construction of the final map. Suzen [57] suggested two options to solve this problem. The first is selection of causative factor maps on the basis of field experience. The second is using stepwise map combination by adding causative factor maps one by one. The resulted susceptibility map is then crossed with the landslide map and checked its accuracy. If the accuracy of the map increases after addition a particular causative factor, such a factor can be included in constructing the final map and vice versa. This method is also recommended by Van Westen [140].

## 2.5 Landslide Events in Malaysia and Cameron Highlands

Landslide together with flood and windstorm are of major natural disaster threats in Malaysia as reported by Sapir, et al. [146] and ADRC [147]. Chan [148] reported that most of landslide events were triggered by heavy rainfall. This relationship can be understood since this country, due to its geographical position, experiences two maritime monsoons namely Northeast and Southwest monsoons. The first monsoon that falls between November and January brings heavier rainfall than the second one

that falls between April and May. In between these two monsoons, there are two inter-monsoon periods that occur for duration of 2-3 months and are characterized by having the highest temperature and driest days. However, during these periods, heavy rainfall with high intensity happens in the northern parts of West Malaysia between June and October as reported by Guha [149]. Thus, the rainfall cycle is somewhat anomalous. In the northern part of Peninsular Malaysia (PM), the average annual rainfall is 3,000 mm/yr which is larger than the average annual rainfall of entire PM with rainfall amount of 2,420 mm/yr.

The relation of landslide events, summarized from JKR [13] database, and monsoonal rainfall of several cities in PM is already shown in Fig. 1.1 of chapter 1. From the figure, it can be concluded that these monsoonal rainfall systems can be considered as the landslide triggering factor in PM. The number of landslide events increases as the rainfall reaches its peak time that coincides with the period of two monsoon systems. October to January and April to June are the months when the frequency of landslide occurrences is high.

The areas that experience landslide events are shown circled in Fig. 2.4. According to landslide records of JKR [13], the most landslide-prone areas is Kuala Lumpur followed by Selangor, Perak, and Pahang. About 55% of the total number landslide events in Malaysia took place at hilly areas such as Fraser's Hill, Cameron Highlands, Genting Highlands (all is in Pahang), Gunung Raya (Langkawi), Paya Terubung (Penang), the mountain ranges in Hulu Kelang (Selangor), and several limestone hills in Ipoh. Among the biggest landslide event is landslide event at Pos Dipang that killed 44 people in 29 August 1996. The most recent landslide occurred at Bukit Antarbangsa, Kuala Lumpur, on 6 December 2008 that killed 4 people, destroyed 14 houses and cut off the access road to the residential area. The total economical loss caused by landslide in Malaysia from 1973 until 2007 was estimated about RM3.0 billion.

Cameron Highlands is a landslide prone area. According to JKR [13], there were 37 costly landslide events in Cameron Highlands from 1961-2007. About 56% of the occurrences were road-related landslides. The remaining was non-road-related landslides (Fig. 2.5a). The first national landslide tragedy in Cameron Highlands

occurred on 11 May 1961 causing 16 people dead. Tapah, Ringlet, Tringkap, *Jalan Belading Tengkak*, Tanah Rata, and Kampung Raja were among places prone to landslides. Besides causing loss of lives, landslides delayed delivery of vegetables and flowers, and cut off links between places.

Site investigation carried out in 2006 and 2008 showed that minor landslides were easy to find along the main road of the study area, more particularly at cut slopes (Fig. 2.5a). Very few landslides occurred at natural slopes. Since 1961 to 2007, the total economic costs due to landslide threat in Cameron Highlands is about RM454 million according to JKR [13] record. There was a big landslide occurred at Km22, Km23.8, and Km24 of the highway connecting Pos Selim, Perak, and Kampung Raja, Cameron Highlands, Pahang (Fig. 2.5b). The road constructed in 1997 was expected to open for public in 2000. Due to the massive landslide occurring in 1999, the opening of the third East-West highway was postponed. There was no loss of lives regarding this landslide. However, the total economic costs for five times maintenance and recovery reached RM466.5 million.

Rainfall also plays important role in triggering landslides in Cameron Highlands. The behavior of landslide occurrences and rainfall intensity variation is shown in Fig. 1.3 of Chapter 1. According to this graph, the number of landslides during rainy seasons is higher than that of dry seasons. On July and August, there are no landslide occurrences. Rainfall of this season might not be significant enough to initiate landslide events.

The natural threat due to monsoonal rainfall system is made worst by anthropogenic activities such as deforestation for farming and expansion of urban areas, settlement and road networks. Cameron Highlands is among regions with a high dynamic economy development such as in producing vegetables and flowers for domestic and overseas market and being a popular tourist destination. The impact of economic development demands the opening of new roads and expansion of farming areas into hill slopes. Both activities mean modification of slopes stability so that in turn they may cause the slopes vulnerable to landslide.





Fig. 2.4 Landslide events distribution in PM from JKR [13] database (1961-2007)



Source: MTD Sdn. Bhd.



Fig. 2.5 Landslides a) along Kampung Raja-Ringlet road, b) at Pos Selim

The abundance of gardening and farming activities in CH has increased soil loss rate. Fortuin [150] reported that the extensive deforestation and indiscriminate land opening for agricultural and housing have increased soil erosion rate over the land surface. Aminuddin, et al. [151] reported that soil loss rate in CH is high due to such activities. The rate was about 24-42 ton/ha/yr under vegetables and 1.3 ton under rain-shelter (plastic-roofed farming). With a high erosion rate, this area becomes prone to landslide.

In relation to human activity, land use changes have been a crucial issue in this area. TNBHidro-Sdn.Bhd. [152] reported on the investigation of land use changes of two catchment areas namely Bertam and Telom. Table 2.4 shows land use/cover changes of both catchment areas from 1950 to 1990. In Bertam catchment, the areas for open land, vegetable/fruit farming expanded significantly from 5.8 to 10.2 km<sup>2</sup>. On the other hand, forest and tea/orchard areas decreased quit significant. In Telom catchment, the forest area decreased significantly from 90.3 to 74.1 km<sup>2</sup>. On the contrary, coverage of vegetable/flower farming expanded enormously. The urban area seemed to slightly expand while tea/orchards areas tended to be constant. In addition, Yusof, et al. [153] reported that more than 19,000 hectares of forest reserve in Cameron Highlands has been proposed for agricultural development and new roads. Such human activities are potential to increase landslide threats on Cameron Highlands and its surroundings.

Table 2.4 Land use changes in Bertam and Telom Catchment

Vegetation/ Land Use	Bertam Catchment [km <sup>2</sup> ]			Telom Catchment [km <sup>2</sup> ]		
	1950's	1980's	1990's	1950's	1980's	1990's
Forest	46.5	45.1	43.5	99.1	90.3	74.1
Tea/Orchards	15.2	10.4	6.6	6.3	6.2	6.2
Vegetable/Flower	5.1	7.0	8.1	5.0	10.7	23.2
Urban	-	4.1	4.2	-	0.5	1.1
Open/Grassland/ Scrub Forest	5.8	6.0	10.2	-	2.7	5.8

Source: TNBHidro-Sdn.Bhd. [152]

## **2.6 The Efforts on Reducing Landslides Hazards**

Knowing that there are many landslide influencing factors, efforts are required to reduce the consequences of landslides such as by locating and predicting hazard zones. Such efforts required mapping zones potential to landslides.

### **2.6.1 Efforts by the Government and Individuals**

Providing LHZ maps have been one of the priorities of Malaysia government in response to this natural disaster threat. The government, through Slope branch of Public Work Department, has launched ten programs of National Slope Master Plan (NSMP) which one of them is providing LHZ maps. Besides the government, individual/non-governmental researchers also showed their awareness in regard to this matter such as Talib [8], Omar, et al. [9], Pradhan and Lee [12], Ramli, et al. [93], Lee and Pradhan [7], and Matori, et al. [154]. The areas commonly used as study areas are Cameron Highlands, Selangor, and Penang Island.

### **2.6.2 Previous Works of LHA in Cameron Highlands**

There were efforts in reducing landslide consequences in Cameron Highlands initiated by various investigators. The efforts discussed in this research are by provision of LHZ maps constructed using different methods or approaches. Existing works on LHA for Cameron Highlands can be divided into three methods namely qualitative, quantitative, and Artificial Intelligent (AI) methods. The qualitative method that uses combination of index maps were applied by Omar, et al. [9], Ramli, et al. [93]. Meanwhile Talib [8] and Lee and Pradhan [10] used the quantitative method that relies on direct comparison between landslide contributing factors and landslide distribution. The AI method which uses a set of reasonably well defined roles to enable the implementation of knowledge-based system in form of artificial neural network has been used by Pradhan, et al. [155] and Pradhan and Lee [12]. The reviews of these works are explained in the following sections.

### *2.6.2.1 LHA in Cameron Highlands using Qualitative Methods*

Omar, et al. [9] applied a qualitative method for constructing LHZ map for Pos Selim to Cameron Highlands areas using GIS and remote sensing data. The study utilized factor maps, i.e. land use land cover (derived from Landsat TM5 image), slope gradient, slope aspect, and height/elevation. The last three maps were derived from DEM (Digital Elevation Model) of topographic map with a scale of 1:50,000. Multi temporal factors were not included in this work. All factors were assigned weight values before proceeding to GIS overlay process for constructing a LHZ map. The authors adopted the weight values from the works of others outside Malaysia rather than extracting from their own study area. For example, Equation 2.3, the probability of high risk model developed by Gao and Lao [81], was used to produce a height risk map. The authors used expert opinion from DeGraff and Romesburg [62] for producing a slope aspect risk map and made their own assumptions for creating a slope risk map. The final LHS showed three level of landslide risk: low risk, medium risk and high risk. About 6.21% of the area was categorized as high risk area while 83.93 % was low risk area. The accuracy of the developed LHZ map has not been known so far because this work did not include process of map validation.

Another investigation on LHZ that used a qualitative method, LHEF rating system, was carried out by Ramli, et al. [93]. The authors utilized GRASS (Geographical Resources Analysis Support System) which is open source GIS software for assessment of LHZ in Tanah Rata, part of Cameron Highlands district. This investigation involved five landslide contributing factors namely lithology, slope angle, structure (lineament), relative relieve, hydrological conditions (water features), and land use land cover. Anbalagan [2] LHEF rating system was modified to suit with the available factors and respective classes. The final LHZ map was divided into five categories namely very low hazard, low hazard, moderate hazard, high hazard, and very high hazard. About 93 percent of the study area fell under low hazard category. Meanwhile, about 15 percent and 0.2 percent of the study area were categorized as moderate hazard and high hazard respectively. None of the area was categorized as very high hazard area. Some notes regarding this work are that expert opinion in form of LHEF rating system was used showing a typical of a qualitative method; secondly,

this work did not take into account the temporal factors; and lastly, this work did not apply map validation, the stage which is important for measuring the accuracy of the developed LHZ map.

#### *2.6.2.2 LHA in Cameron Highlands using Quantitative Methods*

Gahgah, et al. [43] applied another qualitative method which is a combination of heuristic method that is, using expert opinion of Van Westen [111], and index overlay as GIS analysis method for investigation of landslide hazard in Cameron Highlands – Gua Musang road. The final landslide showed five categories of hazard namely very low hazard, low, moderate, high, and very high hazard. Slope and elevations were found to be the most affecting factors for landslide occurrence. This work has the same shortcomings as the previously mentioned work.

Talib [8] applied a bivariate statistical analysis method that is Information Value Method for investigation of slope instability and hazard zonation in Cameron Highlands. The study involved digital elevation data from topographic map, geology map, land use land cover map, distance to fault, drainage, and road map. Weight values were derived from pixel-based pair wise comparison between landslide map and factor maps. The final LHZ map divided the area into three categories: low, medium and high hazard. The author highlighted several places prone to landslide such as, sloping areas at the road and a gardening area in Bertam, Ringlet; some areas near the edge of urban areas in Tanah Rata where settlements were built on sloping hills; road slopes at Berinchang (north of Tanah Rata), Ringlet (near the main lake of CH), and slopes parallel to the Bharat the plantation. All these works have offered the objectivity of defining the relationship between landslide occurrences and causative factors which is implemented in defining a weighting system. However, temporal environmental factors have not been involved in the modeling LHZ and the verification test of the LHZ map was not mentioned in this work.

Back-propagation neural network model has been used to study landslide susceptibility in Cameron Highlands by Pradhan and Lee [12]. Ten landslide contributing factors were involved in this study namely, slope, slope aspect,

topographic curvature, lithology, soil type, rainfall, vegetation index (derived from SPOT 5 satellite image), distance from drainage and lineament. Using an advanced neural network model for analyzing all factors, landslide susceptibility map was produced. This investigation found that the topographic slope has been the most influencing landslide factor followed by the distance to drainage, and lithology. This was indicated by their weight values resulted from back-propagation training method in succession 0.205, 0.141 and 0.117. The final landslide susceptibility map showed a good agreement, 83% accuracy, with landslide data after validation process. This work focused on the introduction of another quantitative method proven to be more satisfactory than the previous method in terms of the accuracy of prediction of susceptible areas. The subjectivity of the expert was removed as this method is considered as data-driven modeling. This work did not take into account the temporal environmental factors.

## **2.7 Remote Sensing and Its Roles in Landslide Hazard Assessment**

Remote sensing has been widely used for landslide hazard assessment. This is because remote sensing offers measurement of objects in landslide areas with no contact while, in fact, the location of landslides is not safe to take measurements. Concept of remote sensing and its associated aspects, applications, and roles in landslide hazard assessment is explained in the following.

### **2.7.1 Remote Sensing: The Concepts**

There are various definitions of remote sensing. A definition given by Lillesand and Kiefer [156] states that remote sensing is the science and art of obtaining information about an object, area, or phenomenon through the analysis of data acquired by a device that is not in contact with the object, area, or phenomenon under investigation. The captured object is usually stored as image data. Early remote sensing technology utilized aerial photographs operating within visible range of the electromagnetic spectrum. For particular purposes, satellite images are used rather than aerial photographs because remote sensing satellites record data using scanners, allowing

the data acquisition at wavelengths longer than visible range such as thermal infrared and microwave spectrum.

Gibson and Power [94] explained that remote sensing systems can be either passive or active. Passive system is known as optical remote sensing while active system is known as microwave remote sensing. Optical remote sensing records electromagnetic radiation reflected or emitted by objects on the surface. Microwave remote sensing transmits electromagnetic radiation of a specific wave length to the surfaces and records the energy reflected or scattered back from the surface. Examples of remote sensing platforms that use passive/optical system are Landsat and SPOT while active platforms are RADARSAT and ERS (European Remote Sensing Satellite).

In this research, the satellite images used are from optical remote sensing. Hence, further description about basic principle of measurement, image processing procedures, and transformation remote sensing data into other data such as NDVI, soil wetness, and LST, is associated with optical remote sensing.

### **2.7.2 Spectral Signatures and Multi Spectral Sensors**

Different features of the landscape such as bush, crop, forest, and water reflect sun energy in different wavelength. The spectral signature of these objects is shown in Fig. 2.6. Green grass appears to be significant in green band of visible spectrum. Within near infrared (NIR) spectrum, green grass shows strong reflectance. This strong reflectance in NIR spectrum is beyond the detection ability of human eye. Dry grass experiences the same thing as green grass. However, dry grass and soil is difficult to distinguish in green band of visible spectrum. Gibson and Power [94] added that plant species are often easy to differentiate in NIR spectrum due to their high reflectances rather than in visible spectrum. It is also difficult to differentiate soil types in visible spectrum because of their very low reflectances in visible. On the contrary soil types can be differentiated based on moisture content in infra red spectrum. Thermal radiation emitted by objects on the earth can be easily detected in infrared spectrum rather than in visible spectrum as explained by Liew [157].

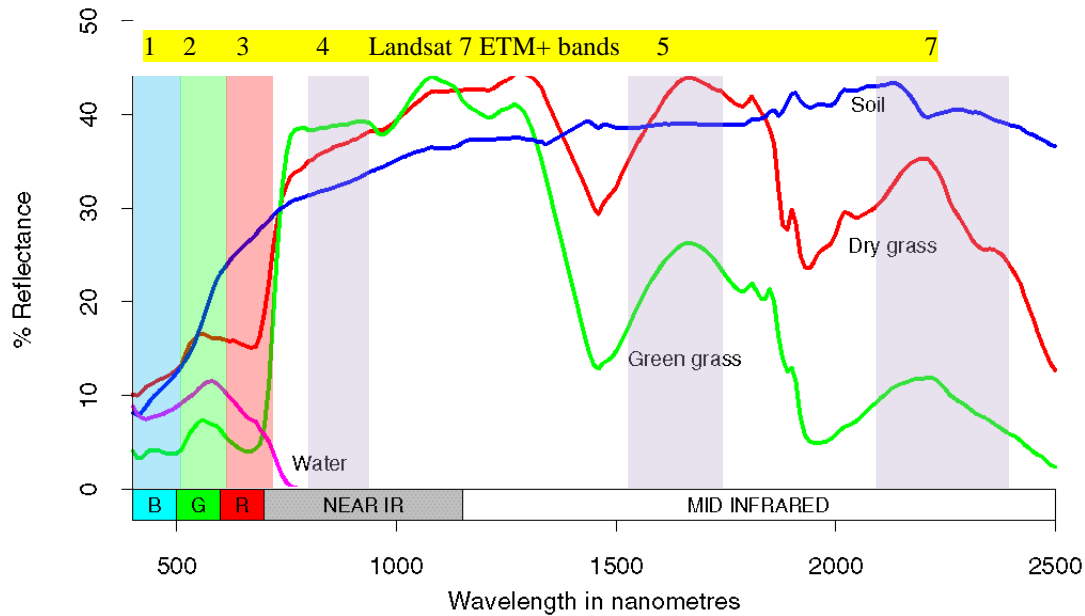


Fig. 2.6 Spectral signatures of different objects and Landsat ETM+ bands

Source: CSIRO [158]

In order to detect objects on earth, most of passive remote sensing satellites are equipped with, at least, sensors working on visible and infrared spectrum as explained by Gibson and Power [94]. A multispectral scanner satellite is an earth observing system (EOS) satellite that brings array of optical sensors the task to acquire information of the same objects on earth at different wavelengths, called ‘bands’. Each band captures a unique spectral signature of the object. Landsat 7 ETM+ and SPOT 5 are example of satellites with multispectral scanner system. The first satellite can detect object using 8 bands (blue, green, red, NIR, 2 mid-infrared/short wavelength infrared, thermal infrared, and panchromatic) while the second can detect 4 bands (green, red, NIR, mid-infrared). Illustration of the position of Landsat 7 bands in electromagnetic spectrum is given in Figure 2.5. Further explanation of two satellite missions currently used in this study is given in the following.

### 2.7.3 Landsat 7 ETM+ Satellite Mission

Landsat 7 ETM+ is part of Landsat program intended to gather information on natural resources of the earth and was launched on April 15, 1999. The program was first



started by The National Aeronautics and Space Administration (NASA) in 1972 and then turned over to the National Oceanic and Atmospheric Administration (NOAA). The distribution of Landsat 'public domain' data is managed by the Earth Resource Observation System (EROS) Data Center of United State Geological Survey (USGS) in Sioux Falls, South Dakota. The program began with the launch of Landsat 1 (1972) followed by Landsat 2 (1975), Landsat 3 (1978), Landsat 4 (1982), Landsat 5 (1984), Landsat 6 (1999), and Landsat 7 (1999). There are only Landsat 5 and 7 that are operational. The typical orbit of Landsat 7 is sun-synchronous, with altitude of 705 km, inclination of 98.2 degree, period of 99 minute, and repeat cycle of 16 days.

The term ETM+ refers to onboard instrument consisting of eight bands of multispectral scanning sensors that able to provide high-resolution image of captured objects of the earth. The instrument features a panchromatic band with 15 m spatial resolution, a thermal Infra Red with 60 m spatial resolution and onboard radiometric calibration. Detail description of all Landsat 7 ETM+ bands along with their application is summarized in Table 2.5 and mostly taken from two Landsat Project websites maintained by Irons [159] and Short [160]. The schematic of the satellite is shown in Fig. 2.7.

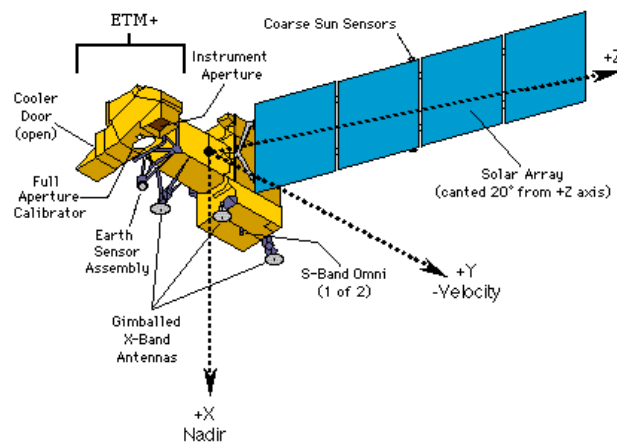


Fig. 2.7 Schematic of Landsat 7 ETM+ satellite

Source: Irons [159] and Geocommunity [161]

Table 2.5 Characteristics of Landsat 7 ETM+ bands

<b>Spectral Bands (<math>\mu\text{m}</math>)</b>	<b>Resolution (m)</b>	<b>Applications</b>
1 0.45–0.52 Visible blue-green	30	Mapping water depth, differentiate soil from vegetation, mapping forest types (deciduous/coniferous)
2 0.52–0.60 Visible green	30	Identify vegetation reflectance peak for discriminating vegetation and assessing plant vigor
3 0.63–0.69 Visible red	30	Absorbs chlorophyll band, suitable from identification of roads, barren land, and types of vegetation
4 0.76–0.90 Near infrared (NIR)	30	Estimates biomass content, separates water bodies from vegetation, detection of shorelines, and discriminates soil moisture
5 1.55–1.75 Mid infrared	30	Discriminates moisture content of soil and vegetation, identifies roads, penetrates thin clouds
6 10.4–12.5 Thermal infrared Low/high gain	120	Maps thermal (heat) emitted by the target and estimates soil moisture, measure vegetation stress, available in two mode: high gain band (6a) and low gain band (6b)
7 2.08–2.35 Mid infrared	30	Useful for mapping rock types and associated mineral deposit based on soil moisture content, useful for interpreting vegetation cover
8 0.52 – 0.9 Panchromatic	15	Black and white images which is useful for enhancing image resolution and image interpretation

Source: NASA [162] and Geoscience-Australia [163]

Landsat data is available at various levels as reported by NASA [162]. The level 1R data product means that Landsat data has been radiometrically corrected. The level 1G data product currently used in this research is Landsat data that has been radiometrically and geometrically corrected. This product is distributed to user in form of grey scale image represented by Digital Numbers (DN's) scaled from 1-255.

Band 6, thermal infra red, of Landsat 7 ETM+ image comes in two modes namely low gain and high gain antenna. Low gain antenna is activated when the average brightness of ground surface is high. Otherwise, high gain antenna mode is 'on' when

the surface brightness is low. This condition means that the antenna is highly focused to the object measured.

#### **2.7.4 SPOT 5 Satellite Mission**

Detail description of SPOT satellite mission can be found in SPOT Satellite Geometry Handbook prepared by Riazanoff [164]. SPOT 5, launched on May 3, 2002, is part of SPOT satellite mission program bringing a series optical remote sensing system. The program was begun with the launching of SPOT 1 satellite on 1986 followed by SPOT 2 (1990), SPOT 3 (1993), SPOT 4 (1998), and SPOT 5, the latest SPOT satellite mission. SPOT is a joint program involving France, Belgium, and Sweden. The primary mission of this program is to gather information of natural resources for purposes such as mapping land use land cover, agriculture study, urban planning, forestry, and water resources management. The satellite is operated by the France Space Agency, Centre National d'Etudes Spatiales (CNES). The typical orbit of SPOT satellite system, including SPOT 5, is sun-synchronous, with altitude of 832 km, inclination of 98.7 degree, period of 101 minute, and repeat cycle of 26 days.

SPOT 5 is equipped with two HRG (High Resolution Geometric) and two HRS (High Resolution Stereo) instruments. The first instrument allows generating 4 resolution levels with 60 km x 60 km swath. The second instrument allows generating stereopair image of a swath 120 km across and 600 km long. HRS provides useful data for generation of Digital Elevation Model (DEM). The satellite offers a resolution in multi spectral mode of 10 m in all visible and NIR bands (Band 1-3). One sensor operating in short wave infrared band (SWIR) is dedicated for monitoring vegetation with a resolution of 20 m. High Resolution Visible (HRS) sensors of SPOT satellite can operate in two modes, multi spectral and panchromatic. During the second mode, SPOT records objects within panchromatic band over the wavelength range of 0.51 to 0.73  $\mu\text{m}$  with 5 m resolution. The characteristics of SPOT 5 bands are given in Table 2.6 and the schematic of the satellite is shown in Fig. 2.8.

SPOT data is available at different product level. Level 1A (raw product), level 1B (system corrected product), level 2A (projected product without ground reference

points), and 2B (projected product with ground reference points). Level 2A is the product currently use in this research. The data is distributed in form of grey scale image represented by DN ranging from 1 to 255.

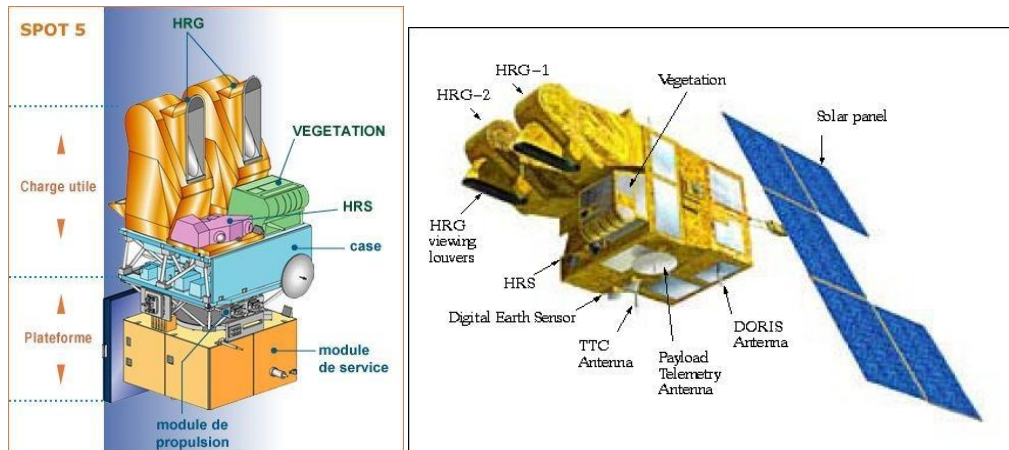


Fig. 2.8 SPOT 5 satellite and onboard instruments

Source: Riazanoff [164]

Table 2.6 Characteristics of SPOT 5 bands

Source: Riazanoff [164], Gao [165]

Band	Spectral Ranges ( $\mu\text{m}$ )	Resolution (m)
Band 1	0.50 – 0.59 (Green)	10
Band 2	0.61 – 0.68 (Red)	10
Band 3	0.79 – 0.89 (NIR)	10
Band 4	1.58 – 1.75 (SWIR)	20
Panchromatic	0.48 – 0.71	5

### 2.7.5 Image Pre-processing

Like other measurements, images produced from remote sensing satellite contain errors as well. Gibson and Power [94] explained that the errors may come from instrumental errors, medium (atmosphere), orbit perturbation that causes image distortion, data transmission from satellite to ground station, and data handling in ground station. Most of instrumental errors and errors during transmission and data

handling in ground station have been fixed by the image producer authority before distributed to public. Geometric and atmospheric corrections are usually delegated to users since it usually requires local requirements, such as local control point in local reference system and local atmosphere correction model, the image producer cannot take over. It is therefore important to apply image pre-processing procedures to ensure that images are free from geometric distortion and atmospheric effects so that distance, polygon area, direction, land cover land use can be accurately extracted. Below is the description of handling geometric and atmospheric errors.

#### *2.7.5.1 Geometric Corrections*

Images produced from remote sensing satellite contain distortions or geometric errors. They need to be freed from such errors to allow extraction any measurements from corrected images. According to Lillesand, et al. [166], the distortions may come from orbit perturbation (e.g. variation of satellite altitude, altitude and velocity due to inhomogeneous land mass and solar pressure), earth curvature, and relief displacement. Image distortions can be either systematic or random/non-systematic. The sources of both distortions are many. An example of systematic distortion is the distortion due to earth's rotation. While Landsat scanning the earth from first to last line at approximately 28 seconds, the target beneath the satellite has move eastward due to earth's rotation. This causes 185 km x 185 km Landsat footprint on the ground become a rhombus shape not square. Such error is usually fixed before the data delivered to users. Random distortions are usually related to orbit perturbation causing the platform unstable so that the altitude (height) and attitude (stability from movement/rotation in x, y, and z directions known as pitching, rolling and yawing) of the platform are disturbed.

The detail procedure of removing random geometric distortion can be found in most of remote sensing image processing literatures such as in Lillesand, et al. [166], Gao [165], Gibson and Power [94], and Unger Holtz [167]. Geometric distortions can be removed by means of rectification process. In doing so, a set of ground control points (GCPs) is required. GCPs can be a georeferenced/corrected map or a set of ground control points whose coordinates are known in a desired (usually local)

reference system. A GCP is required to be easy to find/recognize on both uncorrected image and corrected image. Illustration of rectification process is shown in Fig. 2.9. Rectification process requires collection of the same number and position of GCPs from both images to tie down uncorrected image. It results in a list of coordinates known points extracted from georeferenced image and screen (pixel) coordinates of uncorrected image. Using a polynomial equation, each pixel on uncorrected image is transformed to a position in a real world coordinate system (such as Latitude/Longitude or Easting/Northing) resulting in a new georeferenced image.

A polynomial function is a mathematical equation that can be used to transform uncorrected image to georeferenced image coordinate system. During transformation, uncorrected image undergoes translation, rotation, and scaling. Some image processing softwares provide first order (linear), second order (quadratic), and third order (cubic) polynomial function for rectification process. The higher the polynomial orders the more complex the equation relating both parameters. The following equation is a first order polynomial equation relating coordinates on uncorrected image ( $x_u, y_u$ ) and those on georeferenced/corrected images ( $x, y$ ) as explained in Gibson and Power [94]:

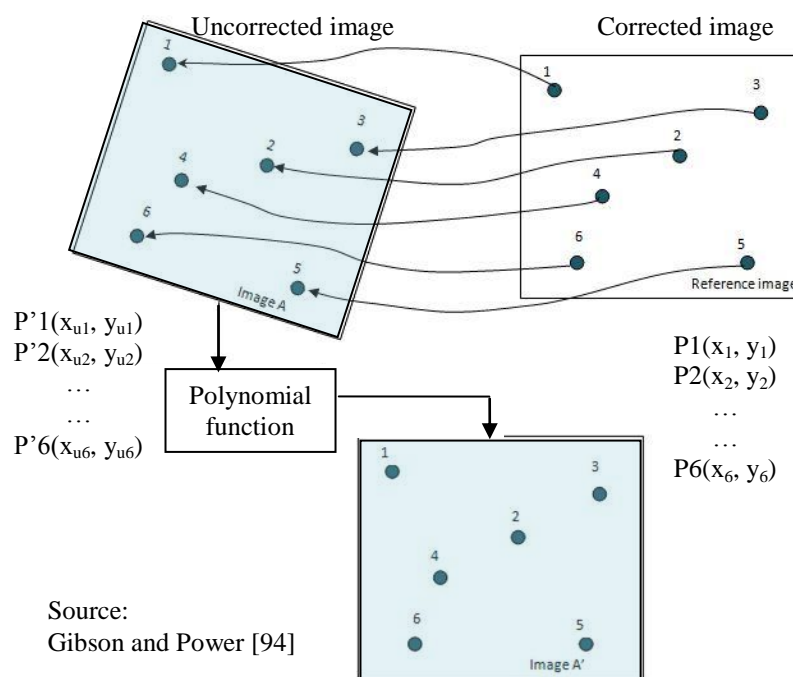


Fig. 2.9 Geometric correction procedures

$$\left. \begin{aligned} x_u &= a_0 + a_1x + a_2y \\ y_u &= b_0 + b_1x + b_2y \end{aligned} \right\} \quad (2.10)$$

First order polynomial only performs translation of uncorrected image to a desired reference system. Second order polynomial links both images using quadratic form, a more complicated polynomial equation, as follows:

$$\left. \begin{aligned} x_u &= c_0 + c_1x + c_2y + c_3xy + c_4x^2 + c_5y^2 \\ y_u &= d_0 + d_1x + d_2y + d_3xy + d_4x^2 + d_5y^2 \end{aligned} \right\} \quad (2.11)$$

To solve Equation 2.10, 3 GCPs are required since it contains 6 parameters (unknown). Meanwhile, 6 GCPs are required to solve Equation 2.11 since it contains 12 parameters.

The quality of rectification result is expressed in RMSE (root mean square error) as explained by Gao [165]. The error is the different between the coordinates of georeferenced image and those resulted from the transformation process. For a given point, it has RMSE values in both directions, Northing and Easting. The magnitude of RMSE of both directions is not necessarily the same. The overall accuracy of transformation equals to the total of RMSE of both directions. Equation 2.12, 2.13, and 2.14 in the following are RMSE of Northing, Easting, and the final accuracy.

$$RMSE_E = \sqrt{\frac{1}{n} \sum_{i=1}^n \delta_{Ei}^2} = \sqrt{\frac{1}{n} \sum_{i=1}^n (\hat{E}_i - E_i)^2} \quad (2.12)$$

$$RMSE_N = \sqrt{\frac{1}{n} \sum_{i=1}^n \delta_{Ni}^2} = \sqrt{\frac{1}{n} \sum_{i=1}^n (\hat{N}_i - N_i)^2} \quad (2.13)$$

$$RMSE_{EN} = \sqrt{\frac{1}{n} \sum_{i=1}^n (\delta_{Ni}^2 + \delta_{Ei}^2)} \quad (2.14)$$

In general, the first two equations indicate the different between the known coordinates from corrected image and the predicted coordinates on uncorrected image

using polynomial transformation. The last equation indicates the total error in both directions. Gao [165] reported that there is no exact standard regarding the acceptable value of overall RMSE. People usually use rule of thumb or conventional wisdom stating that the overall RMSE should not be greater than one pixel size in value. Therefore, for Landsat satellite image with 30 m resolution or SPOT 5 with 10 meter resolution, the overall RMSE should be below 30 m and 10 m accordingly.

There are factors affecting the accuracy of rectification/geometric correction. Gibson and Power [94] identified two factors. The first is the selection of GCPs. GCPs should be easy to identify on both images and do not have possibility to move such as coastal line and river bends, otherwise it may result in a large RMSE. In addition, a sufficient number of GCPs which are well/evenly distributed over the image are required. Having GCPs clustered on a particular part of an image, e.g. east part or west part, will lead to an inaccurate rectification result since the remaining parts of an image are not well tied down.

Illustration of the effect of the number and the distribution of GCPs involved in rectification process on the accuracy of rectification is shown in Fig. 2.10 which is expressed in the changing grid pattern. The grid pattern shows how the rectified image will be distorted. Fig. 2.9a shows rectification result using only 4 GCPs concentrated on upper left corner of the image (shown circled). Grid boxes seem tilted to the east. Adding 4 more GCPs on the upper part of the image, as shown in Fig. 2.9b, causes the lower part extremely distorted westward. Since GCPs on left corner is denser than those on right, the remaining part of the image is dragged to the lower left, showing the expected rectified image. Addition of 2 more GCPs on lower left of the image, shown in Fig. 2.9c, appears to repair the distortion at lower left part left by previous experiment. The lower right part of the image is still distorted. Three more GCPs are added forming a stretch of GCPs from lower left to lower right (Fig. 2.9d). This addition repairs the distortion on the lower right. More GCPs are defined on middle left and right (Fig. 2.9e). The total GCPs are 24. Grid lines seem to have properly aligned. However, center part of the images still experience distortion even though it cannot be seen by human eyes. Finally, addition of 33 more GCPs located mostly on the center part and its surroundings refines the rectification result. These



rectification sequences show visually how the number of GCPs and its distribution affect the result. The actual accuracy is indicated by RMSE.

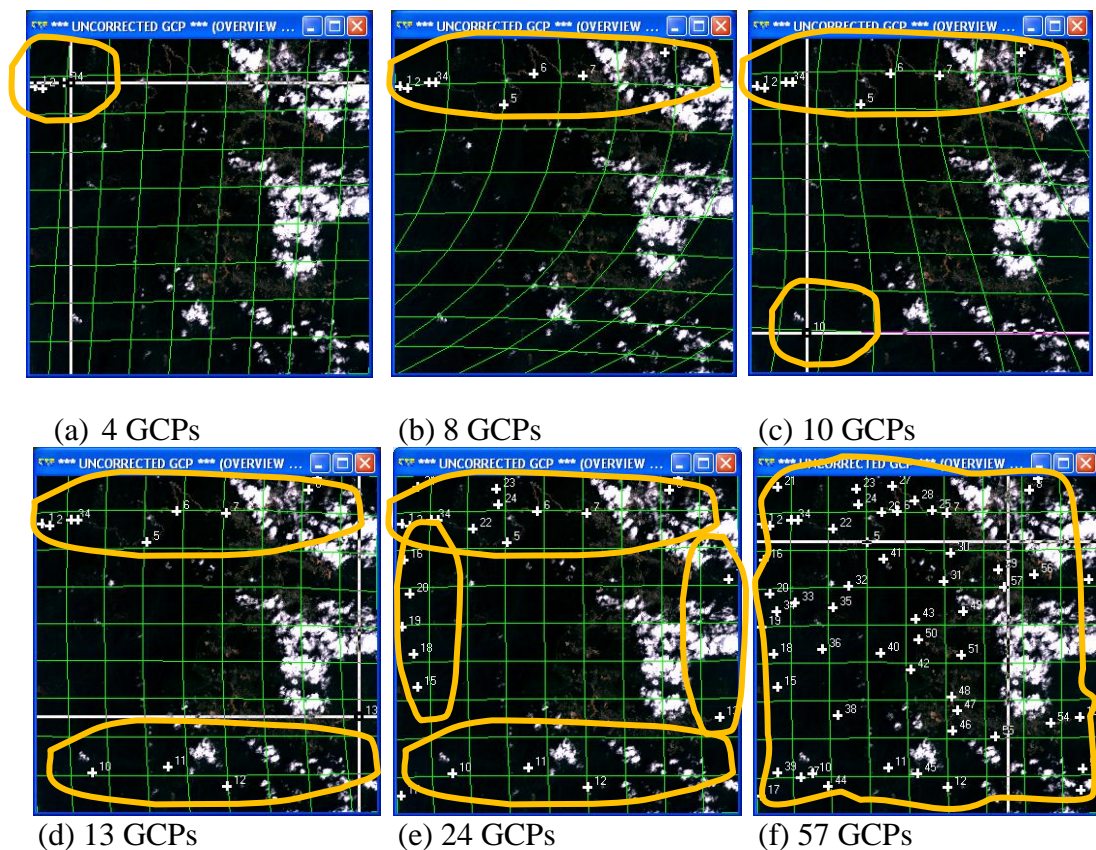


Fig. 2.10 Pattern of distortion due to the number and distribution of GCPs

Gao [165] added other factors affecting the accuracy of rectification. The accuracy of the corrected map, hence the picked GCPs, is an important issue. One has to make sure about the accuracy of the map before using. A set of control points gained from GPS (Global Positioning System) survey would provide more accurate GCPs than those picked up from the georeferenced topographic map. The last factor is the order of polynomial transformation. It is said that by applying high order of polynomial transformation will result in more accurate rectification result.

#### 2.7.5.2 Atmospheric Correction

Atmosphere has significant role in affecting electromagnetic radiation or DN of objects on the earth. The DN/radiance recorded by remote sensing sensor does not

represent the true radiance of targeted object but a mixture of two components as described by Jensen [168], Gao [165] and Hadjimitsis, et al. [169]. They are actual DN of the object and atmospheric factor. The effect of atmosphere can be negative (reduce the DN) by absorbing the radiance or positive (increase the DN) by scattering the radiance. The atmosphere tends to scatter short wavelength bands. The shorter the wavelength bands the higher the scattering degree. Fig. 2.11 shows short wavelength of electromagnetic energy is highly absorbed by the atmosphere as recorded by band 1 sensor. Meanwhile, longer wavelength is less absorbed by the atmosphere as recorded by band 5 sensor.

The effect of atmosphere in altering DN value can be viewed through DN histogram, the graphical representation of DN of an image. Fig. 2.11 shows examples of histogram of band 1 and 5 of a Landsat 7 ETM+ image. Assuming that there are dark pixels, such as cloud shadow, of a given image, these pixels should have DN values of zeroes. However, after examining the histograms, they seem to be shifted from zero. Band 1 on Fig. 2.11 is shifted as far as 49 DN value from the origin while band 5 is shifted by 14. The degree of shifting is different for each band and it depends on the atmospheric conditions as reported by Gibson and Power [94]. For eight bands of Landsat 7 ETM+, the degree of shifting cannot be represented by one single absolute value.

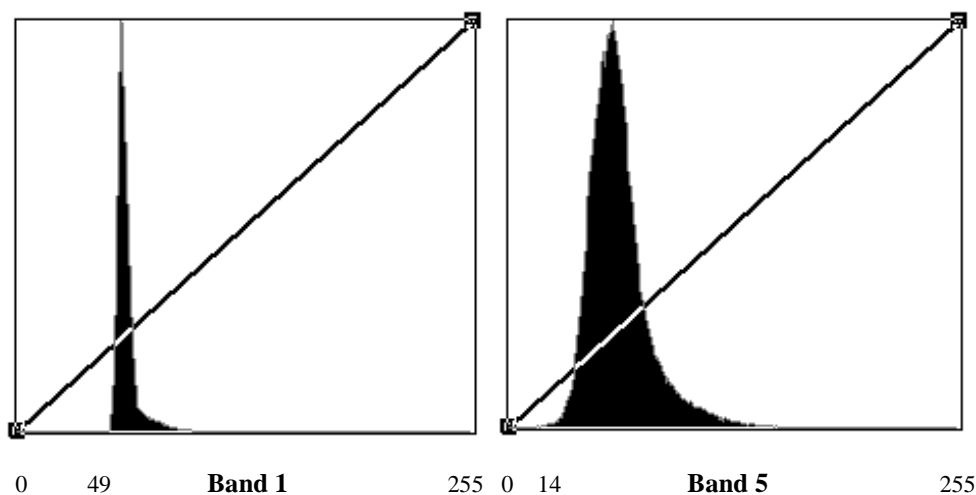


Fig. 2.11 Histogram of band 1 and 5 and the respective offsets

There are various methods to remove atmospheric effect such as optimized cost function and Statistical Estimation developed by Yuzhong and Jakkula [170], QUAC (QUick atmospheric correction) by Bernstein, et al. [171], FLAASH (Fast Line-of-sight Atmospheric Analysis of Spectral Hypercubes) by Jinguo and Zheng [172], and the Darkest pixel (DP) atmospheric correction method, also known as the histogram minimum method applied by Hadjimitsis, et al. [169], or known as Dark Object Subtraction (DOS) the term used by Hall [173]. This method is a first order atmospheric correction by simply subtracting the shifting/offset value from each DN of an image. Therefore, all DN of band 1 image is subtracted by 49 while DN of band 5 image is by 14. However, Gibson and Power [94] suggested that atmospheric correction is not necessarily required before further use of a remote sensing data. The reasons are the image corrected from atmospheric effect has the same appearance as uncorrected one so that human eyes cannot distinguish one from another. The second reason is that the dark pixels are not necessarily present on the image. So, subtracting each DN with the lowest DN value may result in an erroneous image.

### **2.7.6 Image Enhancement**

Image enhancement is intended to improve the spatial quality or interpretability or visibility of an image. Computer-based enhancement is applied to overcome human eyes/mind limitation in distinguishing a slight spectral difference between two different objects. There are many methods for image enhancement such as contrast stretching, ratio images, thresholding, density slicing, filtering techniques, principal component analysis and classification. The detail explanation of such methods can be found in most of image processing of remote sensing literature such as Jensen [168], Gibson and Power [94], Gao [165], and Lillesand, et al. [166]. Gao [165] grouped these methods into two: non spatial image enhancement (such as contrast enhancement and density slicing) and spatial image enhancement (such as spatial filtering and edge detection). Meanwhile, Lillesand, et al. [166] grouped them into three: contrast manipulation (such as density slicing), spatial feature manipulation (such as edge enhancement), and multi-image manipulation (such as band ratioing and principle component analysis). However, Gibson and Power [94] stated that there

is no optimum enhancement technique. The optimum technique is that the one that can enhance the objects/features of investigator's interest.

In this research, image enhancement was mostly carried out by means of applying selected bands combination and contrast adjustment/linear stretching. First order atmospheric correction previously mentioned is also considered as kind of image enhancement method.

#### *2.7.6.1 Band Combination*

Combination of selected bands is usually used to enhance features of interest. Sanaeinejad, et al. [174] found that band combination of RGB (Red Green Blue) 734 or 731 is suitable for soil salinity studies. Ramli and Petley [175] applied various statistical methods such as optimum index factor, maximum variance-covariance determinant, and principal component analysis for selecting best bands combination for landslide studies. Quinn [176] and GDSC [177] listed several band combinations along with their applications. RGB 321 is band combination representing an image in natural color (Fig. 2.12a). This combination best describes the appearance of the landscape in reality. Having an image in natural color is helpful for identification training areas required for image classification for extracting land use land cover. RGB 123 and 432 (Fig. 2.12b) are false color composite (FCC) combinations using which various types of vegetation can be discriminated. Meanwhile, RGB 453 is good for study water content on soil.

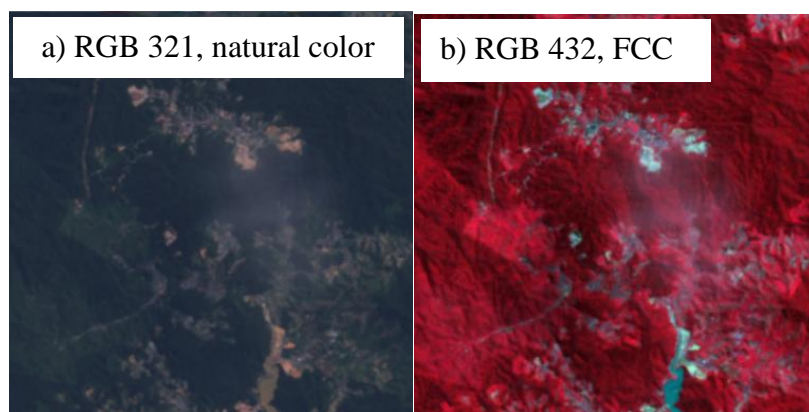


Fig. 2.12 Band combinations: a) natural color and b) FCC

### 2.7.6.2 Linear stretch

The image shown in Fig. 2.12a looks darker compared to that in Fig. 2.12b. Unlike the second image, the first image has not undergone any image enhancement procedures. One of simple methods for image enhancement is linear stretching or so called contrast stretching. The idea is illustrated in Fig. 2.13. An image has digital numbers ranging from 84 to 153. Using linear stretch method, a new image is produced based on the original image by assigning replaces its lowest (84) and highest DN (153) with values of 0 and 255. This operation stretches DN values in between interval 0 and 255 accordingly. This is kind of rubber setting, dragging one end of histogram graph to 0 and another end to 255. Mathematical expression of the stretched image ( $DN_{st}$ ) produced from the original image ( $DN$ ) is given in Equation (2.15).  $DN_{max}$  and  $DN_{min}$  represent the maximum and minimum DN values in the original image.

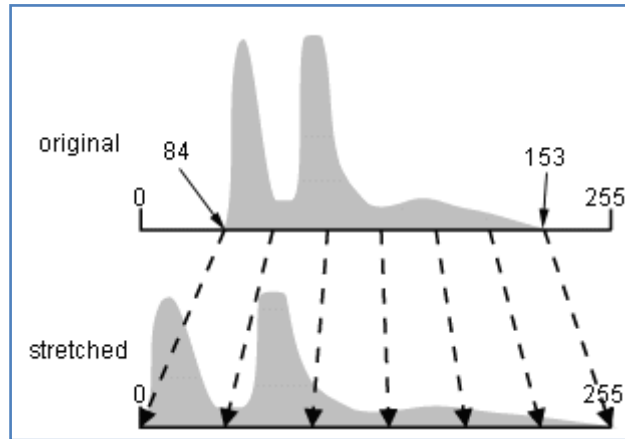


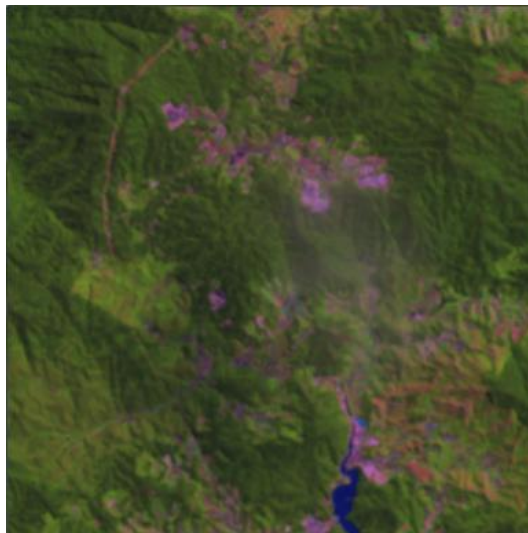
Fig. 2.13 Illustration of linear stretching

Source: CCRS [178]

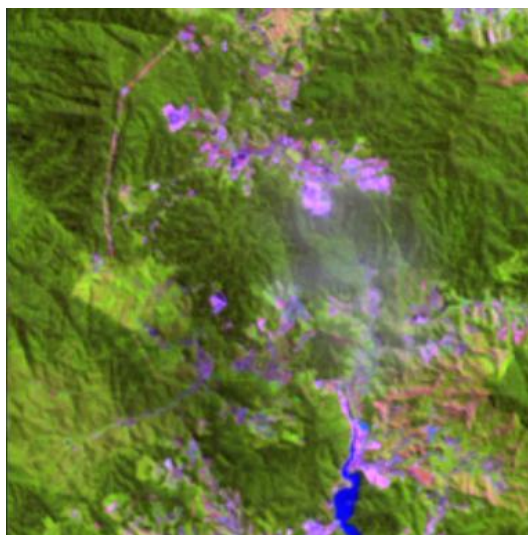
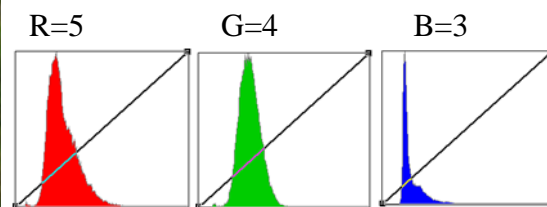
$$DN_{st} = 255 \times \frac{(DN - DN_{min})}{(DN_{max} - DN_{min})} \quad (2.15)$$

Application of linear stretch results in a brighter image than the original one. Fig. 2.14 shows images of part of Cameron Highlands area before (Fig. 2.14a) and after (Fig. 2.14b) application of linear stretch method. This image is constructed using bands combination of RGB 543, enabling the image shown in natural color. The

histograms of original image look narrow. This is why the image looks dark. After applying linear stretch, all histograms occupy a full DN stretch that ranges from 0 to 255. The image is then looks brighter than the original one allowing more information can be extracted. The border between crop land and forest can be well identified and so do the lake, open land and urban. The stretched image is also helpful for delineating homogeneous areas set as training areas for supervised image classification purpose.



a) RGB 543, original histogram



b) RGB 543, stretched histogram

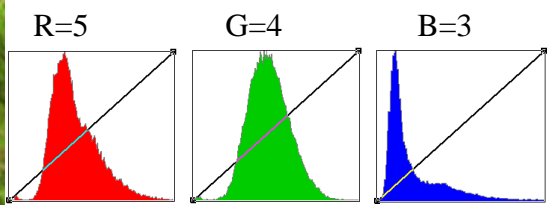


Fig. 2.14 A Landsat image in RGB 543 and the corresponding histogram adjustment:

a) before and b) after linear stretching

### **2.7.7 Image Classification for derivation of Land Use and Land Cover**

Land use land cover (LULC) map is an important landslide contributing factor. To construct such a map from remote sensing imagery, it requires application of image classification processes. Image classification procedure is intended to automatically group all pixels in an image into land use land cover classes as described by Lillesand, et al. [166].

The idea of image classification is that each object on the earth has different reflectance value within electromagnetic spectrum. Thus, objects can be recognized and distinguished one from another based on spectral value. As shown in Fig. 2.6, soil, grass and water show different reflectance patterns within visible, NIR and mid infrared. The principle work of digital image classification is identification of homogeneous groups of pixels in one or more spectral bands based on their spectral/reflectance information as described by CCRS [178]. At the end of classification process, grouped homogeneous pixels are assigned with particular classes or themes such as forest, water, corn farm, etc. The methods of image classification are divided into unsupervised and supervised image classifications. There is also a hybrid classification method which is a combination of automatic and manual classification methods. Detail explanation of classification method can be found in most of image processing of remote sensing image such as Gao [165], Gibson and Power [94], and Lillesand, et al. [166].

#### ***2.7.7.1 Unsupervised Classification***

Unsupervised classification method has pixels of an image grouped into classes/clusters by image processing software. The grouping is based on the reflectance value of pixels that is statistically separable. There is no user (expert/image analyst) intervention or field knowledge required to run unsupervised classification. The classes resulted from this procedure is called spectral classes. User can then identify the land use land cover type of the classes by comparing them with for example, topographic map or field survey data, and finally assign appropriate attributes to those classes.



A good explanation on how this image classifier works was given by Gibson and Power [94]. Once the number of classes defined, the computer software specifies arbitrary DN means to each class and have pixels moved to the nearest mean of classes. The software then recalculates new class means. These values are used to re-evaluate each pixel. The software then relocates pixels to the closest new class means. This procedure can be repeated several times until meet the number of iterations set by the user or achieve the threshold value set by the user. The author said that at a threshold of 0.98, the adjacent iterations left less than 2% of pixels moving. Included as unsupervised classification techniques are *K*-means, ISODATA (Iterative Self-Organizing Data Analysis Technique), and histogram based clustering as described by Gao [165].

#### 2.7.7.2 Supervised Classification

Unlike the previous method, supervised classification requires the user to provide spectral signatures of known land cover lands categories such as forest, urban, barren land, bushes, etc., prior to do image classification. In doing so, such spectral signatures are sampled from the image by delineating several areas of a homogenous type, e.g. forest, then computing statistical parameters, e.g. mean, standard deviation, etc., of their spectral signatures. These areas are called as training areas. The other categories undergo the same procedures so that the statistical parameters of spectral signature of all desired land use land cover categories is made available. The image processing software then compares the DN of each pixel with the statistical parameters and do image classification using statistical techniques so called image classifiers. There three classifiers as described by Liao [47], Lillesand, et al. [166], Gao [165], and Gibson and Power [94] namely, from low to high accuracy, parallelepiped, minimum distance-to-mean or nearest neighborhood, and maximum likelihood classifiers.

Parallelepiped classifier constructs ‘boxes’ using statistical parameters of training areas with mean as the center of boxes and maximum/minimum and standard deviation for determining the width and length of the boxes (Fig. 2.15a). Any pixel falls within a particular box, for example box of forest category, will be grouped to



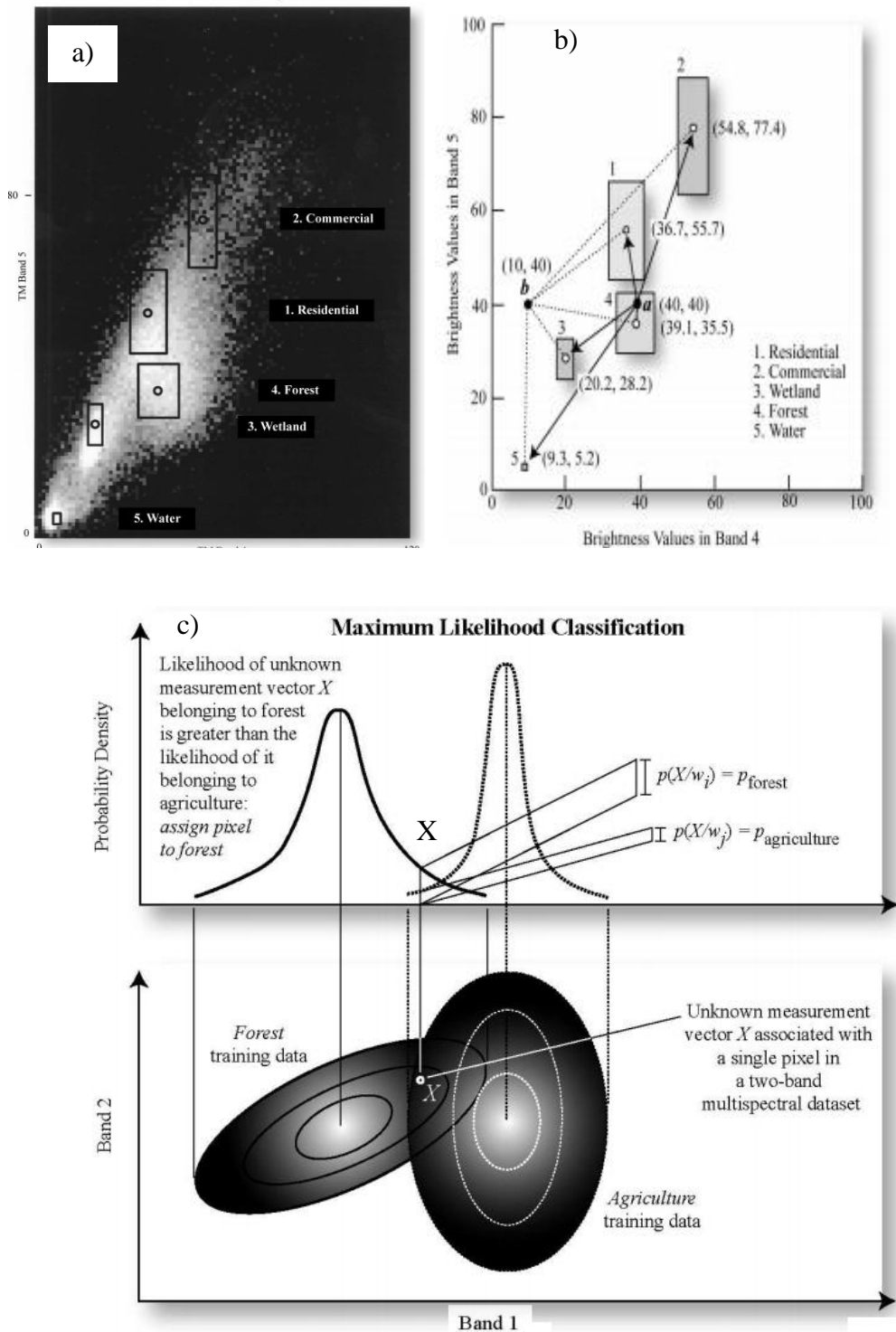


Fig. 2.15 Illustrations of supervised classification classifiers

Source: CCRS [178]

that category. This method offers fast classification but has poor accuracy. Using this method, a pixel can be belongs to two boxes or none of them. In Fig. 2.15b, pixel  $a$

belongs to cluster/class 4 due its location within box 4. Meanwhile, pixel *b* could be unclassified or has no class since there are no boxes containing this pixel. Using Minimum distance-to-mean (Fig. 2.15b), pixel *b* can be grouped to class 3 according to the shortest distance between the distance from pixel *b* to all class mean pixel.

Maximum likelihood is considered as the most useful classifier admitted by Gao [165]. The so-called Gaussian maximum likelihood classifier evaluates any pixels using variance and covariance of spectral signature of land use land cover categories. This method applies an assumption that the distribution of points forming each category, e.g. forest, water, crop land, etc., derived from training areas is Gaussian (normally distributed). Fig. 2.15c shows how point/pixel *X* belongs to forest type rather than to agriculture classes. The reason is that the probability of pixel *X* being grouped to forest class is higher than to agriculture class. The graph of probability density of forest looks more normally distributed than that of agriculture which appears to be a bit narrow.

#### *2.7.7.3 LULC Classification Scheme*

Anderson, et al. [179] designed a classification system for LULC for use with remote sensing data that satisfy the needs of the majority of users. This scheme does not differentiate between land cover and land use. The scheme starts with Level I category for example; urban or built up land, agricultural land, forest land, etc. Urban or built up land is broken down for level II into such as residential, commercial and service, industrial, etc. One thing to take note is that the various types of land use land cover in level II do not necessarily available. Hence, one may reduce or modify it to fit with what available in the study area. The scheme, shown in Table 2.7, contains 9 levels I while the total of level II is many. Level III and IV are left open-ended to users such as federal, regional, state, and local agencies so they can have flexibility in developing more detailed land use land cover according to their particular needs.

LULC classification for level I to IV requires different specification of satellite imageries. Anderson, et al. [179] did not specify detail of satellite mission in accordance to various level of classification. However, the authors only stated about

Table 2.7 Image classification scheme

Category Number	Level 1	Level II
1	Urban or built-up land	11 Residential 12 Commercial & services 13 Industrial 14 Transportation, communications & utilities 15 Industrial & commercial complexes 16 Mixed urban or built-up land 17 Other urban or built-up land
2	Agricultural land	21 Cropland & pasture 22 Orchards, groves, vineyards, nurseries & ornamental horticultural areas 23 Confined feeding operations 24 Other agricultural land
3	Rangeland	31 Herbaceous rangeland 32 Shrub & brush rangeland 33 Mixed rangeland
4	Forest land	41 Deciduous forest land 42 Evergreen forest land 43 Mixed forest land
5	Water	51 Streams & canals 52 Lakes 53 Reservoirs 54 Bays & estuaries
6	Wetland	61 Forested wetland 62 Nonforested wetland
7	Barren land	71 Dry salt flats 72 Beaches 73 Sandy areas other than beaches 74 Bare exposed rock 75 Strip mines, quarries & gravel pits 76 Transitional areas 77 Mixed barren land
8	Tundra	81 Shrub & herbaceous tundra 82 Herbaceous tundra 83 Bare ground tundra 84 Wet tundra 85 Mixed tundra
9	Perennial snow or ice	91 Perennial snowfields 92 Glaciers

Source: Anderson, et al. [179]

the altitude of remote sensing platform. As classification goes deeper (e.g. level IV), low altitude platform with higher resolution is required. As illustration, global

MODIS (The Moderate Resolution Imaging Spectroradiometer) satellite can provide data for level I with resolution range 250 m to 1.1 km. Level II (resolution range of 80 m to 250 m) can be fulfilled by Landsat Thematic Mapper. Level III (30 m to 80 m) can be fulfilled by Landsat 7 ETM+. Level IV (3 m to 30 m) can employ SPOT and aerial photograph to provide such data, and level V, if required, can utilize IKONOS or QuickBird images.

### 2.7.8 Land Surface Temperature

Landsat 7 ETM+ provides sensors working on thermal infrared (band 6) channel to record thermal (heat) emitted by objects on the earth. This data offers an opportunity and at the same time a challenge for users to retrieve land surface temperature (LST). There are methods for retrieving LST from thermal infrared data such as mono-window algorithm developed by Qin, et al. [180], and single-channel algorithm developed Jimenez-Munoz, et al. [181] and the applied by Hua, et al. [182]. Sobrino, et al. [183] estimated LST from the radiative transfer equation using in situ radiosounding data and compared it with the previous two methods.

Mono-window algorithm has been extensively used to retrieve LST from Landsat thermal infrared by such as Chudong, et al. [184], Cheng, et al. [185], Chuansheng, et al. [186], Yang and Wang [187], Zhang, et al. [188], etc. The estimation of LST begins with adoption of basic principle that any objects on earth will emit thermal energy as their temperatures are above absolute zero (Kelvin). Hence, DN<sub>s</sub>, the spectral reflectance, of the objects recorded by the thermal sensors can be transformed to at-sensor radiance using the following equation described in Markham and Barker [189]:

$$L_R = gain \times DN + bias \quad (2.16)$$

$$L_R = 0.0056322 \times DN + 0.1238 \quad (2.17)$$

$L_R$  is spectral radiances ( $\text{Wm}^{-2}\text{sr}^{-1}\mu\text{m}^{-1}$ ); 0.0056322 is *gain*, a general term used to denote an increase in signal power transmission; *DN* is Digital Number of band 6; and 0.1238 is a constant bias. In order to obtain LST, the spectral radiances were then

converted into satellite brightness temperature, which is commonly called as LST, using the following relationship developed by Schott and Volchok [190]:

$$T_B = K_2 / \ln \left( \frac{K_1}{L_R} + 1 \right) \quad (2.18)$$

$T_B$  is at-satellite brightness temperature ( $K^0$ );  $K_1$  and  $K_2$  are two free parameters with the values of  $K_1 = 60.776 \text{ mWcm}^{-2}\text{sr}^{-1}\mu\text{m}^{-1}$ ,  $K_2 = 1260.56 \text{ K}$ .  $T_B$  is uncorrected LST. If required, one may converse the unit of LST from Kelvin degree to Celsius degree using the following relationship:

$$C = K - 273.15 \quad (2.19)$$

As mentioned previously,  $T_B$  is uncorrected LST. Therefore,  $T_B$  represents a mixed signal of different fraction of energy. The fractions include the energy emitted from the ground/targeted object and noises that come from upwelling radiance from the atmosphere, as well as the downwelling radiance from the sky integrated over the hemisphere above the surface. Therefore, the effects of both surface emissivity and atmospheric must be corrected to produce real LST or  $T_s$  as suggested by Yang, et al. [191] and Yang and Wang [187]. To do so, the following mono-window algorithm developed by Qin, et al. [180] is applied:

$$T_s = \frac{1}{C_6} [a_6(1 - C_6 - D_6) + [b_6(1 - C_6 - D_6) + C_6 + D_6]T_B - D_6T_a] \quad (2.20)$$

$T_a$  is the effective mean atmospheric temperature (K),  $a_6$  and  $b_6$  are constants with values of -67.355351 and 0.458606 respectively.  $C_6$  and  $D_6$  can be calculated using the following equations:

$$C_6 = \varepsilon\tau_6 \quad (2.21)$$

$$D_6 = (1 - \tau_6)[1 + (1 - \varepsilon)\tau_6] \quad (2.22)$$

Symbol  $\varepsilon$  represents the ground surface emissivity and  $\tau_6$  the atmospheric transmittance. These three parameters, i.e.  $T_a$ ,  $\varepsilon$ , and  $\tau_6$  are required to convert brightness temperature ( $T_B$ ) to LST or  $T_a$ . Qin, et al. [180] added that  $\tau_6$  can be inferred from atmospheric water content and  $T_a$  can be obtained from near surface temperature ( $T_0$ ) using the following equations:

$$T_a = 25.9396 + 0.88045 T_0 \quad (\text{for United States of America}) \quad (2.23)$$

$$T_a = 17.9769 + 0.91715 T_0 \quad (\text{for tropical}) \quad (2.24)$$

$$T_a = 16.0110 + 0.92621 T_0 \quad (\text{for mid-latitude summer}) \quad (2.25)$$

$$T_a = 19.2704 + 0.91118 T_0 \quad (\text{for mid-latitude winter}) \quad (2.26)$$

### 2.7.9 Vegetation Indices

Described in Gibson and Power [94], vegetation is highly absorbed in the visible red region and highly reflected in the near infra red region. Two different objects on the earth may emit the same radiance in two different electromagnetic bands. Ratioing of both object's radiance can result in additional information compared to evaluation of individual radiance of both objects. This principle is proven to be effective for studying vegetation behavior. The ratio between infrared/red results in a measure of vegetation condition. A simple measure is the presence or absence of vegetation. Pixels with high ratio values show that the vegetation is present and low ratio values indicate that the vegetation is absent. Vegetation index can also be used to measure the biomass and vegetation health. For landslide study, the surfaces such as barren land, open area, non-vegetated slopes, etc. can be mapped for preliminary study of potential unstable areas.

Vegetation index is of image enhancement methods for increasing the spectral contrast between the red and NIR regions of the electromagnetic spectrum. There are various forms of vegetation indices such as Perpendicular Vegetation Index (PVI), Normalized Difference Vegetation Index (NDVI), and Soil Adjusted Vegetation Index (SAVI). NDVI is considered as the most extensively used vegetation index. In most literature, it is formulated as follows:

$$NDVI = \frac{NIR - VR}{VR + NIR} \quad (2.27)$$

Equation 2.27 results in vegetation index values that range from -1 to 1, from no vegetation to completely covered by green-healthy vegetation.

### 2.7.10 Tasseled Cap Transformation for Landsat ETM 7 data

Tasseled Cap Transformation (TCT) was developed by Kauth and Thomas [192] in 1976 as mentioned in Gibson and Power [94]. This is one of image enhancement methods to optimize data viewing for vegetation studies. The first use of this transformation was to monitor crop development in spectral space. Reflectances of soil and wheat in NIR and visible red were monitored as wheat grew up. The effect of shadowing of soil caused by the plant and the sun angle to the reflectances were taken into account. The reflectance of soil and the plant at different phases are put into a single plan, i.e. two-dimensional graph. The plot of these data resembles a cap shown in Fig. 2.16 with tassels of graphs of darker and lighter soil reflectances, originating the name of this transformation technique.

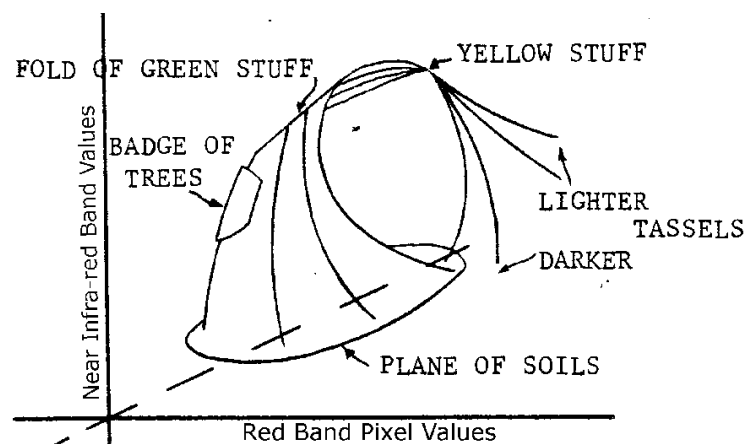


Fig. 2.16 Illustration of Tasseled Cap Transformation

Source: Kauth and Thomas [192]

TCT was first designed for Landsat TM (Thematic Mapper). As Landsat satellite mission evolved with the launching of Landsat MSS (Multi Spectral Scanner) continued by Landsat 7 ETM+, the TCT was then developed to accommodate all six non-thermal bands. These data are transformed into a set of new bands that are useful for interpretation of vegetation including greenness, soil brightness, etc. Equation of TCT for use with Landsat MSS data is linear combinations of green, red, and two NIR bands to produce new four bands of TC1 (Tasseled Cap 1)/greenness, TC2/ soil brightness, TC3/yellowness, and TC4/noise. The Tasseled Cap coefficients were developed by Campbell [193]. For use with Landsat 7 ETM+ imagery, the TCT equations transform the six non-thermal data into new six bands namely TC1 (soil

brightness), TC2 (vegetation greenness), and TC3 (soil moisture), the three most important band. There is no further description regarding the remaining bands TC4, TC5, and TC6. The equation for use with Landsat 7 ETM+ is in form of linear combination. The Tasseled Cap coefficients have been developed by Huang, et al. [194] and are shown in Table 2.8. For example, soil brightness can obtained as follows:

$$\begin{aligned} \text{Brightness} = & 0.3561 \times (\text{Band1}) + 0.3972 \times (\text{Band2}) + \\ & 0.3904 \times (\text{Band3}) + 0.6966 \times (\text{Band4}) + \\ & 0.2286 \times (\text{Band5}) + 0.1596 \times (\text{Band6}) \end{aligned} \quad (2.28)$$

Table 2.8 Tasseled Cap coefficients for use with Landsat 7 ETM+ imagery

Index	Band 1	Band 2	Band 3	Band 4	Band 5	Band 7
Brightness	0.3561	0.3972	0.3904	0.6966	0.2286	0.1596
Greenness	-0.3344	-0.3544	-0.4556	0.6966	-0.0242	-0.2630
Wetness	0.2626	0.2141	0.0926	0.0656	-0.7629	-0.5388
Fourth	0.0805	-0.0498	0.1950	-0.1327	0.5752	-0.7775
Fifth	-0.7252	-0.0202	0.6683	0.0631	-0.1494	-0.0274
Sixth	0.4000	-0.8172	0.3832	0.0602	-0.1095	0.0985

### 2.7.11 The Roles of Remote Sensing in Landslide Hazard Assessment

Remote sensing technology plays important roles in assessment of landslide hazard. It offers non-contact measurement which is helpful for monitoring insecure landslide prone areas. The roles of remote sensing in landslide hazard study include firstly, identification of landslide locations for purpose of construction of landslide inventory map; secondly, provision of large coverage of thematic maps of landslide contributing factors; lastly, monitoring of landslide hazard through changes detection object on the surface ground.

As landslides occur at the earth surface, it attracts scientists to apply remote sensing technologies to exploit landslide areas. When dealing with measurement and monitoring of single landslides with small areas, terrestrial photogrammetry and laser scanning surveys as of remote sensing methods can be suitable methods to apply. These methods have been applied such as by Stylianidis, et al. [195], Bitelli, et al.



[196] and Monserrat and Crosetto [197]. For a larger area, landslides monitoring are carried out by using aerial photogrammetry such as investigations conducted by such as Hervas, et al. [6] and Walstra, et al. [198]. For wide coverage such as medium and regional scale, landslides were monitored using space based-remote sensing imageries such as investigations carried out by Hong, et al. [199], Kyoung-Wook, et al. [19], Shikada, et al. [200], and Mantovani, et al. [124].

Remote sensing imagery has been useful for identification of landslide locations and constructing a landslide inventory map. Shikada, et al. [201] used Landsat TM (Thematic Mapper) satellite image for extracting characteristic properties of landslide areas. Chi, et al. [202] used data fusion of panchromatic and multispectral of SPOT-5 images and DEM to identify landslide scarps. Vohora and Donoghue [97] used Landsat TM and IKONOS images for mapping landslides in Hongkong. Nikolakopoulos, et al. [203] detected landslide areas using Landsat images by means of identification of high reflectance on the image since landslide areas are usually lack of vegetation. Hervas, et al. [6], Nichol and Wong [204], Singhroy, et al. [205] utilized remote sensing images for preparing landslide inventory maps.

Remote sensing offers wide coverage spatial data required for constructing LHZ map. The data that can be derived from remote sensing technology such as, 1) land use land cover as investigations carried out by such as Han, et al. [206], Li, et al. [207], and Khorram, et al. [208]; 2) NDVI, by Gibson and Power [94], Yaowen, et al. [209], and Jiabin, et al. [210]; 3) soil moisture, by Xuhua, et al. [211], Ray and Jacobs [84], and Huang, et al. [194]; and 4) LST, by Alsultan, et al. [212] and Yang, et al. [191], Huang, et al. [194].

Remote sensing satellites have different repeat period. For examples, Landsat 5 and 7 satellites have 16 days repeat period while SPOT (Satellites Pour l'Observation de la Terre or Earth-observing Satellites) 4 and 5 have 26 days repeat period. These repeat periods allow investigators to monitor phases of landslide and detect changes in for example, land use land cover. Another benefit is that multi temporal spatial data such as series of land use land cover, NDVI, soil moisture, LST, etc, can be made available. These data are useful when different conditions of NDVI/soil moisture/LST under different rainfall seasons are required for modeling LHZ. In addition, by having multi temporal spatial data, e.g. land use land cover, one can investigate land use land

cover changes over a particular period; landslide extent can be monitored. For examples, Goetzke, et al. [213] used series of Landsat images for monitoring land use changes due to urbanization in Central European. From 1984 to 2005, the urban areas increased about 37%.

## **2.8 GIS and Its Roles in Landslide Hazard Assessment**

Geographic Information System (GIS) has been a useful tool for very broad applications such as in natural resources, environmental studies, etc. GIS also takes part in mitigation efforts in minimizing loss of lives and damage of infrastructures due to natural hazard threats such, flood and landslides, by providing hazard maps. GIS has been proven to be helpful in LHA as indicated by the abundance of literatures on LHA utilizing GIS tool. Below is the description of the roles of GIS in LHA and brief review of GIS concept and the associated matters.

### **2.8.1. GIS roles in Landslide Hazard Assessment**

Dealing with landslide hazard assessment of medium scale means handling and processing a large amount of spatial data with wide coverage. Without a powerful tool, this work will be cumbersome. GIS offers a powerful tool more than handling and processing data. As defined by Burrough and McDonell [214], GIS a powerful set of tools for collecting, storing, retrieving at will, transforming and displaying spatial data from the real world. Using GIS, modeling and predicting areas potential to landsliding can be made possible.

GIS was first used in landslide hazard assessment (LHA) in the early of 80's as reported by Carrara, et al. [59]. Earlier works used GIS as a tool to display data and results (final map) in an interesting way. During 1980's, GIS was used by few investigators for assessment and prediction of landslide hazard. It became extensively used as the popularity of statistical methods in LHA increased as described by Aleotti and Chowdhury [116] and Van Westen, et al. [49]. Recently, GIS has been proven to be a valuable tool for acquiring, storing data and manipulating data. Morphology factors such as slope, slope aspect, curvature, elevation, etc. can be easily derived

from DEM (Digital Elevation Model) easily using GIS. GIS has become more powerful when it able to handle and undertake image processing works as offered by stand alone image processing software. GIS is also capable in handling spatial data with different reference systems. For use in LHA, GIS encompasses the following components as suggested by Van Westen [108]: data collection, data entry, data management, and data modeling. Roles of GIS in every step of LHA are illustrated in Fig. 2.17. GIS stores required spatial data such as geology and LULC for LHA including remote sensing imageries into a database during data collection phase. Attributing spatial data and generation of DEM are of GIS roles in the second phase. During the third phase, GIS takes part in formation of landslide database and spatial database required for LHA such as hazard factors, elements at risk, and landslide triggering factors. The last phase of GIS role is data modeling. GIS contributes in finalizing LHA by providing landslide hazard/risk map, calculation of risk and vulnerability, etc.

### **2.8.2. Concept of GIS**

Detail information regarding to principle of GIS can be referred to Burrough and McDonell [214]. When explicitly mentioning the hardware used in GIS, Rose [215] defined that GIS is as a computer system capable of assembling, storing, manipulating, analyzing and displaying geographically referenced information, i.e. data identified according to their locations. Besides the hardware, GIS components include GIS computer software, operating personal, geographic data, and data database management including functions to perform data analysis.

In real world, geographic information is represented by location such as location of Bench Mark, petrol station, landslide locations. etc.; attributes such as street name, land cover type, etc.; and spatial relationships such as sharing center line of river and states border, etc. To put such geographic information in a computer for further analysis, GIS is required. There are three steps to go from real world geographic objects to those on a computer: 1) representation of geographic objects, 2) relating attributes to geographic representation, and 3) spatial relationship between geographic representations.

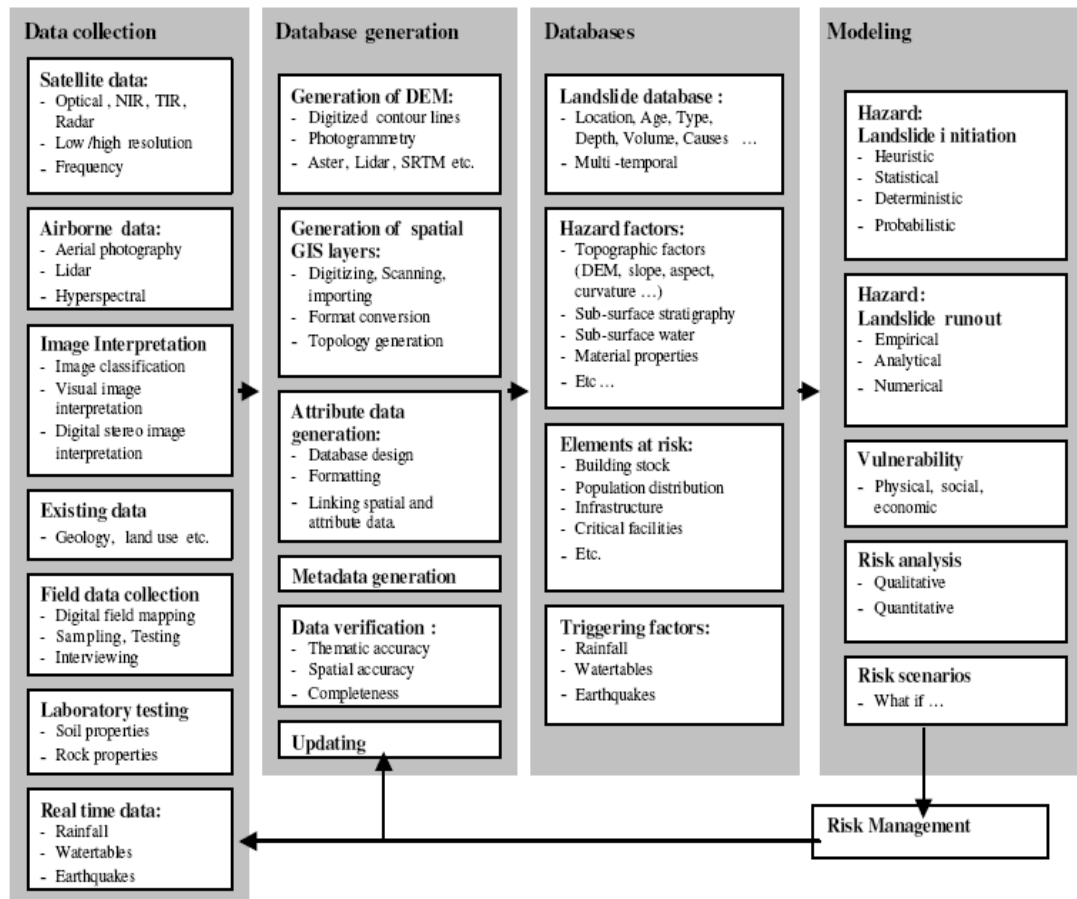


Fig. 2.17 GIS roles in phases of LHA

Source: Van Westen [108]

In GIS, there are two types of data models/formats as representation of real world objects in computer namely vector and raster data model (Fig. 2.18). In vector data model, real world geographic objects are represented by spatial features i.e. point (e.g. electric pole, control point, etc.), line (e.g. center line of river and road, geology lineament), and area (e.g. building, island, etc.). The coordinates of points and the points forming line/area can be obtained from measurement e.g. using GPS, picking up from topographical map, etc., and stored in GIS. Vector data model is good for representing accurate position of objects and is helpful when used for defining spatial relationship between objects. Raster data model uses regular grid of evenly size cell to represent real world objects in computer. Each represents a portion of area on earth. For example, a grid may represent 10 x 10m of area on earth and could be assigned a value of geology type, soil type, elevation, etc. Examples of raster data are slope, slope aspect, remote sensing imageries. Raster data is suitable for representing

continuously changing attributes such as elevation, reflectance, temperature, etc. However, raster data is not suitable when dealing with accurate measurement on GIS.

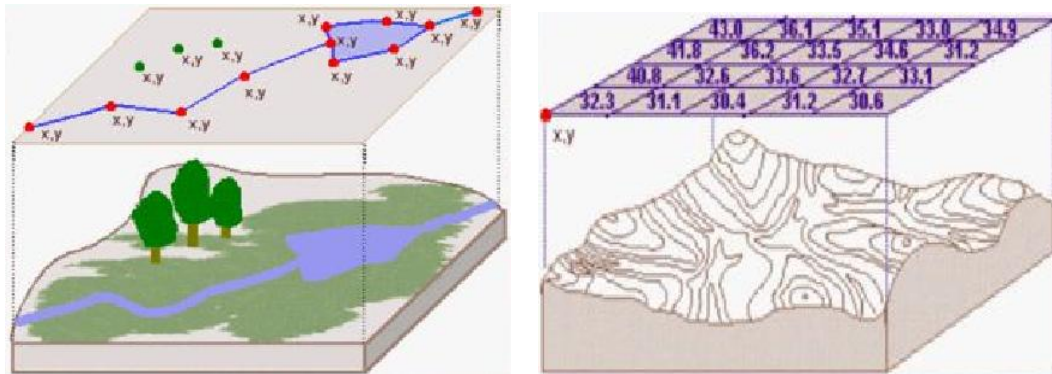


Fig. 2.18 Vector and raster data model

Source: Rose [215]

The next step for bringing real world geographic objects into a computer is by linking attributes of geographic representation. Attributes are non-spatial data associated with geographic representation. For example, one needs to input geology type on geology layer or street name on street layer. Tables are prepared to store the attributes associated with the objects. GIS with capability of database management and manipulation is able to link between spatial and attribute data and allow analysis and query of both data. The last step is building spatial relationship between geographic representations. Spatial relationships of individual object are length, area, shape, and perimeter. Meanwhile, spatial relationship among 2 objects or more could be distance, direction, and topology. Topology is simply defined as the spatial relationships between adjacent or neighboring features. For example, end of two roads may share the same endpoint; a river and the adjacent land cover may share boundaries or segments of the boundary, etc. Spatial distribution of objects described how a particular object is spread out on the map. For example, the spatial distribution of forest may across various type of geology.

### 2.8.3. GIS Software

There are non-commercial/open source and commercial GIS softwares. GRASS (Geographic Resources Analysis Support System) is an example of non-commercial software while ArcGIS, the software currently used in this work, is commercial software. Like any other GIS softwares in general, this software is capable for undertaking all previously mentioned GIS works as described in ESRI [63]. For use in LHA, the software offers facilities to cover all required processes i.e. data collection, data entry, data management, and data modeling. In data collection phase, a required landslide contributing factor, e.g. geology map, can be made available by digitizing a scanned geology map. A geocoding toolbox can be used to tie down the digitized map to the desired projection system. In addition, the software can perform image processing of satellite images to produce LULC, one of important landslide contributing factor. In the second phase, the software facilitates attributing of spatial data. The next phase, the software can be used to derive spatial data from DEM such as slope, slope aspect, curvature, etc. from DEM. The main function of the software in this phase is database management, to prepare all contributing factors, including attributing weightage values, to be ready for final stage. The final phase is executing the landslide hazard assessment model in order to produce a final landslide hazard map.

Talking more detail about ArcGIS software, the software has two powerful toolboxes for LHA purpose namely 3D Analyst and Spatial Analyst. The first is useful for deriving spatial data categorized as 3 dimensional (3D) surfaces such as TIN (Triangulated Irregular Network). This 3D surface is a main data used by Spatial Analyst to derived data such as slope, slope aspect, curvature, and elevation. Spatial analyst offered spatial analysis tools required for modeling landslide hazard such as extraction menu for evaluating the relationship between past landslide occurrences and causative factors and overlay tools using which the final landslide hazard maps are constructed.

## 2.9 Chapter Summary

This chapter has presented a general review of landslide hazard assessment (LHA) including the terminologies and associated concepts. Several factors were discussed in term of their significance of causing instability of slopes. Ten static contributing factors namely lithology, proximity to geology lineament, soil, slope, slope aspect, elevation, curvature, proximity to water body, LULC, and proximity to cut slope which is associated with road, were found to be relevant to involve in LHA. In review of multi temporal environmental factors i.e. NDVI, soil moisture and LST, it was noted that such factors indicate changes due to different rainfall seasons. In regard to selection of appropriate scale, medium scale is suitable for LHA utilizing remote sensing imageries.

There are various methods in LHA which can be grouped into qualitative and quantitative methods. Unlike qualitative methods that are subject to expert subjectivity, quantitative methods offer objectivity in obtaining relationship between past landslide occurrences and relevant landslide contributing factors and the final landslide hazard map. From literature review, it was noted that most of previous works of LHA involved 'static' landslide contributing factors. Investigation on landslide susceptibility that utilizes multi temporal rainfall maps is quite rare. The spatial resolution of available rainfall map for large until medium scale mapping is coarse. As replacement to this data, remote sensing offers environmental data that are responsive to cycle of rainfall such as vegetation index (in form of NDVI), soil wetness, and LST. Such data in form of multi temporal are rarely taken into account in modeling landslide susceptibility either in local or abroad investigations.

A number of studies of LHZ have been conducted for Cameron Highlands. Both methods, qualitative and quantitative methods, were applied. Reviewed literatures of local investigations showed that most of the studies did not take into account the temporal conditions of landslide contributing factors affected by rainfall cycle in the landslide hazard model. Landslide records showed that the number of landslide occurrences increased within rainfall seasons. Previous works left a gap that is the absent of multi temporal factors and put an opportunity to apply multi temporal factors derived from satellite imageries in LHA.

Basic techniques of image processing of remote sensing data were described in order to produce corrected satellite images. Procedures of converting corrected satellite data to other spatial data such as LULC, NDVI, soil moisture, and LST were explained. Finally, a brief review of GIS concept and its capability were discussed. The presence of GIS has been helpful in covering all steps in LHZ from data collection to presentation final landslide hazard map.



## CHAPTER 3

### DATA AND METHODOLOGY

#### **3.0 Overview**

This chapter describes the characteristic of the study area, spatial data involved, and the methodology of the research implemented in this study. The description of the methodology begins with data preparation, data processing, and analysis of the result. The scenario of data processing was designed so that the objectives of the research can be achieved.

#### **3.1 Characteristics of Study Area**

The study area has special characteristics of topographical parameters, LULC, and the climate. In addition, characteristic of landslides in the study area occurrences in Cameron Highlands are explained as well.

##### **3.2.1 Limits of Study Area**

The study area is part of Titiwangsa mountain range. The area covers 30 km x 30 km (about 900 km<sup>2</sup>) that conforms to the coverage of 1: 25000 topographic map, published by Department of Survey and Mapping Malaysia. As shown in Fig. 3.1, the study area mainly includes main part of Cameron Highlands district, Pahang state, and eastern part of Kinta District, Perak state. Small part of study areas are occupied by Gua Musang district, Kelantan state, and Batang Padang district, Perak state, which are located at the Northeastern and Southern of the topographic map respectively. The boundary coordinates of the study area are presented in Table 3.1 in

three formats namely, 1) RSO (Rectified Skew Orthomorphic) which is the projection system use for topographical mapping in Malaysia, 2) geodetic system and 3) Universal Transverse Mercator (UTM) system.

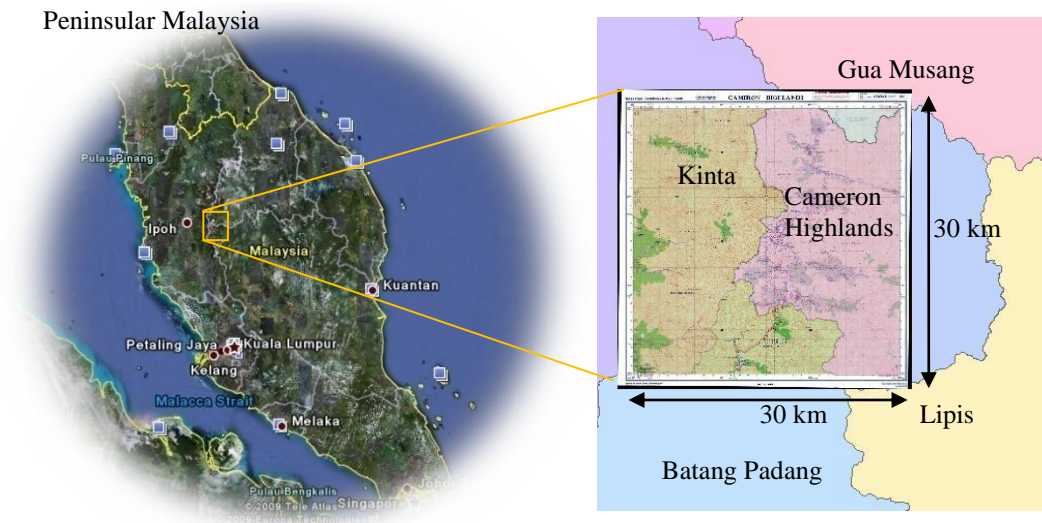


Fig. 3.1 Location of the study area

Table 3.1 The Coordinates of the study area corners

	Upper left coordinates		Bottom right coordinates	
RSO	X: 360000 m	Y: 510000 m	X: 390000 m	Y: 480000 m
Geodetic	$\lambda$ : $101^{\circ} 13' 48''$	$\phi$ : $4^{\circ} 36' 29.1''$	$\lambda$ : $101^{\circ} 30' 4.3''$	$\phi$ : $4^{\circ} 20' 16.4''$
UTM North 47	747417.5 E	509730.8 N	777615.51 E	479934.06 N

### 3.2.2 Topography, LULC and Soil of Cameron Highlands

The study area is located at mountainous terrain. The elevation ranges from 80 meter to 2100 meter. The lowest height is located at lower left of the map which is rubber plantation area located in Perak state. The highest elevation is at top of Mount Irau, followed by the top of Mount Berincang that is 2110 m and 2031 m above mean sea level respectively. The average height is 1108 meter indicating that the study area is deserved to be called as highlands area. About 60% of the total of study area is located at elevation above 1000 m.

According to slope classification by Omar, et al. [9], the slopes at the study area are mainly dominated by the critical slopes that range from  $20^{\circ}$  to  $35^{\circ}$  and occupies 47% of the total area. About 33% of the study area has moderate slopes that range from  $12^{\circ}$ - $20^{\circ}$  and  $20^{\circ}$ - $41^{\circ}$ . The remaining areas are considered as flat (18%) with slopes that range from  $0^{\circ}$ - $12^{\circ}$  and areas with the steepest slope (4%) that range from  $41^{\circ}$ - $88^{\circ}$ .

LULC of the study area is dominated by forest (92%) followed by cropland (7%) and built up (1%). The corresponding areas are 833.6 km<sup>2</sup>, 61 km<sup>2</sup> and 5.5 km<sup>2</sup> respectively. This information was extracted from topographic map constructed using aerial photo acquired in 1981. In recent condition, these portions of LULC have surely changed. Investigation performed by TNBHidro-Sdn.Bhd. [152] showed that the development of cropland and built up increased significantly. The number of open land and crop land has expanded significantly in Bertam and Telom catchments, two areas in Cameron Highlands. The increase of these two land uses implicitly means the decrease of forest areas.

The soil in Cameron Highlands is generally sandy and easy to erode as reported by Van der Ent and Termeer [216]. Having this soil type combined with critical slopes and high rainfall intensity, the potential of landslide occurrences in Cameron Highland becomes higher.

### **3.2.3 Climate of Cameron Highlands**

The annual rainfall of the study area is quite high ranging from 2412 mm to 3172 mm based on Malaysia Meteorological Department (MMD) data record acquired from 2000 until 2005 as shown in Fig. 3.2. The monsoon system plays an important role in controlling rainfall distribution. As explained by Guha [149], the Northeast monsoon that falls between November and January brings heavy rainfall over Malaysia, particular in the east coast of Peninsular Malaysia (PM). In the western part of PM, the rainfall intensity is lesser than that of the eastern part. Meanwhile, during the southwest monsoon period that falls between April and May, less rainfall occurred in PM compared to that of northwest monsoonal period. The hottest and driest days take

places during inter monsoon period. On the contrary, heavy rainfall with high intensity takes place in the northern part of PM.

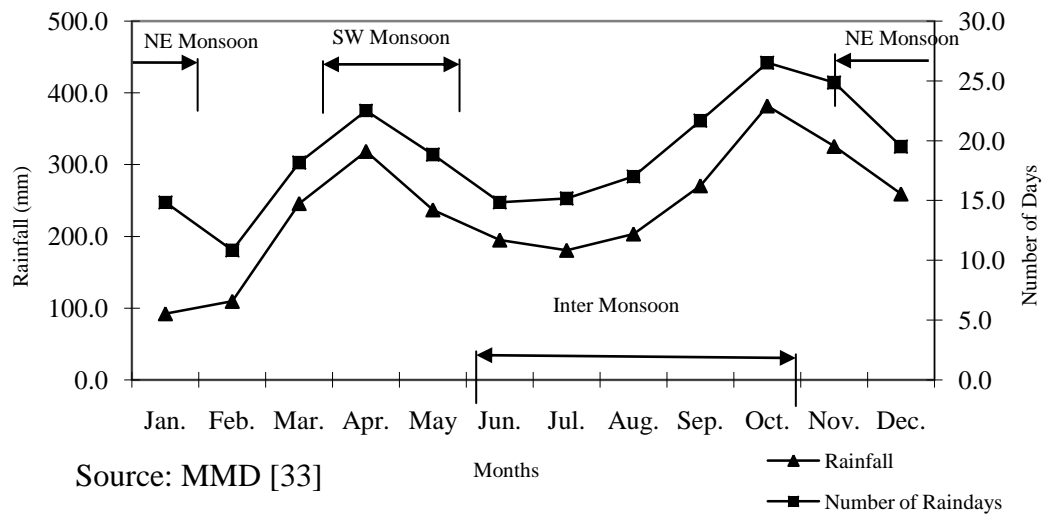


Fig. 3.2 Monthly averaged rainfalls of Cameron Highlands (2000-2005)

Comparison between rainfall data of MMD and monsoonal periods shows that the peak of heavy rainfall started early before northeast monsoon period. The rainfall intensity starts to increase from September and decreases on January. The intensity of rain reaches its peak on October as indicated by the maximum number of rain days by 26.5 days per month averaged over 5 years of rainfall data. As the consequence, the amount of rainfall in October, which is 381.6 mm, is the highest one for the entire year. During southwest monsoon, the rainfall intensity reaches its peak on April with 22.5 rainy days and 318.3 mm rainfall amount. This number is slightly smaller compared to that of northeast monsoon period. There are two driest seasons which takes place during inter monsoon periods indicated by low rainfall intensities. The peaks of these seasons occur on February and June and the rainfall intensities are 117.6 mm and 141.8 mm respectively. Meanwhile, there is an agreement between monthly rainfall amount and the number of rainy days.

The temperature range is 14.5<sup>0</sup>C (minimum) - 22.4<sup>0</sup>C (maximum) according to the data from Worldclimate [217] averaged from 1966-1975. This area is also called cloud forest due to the existence of mountains intercepting circulation of air, forcing it upward where it cools and water vapor condenses into cloud. The clouds that

frequently exist in the study area cause a problem in data acquisition using optical remote sensing technique.

#### **3.2.4 Geology of Cameron Highlands**

The geology of the study area mainly consists of granite. The primary granite type is acid intrusive granite formed in the Late Triassic period. The granite is divided into a medium to coarse grained, porphyritic, biotite granite as mentioned in Van der Ent and Termeer [216]. The porphyritic biotite granite is found abundant in the study area. The conditions of granite rocks vary. Some of them are covered with sandy soil mixed with peat; some are studded with Granite boulders; and some are covered with loamy soils and beds. Granite looks decaying in some places with colors vary from deep red, yellow to almost white. The color of the weathered overlying soil also varies from deep red, light yellow and pink. Along fresh cut slope, the different color of weathered underlying soil. Discontinuity exists within granite rock that ranges from 0.3 to 1 meter.

Alluvium rock type also exists in the study area. This rock type consists of deposit of clay, silt and sand left by flowing water in a river valley or delta. This type of rock typically produces fertile soil. Another existing rock type is Schist, a kind of metamorphic rocks. In the study area, schist is the oldest rock. It was intruded by granite so that schist is normally situated at the upper part of lithological boundary. A detail explanation of geology of the study area can be found in Bakar and Madun [218] and Jamaluddin [219]. There is *undifferentiated* which is described in geology map as sedimentary rock.

#### **3.2.5 Landslide Occurrences in Cameron Highlands**

The main source of landslide occurrences record was obtained from Malaysian Public Work Department (Jabatan Kerja Raya, abbreviated as JKR) report documented in JKR [220]. Table 3.2 shows the summary of landslide occurrences in Cameron Highlands from 1961 to 2007 and the corresponding rainfall intensity. The number of

road related landslide is higher (57%) compared to non-road related one (43%). A more meaningful illustration on relationship between landslide and rainfall intensities is already shown in Fig. 1.3 of Chapter 1. Starting from November to January, high intensity of rainfall driven by Northeast monsoon is followed by the high number of landslide occurrences. Meanwhile, during southwest monsoon with lower rainfall intensity than that of northeast, the number of landslide occurrences is lower as well. On July and August which are the hottest and dries months, there are no landslide occurrences.

Table 3.2 Number of landslide occurrences in Cameron Highlands (1961-2007)

Month	Landslide Occurrence Number	Monthly Average Rainfall (mm)		Landslide Type	
		Malaysia	Cameron Highlands	Non-road related	Road related
Jan	5	92.1	141.8	2	3
Feb	1	109.3	117.6	0	1
Mar	1	245.6	200.8	1	0
Apr	2	318.3	289.8	1	1
May	3	236.8	260.5	2	1
Jun	3	194.8	157.8	0	3
Jul	0	180.5	141.8	0	0
Aug	0	203.2	171.8	0	0
Sep	1	270.4	240.8	1	0
Oct	10	381.6	340	5	5
Nov	6	325.2	316.5	2	4
Dec	5	258.9	222.4	2	3
Total	37		Total	16	21
			Percentage (%)	43	57

Source: JKR [13]

Among the areas that experiencing landslide events according to JKR [13] and Chan [148] record are Tanah Rata/Brinchang (6 cases), Ringlet (3 cases), Tapah-Cameron Highlands road (8 cases), Kampung Raja (2 cases), Tringkap (1 case), Kuala Terla (5 cases), Lata Iskandar (1 case), Blue Valley (1 case), Simpang Pulai-Cameron Highlands (5 cases) and Gua Musang-Cameron Highlands road (1 case). According to Chan [148], landslides in Ringlet (1961), Kampung Raja (1966) and Tanah Rata-Brinchang road (200) are considered as the killing landslide that killed 16 people for the first case and 6 people for the last 2 cases. Meanwhile, a landslide at

Pos Selim, located at Simpang Pulai-Kampung Raja road near Perak-Pahang boundary, was considered as a big massive landslide occurred in 1999 with wide coverage. There were no people killed but the total economic loss costs about RM 354.6 million. The total cost includes such as fatalities, injuries, distance related transportation cost, time related transportation cost, time related productivity cost, and restoration cost. Fig. 3.3 shows two conditions of landslide at Pos Selim at KM33 of Simpang Pulai Kampung Raja road recorded in 2001 and 2006.

### **3.2 Hardwares and Softwares**

Garmin E-Trex V and Garmin iQue® 3000 PDA GPS (see Fig. 3.4) were used to record landslide locations during field surveys carried out on 6 December 2006 and 4 May 2008 respectively. A pocket camera was used to capture current and past landslides objects. One unit of computer with high speed processor and video graphic was used for image processing and GIS analysis. Softwares used in this research mainly consisted of Image Processing softwares namely, ER Mapper® 6.4, and GIS software namely AutoCAD Land Development 2004, ArcView® 3.2a, ArcGIS® 10. MapSource® was used to download and display GPS data of landslide locations.

### **3.3 Source of Spatial Data**

The main data used in this research are shown in Table 3.3. The data came with various format and scale and originated from different sources. The detail description of each data is explained in the following sections.

Some of these data were used to derive spatial data, i.e. landslide causative factors, required for landslide susceptibility modeling. These data include topographic map, Landsat 7 ETM+ images, geology map, and soil map. The discussion of derivation of landslide causative factors is given in section 3.4.

Table 3.3 Data source for deriving landslide causative factors

Data	Format	Scale	Source
Topographic map	Analog and digital maps	1 : 25,000 1 : 50,000	Department of Survey and Mapping Malaysia (DSSM) or JUPEM
SPOT 5 image	Digital	-	Malaysia Remote Sensing Agency (ARSM)
Landsat 7 ETM+ images	Digital	-	Malaysia Remote Sensing Agency (ARSM) and EROS- USGS at <a href="http://glovis.usgs.gov/">http://glovis.usgs.gov/</a>
Soil map	Analog map	1: 1,500,000	European Soil Portal at <a href="http://eusoils.jrc.ec.europa.eu/">http://eusoils.jrc.ec.europa.eu/</a>
Geology map	Analog map	1: 250,000	Minerals and Geoscience Department Malaysia
Rainfall data	Digital	-	Malaysian Meteorological Department (MMD)
Landslide map	Digital map	-	Malaysia Remote Sensing Agency (ARSM) reported in Pradhan and Lee [12]

### 3.3.1 Topographic Map-Derived Spatial Data

The topographic map used was the map with the following particular information: sheet No. 3662, series No. L7030, published as second edition in 1994, and scale of 1:50,000. This map was obtained from DSMM or known as JUPEM (Jabatan Ukur dan Pemetaan Malaysia) in hard copy/analog format. According to the information on the map legend, the map was constructed based on aerial photographs taken in 1981. The road network on the map was updated in 1994 by DSMM. The digital version of the map was available at scale 1:25,000.

Topographic map had two functions. The first, it served as a base map from which landslide causative factors were derived. The second was as a reference map to rectify all satellite images. The first was the function of digital topographic map and the second was the function of analog topographic map after being geometrically corrected. There were six landslide causative factors derived directly and indirectly from topographic map. Road and river/lake maps were directly extracted directly



from the digital topographic map by separating these two layers from the map. Maps of slope, slope aspect, curvature and elevation were indirectly derived from the digital map through DEM. DEM was first generated from contour map extracted/digitized from the corrected map. Once a scanned topographic map has been geometrically corrected, it can be used as a reference map to rectify any remote sensing images. SPOT image was rectified using the corrected topographic map. Derivation of spatial data from topographic map is illustrated in Fig. 3.12 and discussed in detail in section 3.4.

### **3.3.2 SPOT 5 Satellites Data**

SPOT 5 satellite image was mainly used for providing a reference/corrected satellite image to rectify all Landsat images using image-to-image registration and for updating road map which was first extracted from the topographic map. Detail discussion of rectification process is described in section 3.4. The main updated road was the road connecting Simpang Pulai and Kampung Raja. Based on the first purpose, a good SPOT 5 image with minimum cloud coverage with a good contrast was selected. Below is the particular of the image:

- Date of acquisition : 19 April 2005
- Path/Row : 268/341
- Cloud cover (%) : 5%
- Projection system : UTM (Universal Transversal Mercator)
- Time of acquisition : 3:16 GMT or 11:16 AM in local time
- Number of bands : 4 bands

With such a time of acquisition, when the sun is almost at the zenith, the energy of the sun is sufficient to provide a good contrast of the acquired image and it provides minimum shadowing effect caused by cloud. The preview of SPOT 5 satellite image is shown in Fig. 3.5. The area of study is indicated by a square of 30 km x 30 km.

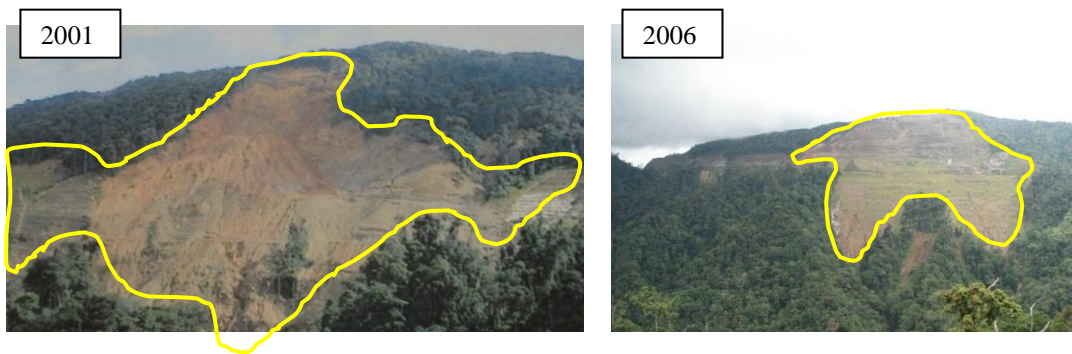


Fig. 3.3 Different conditions of landslide at Pos Selim



Fig. 3.4 Handheld GPS device for data collection

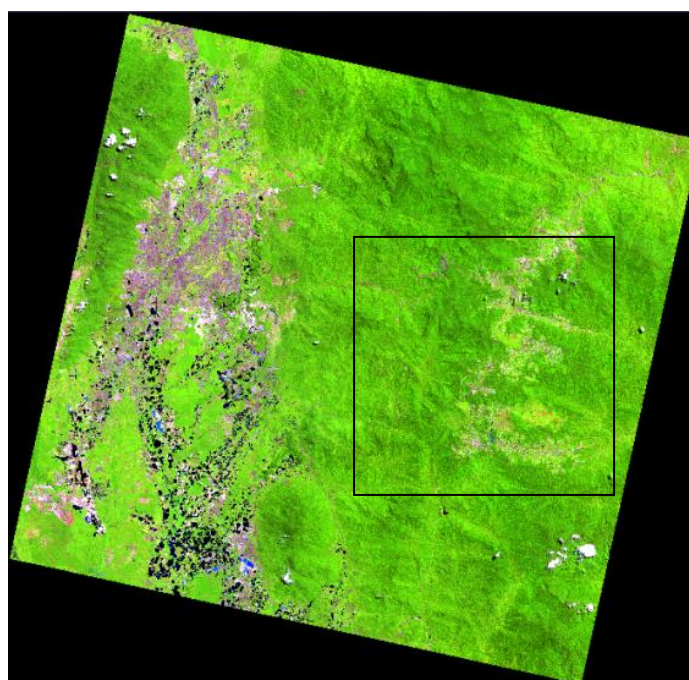


Fig. 3.5 Preview of SPOT 5 image

### **3.3.3 Landsat 7 ETM+ Satellite Data and Strategy of Data Selection**

All Landsat data used in this research is from the same path/row index that is 127/057. Landsat data were used to derive LULC and multi temporal factors of, NDVI, soil wetness, and LST. Since the objectives of the study are to model susceptibility taking into accounts the multi temporal factor due to monsoonal rainfall and hence, the evaluation of the temporal factors at once, a careful data selection was undertaken. There were four Landsat images to select in accordance to the peak time of two rainy and dry seasons.

The selection of Landsat images was based on the following conditions:

1. Landsat images were required to represent monsoonal rainfall cycle as much as possible. It means that the time of images acquisition should be the same as the peak time of rainy and dry seasons of Cameron Highlands annual rainfall cycle.
2. Landsat images with SLC (the Scan Line Corrector)-on mode were selected. This means the images taken after 31 May 2003, were omitted. The images taken from September 1999 until 31 May 2003 were available to select. Those with SLC-off mode were not selected due to the presence of instrumental errors.
3. Landsat images with minimum cloud cover/haze and offered by EROS as free downloadable images were selected.

Calling back monsoonal rainfall cycle of Cameron Highlands which is shown in Fig. 3.6, it can be highlighted that there are two pronounced rainy (shown in solid lines) and dry seasons (shown in dashed lines). Peak times of rainy seasons occurred in April and October while those of dry seasons occurred in February and June. Based on these peak times and requirements to meet conditions number 2 and 3 mentioned above, four Landsat images were identified and shown in Table 3.4. The selection of 4 images that corresponds to two peak time of rainy and dry seasons was intended for first, to limit the volume of research work, and the second is to ensure to produce distinctive maps representing different conditions of rainfall cycle.

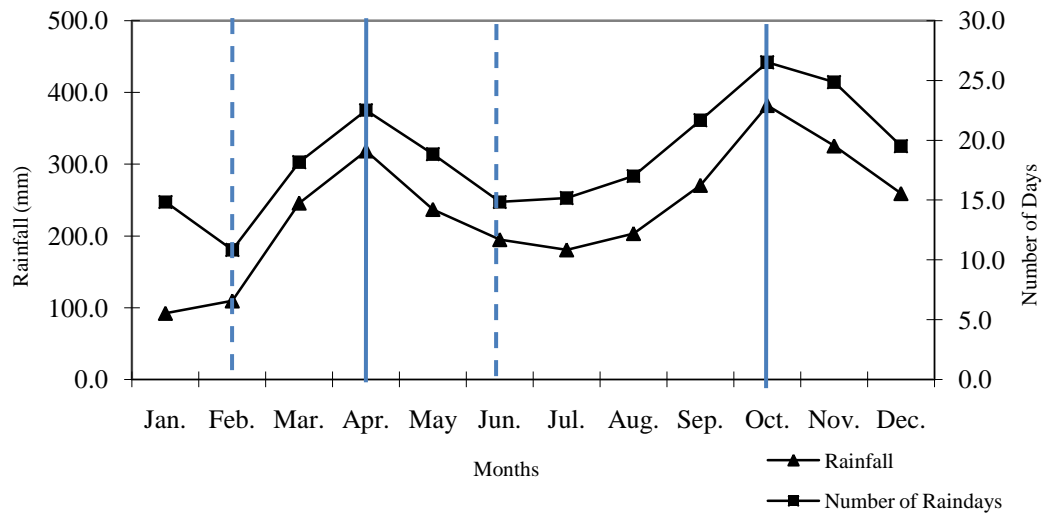


Fig. 3.6 Identified peak time of rainy and dry seasons for Landsat data selection

Table 3.4 Selected Landsat 7 ETM+ images

No	Peak time of Rainfall cycle	Seasons	Dates of possible Landsat 7 images	Cloud cover
1	February	Dry	24 February 2001	22 %
2	April	Rainy	31 May 2001	19%
3	June	Dry	19 June 2002	25%
4	October	rainy	20 September 2001	13%

Selection of desired Landsat data encountered some problems and seemed to be unsatisfactory. The problems were mostly due to the availability of the image of interest that matched with peak times of both seasons and the status of ‘not free to download’. Sometimes, the images were unavailable with no further explanation from the image provider. Cloud cover and short period of SLC-on mode have been limitations to get the desired images. The author concerned to have all images available in a year in so that all multi temporal data have a common time frame, more particularly in the same year. This is to avoid different behavior of rainfall cycle due to the global climate change issue. However, that was not the case. Year 2001 contains good and nearly complete data availability. For the first dry season on February, Landsat data was available. There was no data on April, the first rainy season. Landsat data acquired on May was selected for the replacement. The same case went to the second rainy second on October. Landsat image taken on September

was selected as the replacement. Meanwhile, there was no image on June, the second dry season. As the replacement, the image acquired on the same month in 2002 was chosen. All selected Landsat images are shown in Fig. 3.7. A rectangle on each image indicates the study area.

As mentioned previously, there are four spatial data that can be derived from Landsat images that are LULC, NDVI, soil wetness and LST. Band 1-5 and 7 were used to extract land use land cover map through image classification and perform Tasseled Cap Transformation to produce soil wetness map. Band 3 (visible red) and 4 (near infra red) were used to produce NDVI map. Band 6, either low or high gain mode, was used as the main data for generating LST map. In addition, the original projection system of these data is in UTM. For further utilization, these images are required to be tied down to a local projection system using rectification process.

### **3.3.4 Soil Map**

Soil is defined in Mulders [221] as natural bodies, each with a unique morphology resulting from a unique combination of climate, living matter, earthy parent materials, relief and age of landform. Soil map may show level of weathered and types of material composing soil. The more weathered soil composing materials the more likely to slide slopes covered with that particular soil composing materials. In addition, soil can be composed from strong or weak material according to Mohr's scale of hardness. Hence, soil map is one of important landslide causative factors.

The soil map is available at a small scale that is 1:1,500,000. This data was obtained from European Digital Archive of Soil Maps as the works conducted by Selvaradjou, et al. [222] which was sponsored by Soil Science Division, Ministry of Agriculture Malaysia. The map is available online and can be reached at <http://eusoils.jrc.ec.europa.eu/>. Preview of soil map of PM and portion of CH are shown in Fig. 3.8.

In order to be used in landslide susceptibility modeling, soil map is required to have the same projection system as topographical map. It was done through



rectification process. The rectification procedure of the soil map is discussed in section 3.4.

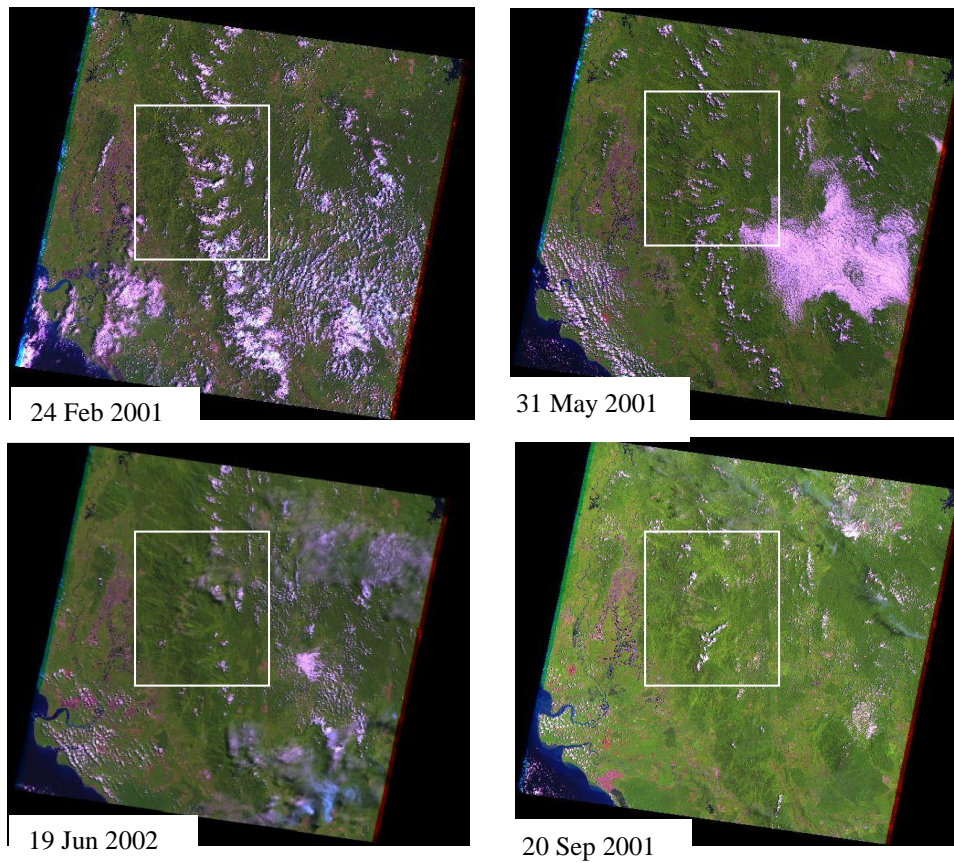


Fig. 3.7 Selected Landsat 7 ETM+ satellite images

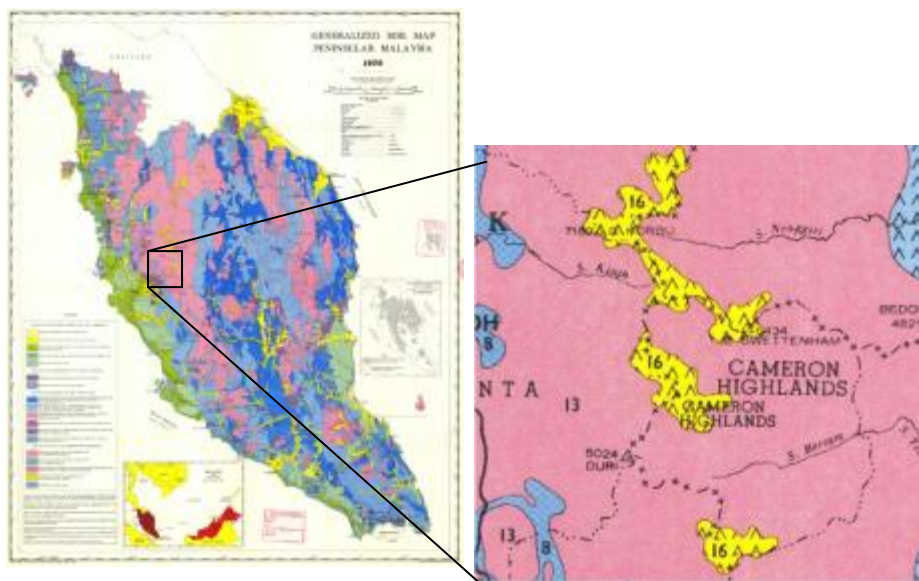


Fig. 3.8 Soil map of PM and CH

### 3.3.5 Geology Map-Derived Spatial Data

Geology of Perak and Pahang maps were obtained from Minerals and Geoscience Department Malaysia, at Perak state branch. The area of study is separated into two sheet maps as shown in Fig. 3.9a and Fig. 3.9b. The map consists of lithology (rock types) and lineaments (fault). For Pos Selim and Tanah Rata areas, more detail geology maps of works of Bakar and Madun [218] and Ramli, et al. [93] were added into the existing geology map as shown in Fig. 3.9c and Fig. 3.9d. Meng [223] reported that there are eight major faults of Peninsular Malaysia. One major fault crosses Cameron Highlands area namely Bentong Suture fault. Minor faults exist in the study area.

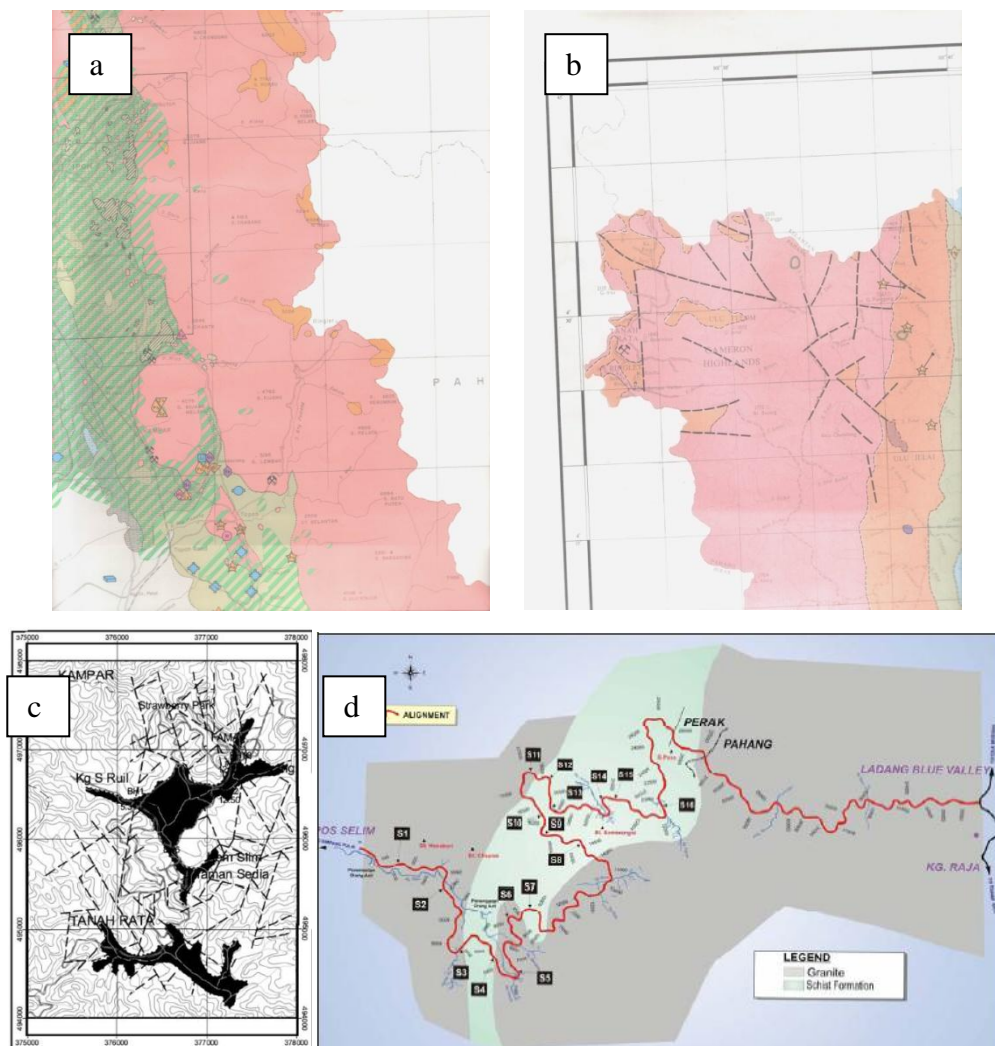


Fig. 3.9 Source of geology maps of the study area

All geology maps shown in Fig. 3.9 were scanned from their original hardcopy format. For further use, these maps were required to be rectified to the local projection system. The rectification enables all maps to be joined together. Rectification of these maps is discussed in section 3.4.

### 3.3.6 Rainfall Data

The rainfall data is not a map but time series of rainfall data recorded at Tanah Rata weather station. The data was provided by Malaysia Meteorological Department. The rainfall data spans from 2000-2005 and available as monthly average rainfall. The graph of rainfall data is shown in Fig. 3.10 and the rainfall data is presented in Appendix A.

Rainfall data was used for month by month comparison between landslide occurrences and rainfall intensity as portrayed in Fig. 3.11 (rainfall versus landslide occurrences in PM) and Fig. 1.3 (rainfall versus landslide occurrences in Cameron Highlands). Yearly average rainfall data was used to select Landsat data as discussed in subsection 3.3.3.

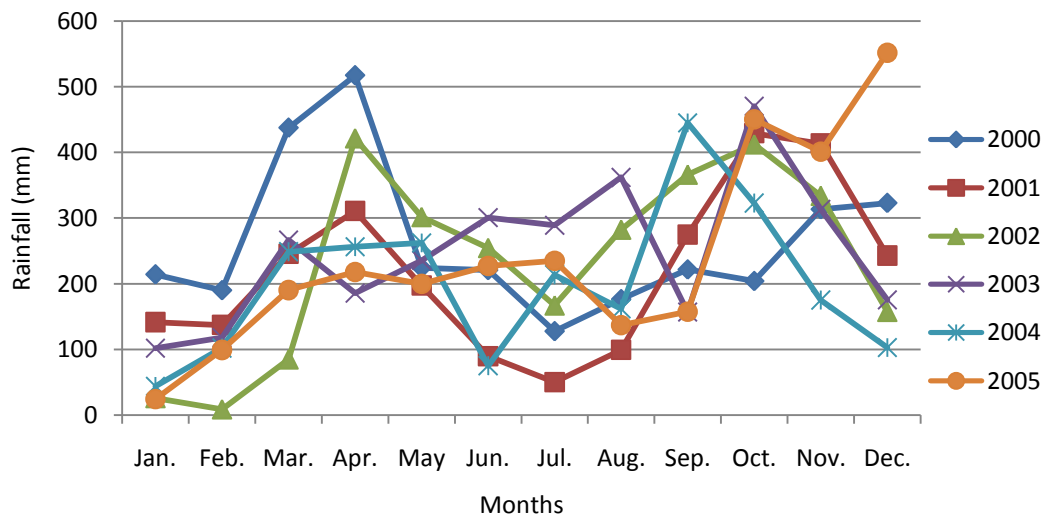


Fig. 3.10 Rainfall data at Tanah Rata, Cameron Highlands



### 3.3.7 Landslide Inventory map

Landslide map has two functions namely for use in deriving spatial relationship between landslide causative factors and past landslide occurrences and in validating the final landslide susceptibility map. Detail information of these data source is explained in the following.

Landslide inventory map consists of location of landslides or slope failures regardless the magnitudes. The map was constructed from two sources. The first was from site surveys of landslide and slope failure locations using handheld GPS device which were carried out twice, in 6 December 2006 and 6 May 2008. The second was landslide map issued by ARSM as reported in Pradhan and Lee [12]. This map was constructed from image interpretation of aerial photographs taken from 1981-2002, SPOT 5 panchromatic images, and landslide report over 21 years. Liao [47] identified that creating a landslide map from image interpretation has disadvantageous that may lead to errors during processing. Landslide scarp may be difficult to differentiate with barren land or cut slope.

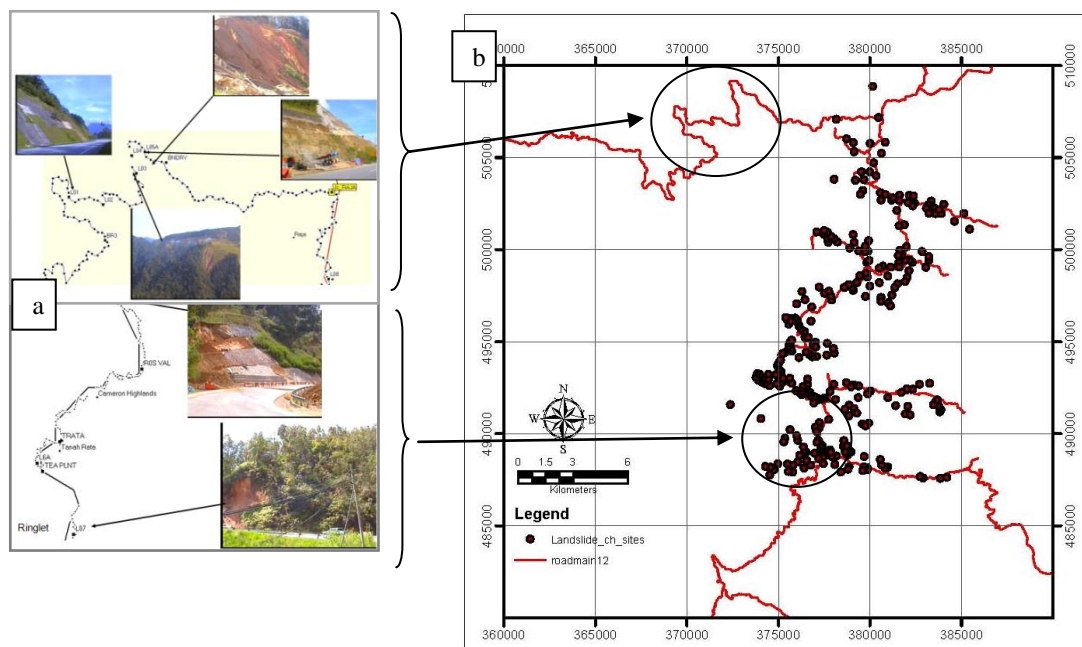


Fig. 3.11 Source of landslide map: a) site survey, b) the map from ARSM

Two sources of landslide map are shown Fig. 3.11. Fig. 3.11a shows GPS tracks along Simpang Pulai to Kampung Raja (upper image), Kampung Raja to Ringlet (lower image), identified landslide/slope failure locations and the corresponding pictures. Fig. 3.11b shows landslide map issued by ARSM.

The coordinates of landslide/slope failures gained from site survey were already in local projections system that is RSO. Meanwhile, the landslide map was available in digital format with no projections system. A rectification process was then required in order to be compatible with field data and other spatial data. Data processing for rectification of landslide map and preparation of landslides locations layer are explained in section 3.4.

### **3.4 Data Processing and Derivation**

Data processing at this stage is intended to process all relevant data sources listed in Table 3.3 to produce landslide causative factors. There are ten ‘static’ causative factors (shown in grey boxes) and three multi temporal factors (shown in black boxes) produced from data sources. The overview of data source and the associated derivative spatial data are illustrated in Fig. 3.12. Briefly, data processing was begun with description of RSO projection system and provision of corrected digital topographic map through rectification process. RSO was set as the projection system. A number of spatial data (landslide causative factors) were derived from the corrected topographic map. The map was also used as a reference map using which other spatial data were georeferenced. The following sections describe the detail process of derivation of spatial data.

#### **3.4.1. RSO Reference System**

The projection system used for all spatial data in this work is RSO, Rectified Skew Orthomorphic, which is based on MRT (Malayan Revised Triangulation) geodetic reference system. This is an oblique Mercator projection as explained in Kadir, et al. [224] that provides optimum solution for topographical mapping in Malaysia in the

sense of minimizing distortion and maintaining conformal. The scale factor varies from 0.99984 to 1.0016 that leads to maximum scale distortion of 1:6250. The detail information of RSO projection parameters can be found in Appendix B. The RSO projection system for Peninsular Malaysia has different parameters compared to the one for Sabah Serawak area. Fig. 3.13 shows RSO projection parameters specified in ArcGIS environment.

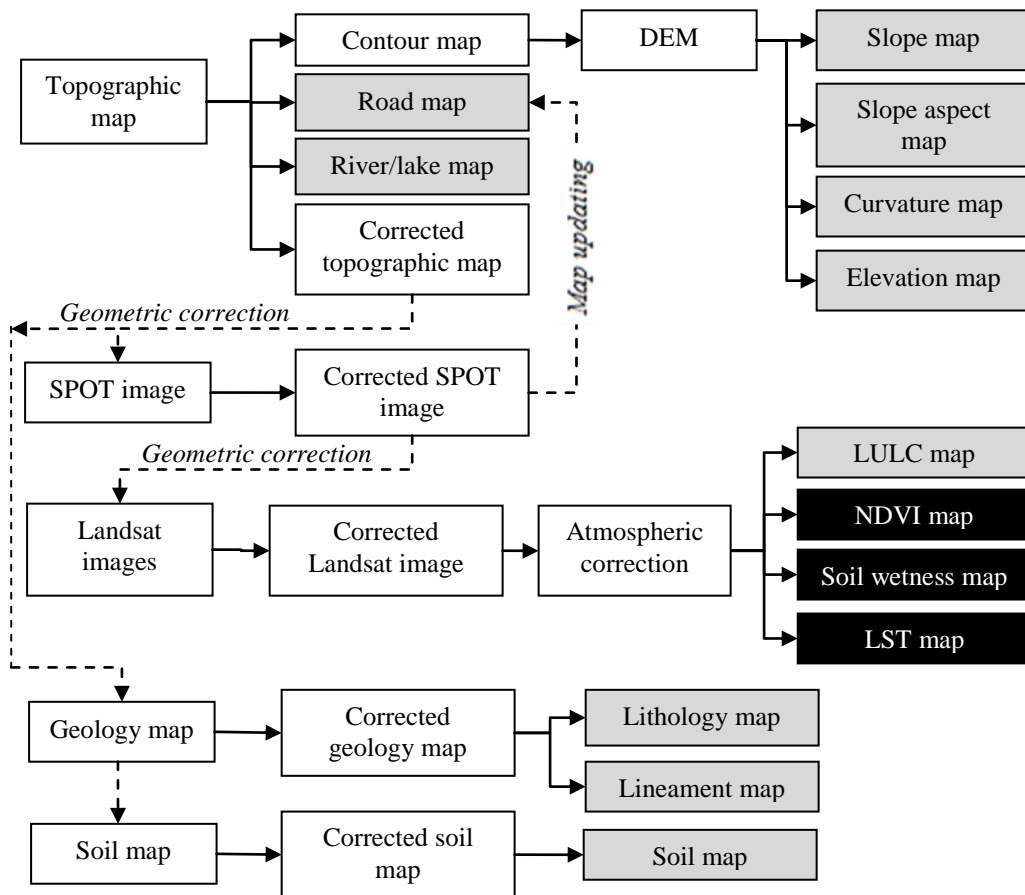


Fig. 3.12 Derivation of spatial data for landslide susceptibility modeling

The spatial data came in different or with no projection systems. Spatial data derived from digital topographic map such as contour, DEM, slope, slope aspect, curvature, road network, river lake maps have coordinate extents in RSO system. However, RSO system has not been assigned to those data. Less work was needed to make these data in RSO system. In ArcGIS, RSO parameters were assigned to these spatial data. Satellite images (i.e. Landsat 7 ETM+ and SPOT 5 images) came in UTM (Universal Transverse Mercator) projection. Rectification process was applied

to these data to convert their projection systems into RSO system. Scanned geology and topographic maps had no projection systems. The scanned topographic map was the first map to rectify to RSO system. Having this map rectified, it served as a reference image for rectifying other spatial data such as satellite images, geology, and soil maps.

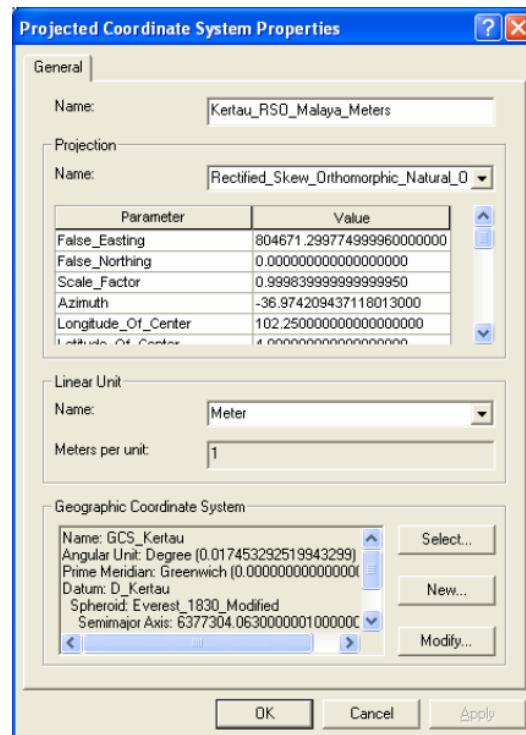


Fig. 3.13 RSO projection parameters defined in ArcGIS environment

### 3.4.2. Digital Elevation Model (DEM)

DEM is a raster representation of continuous surface, usually referencing the earth surface. DEM is a 3D surface which is usually derived or calculated using specially designed algorithms that sample point, line or polygon data and convert them into a digital 3D surface. There are three type of surface models namely, TINs (Triangulated Irregular Networks), raster, and terrain surfaces. The first surface illustrated in Fig. 3.14 was selected for the first conversion product of contour line map to 3D surface.

In this research, the contour line data was split from the digital topographic map using AutoCad Land Development software. Major and minor contour lines were

selected and saved into an individual file. Using ArcView software, the contour line map was converted into a polyline shape file (\*.shp), one of the vector formats in which the data was stored. The contour layer was converted into TINs surface using 3D Spatial Analyst of ArcGIS environment. The algorithms triangulated points at contour lines which were treated as vertices. The vertices were connected with a series of edges to form a network of triangles. The resulting triangulation should meet the Delaunay triangle criterion requiring that no vertex lies within the interior of any of the circumcircles of the triangles in the network. The detail explanation in regard to TINs concept can be found in ESRI [63]. Fig. 3.15 shows the contour line and its TINs surface of the study area.

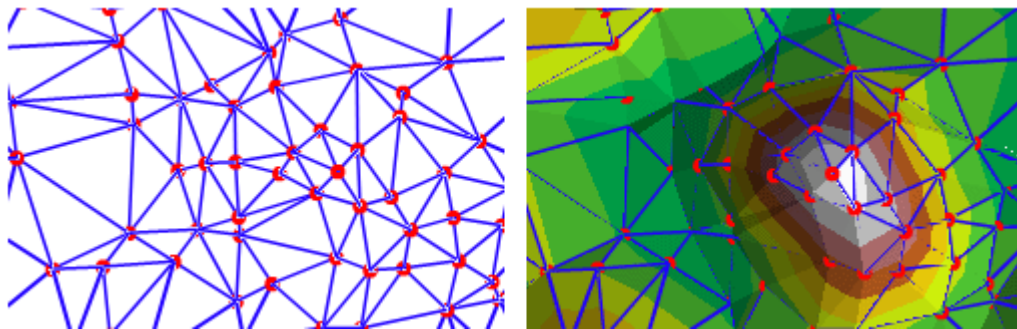


Fig. 3.14 TINs surface

### 3.4.3. Elevation

Elevation has a role in slope instability. The higher the location the stronger the gravitational force acting on a mass body. In ArcGIS, elevation is a raster surface model. Elevation of points can be extracted directly once 3D surface has been created. Either TINs or raster surface provides elevation data at fixed points with the help of interpolation methods such as Inverse Distance Weighted, Spline, Kriging, and Natural Neighbors. The detail of these methods can be found in ESRI [63]. Elevation layer is the product of conversion of TINs surface into grid/raster format. There is no difference elevation value at a given location in both surface formats. Fig. 3.16 portrays a raster surface (elevation) with 30 x 30 meter square pixel size.



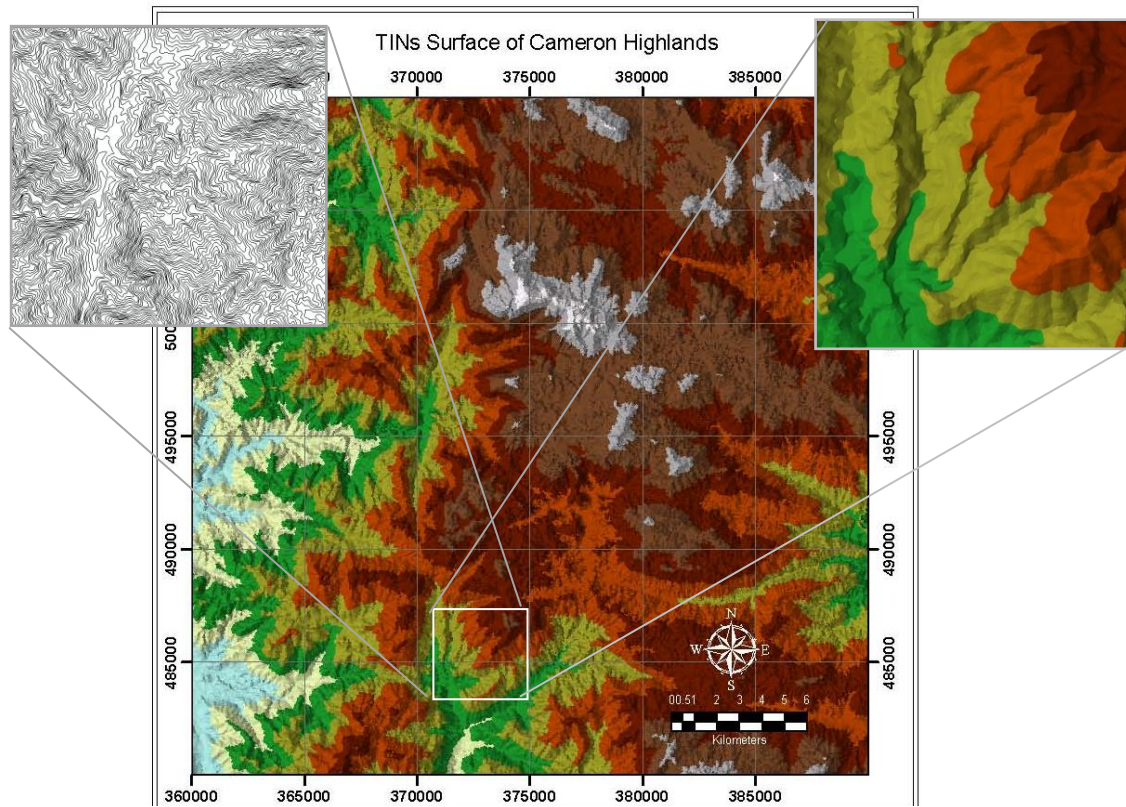


Fig. 3.15 Contour lines and TINs surface

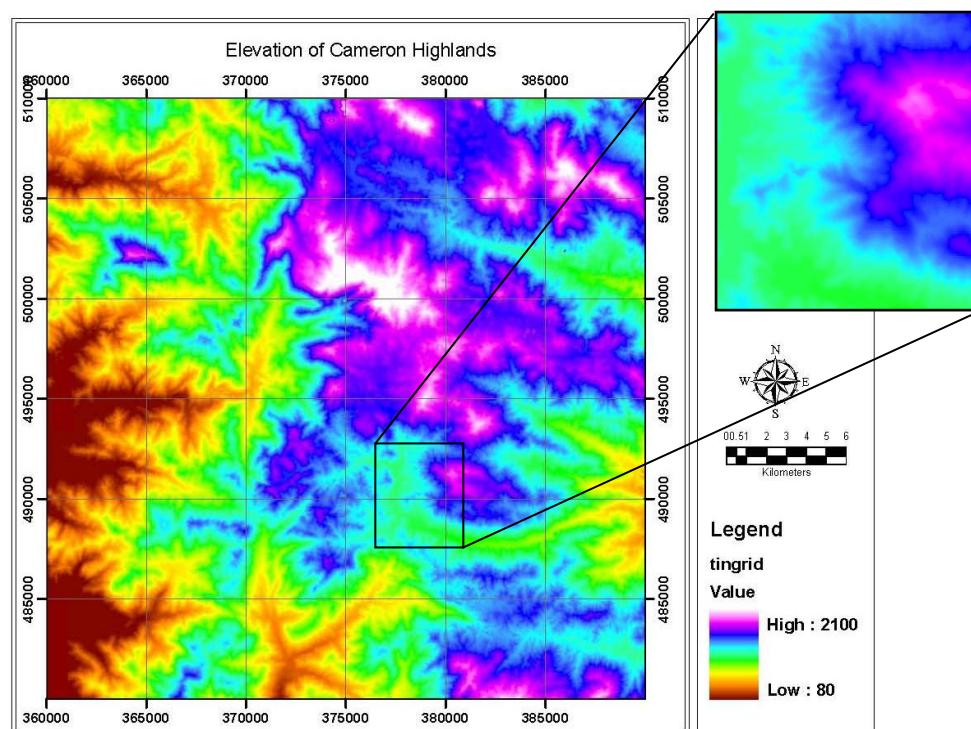


Fig. 3.16 Raster surface of part of the study area

The selection of this resolution is intended to conform to that of band 1-5 and 7 of Landsat images. Table 3.5 shows the distribution of elevation at the study area after being classified into five classes using natural break method. About 70% of the study area is above 900 meter and the average height is 1106 meter. These facts confirm why this place is called a highlands area.

Table 3.5 The distribution of elevation at the study area

Elevation (m)	Area (km2)	%
80 - 600	93	10.3
600 - 924	190	21.2
924 - 1200	213	23.7
1200 - 1452	227	25.3
1452 - 2100	175	19.5

#### 3.4.4. Slope

The steepness of the slope plays an important role in slope stability. Slope map can be derived either from each triangle in TINs or each pixel in raster surface. For a given cell/point, slope is computed based on elevation values of its eight neighbor cells. The slope function fits a plane to the z-values of 3x3 cell neighborhood around the processing or center cell (Fig. 3.17a). The slope value of this plane is calculated using the average maximum technique as described in ESRI [63]. The direction of the plan faces is the aspect for the processing cell. The output slope raster can be either in degree or percent (called ‘percent rise’) unit. Fig. 3.17b illustrates slopes in degree and rise. The lower the slope value the flatter the terrain; the higher the slope value the steeper the terrain. In this research, the unit in degree was chosen.

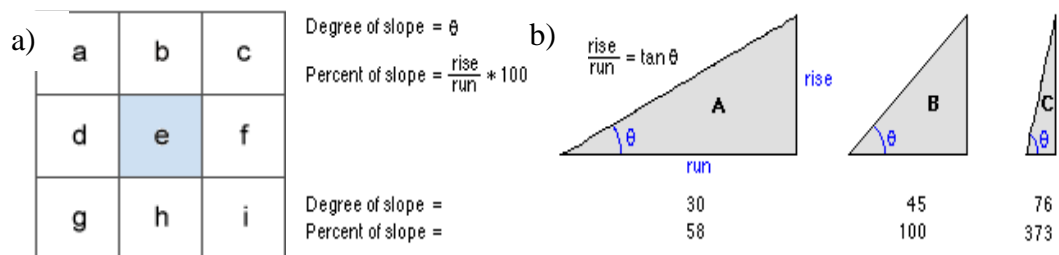


Fig. 3.17 a) A 3x3 neighborhood cells for slope computation, b) slope in degree and rise (Source: ESRI [63])

The rate of change (delta) of the surface in the horizontal (dz/dx) and vertical (dz/dy) directions from the center cell determines the slope. Referring to Fig. 3.17a, the rate of change of center cell 'e' is determined by the values of cell 'a' to 'i'. The rate of change in the x and y directions for cell 'e' are computed using equations described in ESRI [63] as follows:

$$[dz/dx] = ((c + 2f + i) - (a + 2d + g)) / (8 * x\_cell\_size) \quad (3.1)$$

$$[dz/dy] = ((g + 2h + i) - (a + 2b + c)) / (8 * y\_cell\_size) \quad (3.2)$$

The slope is calculated using the following equation described in ESRI [63]:

$$\text{slope\_degrees} = \text{ATAN} ( \sqrt{ ([dz/dx]^2 + [dz/dy]^2 ) } ) * 57.29578 \quad (3.3)$$

The slope map of the study area is shown in Fig. 3.18. The slope unit is in degree. Each slope cell represents an area of 30 x 30 meter square. The distribution of slopes is shown in Table 3.6 after the slopes classified into 5 classes using natural break method. Moderate slopes dominate the study area (31%) followed by shallow slopes (25%). Steep and the steepest slopes cover about 29% of the area while the remaining area is flat slope that occupies 15% of the area. The names of slope criteria were adopted from Berset and Sangakkara [225].

Table 3.6 The distribution of slope at the study area

Slopes (degree)	Area (km2)	%	Slope criteria
0 – 7.6	134	15	Flat
7.6 – 19.6	222	25	Shallow
19.6 – 27.6	280	31	Moderate
27.6 – 37.6	198	22	Steep
37.6 – 89.6	67	7	Extreme steep

### 3.4.5. Slope Aspect

There is an assumption stated by DeGraff and Romesburg [62] that slopes facing the sun, especially the afternoon sun, tend to have higher soil temperature, lower soil moisture, less vegetation and hence, more erosion could possibly take place. In this research, slope aspect is included as a landslide causative factor.



Slope aspect is the direction that a slope faces. Slope direction is commonly known as the compass direction of a hill faces. It can be calculated for each triangle in TINs and for each cell in raster. Slope aspect is measured clockwise in degree from 0, towards North, to 360, towards North again, forming a full circle. The direction of each cell's slope face is indicated by the slope aspect value. For flat areas, the directions are given a value -1. Fig. 3.19 shows a compass direction, an input elevation dataset and the output slope aspect in raster format.

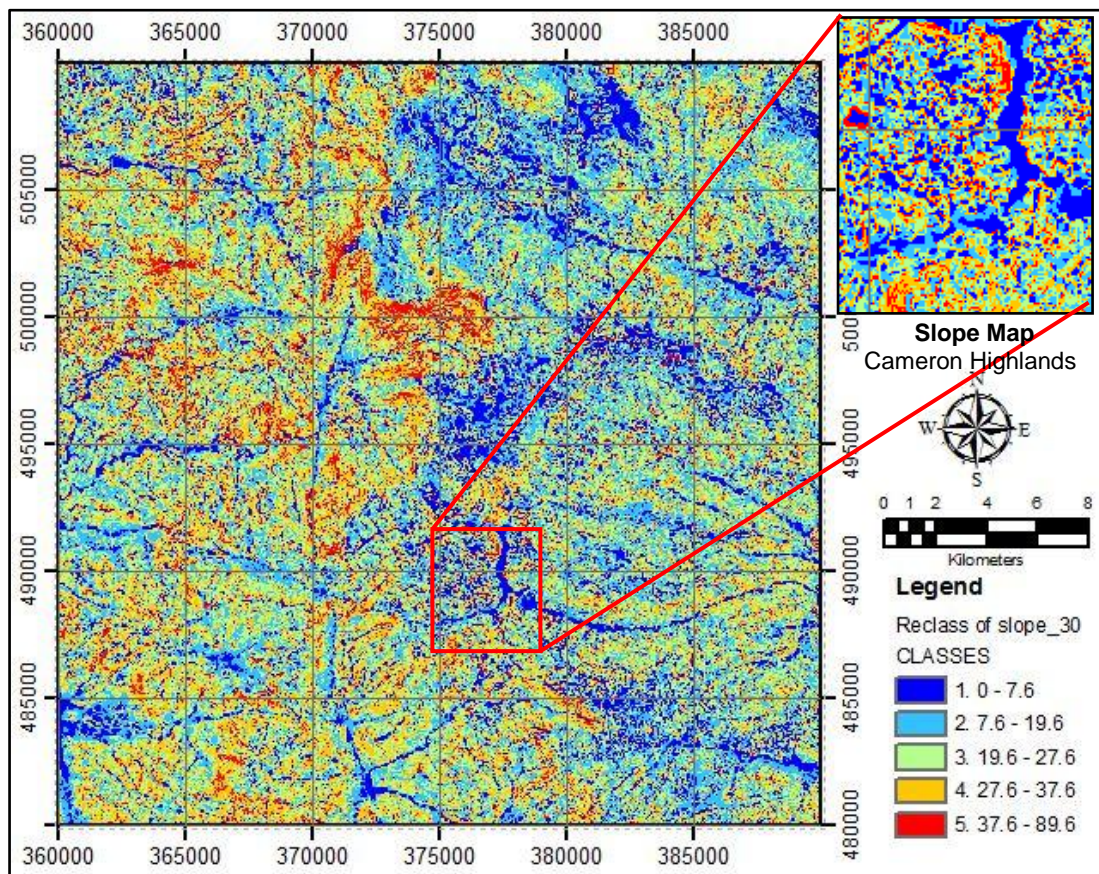


Fig. 3.18 Slope map of the study area

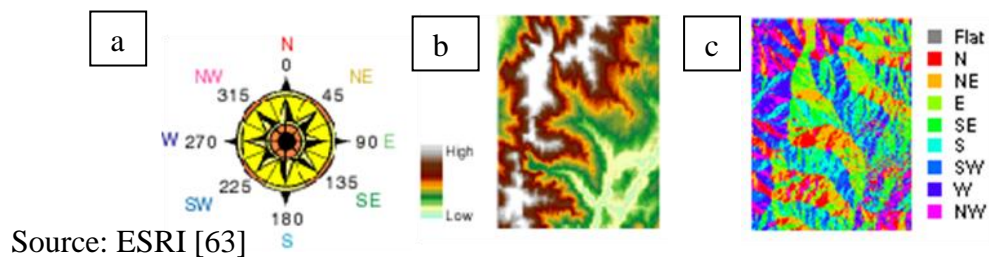


Fig. 3.19 a) compass direction, b) elevation (input), c) slope aspect (output)

Conceptually, the slope aspect function fits a plane to the z-values of a 3 x 3 cell neighborhood around the processing or center cell. Using a moving 3 x 3 window, it visits each cell in the input raster. For each cell in the center of the window (the same illustration as in Fig. 3.17a), an aspect value is calculated using an algorithm that incorporates the values of the eight cell, cell 'a' to 'i', surrounding the center cell, 'e'. The procedures of calculating slope aspect are explained in ESRI [63] as follows:

1. Calculation of the rate of change in the x and y direction for cell 'e' using the following algorithm:

$$[dz/dx] = ((c + 2f + i) - (a + 2d + g)) / 8 \quad (3.4)$$

$$[dz/dy] = ((g + 2h + i) - (a + 2b + c)) / 8 \quad (3.5)$$

2. Calculation of aspect values using the following algorithm :

$$\text{aspect} = 57.29578 * \text{atan2} ([dz/dy], -[dz/dx]) \quad (3.6)$$

3. Conversion the aspect values to compass direction values (0-360 degrees) using the following rule:

if aspect < 0

cell = 90.0 - aspect

else if aspect > 90.0

cell = 360.0 - aspect + 90.0

else

cell = 90.0 – aspect (3.7)

Slope aspect map with 30 m x 30 m resolution of the study area is shown in Fig. 3.20. It is difficult to interpret visually due to the pixel size. According to Table 3.7, there is no a dominant direction of slope cells. All slope directions, except flat areas, occupy almost the same areas ranging from 12-13% of the study area. A more detail explanation on slope aspect matter can be found in ESRI [63].



Table 3.7 The distribution of slope aspect of the study area

Slopes Aspect (degree)	Compass Direction	Area (km2)	%
-1	Flat	4	0
0 - 22.5	North	58	6
22.5 - 67.5	Northeast	111	12
67.5 - 112.5	East	114	13
112.5 - 157.5	Southeast	107	12
157.5 - 202.5	South	115	13
202.5 - 247.5	Southwest	111	12
247.5 - 292.5	West	115	13
292.5 - 337.5	Northwest	108	12
337.5 - 359.9	North	56	6

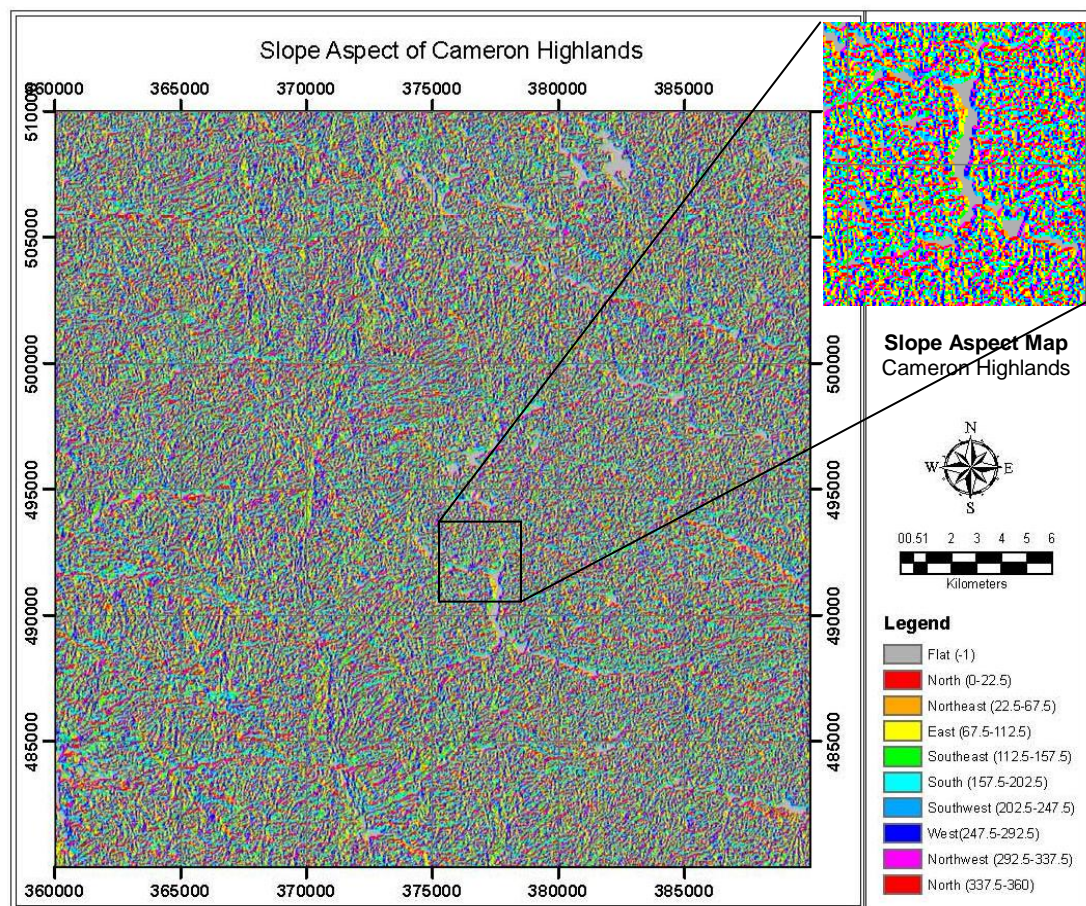


Fig. 3.20 Slope aspect map of the study area

### 3.4.6. Curvature

The curvature of a surface, e.g. raster or TINs surface, is calculated on a cell-by-cell basis using a fourth-order polynomial described in ESRI [63] as follows:

$$Z = Ax^2y^2 + Bx^2y + Cxy^2 + Dx^2 + Ey^2 + Fxy + Gx + Hy + I \quad (3.8)$$

This function fits to a surface composed from a 3 x 3 window. The coefficients A, B, C, and so on, are calculated from this surface using Equation 3.10. L is the distance between the centers of cell/pixel which equals to pixel size (30 meter). The illustration of calculating curvature is given in Fig. 3.21. The relationship among nine values of elevation of each numbered cell for calculating curvature follows the following equations as described in ESRI [63]:

$$\begin{aligned} A &= [(Z1 + Z3 + Z7 + Z9) / 4 - (Z2 + Z4 + Z6 + Z8) / 2 + Z5] / L^4 \\ B &= [(Z1 + Z3 - Z7 - Z9) / 4 - (Z2 - Z8) / 2] / L^3 \\ C &= [(-Z1 + Z3 - Z7 + Z9) / 4 + (Z4 - Z6) / 2] / L^3 \\ D &= [(Z4 + Z6) / 2 - Z5] / L^2 \\ E &= [(Z2 + Z8) / 2 - Z5] / L^2 \\ F &= (-Z1 + Z3 + Z7 - Z9) / 4L^2 \\ G &= (-Z4 + Z6) / 2L \\ H &= (Z2 - Z8) / 2L \\ I &= Z5 \end{aligned} \quad (3.10)$$

The curvature is also known as the second derivative of the surface, i.e. the slope of the slope. It is formulated in ESRI [63] as follows:

$$\text{Curvature} = -2(D + E) * 100 \quad (3.11)$$

Curvatures are indicated by negative to positive values. The unit of curvature is inverse distance that is 1/m. A positive curvature indicates the surface is upwardly convex at that cell. A negative curvature indicates the surface is upwardly concave at that cell. A value of zero indicates the surface is flat. In this research, curvature data is used to evaluate the type of curvature the landslides may occur.

The curvature map of the study area is shown in Fig. 3.22. The map is difficult to interpret visually due to the pixel size that is 30 meter. The study area mainly consists



of moderate concave to flat areas that occupy about 46% of the total area. The moderate concave and convex types occupy almost the same area, about 20-22%, as well as high concave and moderate convex as shown in Table 3.8. The latter occupies 11% of the total area.

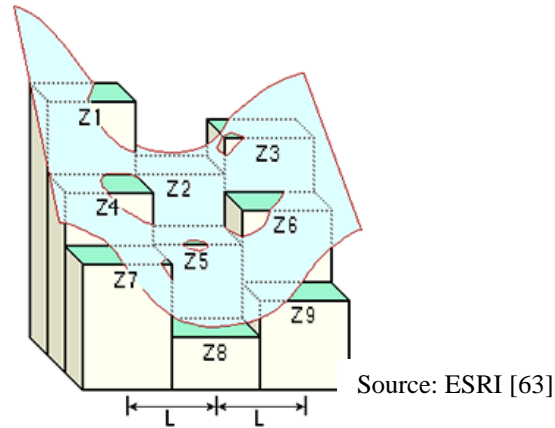


Fig. 3.21 The concept of calculating curvature

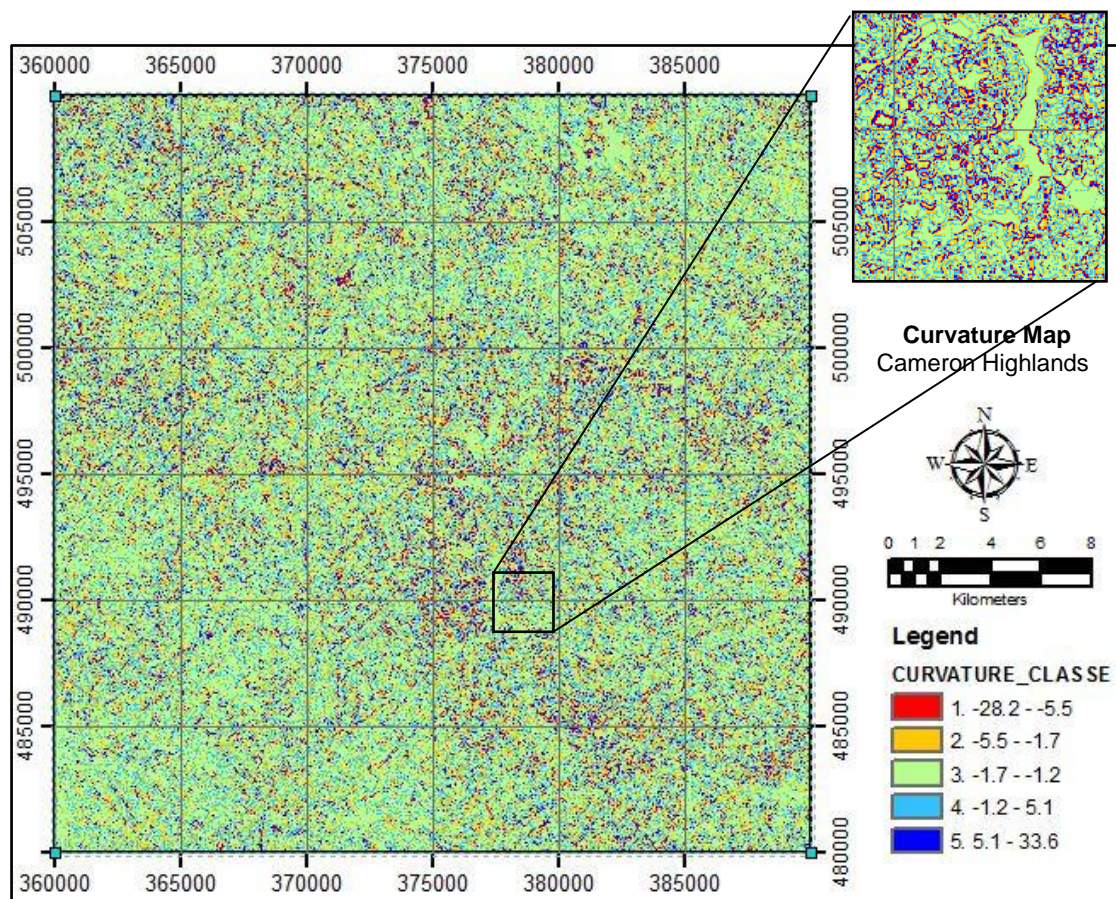


Fig. 3.22 Curvature map of the study area

Table 3.8 The distribution of curvature at the study area

Slopes Aspect (degree)	Curvature type	Area (km <sup>2</sup> )	%
-28.2 - -5.5	High concave	44	5
-5.5 - -1.7	Moderate concave	179	20
-1.7 - 1.2	Concave to Flat	418	46
1.2 - 5.1	Convex	202	22
5.1 - 33.6	Moderate Convex	57	6

### 3.4.7. Road Network and River-Lake

The road network map of the study was extracted from the old database of topographic map by separating this layer from the main database. Road networks mainly consist of Simpang Pulai - Pos Selim - Kampung Raja - Gua Musang stretch and Kampung Raja – Teringkap - Tanah Rata – Ringlet - Jalan Tapah stretch. The old road database, which was derived from aerial photograph taken in 1981, did not contain, for example, the new road connecting Simpang Pula to Kampung Raja (section I) and Kampung Raja to Gua Musang (section II) as shown in upper part of Fig. 3.23. These two road networks were extracted from SPOT 5 image by means of on screen digitizing. The extraction of new road from the image was carried out after the image has been geometrically corrected. Detail procedures of geometric correction of the image are discussed in subsection 3.4.10.

Road map has been commonly used as a landslide causative factor as previously discussed in section 2.2.5.2. It is not road itself that causes landslide. However, road development is often associated with clearing and cutting natural (vegetated) slopes. This may disturb the stability of such slopes. The closer the distance from the road means the higher the potential threat of landslide/slope failure as the result of slopes clearing and cutting for road development. In regard to landslide susceptibility modeling, Euclidean distances from road were computed using Spatial Analyst toolbox in ArcGIS. Euclidean distance is a straight line distance from each cell to the closest source cell. Euclidean distance from the road of the study area is shown in Fig. 3.24.

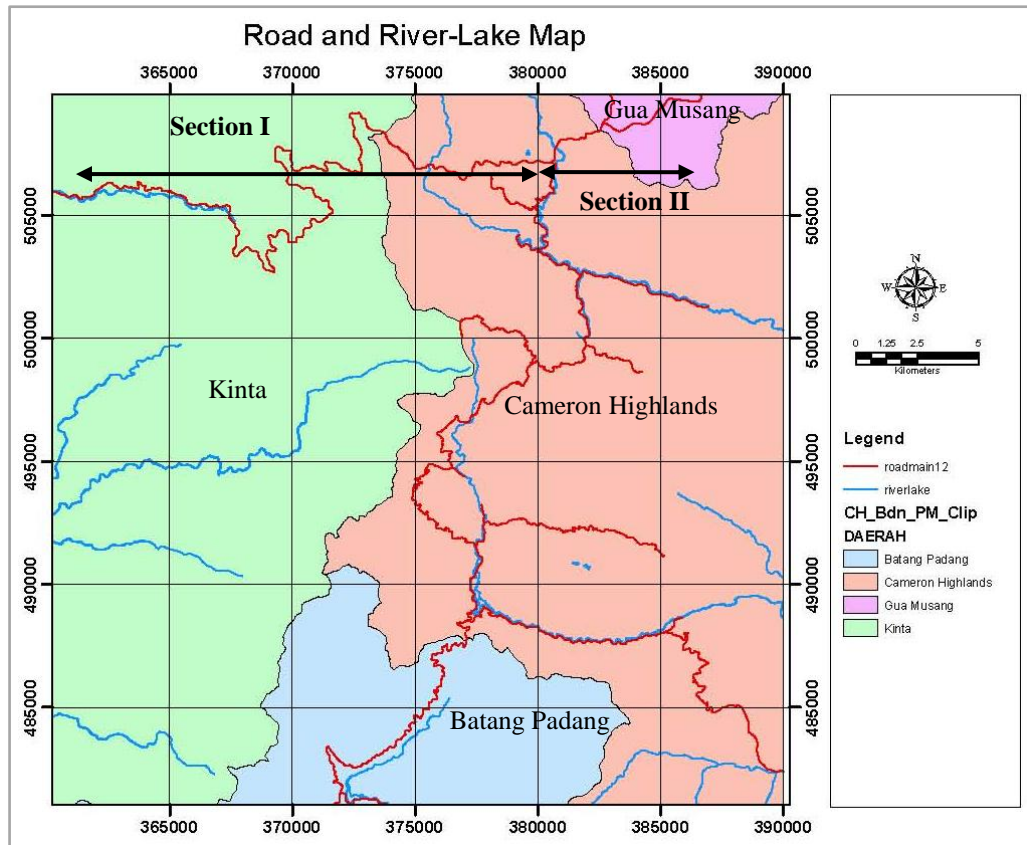


Fig. 3.23 Updated road network map

### 3.4.8. River and Lake

Erosion and slope failure often take place along the moving water body. The contribution of water bodies to slope instability has been previously discussed in section 2.2.3.2. In addition, high level of landslide hazard took place along the river as stated by Liu, et al. [89]. Zhu and Huang [226] and Chuanhua and Xueping [42] found that proximity to rivers has been one of factors contributing landslide occurrences. In this research, river and another water body i.e. lake, were added for landslide susceptibility modeling.

The way river and lake layer extracted from old database of topographic map was the same as that of road network. There were only main rivers extracted. The rivers include *Sungai Bertam*, *Sungai Terla*, *Sungai Kampar*, *Sungai Bertam*, *Sungai Geruntom*, *Sungai Geroh*, *Sungai Lemoi*, *Sungai Dipang*, and *Sungai Batang Padang*.



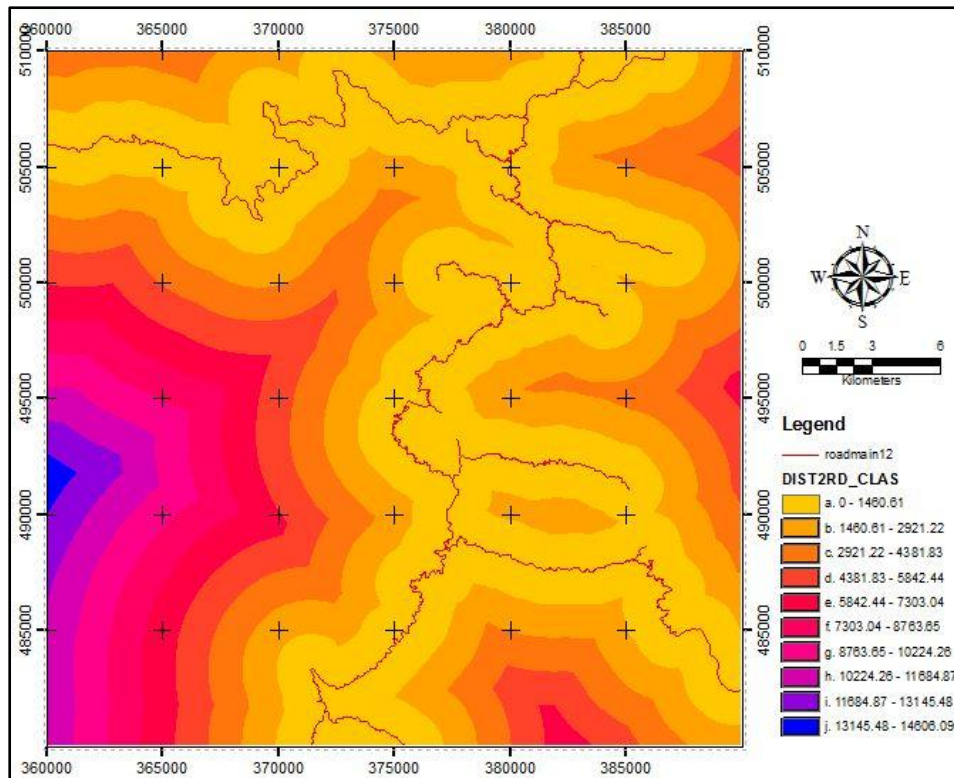


Fig. 3.24 Distance from road map of the study (in meter)

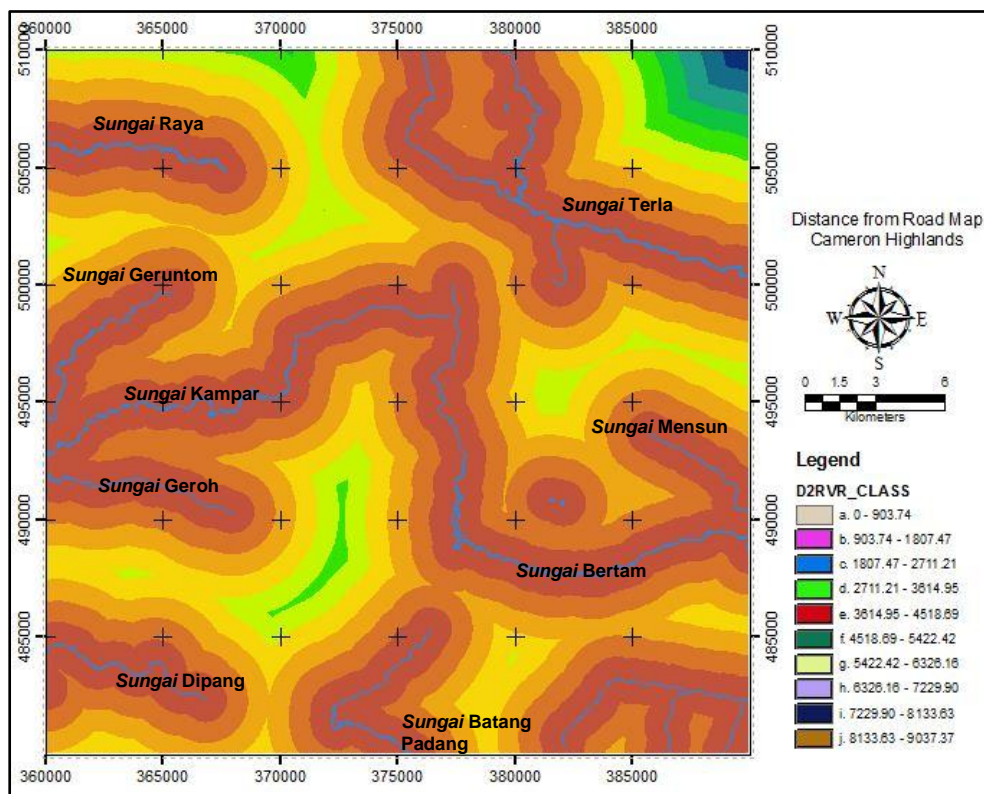


Fig. 3.25 Distance from river map of the study area (in meter)



Some rivers and small lakes were added to the old database by means of on screen digitizing of the georeferenced SPOT 5 image. For landslide susceptibility modeling, Euclidean distances from the rivers were computed (Fig. 3.25) and included in the modeling. This is the way this spatial data prepared for GIS process. Theoretically, the effect of river diminishes as the distances from river increase. Erosion and slope failures generally take place along the river banks.

#### **3.4.9. Geometric Correction of Topographic Map**

As mentioned earlier, all the satellite images came with projection systems other than RSO. To fix this problem, geometric correction should be applied to all images. In doing so, a set of GCPs is required. In this research, GCPs were obtained from a corrected-scanned topographic map. The procedures to prepare a corrected topographic map are explained in the following.

The hardcopy of Cameron Highlands topographic map was scanned. Since the image produced from scanning process contained distortions, geometric corrections have to be applied. Beforehand, the image was subset to remove unnecessary part i.e. the information contained in map legend part (Fig. 3.26a). Using Geocoding Wizard in ERMapper environment, geometric correction was carried out by first selecting third order (cubic) polynomial as the mathematical model (see section 2.7.5.1) to relate the uncorrected image, namely a scanned topographic map, with the georeferenced database or set of known coordinates of points at recognizable positions on the map. These points can be obtained from GPS surveys or grid coordinates on the hardcopy of topographic map (see Fig. 3.26b). As the output coordinates, Kertau was selected as the geodetic datum; Oblique Mercator of West Malaysia RSO was chosen as the geodetic projection system; and Easting/Northing was chosen as the coordinate type. About 150 GCPs which mostly consists of points of crossing grid lines were selected. In doing geometric correction, center of grid points on the uncorrected image were identified and marked on the screen. The corresponding coordinates, e.g. Easting and Northing, were inputted on screen as well.

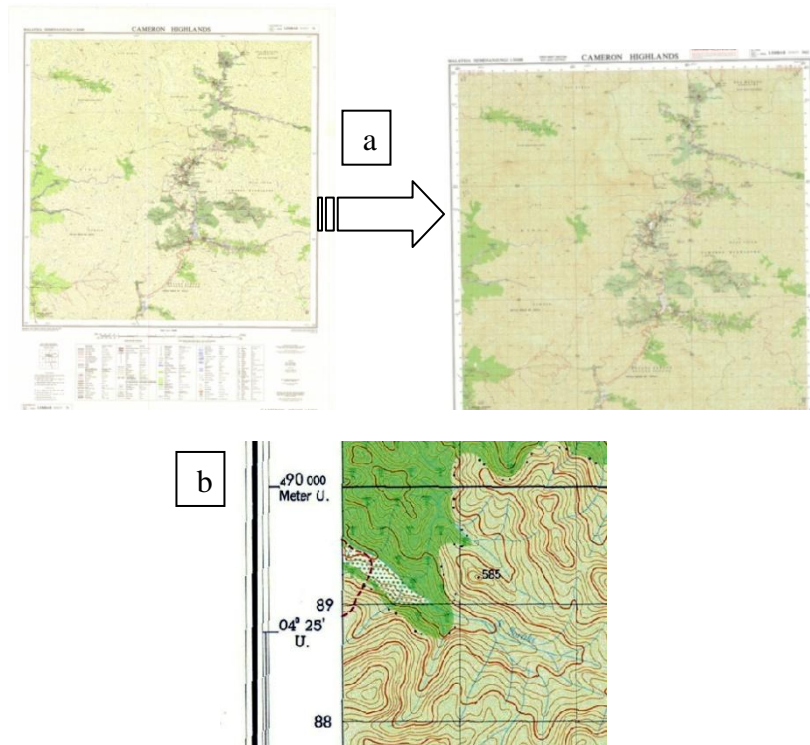


Fig. 3.26 a) Scanned and cropped topographic map, b) the grid coordinates

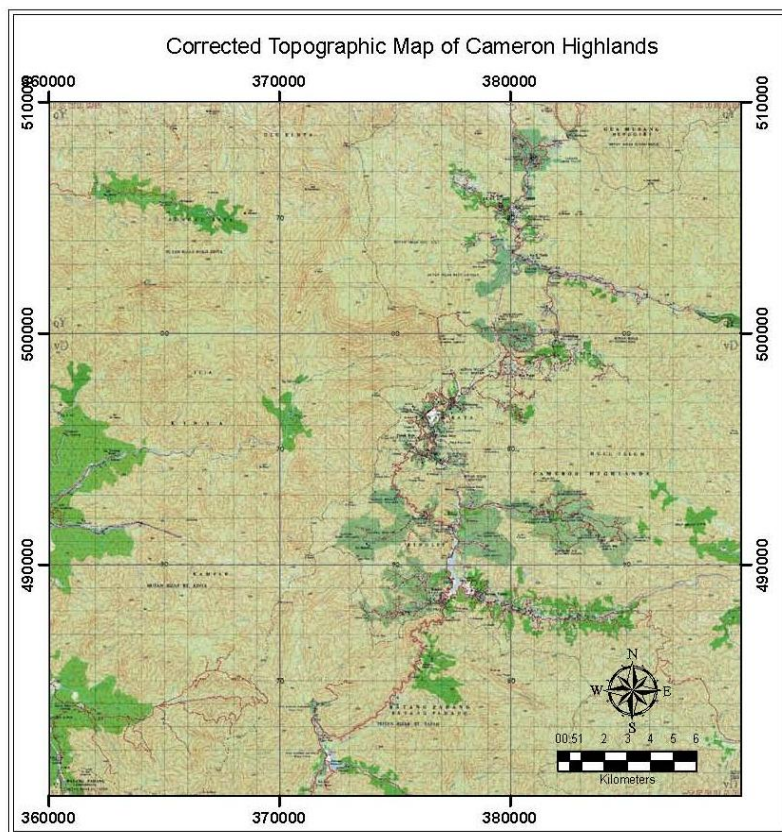


Fig. 3.27 Geometrically corrected topographic map of Cameron Highland

A number of 141 GCPs was finally selected as the final GCPs because these GCPs resulted in the average Root Mean Square Error (RMSE) that was 0.546 (pixel), about a half pixel. It is the value that nearly meets the recommended requirement that is 0.5 (pixel). The discussion on the accepted RMSE can be found in section 2.7.5. The list of GCP coordinated can be found in Appendix C. The corrected topographic map is shown in Fig. 3.27. The corrected image is sometime called as georeferenced or rectified image, the image that has been corrected from geometric errors/distortions.

#### **3.4.10. Image Pre-Processing for SPOT and Landsat Images**

In general, image pre-processing procedures include image subsetting, image enhancement, geometric correction, and atmospheric correction. The following sections explain these procedures.

##### *3.4.10.1 Image Subsetting*

All satellite images were subset to conform to the size of study area to fit the size of the corrected topographic map. Fig. 3.28 shows cropped SPOT 5 and Landsat 7 ETM+ image. The size of the image is about 30 km x 30 km cropped from 60 km x 60 km, a full scene size of SPOT image, and 185 km x 185 km, a full scene size of Landsat 7 ETM+ image. The projection system of the images was in UTM. To make them compatible to process with other spatial data, the images were transformed to RSO projection system through geometric correction process.

##### *3.4.10.2 Dealing with Atmospheric Effects*

As discussed in section 2.7.5.2, the DN recorded by a satellite sensor consists of the radiance of an object and the atmosphere effects. The atmospheric effect can either increase or decrease the radiance of the object. The effect can be seen through the DN histogram of different bands and explained in the following. A simple

atmospheric correction was applied by means of adjusting the histogram of each band of the images.

Fig. 3.29a shows histogram of band 1 and band 5, the shortest wavelength and a longer one respectively, of Landsat image acquired on 19 June 2002. The DN of band 1 is shifted from zero by 49 larger than that of band 5 that is by 14. The DN shifts for all bands of Landsat and SPOT 5 images are listed in Table 3.9. The effect of atmosphere on Landsat bands is apparent. The shorter the wavelength of band the greater the DN shifts. Thermal band is shifted by 102 from the origin. Fig. 3.29b proves that SPOT 5 image is a perfect one due to no shifting of the DN of all bands. This image was then selected as the reference image for further processes.

Table 3.9 shows the ranges of offset of Landsat images. The offset ranges were calculated from 4 Landsat images for each band. The offsets vary time by time. Therefore, it is not possible to give absolute offsets for each band that are applicable in all situations. To fix this problem, a first order atmospheric correction was applied by subtracting the offset from each DN. For this current study, the average offset of each band was applied to correct atmospheric effect.

Table 3.9 Offsets of Landsat and SPOT bands

Bands	Landsat DN shifts		SPOT 5 DN Shifts
	Shifts	Average	
Band 1 (visible blue)	49-57	52	0
Band 2 (visible green)	30-35	32	0
Band 3 (visible red)	20-26	23	0
Band 4 (NIR)	16-20	18	0
Band 5 (middle IR)	7-14	11	Not Available
Band 6 (thermal IR)	102-113	108	
Band 7 (middle IR)	9-10	10	
Band 8 (panchromatic)	16-19	18	

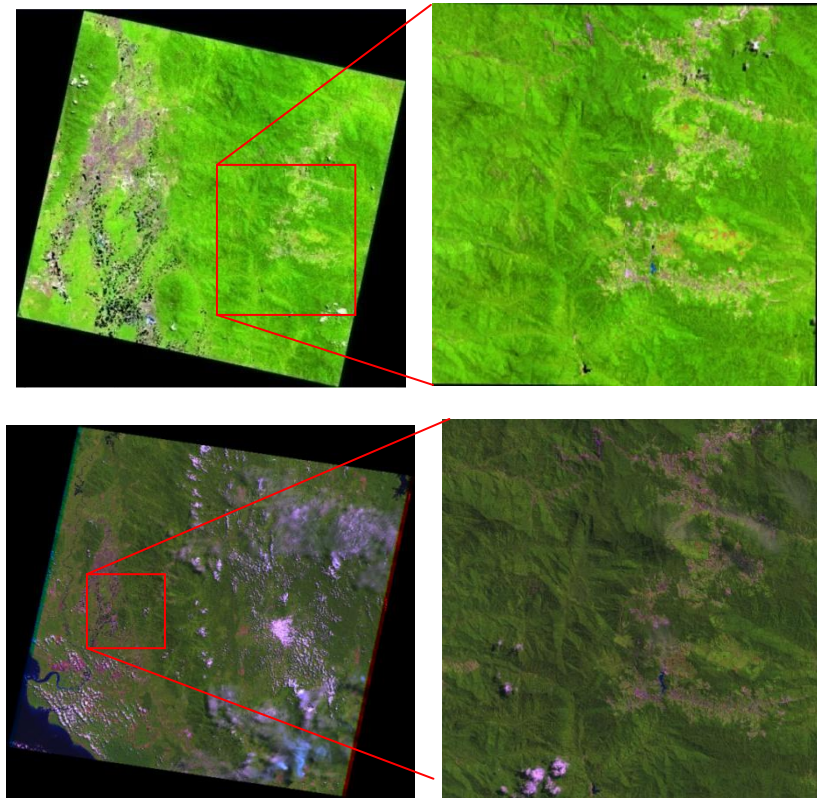


Fig. 3.28 Subsetting a SPOT 5 and Landsat 7 satellite image

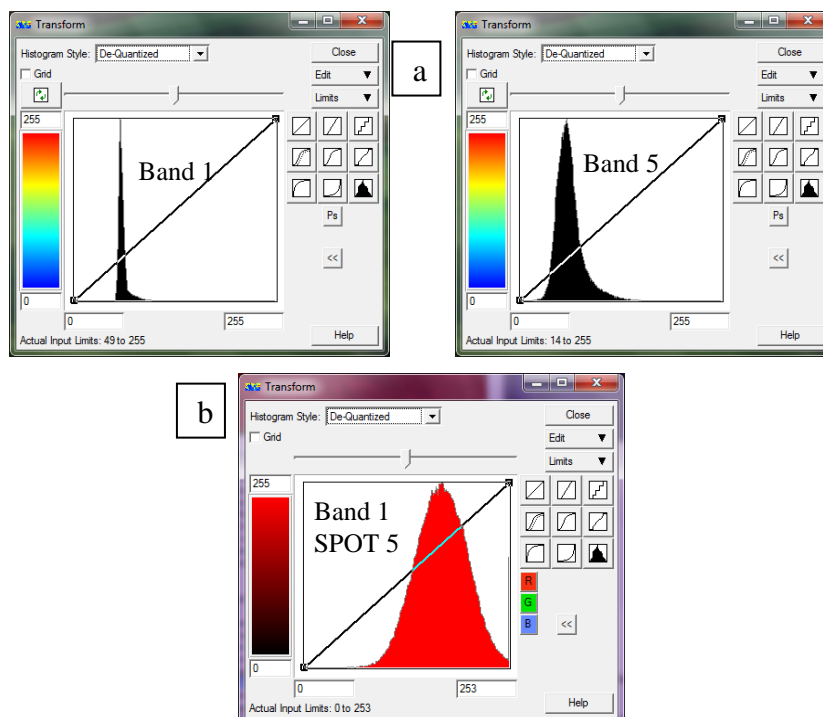


Fig. 3.29 a) Histogram of band 1 and 5 of Landsat image, b) histogram of band 1 of SPOT 5 image

The first order atmospheric correction approach uses an important assumption that there are pixels within the scene whose true DN is zero which is associated with the reflectance of water bodies. Fortunately, there are lakes/water bodies in the study area. Lakes in the study area have different DNs that are 0, 10, and 183. The problem arose when knowing that cloud shadow has the same DN value as lakes that are 0. With the limitation of ERMapper software used in this study in handling atmospheric effects, there were no attempts to perform further atmospheric correction. In regard to handling cloud shadow and cloud itself, it is discussed in section 3.4.15.

#### *3.4.10.3 Geometric Correction of SPOT and Landsat Images*

Geometric correction at this stage was meant to remove geometric errors and transform the projection system of all satellite images from UTM to RSO. Image to image registration would be preferable rather than image to topographic map registration. The latter is more cumbersome to do because recognizing the same objects on the map and the satellite image is not easy task. In doing so, one satellite image was selected as a reference image to which the remaining satellite images were referred during geometric correction process. The reference image was first georeferenced to RSO using georeferenced topographic map. This process is described below.

Due the clarity of the image quality and the superiority in image resolution, SPOT 5 image acquired on 19 April 2005 was selected as the reference image. Geometric correction was using two ways. The first was application of map to map projection and the second were application of image to image registration.

Map to map projection is a simple way to transform from one projection system to another. UTM to RSO transformation algorithm was applied. There are no GPCs required. The result was not satisfying. When overlaid with the existing road network, the identified road network on the corrected image, indicated by number 1, was somehow shifted to the left of the existing road network, indicated by number 2, as shown in Fig. 3.30a. This method and, hence, the resulted image using this method were no longer used for further works.



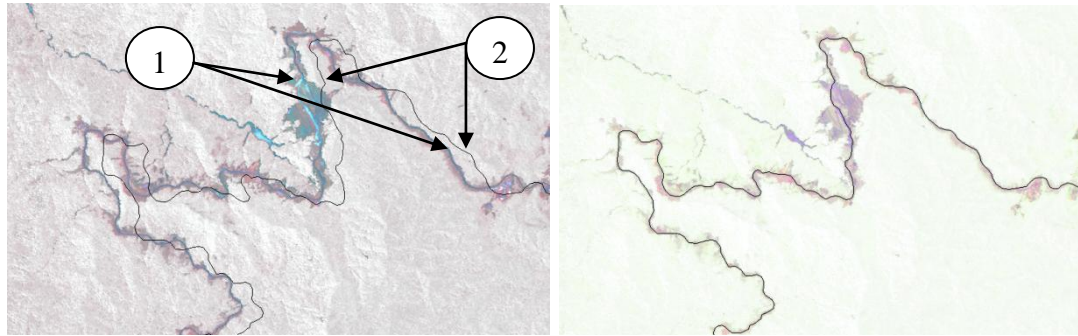


Fig. 3.30 a) Inaccurate and b) accurate geometric correction

Having been disappointed by the previous result, geometric correction using polynomial function was then carried out. A third order polynomial was selected. As GCPs point, geocoded image option was chosen. This was followed by selecting the corrected topographic map as the geocoded image. Geometric correction was carried out by means of pin pointing the same objects on the uncorrected SPOT 5 image and on the corrected topographic map (Fig. 3.31). A number of 254 points was picked up as GCPs. The total RMS error was 0.304 (pixel), the value that meets the acceptable limit. The corrected image is shown in Fig. 3.32. As the result, road network on the image coincide with the existing one (Fig. 3.30b).

Geometric correction was applied to all Landsat images using the same procedures. The number of GCPs involved might be different for each image due to the degree of recognizable of the objects on those images. The GCPs were selected as the distinctive physical features recognizable on both images (corrected and uncorrected image) such as road junctions, edges or corners of features, and deflection points of river and road. The minimum number of required GCPs is 10 for performing third order polynomial transformation. RMSE of geometric correction is computed using Equation 2.14. Table 3.10 shows the number of retained GCPs and RMSE of each image. The number of GCPs was actually larger than the one shown in Table 3.10. GCPs shown in Table 3.10 are the retained ones that result in the acceptable limit of RMSE that is about a half pixel size.

The number of GCPs used for geometric correction of all images has satisfied the required number for performing third order polynomial transformation that is 10

GCPs. Meanwhile, the distribution of GCPs has been maintained so that GCPs were distributed evenly over an uncorrected image.

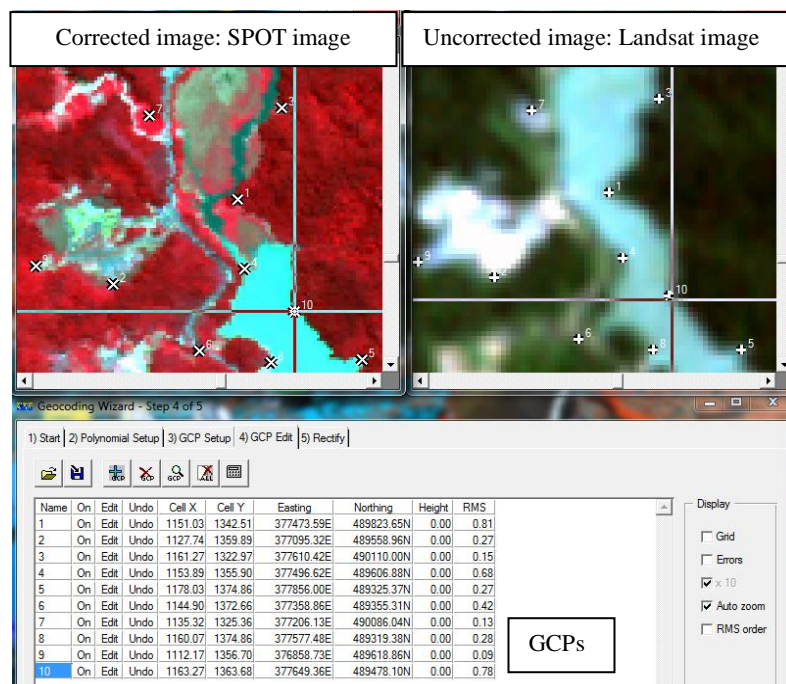


Fig. 3.31 Snapshot of image-to-image geometric correction

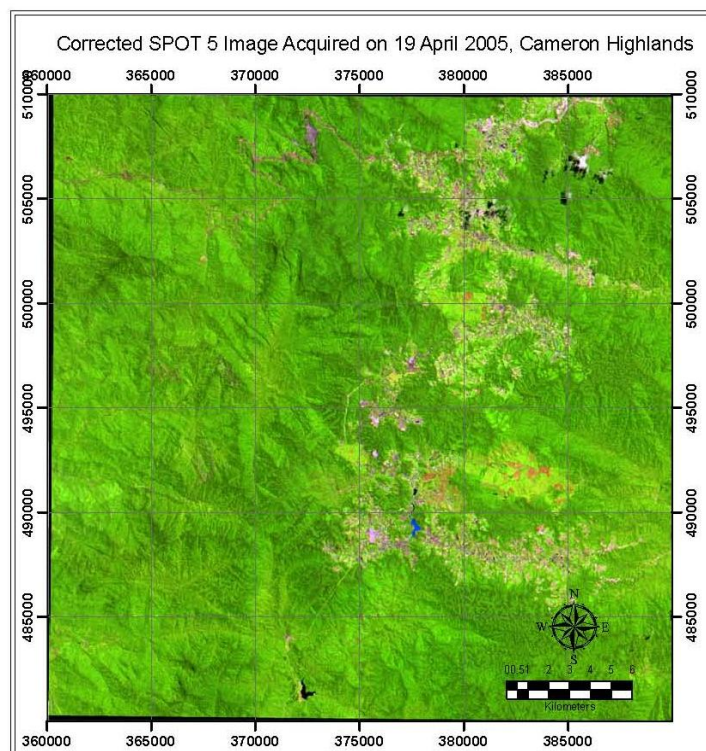


Fig. 3.32 Geometrically corrected SPOT 5 image



Table 3.10 Geometric correction results of Landsat images

Acquisition Date	Number of GCPs	RMSE
24 Feb 2001	60	0.580
31 May 2001	59	0.580
19 Jun 2002	58	0.567
20 Sep 2001	62	0.557

#### 3.4.10.4 Image Enhancement

Image enhancement techniques have been explained in section 2.7.6. For SPOT 5 image, there was no further image processing required since its jobs for providing a reference image for correcting all Landsat images and updating road network have done.

Image enhancement was meant to get a better view of the images to provide a better image interpretation especially during image classification to produce LULC map. Either image in natural color or false color composite was used mainly for identification of training areas described later. For natural color, bands combination of RGB 321 shows image in natural color and 543 enhances the contrast of object under thin layer of cloud/haze in natural color. False color composites of RGB 123 and 432 were also used to enhance different type of vegetation.

#### 3.4.11. Land use land cover map

In this section, image processing was continued to produce LULC. LULC map was assumed to be a non-temporal factor. Landsat image acquired on 20 September 2001 was selected as the data source for extracting LULC due to its good clarity among the others. Another reason was the time frame of the research work which was set to year 2001. Workflow of image classification procedures is shown in Fig. 3.33.

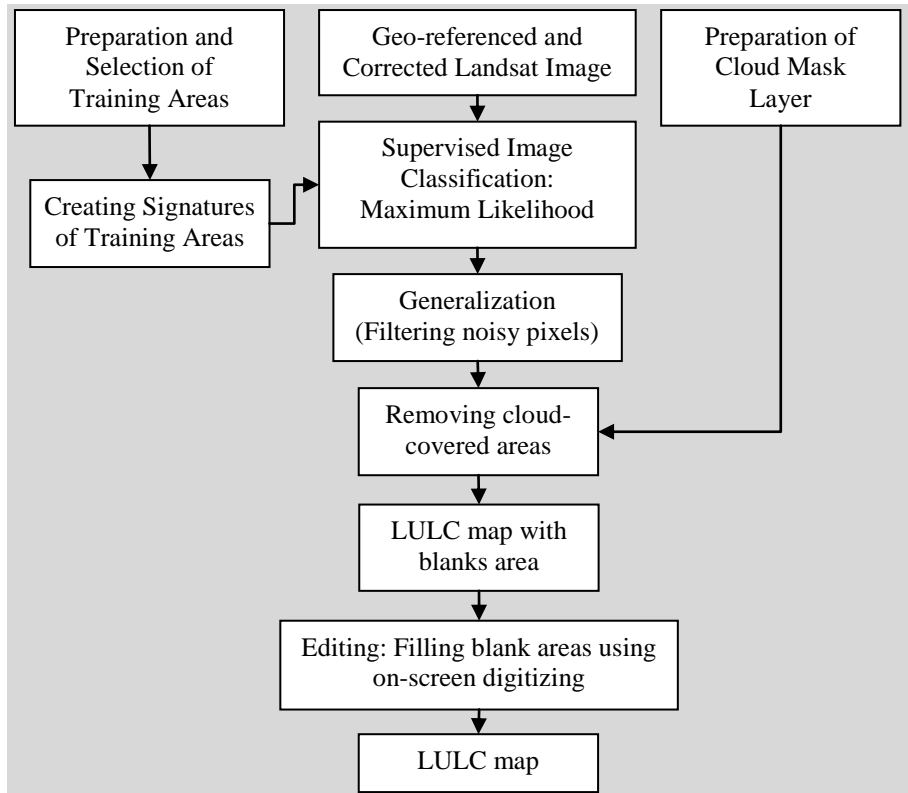


Fig. 3.33 Image classification procedures

Image classification was started by setting up the Landsat corrected image as the input image. Training areas were defined in order to generate reflectance signature of each class. Using supervised classification, the signature was used to cluster the pixels with homogenous reflectance on the image. Filtering was applied to remove small pixels and to generalize the objects. Area covered by cloud and its shadow was delineated, removed and filled with the classified images from the other Landsat images.

#### 3.4.11.1 Image classification scheme

Image classification scheme created by Anderson, et al. [179] has been adopted and modified to simplify the image classification process. It has 9 Level I categories. Not all of categories are available in the study area such as glaciers, and beaches. The number of categories was then reduced to four. Table 3.11 shows LULC classification categories from level I to level II. Level III was omitted for simplification reason

during image classification. Level II in this research was mainly adopted from information on topographic map legend of the study area and from knowledge gained during site visit. The author added cut slope, barren land, thin vegetated area, and open land classes for landslide susceptibility modeling purpose.

Table 3.11 Modified image classification scheme for LULC mapping

Category Number	Level I	Level II	Level II (Used in this research)
1	Urban and developed area	Urban areas Developed area Barren land	<b>Urban/Built up</b> <b>Cut slope</b> <b>Barren land</b> <b>Open land</b>
2	Herbaceous land	1. Pasture 2. Agriculture 3. Grassland	<b>Thin vegetated areas</b> <b>Cropland</b> <b>Bushes</b>
3	Forest	1. Deciduous forest 2. Coniferous forest	<b>Forest</b>
4	Water	Water	<b>River and lake</b>

Urban/built up, cut slope, barren land/open land were grouped as urban and developed area. Urban includes settlement, cemented/asphalted surface and buildings. Cut slope is barren land along the road while open land is barren land and cut slope that have no relation with the road. Land covers related to herbaceous land are cropland, bushes and thin vegetated area. The latter was interpreted visually from the satellite image as bright green areas within dark green areas (forest) and concluded as thin vegetated areas. It may consist of small vegetation and bushes. There is only one Level II of forest that is forest itself. Both deciduous and coniferous forest is not typical forest of the study area. Meanwhile, river category was subdivided into river and lake. There are two big lakes that are located near the center and lower center of the corrected image. A small one is near upper center of the area study. Rivers also exist in the study area. Two big rivers, *Sungai Bertam* and *Sungai Terla* are the main rivers in Cameron Highlands. The others are considered as narrow rivers with the water flows away from the study area. Many upstream of big rivers, such as *Sungai Kampar* and *Sungai Dipang*, are located within the study area.

#### *3.4.11.2 Ground Truthing, Training Sites and Signatures Generation*

Ground truth for image classification is the actual information of LCLU of each category of LULC. In this research, ground truth was obtained from topographical map, visual interpretation of the Landsat and SPOT 5 images, and field survey using GPS. The latter was carried out along the main road. The picture of each category of LULC was recorded using a digital camera. Fig. 3.34 portrays sample of LULC categories.

The information of ground truth gained from was used to assist digitizing the homogeneous areas on the Landsat image using polygon tools. The polygons of homogeneous area are called as training sites. Training areas for each LULC Level II categories were digitized over the Landsat image based on visual interpretation of recognizable homogeneous areas. Classified image resulted from unsupervised classification was also used to assist identification of homogeneous areas for use as training areas in supervised classification. Visual interpretation of SPOT 5 image provided useful aid for clustering the object because of the high clarity and resolution of this image. Digitization of training areas was done using ArcGIS. A polygon shape layer was first prepared and assigned with RSO projection system. All the training areas are shown in Fig. 3.35.

In order to distinguish among the training areas, each of them was assigned a specific code as follows: 0-forest, 1-lake/river, 2-urban, 3-small vegetation/cropland, 4-cut slope/barren land, 6-open land. Before classification carried out, the spectral signatures were derived from each training areas. The spectral signatures were used to examine the signature separability between each class to see the level of separation between pairs of classes. Signature separability determines the accuracy of the classification.

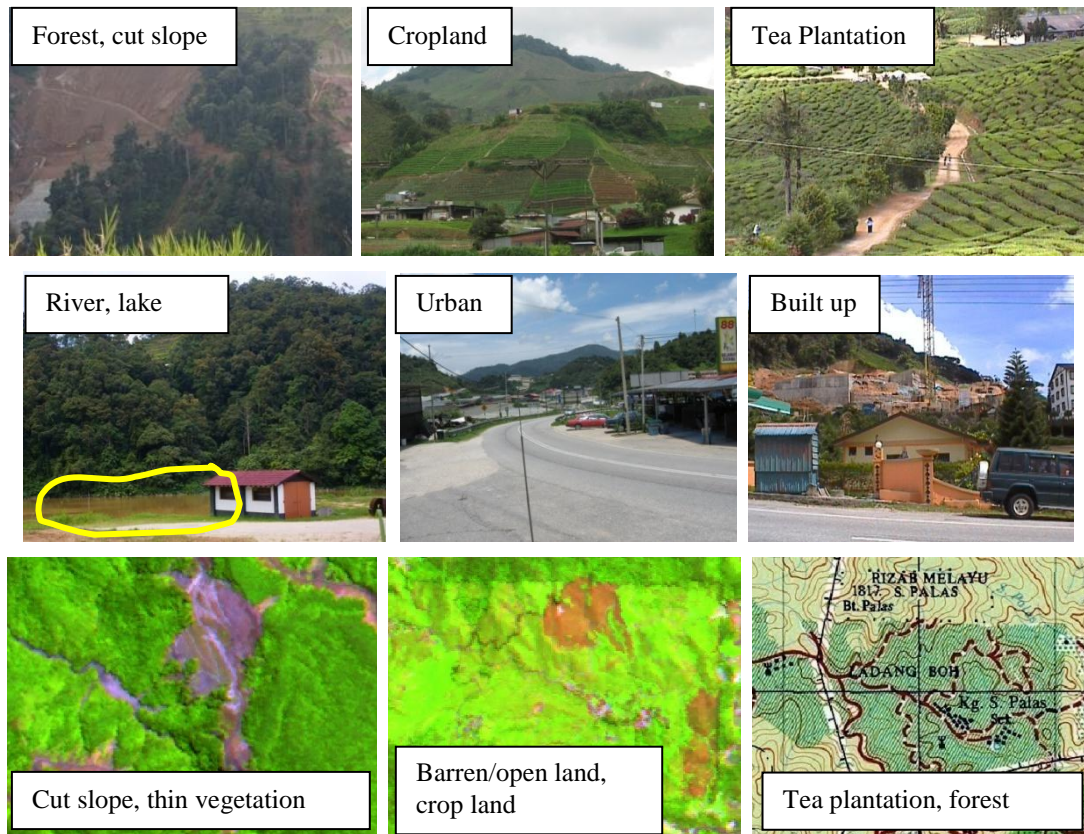


Fig. 3.34 Various ground truth for LULC classification

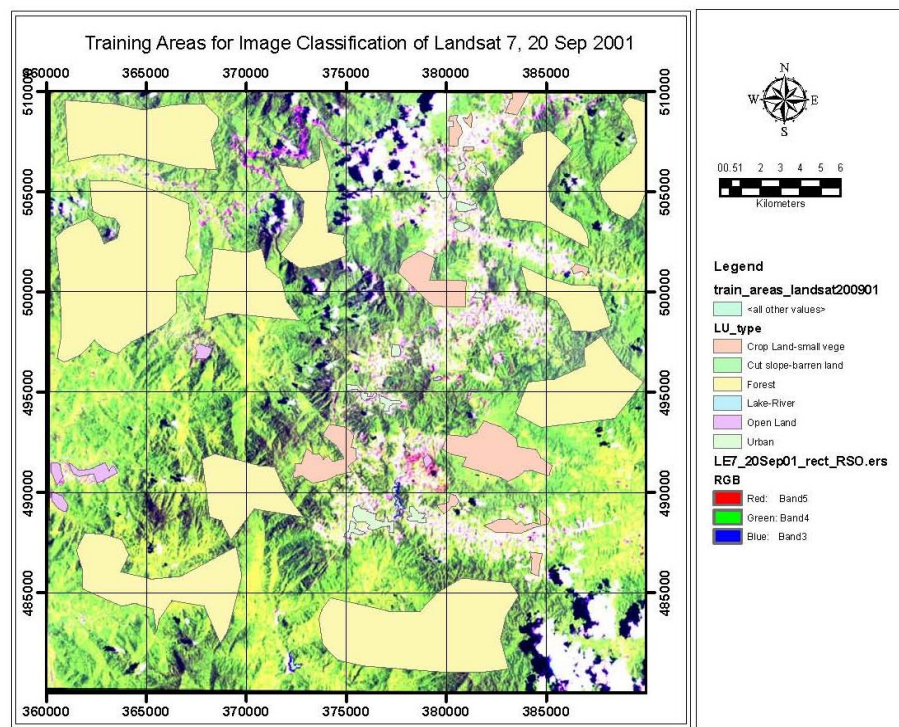
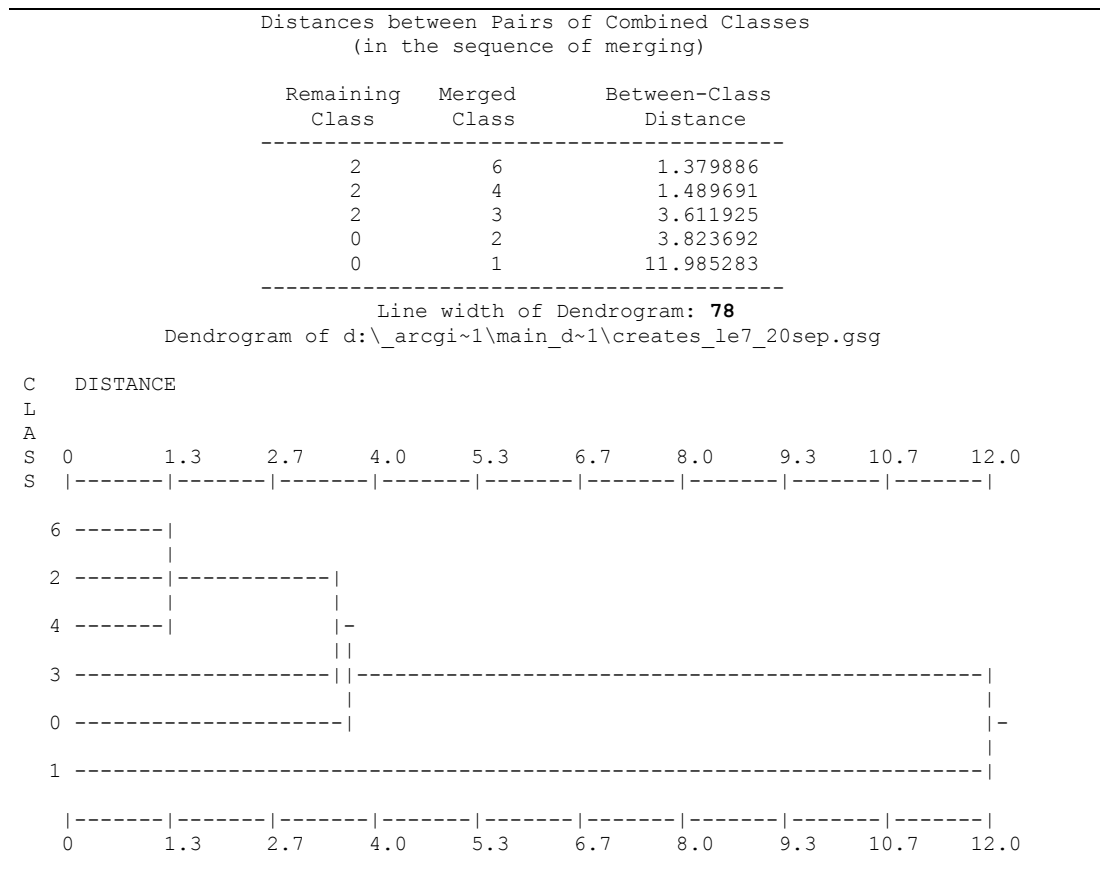


Fig. 3.35 Training areas for image classification of the Landsat image

The signature separability of classes is presented in a dendrogram. A dendrogram is explained in ESRI [63] as a diagram that describes the attribute distances between each pair of sequentially merged classes. The diagram is graphically arranged so that members of each pair of classes to be merged are neighbors in the diagram to avoid crossing lines. A dendrogram has classes or clusters in a signature file arranged relative to one another using the multidimensional distance separating the classes in attribute space. The signature file of the Landsat image was used as the input for dendrogram function. The output of the dendrogram is shown in Table 3.12.

The dendrogram is explained as follows: firstly, urban/built up (2), Open land (6), and cut slope/barren land (4) have low separability. The next, at a distance of 1.380, urban/built up and open land will merge; urban/built up and cut slope/barren land will merge at distance of 1.490. Small vegetation coverage/cropland (3) has a larger distance of 3.611 to separate from urban (2). Meanwhile, forest (0) can be easily separated from urban (2) and lake-river (1) because it has farther distances by 3.824 and 11.985 respectively. The term distance in this case is the distance between pairs of classes calculated based on their means and variances that can be found in output file of signature generation. The distance can also be viewed as the distance in a multidimensional space. Low separability between pairs of classes will reduce the accuracy of image classification. Low separability of built up (2), open land (6) and cut slope/barren land (4) was overcome by means of merging open land and cut slope/barren land as one class. Urban/built class was clearly distinguishable from open land/barren land/cut slope (Fig. 3.36). This class is shown in red. The surrounding areas are open land and barren land. Based on these signatures, the final classes were expected to have 5 LULC categories: urban/built up, forest, lake/river, cropland/thin vegetation/small vegetation, open land/barren land/cut slope.

Table 3.12 Dendrogram of the Landsat image Signatures



### 3.4.11.3 Image Classification and Raster Generalization

The next step after collecting object signatures and analysis their separability was to undertake supervised classification. This process is intended to assign each cell of satellite image of the study area to a known class as using statistic of signature information of each class. It contains multivariate statistics of each class or cluster necessary to conduct image classification. The expected result is a map containing partition of the study area into known classes of LULC.

A supervised image classification was applied to a Landsat image acquired on 20 September 2001 particularly using reflectances of band 5, 4 and 3. It was conducted by using maximum likelihood classifier. LULC map resulted from this process comprises of five features namely urban/built up, forest, lake/river/water-like surface, cropland/thin vegetation/small vegetation, open land/barren land/cut slope (Fig. 3.37). The pixel size of the map is 30 m x 30 m.



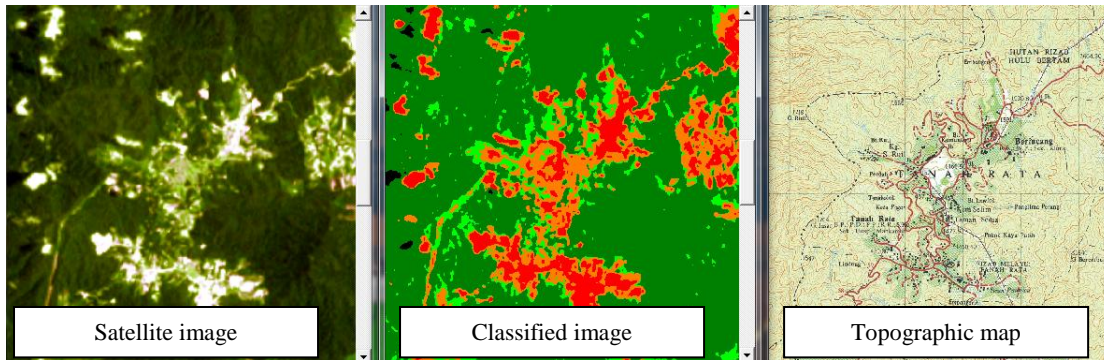


Fig. 3.36 Separability of urban with the surroundings seen on classified image and the corresponding image and topographic map

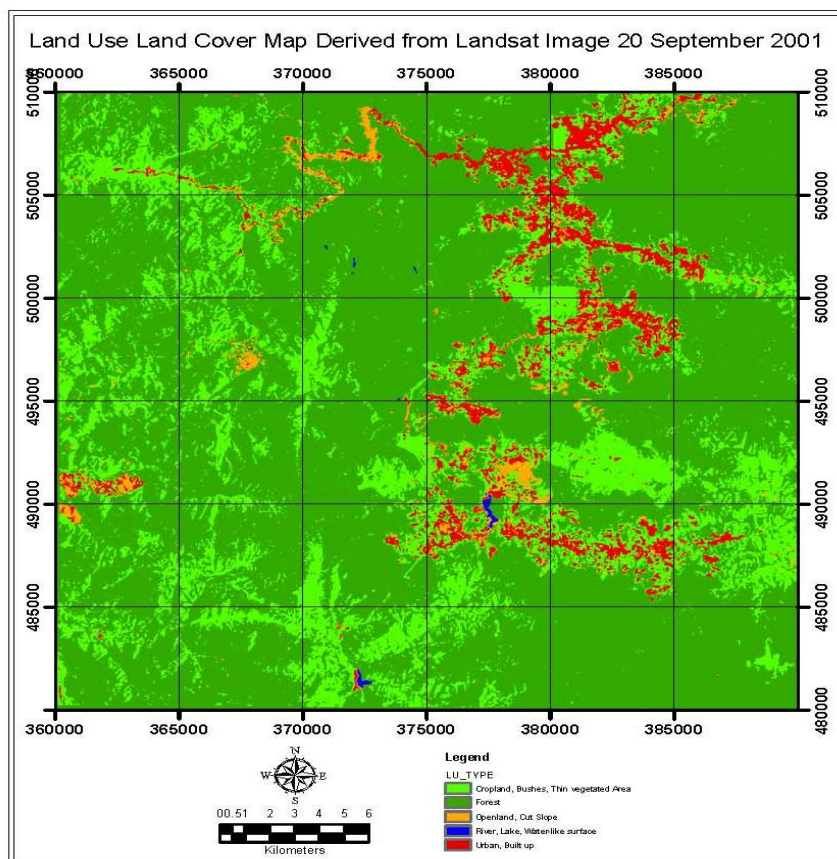


Fig. 3.37 Land Use Land Cover Map

The classified image contains a large number of small clustered pixels that is usually called as ‘noise pixels’. Before further utilizing the classified image, raster generalization was applied to the classified image in order to either to clean up small erroneous pixel in the raster data or to generalize the data to remove or smooth unnecessary detail for a more general analysis. The erroneous pixels may be



unclassified data originating from the satellite image. In doing so, raster generalization was performed by using Majority Filter method. This method replaces cells in a raster based on the majority of their contiguous neighboring cells. Contiguous means sharing an edge for a kernel of EIGHT and sharing a corner for a kernel of rectangular regions. This work used a kernel of EIGHT. Detail explanation in regard to this subject can be referred to ESRI [63].

Illustration of raster generalization is given in Fig. 3.38a. The input raster contains small clustered pixels such as pixels with values of 6, 0 -3, and 2. After applying Majority Filter Generalization, these erroneous pixels in output raster are replaced by the majority contiguous neighboring cells. Fig. 3.38b portrays generalization result applied to classified image of part of the study area. Left picture is the original classified image while right picture displays the image after application of generalization. Erroneous pixels within the delineated lines (left picture) were removed (right picture).

Calculation of the area of all classes was done after raster generalization completed. The number of pixels of each class was multiplied by 30 m x 30 m and the result is shown in Table 3.13. Forest dominates the study area by occupying 74% of the area followed by cropland/small vegetation that occupies 20% of the area. Small part of the area is occupied by open land, river/lake and urban with their respective areas are 5%, 2% and less than 1% of the total area. The value of the area of all classes has been corrected from the effect of cloud and its shadow. The actual image contains cloud cover around 9% of the total area. The procedure in regard to fixing cloud cover problem is discussed in section 3.4.15.

Table 3.13 Statistic of LULC map derived from the Landsat image

Land Use Type	Number of pixel	Area (km <sup>2</sup> )	%
Cropland, Bushes, Thin vegetated area	197,954	178.2	20
Forest	713	664.3	74
River, Lake, Water-like surface	738,129	15.8	2
Urban, Built up	45,685	0.6	0
Open land, Cut slope	17,502	41.1	5
Total Area		900	

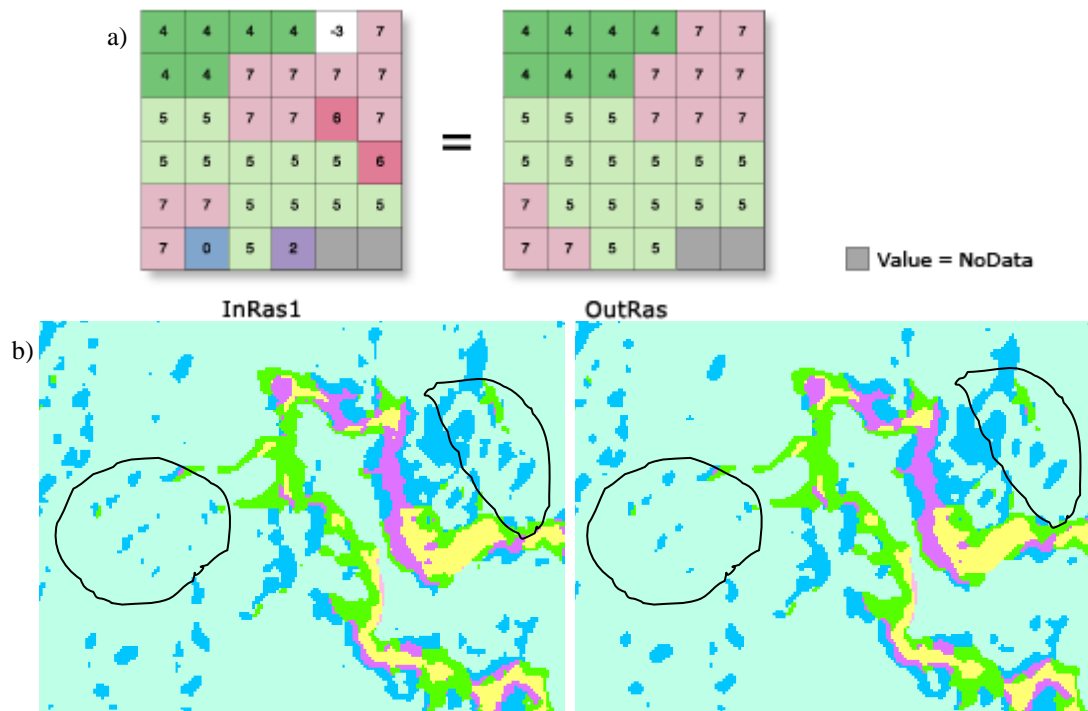


Fig. 3.38 a) Illustration of generalization, b) before and after generalization

The reason to provide only five categories of LULC was meant to conform to the final landslide susceptibility map that divides the susceptibility of the study areas into five categories: very high, high, moderate, low, very. In addition, it was also mean to facilitate derivation of weighting system.

### 3.4.12. Normalized Difference Vegetation Index (NDVI)

Multi temporal NDVI maps were used as representation of the effect of monsoonal rainfall. These maps were included in landslide susceptibility modeling taking into account environmental change due to monsoonal system. NDVI is one of the factors affected by seasonal rainfall as discussed in section 2.2.7.1. The inclusion of multi temporal NDVI maps was intended to investigate their roles in affecting the accuracy of the final landslide susceptibility maps and to seek possible replacement for rainfall data. In addition, NDVI can be used as indirect indicator of slope stability. High NDVI at a particular area means that this area is covered with healthy green vegetation and vice versa.

NDVI maps were derived from four Landsat images as presented in Table 3.4 involving visible red (band 3) and NIR (band 4). Computation of NDVI was carried out within ERMapper environment. It employed Equation 2.27 described in section 2.2.4.2. Equation 2.27 produced NDVI values ranging between -1 (no vegetation) and +1 (completely healthy green vegetation cover). When the NDVI image moved to ArcGIS environment, the index value was re-mapped into grayscale index ranging from 0 to 255 using scaling method as follow:

$$\text{Scaled NDVI} = 100(\text{NDVI} + 1) \quad (3.12)$$

Fig. 3.39a shows an example of NDVI image of Tanah Rata-Ringlet area and the corresponding false color composite image (RGB 543) image shown in Fig. 3.39b. Area with the brightest color is forest. Crop land area is a bit darker than the forest. Built up and open land area are shown darker compared to crop land. This may be due to the absence of vegetation within this area or due to the presence of sparse vegetation or small vegetation coverage. Meanwhile, lake is shown as black area since there is no vegetation within the lake and the nature of the reflectance of water body is usually zero; therefore, it appears in black, the darkest tone in grey scale display. The areas bound by line are cloud covers and their shadows. Multi temporal of NDVI maps was produced so that they were able to represent vegetation condition during two peaks of rainy and dry seasons. All NDVI maps is shown in Appendix E.

#### **3.4.13. Soil Wetness from Tasseled Cap Transformation**

Soil wetness can be an indicator of the effect of seasonal rainfall on the wetness of the soil. As discussed in section 2.2.7.2, change in rainfall amount and pattern can affect soil moisture. Monsoonal rainfall, of course, pours different rainfall amount in a year in the study area. As the case of NDVI, multi temporal soil wetness maps were included in landslide susceptibility modeling with intention to investigate their roles in affecting the accuracy of the final landslide susceptibility maps and to seek possible replacement for rainfall data.

Multi temporal of soil wetness maps were derived from four Landsat image presented in Table 3.4. Soil wetness map was computed using linear transformation

of TCT equations as presented in Equation 2.28. It involves linear combination of bands 1-5 and 7 excluding thermal infrared and panchromatic bands. The coefficients in Equation 2.28 were replaced by the ones for computing soil wetness as listed in Table 2.8. The equation for computing soil wetness using TCT is explained in Huang, et al. [194] as follows:

$$\begin{aligned} \text{TC3 (Wetness)} = & 0.2626 \cdot \text{ETM1} + 0.2141 \cdot \text{ETM2} + 0.0926 \cdot \text{ETM3} + \\ & 0.0656 \cdot \text{ETM4} - 0.7629 \cdot \text{ETM5} - 0.5388 \cdot \text{ETM7} \end{aligned} \quad (3.13)$$

The generation multi temporal soil wetness was carried out within ArcGIS environment so that the resulted maps were already re-mapped into grayscale index ranging from 0 to 255. All soil wetness maps are stored in Appendix F. Snapshot of soil wetness of Tanah Rata is portrayed in Fig. 3.40. In general, soil moisture of forest areas surrounding Tanah Rata town is higher than that of open and built up areas

#### **3.4.14. Land Surface Temperatures**

As discussed in section 2.2.7.3, LST changes as rainfall intensity varies. LST was computed employing Equation 2.16 to 2.19 and not to continue to Equation 2.24 due to the absence of some parameters such as  $\varepsilon$  (the ground surface emissivity) and  $\tau_6$  (the atmospheric transmittance). Therefore, the computed LST still contains radiance of surrounding objects and the effect from atmosphere. LST resulted at this stage is known as brightness temperature. In this study, this parameter is assumed to be LST. In addition, reduction of LST to local values was intended to approximate these values to in situ temperature. Reduction was referred to monthly temperature data at Tanah Rata weather station averaged from 1930-1975. This station is located at 4.50°N 101.40°E, and about 4487m above mean sea level.

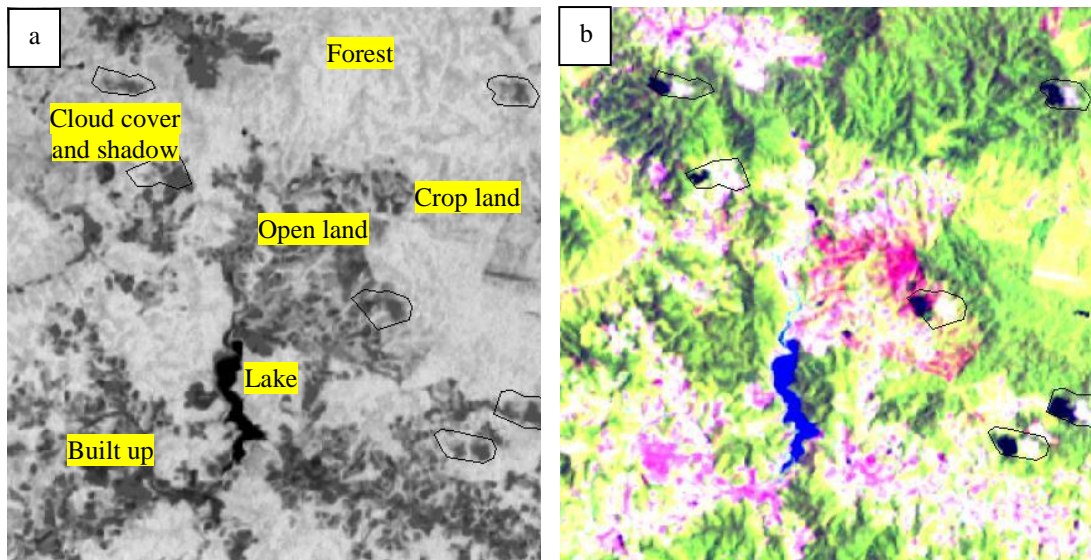


Fig. 3.39 NDVI (a) and RGB images (b) of Tanah Rata-Ringlet

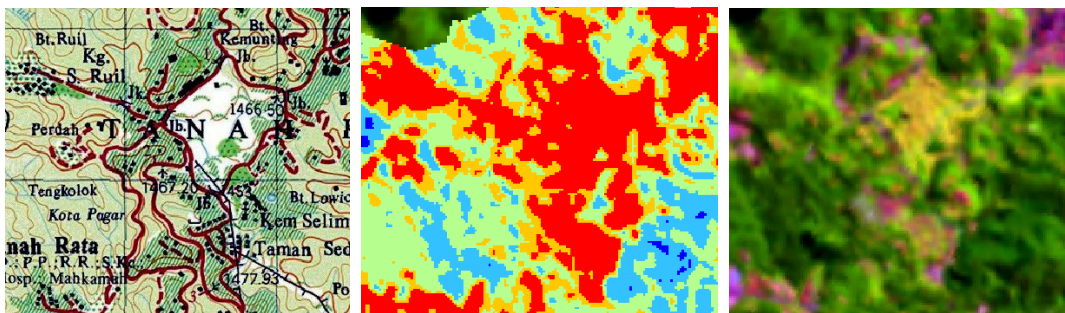


Fig. 3.40 Snapshot of soil wetness at Tanah Rata (center), topographic map (left), and the corresponding image (right)

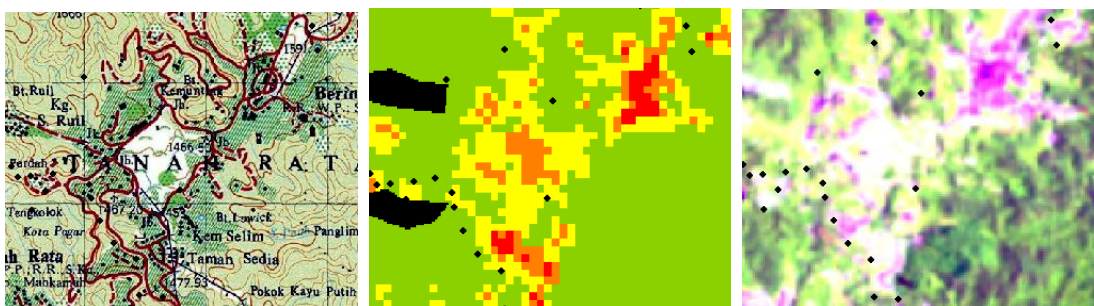


Fig. 3.41 Snapshot of LST at Tanah Rata (center), topographic map (left), and the corresponding image (right)

The main input to Land Surface Temperature (LST) data is four thermal infrared (band 6) images. The high gain antenna mode 6 was chosen rather than the low one.

The selection was based on the consideration that the condition of surface brightness of most of satellite images was low. The high gain antenna mode means that the antenna is highly focused. Fig. 3.41 shows that LST of urban areas is higher than that of the surrounding sparse vegetated areas. Meanwhile, LST of sparse vegetated areas is higher than that of forest area. All LST maps can be found in Appendix G.

### 3.4.15. Dealing with Cloud Cover Problem

Cloud cover has been a frequent problem when dealing with satellite images of highlands area. Cloud cover and cloud shadow prevent extraction of spatial information e.g. land use land cover, LST, NDVI, and TCT soil wetness of the areas covered by clouds and their shadow. In this research, the concern is to remove the covered area from the image either automatically or manually. In doing so, a mask layer for removing clouds and their shadows should be created. ERMMapper provides the following algorithm for cloud masking that utilizes ratio of band 1 as input 1 (I1) and band 6 (thermal infrared) as input 2 (I2):

$$\text{IF } (I1/I2 > 1.70) \text{ THEN } 255 \text{ ELSE } 0 \quad (3.14)$$

As the results, the built in algorithm can only delineate areas covered by cloud excluding areas covered by cloud shadow that are shown Fig. 3.42 as delineated areas in red color beside the clouds. To overcome this problem, cloud and shadow mask were created by on-screen digitization on four Landsat satellite images from which LULC, TCT soil wetness, NDVI and LST maps are derived. Polygon shape files were prepared for creation of multi temporal cloud and shadow masks. Fig. 3.43 shows cloud and shadow mask for Landsat dated on 20 September 2001. The remaining masks can be found in Appendix H. The percentage of cloud cover and its shadow areas of the first, second, third and forth Landsat images is 24.2%, 23.7%, 3.4% and 10.4% of the total area respectively. The first two Landsat images contain a wide coverage of cloud covers and the associated shadows.

As these masks were used to remove clouds and their shadows, it left ‘holes’ or blank areas on the images of LULC, NDVI, TCT soil wetness, and LST. For LULC maps, the ‘holes’ were replaced by the image classification results from other Landsat

data i.e. Landsat images acquired on 24 February 2001 and 31 May 2001. The author made an assumption that the LULC remained unchanged during the study. Fig. 3.44 illustrates the procedures of filling up the ‘holes’ due to cloud cover and the shadow of Landsat image acquired on 20 September 2001.

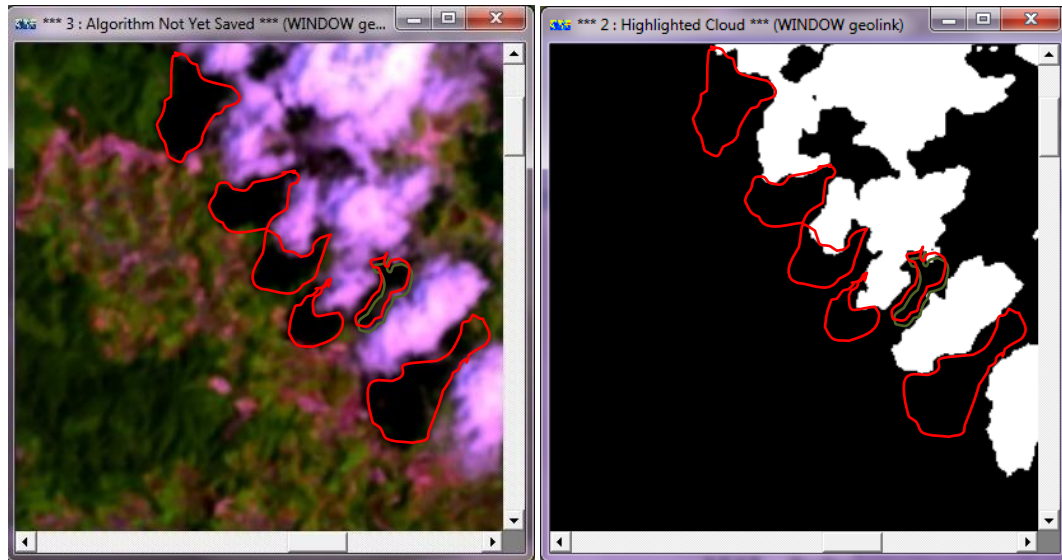


Fig. 3.42 A Landsat image with cloud and shadow (left); cloud mask and remaining cloud shadows (right)

In case of NDVI, TCT soil wetness and LST, the holes are kept as they were. No attempt was made to fill up the holes. This is due to the author’s assumption that these data are of time varying factors. Therefore, there is no need to fix this problem. The only reasonable solution is to fill these holes with the images of adjacent date of acquisition. However, this will take extra works and will be cumbersome to carry out. In addition, different date of acquisition will result in different values of NDVI, TCT soil wetness and LST due to different atmospheric effects. These blank areas were then assigned as ‘no data’ for further GIS analysis.

#### **3.4.16. Lithology and Lineament Maps**

Three different sources of geology map were scanned and georeferenced using a polynomial function with respect to the following georeferenced maps:



1. Coastline map from geology database for georeferencing geology maps of Perak and Pahang,
2. Topographic map for georeferencing geology maps of Pos Selim and Tanah Rata.

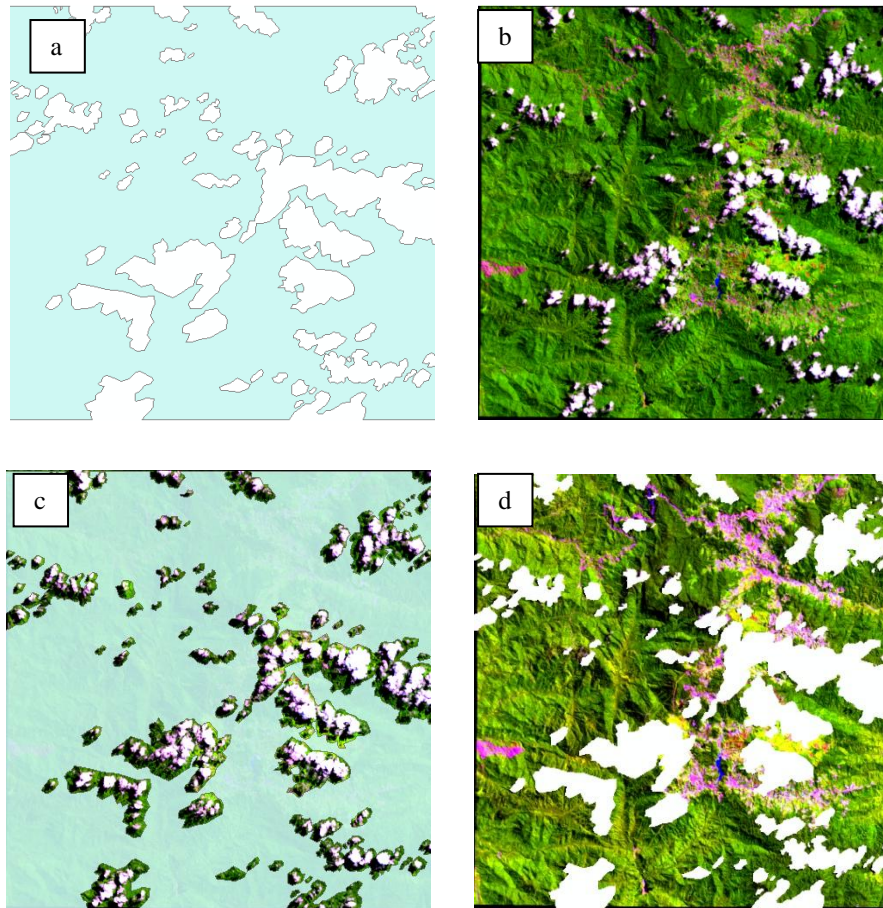


Fig. 3.43 (a) Cloud and shadow mask, (b) the satellite image, (c) the mask over the image, (d) cloud free image



Fig. 3.44 (a) a classified image with 'holes'; (b) a classified image with 'holes' on top of another classified image; (c) 'holes' have been filled up



In order to allow geology maps to be compatible with other spatial data, a polygon shape file was prepared using ArcGIS to store geology data from different sources. Lithology boundaries were onscreen digitized. The respective attributes that consist of alluvium (83% of the study area), *undifferentiated*/sedimentary rock (14.45%), schist (2.41%) and granite (0.14%) were added to geology layer. This layer was then converted into raster format for GIS analysis purpose and is shown in Fig. 3.45.

Geology lineament (or geology fault) map was extracted from the georeferenced geology map by means of on-screen digitizing. A polyline shape file was prepared to record the digitized lineaments. Geology lineament map is also shown in Fig. 3.45. For GIS analysis purpose, Euclidean distances (Fig. 3.46) were computed to provide assessment on the effect of distances from lineaments to landslide occurrences.

#### **3.4.17. Soil Map**

Soil map is an important landslide causative factor as described in section 2.2.1. Soil map explains weakening of slope forming material due to natural processes such as weathering and tectonic uplift as reported by Zhou, et al. [51].

Soil map was in digital format with no projections system. This map was first georeferenced so that soil layer can be extracted. Coastline map from geology database was used as the reference for georeferencing. First order (linear) polynomial was used as transformation function requiring at least three GCPs. Six GCPs were prepared to allow a better georeferencing result. Using only six GCPs, accuracy is not the main concern due to the fact that the scale of both maps is very small. Georeferenced soil map is shown in Fig. 3.47.

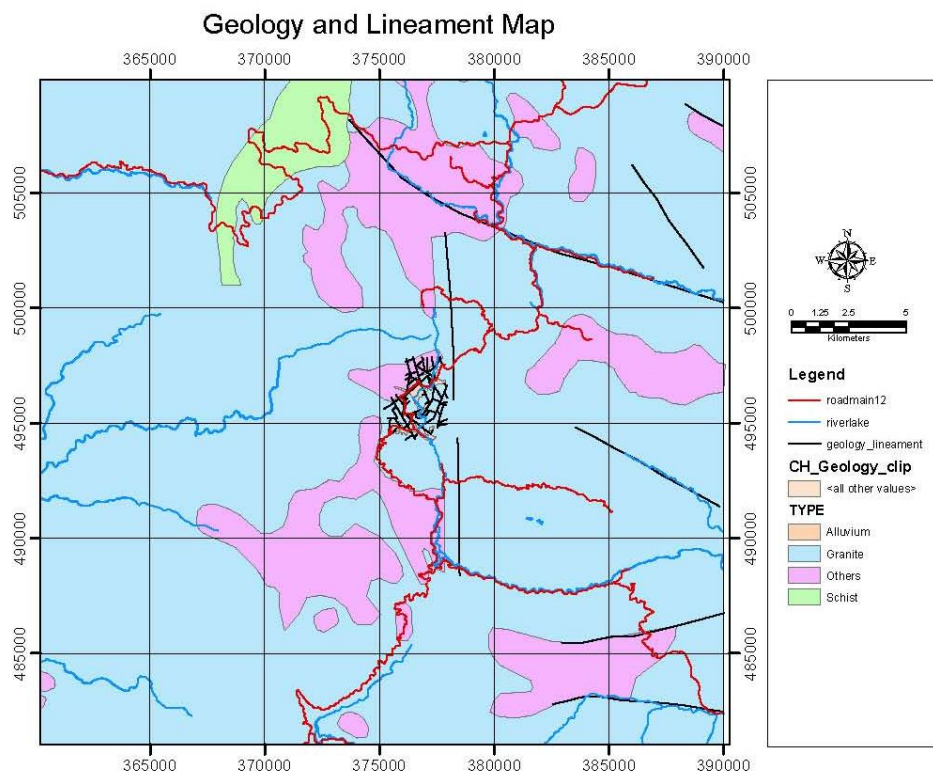


Fig. 3.45 Geology and lineament map

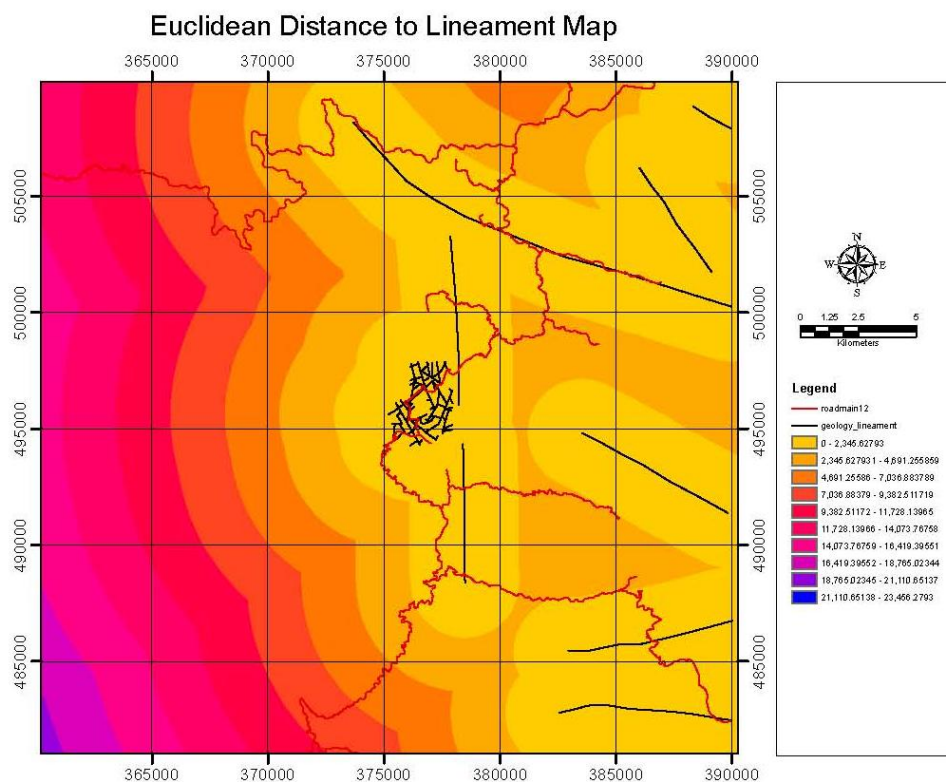


Fig. 3.46 Euclidean distances from geology lineament

The next step was to prepare a polygon shape layer in which soil type boundaries were digitized then stored, and soil attributes were assigned. Soil map of the study area consists of three soil types namely (1) Red-Yellow Podzolic soil with Reddish-Brown Lateritic soils on residual materials from acid to intermediate igneous rocks, arenaceous, argillaceous, and mixed sediment (2) Podzols and Lithosols on acid igneous rocks at elevations above 5000 feet, and (3) Red-Yellow Podzolic soils with Lithosols on acid to intermediate igneous rocks. The latter dominates 86.2% of the study area followed by the soil type (1) and (2) that occupy 12.4% and 1.4% of the study area respectively.

#### **3.4.18. Landslide Inventory**

As described in section 3.3.7, landslide and slope failures location were available in form of a list of coordinates obtained from site survey and a digital map. To merge both data, a point shape file was prepared to store both data. Landslide data from site survey was exported to ArcGIS from its native format produced by Map Source software. Meanwhile, landslide map from ARSM was digitized on-screen. Prior to on-screen digitizing, the landslide map underwent rectification process. The result of merging both data is a landslide inventory map of the study area consisting of 258 landslide points as portrayed in Fig. 3.48. This map is used for deriving spatial relationship between landslide causative factors and past landslide occurrences and for map validation.

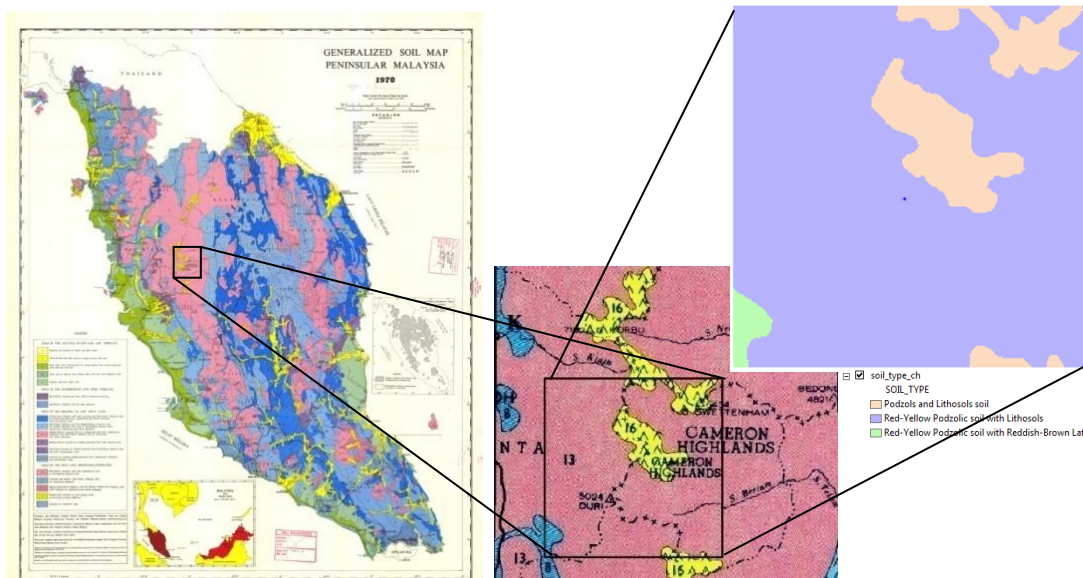


Fig. 3.47 Soil map of the study area

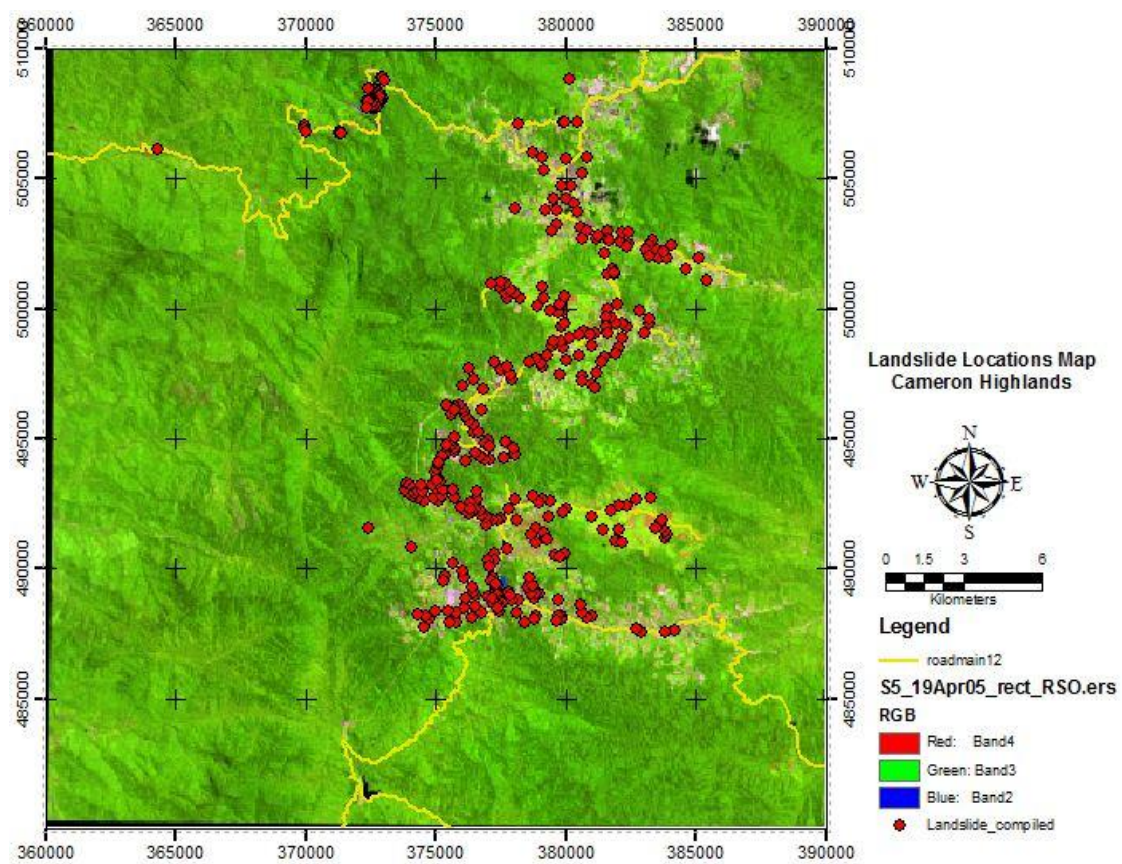


Fig. 3.48 Landslide map of the study area

### **3.5 Landslide Susceptibility Modeling**

The works at this stage are manifestation of the objectives of the research. In regard to achieve the research objectives, strategies of data processing and analysis were arranged. Fig. 3.49 shows work flow for data processing and analysis. The works begin after all required thematic map of landslide causative factors gathered. All thematic maps are required to be in raster format. Spatial relationship between landslide factors and past landslide events is derived for use in deriving weighting system. All classes are awarded weight values according their influences allowing provision of weighted thematic maps. Four scenarios of data processing were designed to compensate multi temporal factors and assessment of their roles. LSMs resulted from these scenarios are analyzed to provide answers for the research objectives. The detail of these works is explained in the following sections.

#### **3.5.1 Extraction of Terrain Attributes of Landslide Sites**

Extraction of terrain attributes of landslides sites is intended to determine the spatial relationship between landslide causative factors and past landslide events. The characteristics of landslides at the study area were obtained by means of crossing of each causative factor with landslide locations on the landslide map. It is assumed that there is no correlation between landslide causative factors. Using Extraction Values to Points function in Spatial Analyst Toolbox of ArcGIS, the attributes of each landslide location such as LULC, lithology, elevation, and elevation, were extracted.

A number of 358 landslide points with size of 30 m x 30 m were used to extract landslide attributes. The extraction procedure is illustrated in Fig. 3.50. Fig. 3.50a is a layer of landslide map and Fig. 3.50b is a layer of slope map. Both layers are overlaid and crossed (Fig. 3.50c) so that it results in a new layer of point shape with the corresponding slope attribute table (Fig. 3.50d). This table is used to construct landslide frequency diagram (Fig. 3.50e) to facilitate interpretation of landslide occurrences in relation with slope classes.

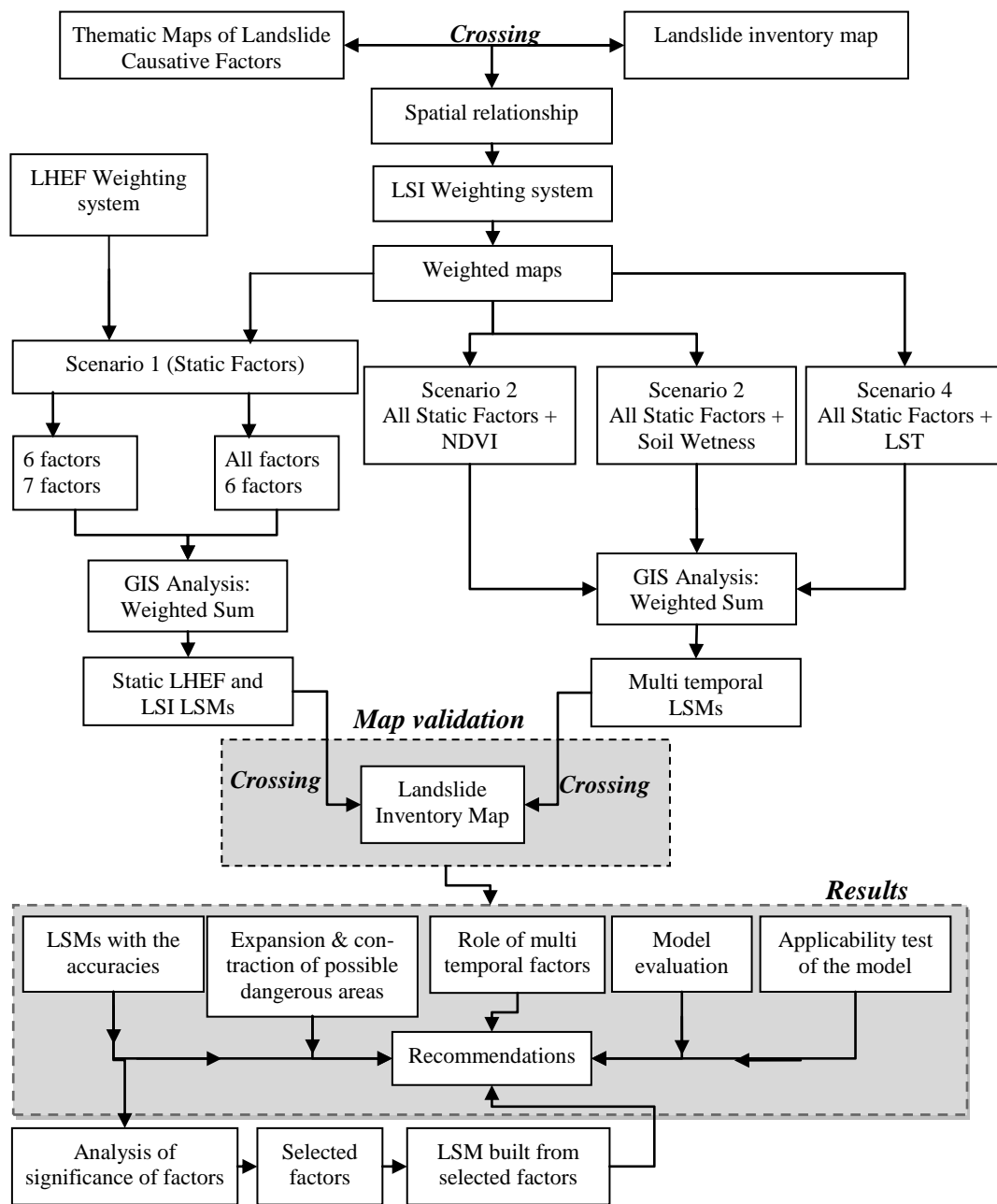


Fig. 3.49 Work flow of landslide susceptibility modeling

Crossing landslide map with remaining causative factors were carried out so that each causative factor has landslide occurrences distributed to its classes. Classes with associated landslide occurrences number were used to compute landslide indices, i.e. Landslide Susceptibility Index (LSI) and Landslide Frequency Index (LFI).



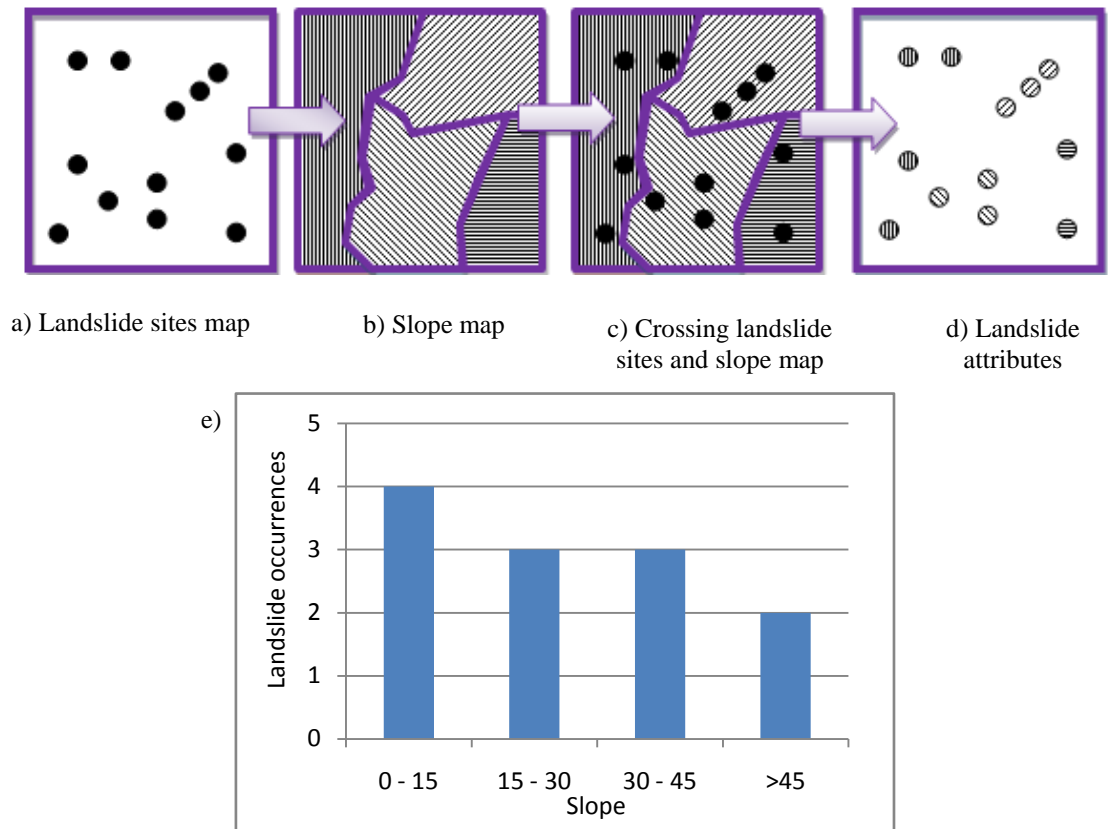


Fig. 3.50 Crossing landslide map and slope map

### 3.5.2 Landslide Attributes Reclassification

Based on the result of crossing, landslide attributes of each landslide causative factor were classified into five categories. The classification was based on ‘natural breaks’, an option offered in ArcGIS environment during reclassification process, referring to the natural break of the data. The selection of the class number, that is 5, is meant to facilitate assigning 5 susceptibility statuses namely, very high, high, moderate, low, and very low. Fig. 3.51 below is an example of reclassification of slopes into 5 categories using natural breaks method. Five classes of slope (in degree) along with the number of landslide occurrences are as follows: 0 – 7.8 (84 occurrences), 7.8 – 19.4 (76), 19.4 – 27.4 (90), 27.4 – 36.4 (63), and 36.4 – 51.0 (37).

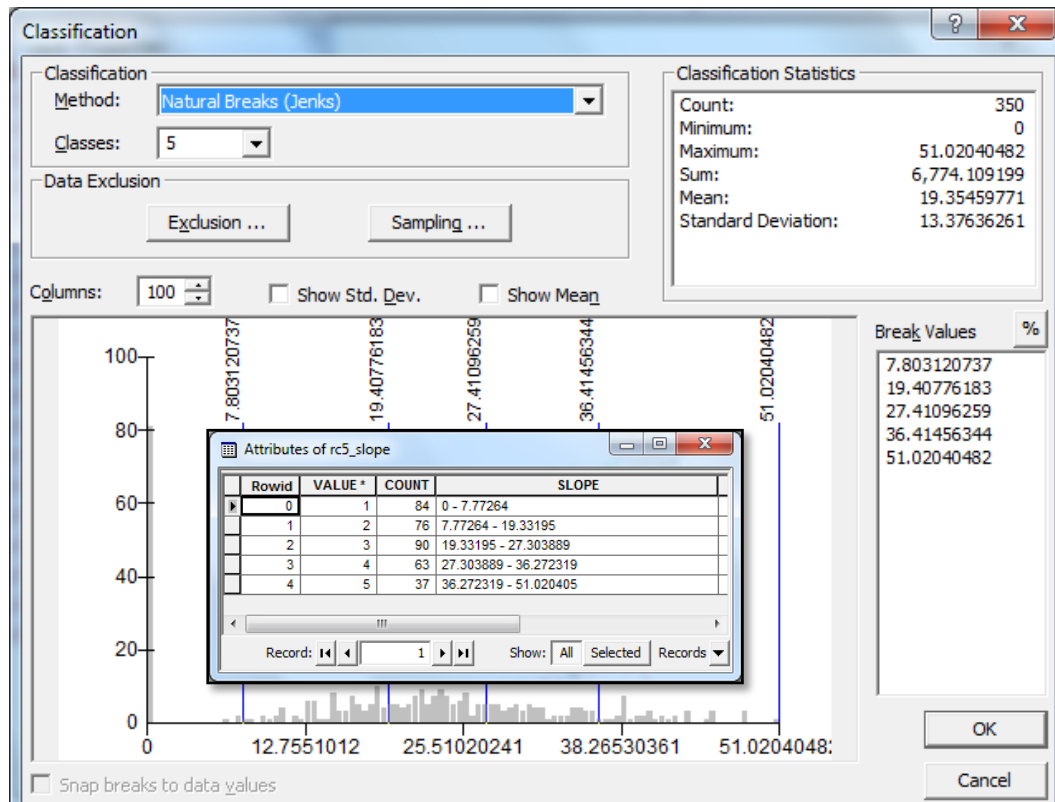


Fig. 3.51 Classification of slope attributes into five

Landslide causative factors that can be reclassified are:

1. Slope
2. Elevation
3. Distance from road
4. Distance from river-lake
5. Distance from lineament
6. Curvature
7. NDVI
8. TCT soil wetness
9. LST

Slope aspect map cannot be reclassified because its classes are fixed. The classes determine compass directions the slopes face. Lithology, LULC, and soil map also cannot be reclassified because they are not continuous surface. Each map has fixed classes.



### **3.5.3 Weighting System**

Relative contribution between causative factors is difficult to identify. This is the problem encountered by Liao [47] during constructing landslide hazard map of counties of Arkansas. However, Chan [148] reported that most of landslide occurrences in Malaysia were triggered by rainfall; more appropriately is after prolonged rainfall. This is also the trend of landslide occurrences in the study area. Therefore, landslide causative factors related to rainfall, i.e. NDVI, soil wetness, and LST deserve to be awarded higher weight values over the others. In addition, high level of erosion occurred in agriculture area as reported by Aminuddin, et al. [151]. Cropland, as related with agriculture area, also deserves to have a high weight value. Anbalagan [2] set the maximum weight values to 2 or 1 in LHEF rating system for different causative factors during investigating landslide hazard in Himalaya. This assignment of weight values mostly depends on expert's opinion/knowledge. In this study, the significant role of all causative factors was treated the same. This is also intended to avoid subjectivity by the author in assigning different weight values for each causative factor. However, relative importance between classes was considered.

Bivariate statistical method described in section 2.4.2.1 was chosen as the method to derive weighting system. There are two types of expressing relationship between landslide causative factors and landslide occurrences, i.e. using area density which is also known as LSI, expressed in Equation 2.4, and number density known as LFI, Equation 2.5. These two methods were evaluated and applied in this study.

### **3.5.4 Final Landslide Susceptibility Maps and Scenarios**

Final landslide susceptibility maps (LSMs) were constructed by summing up weighted thematic map of landslide causative factors. Cross correlation between landslide causative factors was assumed to be ignored. LSI and LFI values were used to derive weight values of classes of a particular causative factor. The following section is the description of derivation weight values of slope classes.

In section 3.5.2, slope map has been reclassified based on slope intervals obtained from crossing process. There is an attribute table accompanying slope layer consisting

slope classes and the number landslide occurrences. Using built in mathematic functions in ArcGIS, area of each class can be computed. Area of landslide of each class can be computed as well by multiplying the number of landside occurrences with the resolution of working image that is 30 m x 30 m. Therefore, a slope class with 84 landslide occurrences means that the area of landslide occurrences within this class is  $84 \times 30 \times 30 = 75,600$  square meter. The areas of the remaining classes are calculated using the same procedure. Ratio of area of landslide and area of respective class determine the LSI value. Ratio of all classes is calculated. To avoid the small value of the ratio result, Suzen [57] provided 1000 as a multiplication factor as expressed in Equation 2.4. For awarding a weight value, a class with the largest LSI value is awarded weight value of 100. The remaining classes are awarded weight values proportional to a class with the largest LSI value. Ratio of LSI of a slope class and LSI of a slope class with the largest LSI value multiplied by 1000 determines weight value of a particular slope class. Calculation of weight value of classes of the remaining landslide causative factors follows the mentioned procedures. After all classes of all causative factors have been assigned weight values, the weighted thematic maps are ready to use in landslide susceptibility modeling.

Another weighting system that is LHEF rating system was also applied. This weighting system is part of qualitative method. The way classes of a particular landslide causative factor awarded a weight value is based on LHEF rating system developed by Anbalagan [2]. The application of this weighting system was intended to provide a comparison result to bivariate statistical method.



The final LSMs were constructed by summing up all weighted map using Equation 2.9, mentioned in section 2.4.3. In ArcGIS, it was done by applying weighted sum overlay method. The final LSMs were divided into 5 categories of susceptibility ranging from Very High (VHS), High (HS), Moderate (MS), Low (LS), and Very Low susceptibility (VLS). These abbreviations are applied for further discussing the results.

The method of construction of the final LSMs is the simple one that is weighted sum. The underlying reasons of selecting this method is that the method of zoning an area into different level of potential landslide threats is open for exploitation as

suggested by Guzzetti [29] and there is no single method proven to be superior in every area and for all types of landslide. Jamaluddin, et al. [227], a local landslide expert, added that there is no satisfactory slope assessment system in Malaysia. Therefore, the author took advantage about this matter by applying the simple method. Another important underlying reason is that this study focuses on modeling landslide susceptibility that incorporates the changing environmental factors due to the effect of monsoonal rainfall system acting on the study area. Their roles in explaining landslide occurrences and seasonal rainfall amount were investigated.

Table 3.14 Scenario of data set for landslide susceptibility modeling

No.	Landslide causative factors	Scenario I			Scenario II	Scenario III	Scenario IV
1	Slope	√	√	√	√	√	√
2	Slope aspect				√	√	√
3	Elevation				√	√	√
4	Curvature				√	√	√
5	Dist. from road				√	√	√
6	Dist. from river/lake	√	√	√	√	√	√
7	Dist. from lineament	√	√	√	√	√	√
8	Geology	√	√	√	√	√	√
9	Soil	√	√	√	√	√	√
10	LULC	√	√	√	√	√	√
11	NDVI				√		
12	Soil Wetness		√			√	
13	LST						√

 Data not involved     
  Multi temporal factors

To achieve the stated research objectives, four scenarios of data processing were designed. Table 3.14 presents the scenarios in which different list of landslide causative factors are included. The total number of ‘static’, i.e. non-change in time, factors, is 10 while the number of multi temporal factors is 3 namely NDVI, soil wetness, and LST. Scenario I is called as a ‘static’ scenario because it involved static causative factors. Within scenario I, there are 4 sub scenarios namely LHEF 6, LHEF 7, LSI 6 and LSI 10 (all factors). The application of these 4 sub scenarios was intended to evaluate which method, between qualitative and quantitative methods, results in satisfactory result; to evaluate the number of causative factors involved in the modeling; and to provide a benchmarking result that can be used to evaluate the

roles of multi temporal causative factors namely NDVI, soil wetness, and LST, in the developed LSMs. Scenarios II, III and IV used the same data set of scenario I that is ten factors with additional multi temporal data of NDVI, TCT Soil Wetness, and LST respectively. For each scenario, four LSMs were produced.

### **3.5.5 Validation of Final LSMs**

Validation of landslide models applies well known and widely applied principle that is '*the past and present are keys to the future*' as mentioned by Varnes [38], and Carrara, et al. [228]. This principle implies that slope failures/landslides in future will be more likely to occur under those conditions which led to past and present instability. Map validation is intended to measure the accuracy of the final LSMs produced from various scenarios. By knowing the accuracy of the final LSMs, the role of a particular causative factor can be judged; the model of landslide susceptibility can be evaluated; and a recommendation on landslide susceptibility modeling can be drawn.

The landslide map expressing the distribution of landslide and slope failure locations in the study area is an important key to assess the accuracy of the final LSMs. The procedure to assess the accuracy is by using the same procedures described in section 3.5.1 that is by crossing the final LSMs with the landslide map. This process results in a new layer with an attribute table containing a list of landslide points/locations and the respective susceptibility attributes e.g. VHS, HS, MS, LS, and VLS. The author made an assumption that the landslide/slope failure locations on the landslide map should fall in VHS and HS categories in the final LSMs when both maps are overlaid. The number of landslide points having both status (VHS and HS) categories is used to measure the accuracy of the final LSMs. Susceptibility statues of MS, LS, and VLS are considered as secure. Hence, the greater the number of landslide points falling in VHS and HS categories, the more accurate the landslide susceptibility model. After map validation is completed, the following things, as portrayed in Fig. 3.49, can be concluded:

1. Landslide susceptibility models indicated by the accuracy of LSMs,
2. The role of each multi temporal factor,
3. Possible expansion and contraction of potential dangerous areas, i.e. with VHS and HS statuses,
4. Suitable weighting system.

### **3.5.6 Analysis of Relative Role of Causative Factor**

It has been mentioned in section 3.5.3 that relative role of each landslide causative factor is not easy to measure. However, this study also made an attempt to evaluate the relative important/role of a landslide causative factor to other factors. The factors identified as the significant ones are used to produce LSM. The underlying idea is that an appropriate weighting system combined with selected significant causative factors would result in a more accurate LSM.

### **3.5.7 Test of Applicability of the Developed Model**

Penang Island is considered as a landslide prone area. A number of landslides have occurred (Fig. 3.52). The spatial data required for conducting a study on landslide susceptibility modeling are available. These two conditions underlined the selection of this place as test site for the applicability of the developed mode regardless the fact that this place is not considered as highlands areas as the case of Cameron Highlands. Either qualitative or quantitative method proven to be superior in producing a more accurate LSM will be chosen. The causative factors proven to be the significant ones will be adapted for applicability test in the test site. Assessment of the accuracy of the final LSM of Penang Island constructed using Cameron Highlands landslide susceptibility model was carried out using the same procedures mentioned in sub section 3.5.5.

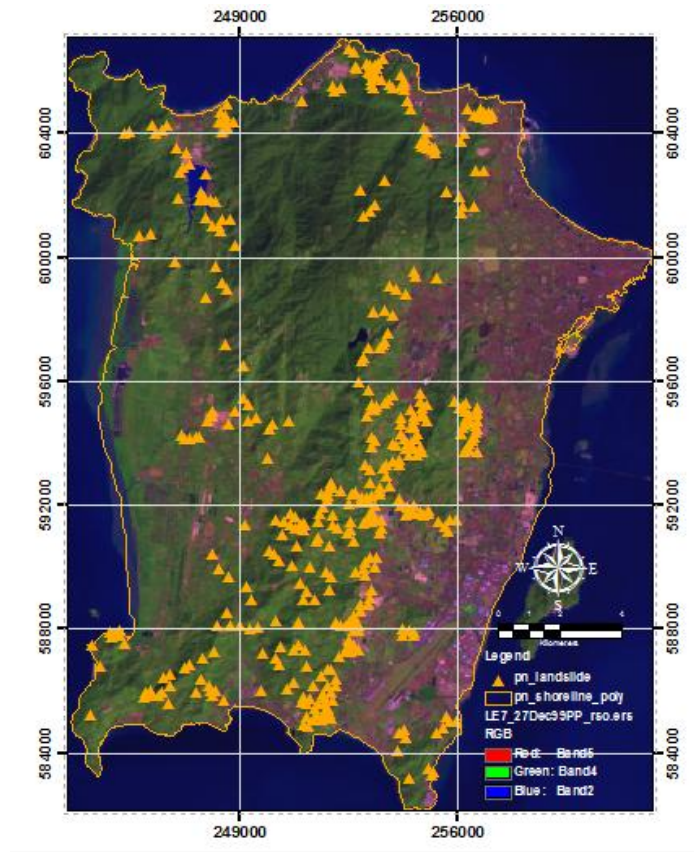


Fig. 3.52 Landslide map of Penang Island on top of a Landsat image

### 3.6 Chapter Summary

This chapter has presented characteristics of the study area, data required for modeling landslide susceptibility and the overall methodologies employed to achieve objectives of the research. The summary is depicted in Fig. 3.53.

The characteristics of the study area have ensured that this area is feasible for conducting modeling landslide susceptibility. The relevant characteristics include high frequency of landslide occurrences during rainy seasons, monsoonal rainfall system, high rate erosion, road development, extensive gardening and farming, etc. The most interesting factor to conduct the modeling is the nearly synchronous between rainy cycle and frequency of landslide occurrences.

Relevant data from different sources and format were gathered. The data mainly consists of Landsat 7 ETM+ and SPOT 5 satellite images, topographic map, soil map,

geology map, rainfall data, and landslide map. Data preprocessing such as geometric correction and atmospheric correction were applied for the satellite images. Soil, geology and hardcopy of topographic maps underwent geometric correction as well so that the spatial data extracted from these maps are compatible with other spatial data already in RSO projection system. The data were further processed to produce thematic maps consisting of 10 static factors and 3 multi temporal factors. The first factors consist of maps of slope, slope aspect, curvature, elevation, road network, river/lake, lineament, lithology, soil, and LULC. The second consist of NDVI, soil wetness, and LST. Cloud and shadow has been problems in preventing to acquire a full map. The areas affected by both features were left blank for NDVI, soil wetness, and LST maps and filled with the information gained from the adjacent date of acquisition image.

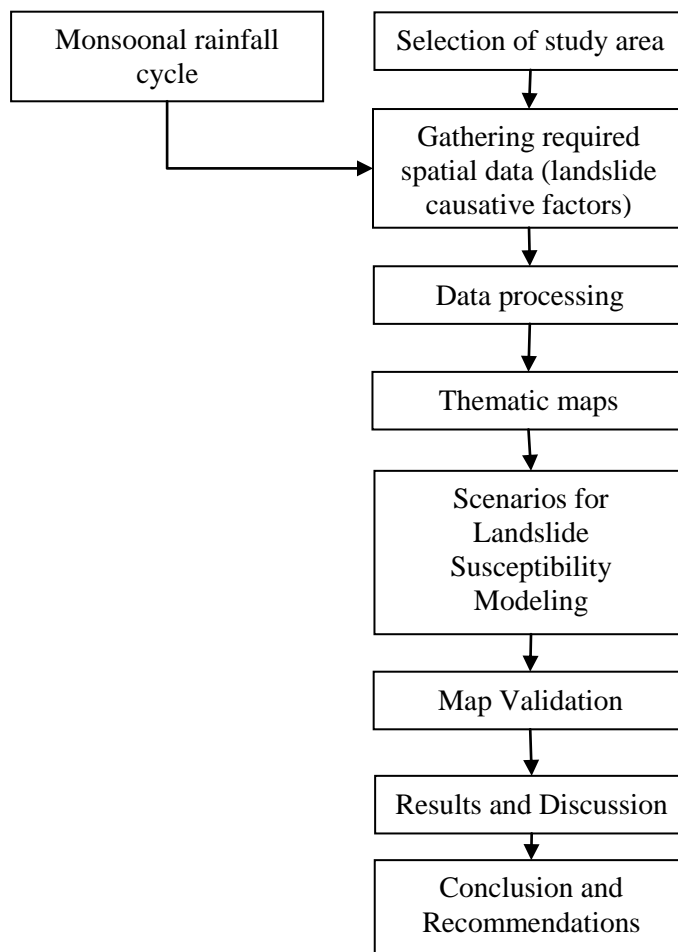


Fig. 3.53 Flow chart of chapter 3

Landslide susceptibility modeling begins with determining the spatial relationship between past landslide occurrences and causative factors. The relationship of both factors underlies the derivation of a weighting system, the assignment of weight values to classes of each causative factor, and the preparation of weighted thematic maps.

There are four scenarios of modeling. The first scenario includes only static factors; the second to fourth scenarios involve all static factors with additional multi temporal factors namely NDVI, soil wetness, and LST respectively. The scenarios were designed to answer objectives of the research on the roles of multi temporal factors in modeling landslide susceptibility. Map validation is applied to investigate the role of multi temporal factors. From scenarios of landslide susceptibility modeling, conclusions and recommendations can be drawn.



## CHAPTER 4

### RESULTS AND DISCUSSION

#### **4.0 Overview**

This chapter describes the spatial relationship between landslide map and causative factors from crossing process, discussion on derivation of weighting system using two indexes, LSI and LFI, and using LHEF rating system. Results of landslide susceptibility modeling using scenario 1 to 4 are discussed and evaluated with the mentioned research objectives. The roles of multi temporal factors introduced in the modeling and the develop landslide model are evaluated.

#### **4.1 Weighting System and Construction of Thematic Maps**

Table 4.1 shows four landslide causative factors of the study area namely land use land cover, geology, elevation and slope. This table explains the number of landslide on each class of a causative factor (column 3), the area of landslides (column 6), the exposure areas of that sub category (column 7), the computation of LSI (column 8) and LFI (column 9), and weight values computed using LSI (column 10). The remaining causative factors are shown in Table 4.2 to Table 4.7. The assignment of weight values to classes of every causative factor is intended to construct the weighted thematic map of all scenarios.

The distribution of landslide occurrences in classes of a particular causative factor were determined from two processes namely crossing between landslide map and that particular factor and reclassification. Therefore, the resulted LSI values were solely generated from crossing process, more particularly the accuracy of landslide inventory map. Sometimes the results of crossing, i.e. LSI values, are somewhat

contradictory according to geotechnical point of view such as the case of slope LSI values. Adequate explanation is given to LSI of all causative factors. However, one thing to take notes is that the method used to derive LSI is bivariate statistical approach. The method is typically data driven process regardless the role of thumbs in geotechnical perspective.

#### **4.1.1 Weight Values and Thematic Map of Land Use Land Cover**

The study area that covering 900,000,000 square meter was divided into five categories of LULC. They are 1) cropland, bushes, thin vegetated area in a group; 2) forest; 3) urban and built up; 4) open land and cut slope; and 5) river and lake.

The distributions of landslide occurrences within LULC types as well as the LSI values are shown in Fig. 4.1. The Figure shows that the high number of landslide occurrences in a particular class does not necessarily produce high LSI values. As the example of this case is the forest class. The number of landslide occurrence at this class is the highest one, 138. However, the LSI value is the lowest one, 1.87. Crop land-bushes-thin vegetated area class has a similar condition with forest. This is the consequence of using bivariate statistical method. This method offers an objective measure of landslide occurrence relative to different types of land use land cover by means of comparing the area of landslides within a class, i.e. forest, and the area of the respective class, i.e. forest. The size of the study area and the distribution of landslide sites affect the values of LSI. The remaining classes show inconsistencies between the number of landslide occurrences and LSI values. LSI value of open land-cut slope is the highest one, 32.57, although the corresponding number of landslide occurrences is the lowest one, 57. The second highest LSI values, 19.70, belongs to urban-built up class even though the corresponding number of landslide occurrences, 90, is higher than that of open land-cut slope class. The LSI values of these last two classes can be a preliminary indicator of intervention of human in contributing instability of slopes by changing natural slopes into for examples, cut slopes for road development, urban expansion, open land for constructions, etc. Since there is no landslide within lake or river, the respective LSI value is zero.

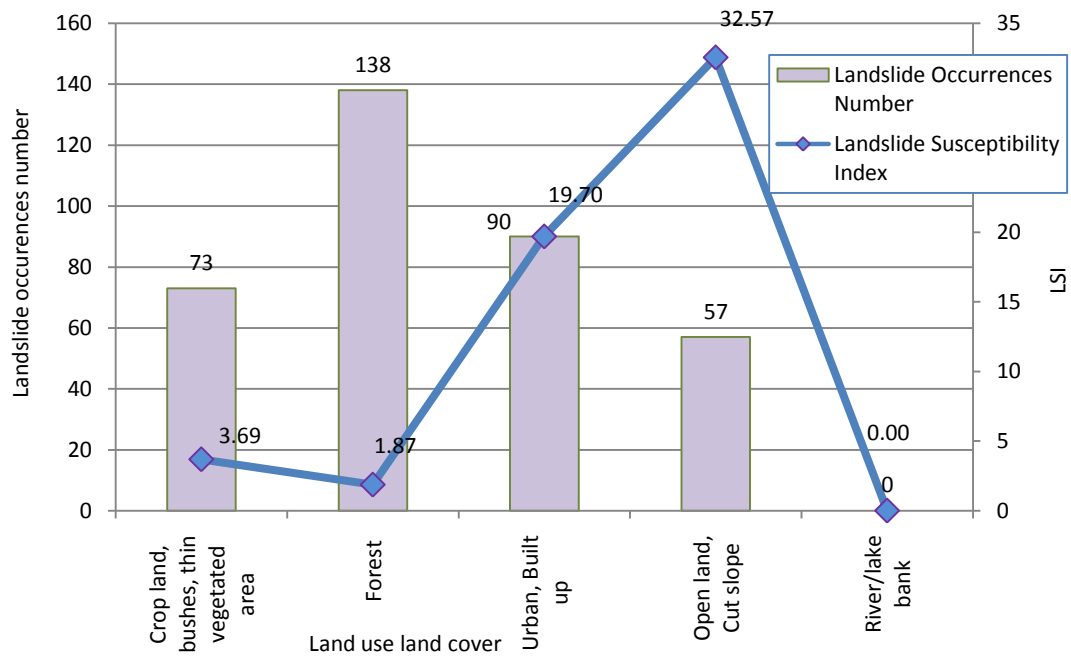


Fig. 4.1 Landslide occurrences number and Landslide Susceptibility Index of land use land cover

The identified landslide locations on the landslide map were mostly located in places that were formerly covered by forest. It seemed to be a contradiction to the fact that forested areas generally tend to increase the stability of the slopes. A reasonable explanation regarding this contradictory is that the sources of spatial data used for constructing the landslide map of Cameron Highlands are mainly from interpretation of aerial photographs acquired during the period of 1981-2002 by Malaysian Center for Remote Sensing as reported by Pradhan and Lee [229]. These authors added that landslides were recognized through image interpretation process as breaks in the forest canopy, bare soil, or geomorphological features such as head and side scarps, flow tracks, soil and debris deposits below a landslide scar. Fresh landslide scars were also found during field investigations conducted in 6 December 2006 and 4 May 2008.

The next step is to derive LSI values from which weight values of classes of a particular causative factor can be computed. The theoretical background can be found in Liao [47] and is explained in section 2.4.2.1. LSI is derived using Equation 2.4. Adjustment of multiplication factor was applied to avoid a number of decimals and

facilitate computation of weight values. The detail explanation of obtaining LSI values is given as follows.

In Table 4.1, LSI values presented in column 8 were obtained by dividing area of landslides occurring within each class (column 5) with the total area of that class (column 7). This process produced very small values. As an example, landslide area of cropland is  $65,700\text{m}^2$  while cropland area is  $178,158,600\text{m}^2$ . The division of the first value over the second one produced a very small value of 0.000368773. To facilitate calculation, this number was multiplied by 10,000 so that it resulted in a value of 3.69. This procedure was applied to compute all LSI values. The LSI values were used to derive weight values.

Another way to develop weight values was by using LFI values. Equation 2.5 was used to derive LFI. Adjustment of multiplication factor was also applied to avoid a number of decimals and facilitate computation of weight values. Practically, LFI values were derived from the ratio between the number of landslide occurrences within a class (column 3) and the total area of that class (column 7). As an example, the number of landslide within cropland area is 73. Division of this number with cropland area results in a value of 0.00000040974727. Again, to facilitate calculation, this value was multiplied by  $10^7$  so that it equaled to 4.10. Computation of LSI and LFI values for all classes of each causative factor was done using this manner. This method has been widely used such as by Liao [47], Lee, et al. [230] and Lee, et al. [231].

According to Liao [47], both LSI and LFI values can be used as an objective measure for landslide occurrences that respect to different types of land use land cover. The higher the LSI or LFI values the more prone to landslides. Fig. 4.2 shows that LSI and LFI values indicate the same trend. In this research, LSI was used for generating rating weight values rather than LFI for reasons: 1) LSI measures the

Table 4.1 Landslide attributes from land use, geology, elevation, slope maps, and weighting systems

Landslide factors	Sub-Categories	Landslide number, (%)	Landslide areas (m2)	Number of Pixel of each category	Area of each sub category (m2)	Landslide Susceptibility Index (LSI)	Landslide Frequency Index (LFI)	LSI-based Weight Values
(1)	(2)	(3)	(5)	(6)	(7)	(8)	(9)	(10)
Land use land cover	Crop land, bushes, thin vegetated area	73, (20)	65700	197954	178158600	3.69	4.10	11
	Forest	138, (39)	124200	738129	664316100	1.87	2.08	6
	Urban, Built up	90, (25)	81000	45685	41116500	19.70	21.89	60
	Open land, Cut slope	57, (16)	51300	17502	15751800	32.57	36.19	100
	River and lake	0, (0)	0	713	641700	0.00	0.00	0
Lithology (Rock types)	Granite	231, (65)	207900	830016	747014400	2.78	3.09	15
	Sedimentary rock	82, (23)	73800	144535	130081500	5.67	6.30	31
	Alluvium	1, (0)	900	1429	1286100	7.00	7.78	38
	Schist	44, (12)	39600	24062	21655800	18.29	20.32	100
Elevation	80 - 540.96	0, (0)	0	80293	72263700	0.00	0.00	0
	540.96 - 1130.56	54, (15)	48600	405843	365258700	1.33	1.48	16
	1130.56 - 1249.51	92, (26)	82800	113435	102091500	8.11	9.01	100
	1249.51 - 1394.33	75, (21)	67500	142847	128562300	5.25	26.30	65
	1394.33 - 1585.69	100, (28)	90000	184277	165849300	5.43	6.03	67
	1585.69 - 1864.97	29, (8)	26100	69831	62847900	4.15	4.61	51
	1864.97 - 2100 (max)	0, (8)	0	3466	3119400	0.00	0.00	0
Slope	0 - 7.8	84, (23)	75600	149100	134190000	5.63	6.26	100
	7.8 - 19.3	76, (21)	68400	235235	211711500	3.23	3.59	57
	19.3 - 27.3	90, (25)	81000	310770	279693000	2.90	3.22	51
	27.3 - 36.3	63, (18)	56700	215813	194231700	2.92	3.24	52
	36.3 - 51	37, (10)	33300	83446	75101400	4.43	4.93	79
	51- 89.6 (max. slope)	0, (0)	0	5628	5065200	0.00	0.00	0

proportion of landslide areas, and 2) LSI considers the size of landsides while LFI disregards it.

The assignment of weight values for each class of lands use land cover is described as follows. The land use type that has the highest value of LSI is assigned the maximum weight value of 100. The other land use types are assigned weight values proportional to their LSI values divided by the largest LSI of a class within land use land cover category. For example, open land has the highest LSI value of 32.57 so it is assigned the maximum rating weight value of 100. Crop land is assigned a rating weight value by means of dividing its LSI value, 3.69, by 32.57, the highest LSI value. Hence, the rating weight value of crop land is  $3.69/32.57 \times 100 = 11$ . The rating weight values for the remaining classes were derived using the same manner.

Thematic map of land use land cover was constructed based on weight values derived from LSI. Fig. 4.3 shows thematic map of land use land cover that has a similar appearance as the original land use land cover map except that the map replaces the attribute of land use land cover types with LSI values. The LSI values for open land-cut slope, urban-built up, cropland-bushes, forest and river-lake are 100, 60, 11, 6, and 0 respectively. Areas with the highest weight values are mainly located along roadsides. Few of them are located in the middle of forest and the surrounding of urban/built up areas.

#### **4.1.2 Weight Values and Thematic Map of Lithology**

Crossing between landslide map and lithology/rock map shows that granite-covered area has the highest landslide occurrences number namely 231 (65%) landslides (Table 4.1). It is followed by acid intrusive (sedimentary rock), schist and alluvium with landslide number of 82 (23%), 44 (12%), and 1 (0%). The granite rock type was formed in the late Triassic period, over 200 million years age. Fortuin [150] reported that the depth of the rock may vary from about 5 m to over 25 m.

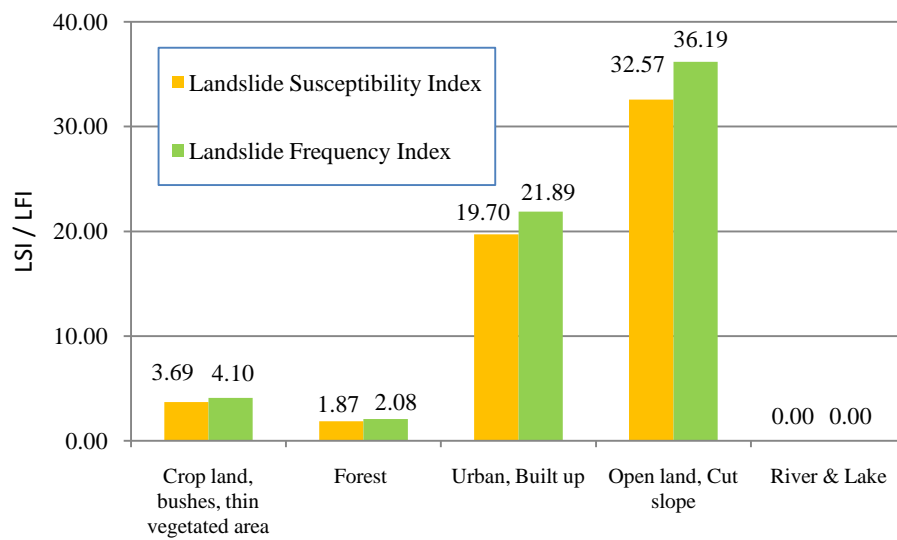


Fig. 4.2 Landslide Susceptibility and Landslide Frequency Indices of LULC

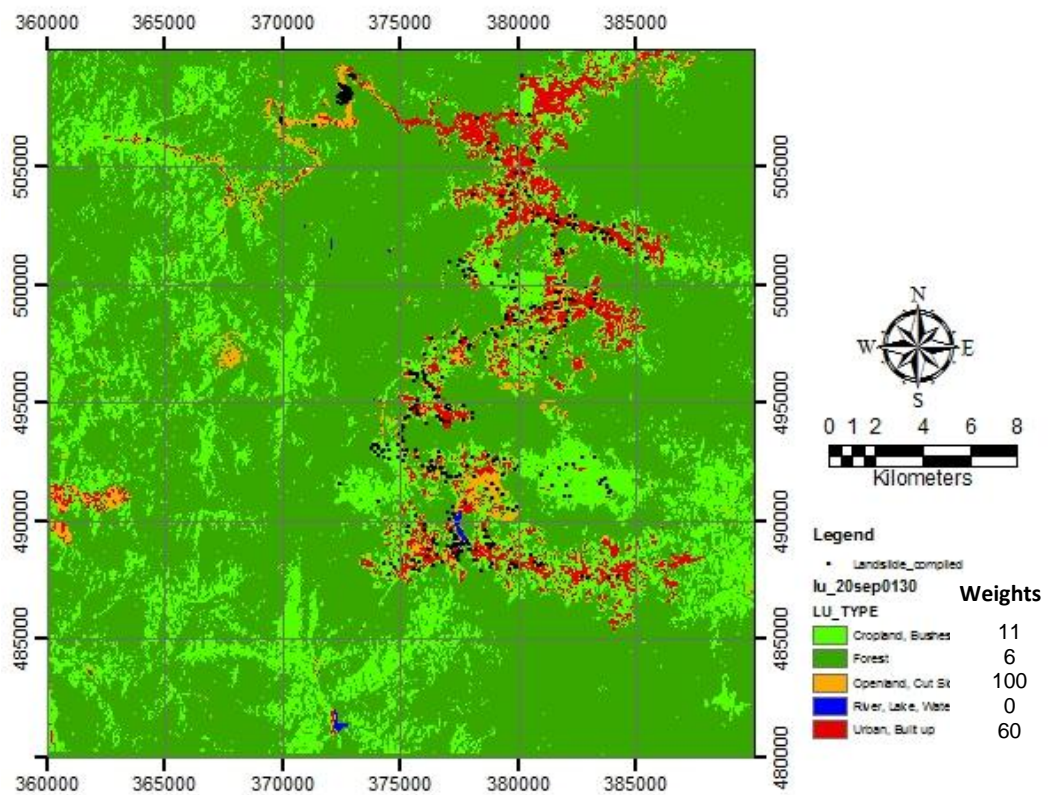
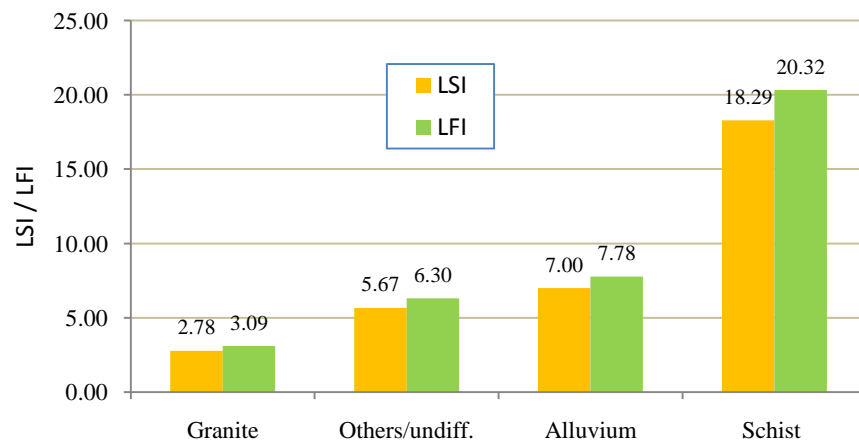


Fig. 4.3 Thematic map of land use

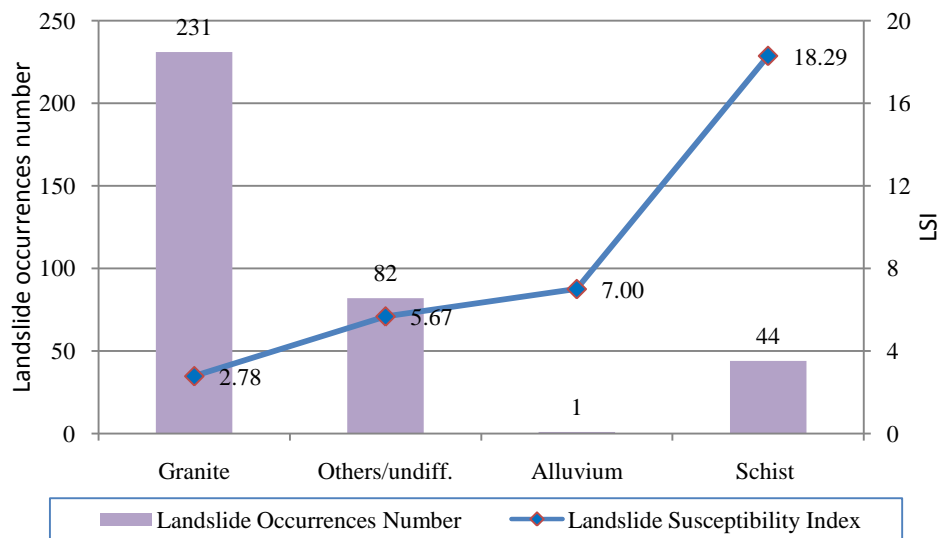
The LSI and LFI values indicate the same trend as shown in Fig. 4.4 (a). Fig. 4.4 (b) shows a different trend between the number of landslides and LSI of lithology type. Granite-covered areas had the lowest LSI value, 2.78, even though this area had the highest number of landslide occurrences, 231. The wide range of granite coverage was responsible in determining this small value of LSI. Almost similar condition went to sedimentary rock type. Schist-covered area was found to be the most prone slopes to fail referring to its highest LSI value, 18.29. As mentioned previously, this is the consequence of applying bivariate statistical approach to produce an objective measure of landslide occurrence relative to different types of lithology. From high to low, LSI values of 18.29, 7.0, 5.67, and 2.78 belongs to schist, alluvium, others/undifferentiated, and granite types respectively.

The existence of a large number of landslides on granite-covered areas has been a questionable phenomenon. According to Mohr's scale of hardness, the hardness of granite is quite high, about 7–8. LHEF of Anbalagan [2] also put granite rock type as having a small rating value meaning that granite rock type was quite hard. Hence, slopes covered with this rock type are least likely to fail. It seemed to be a contradiction having these facts. However, previous investigations along Pos Selim-Cameron Highlands highway, part of the study area, carried out by Jamaluddin [219] showed that the discontinuities existed in the bedding planes of rock mass, both granite and metamorphic bedrock. The area experienced weathering both chemical and physical weathering. There were two weathering profiles of granite that tended to cause rock falls and landslides. The thickness of overburden soil was about 5-20m. Overlay of maps of lithology, landslide sites and river including tributary rivers shows that most of post landslide events occurred near or alongside the rivers. High rate of erosion along the riverside accelerates the weathering process of respective rock mass (Fig. 4.5). Maps overlay of land use land cover, lithology, and landslide site shows that the land use types on top of granite covered area are dominated by urban or built up and crop land types (Figure 4.5b), as the result of image classification. This means that anthropogenic activities might have changed the land cover from the original type into both types. During which, the land cover might appear as landslide scars and then recognized as landslide sites during construction of landslide inventory map by ARSM.





(a)



(b)

Fig. 4.4 (a) LSI and LFI, (b) Landslide occurrences number and Landslide Susceptibility Index of lithology

The rating weight values for lithology were computed the same manner as land use land cover causative factor. Schist was assigned the maximum weight value of 100 due to its maximum LSI value. It was followed by alluvium, sedimentary rock, and granite with their corresponding weight values are 38, 31, and 15. These weight values were computed proportional to their susceptibility indexes (see Table 4.1). Using all these weight values, thematic map of lithology was constructed (Fig. 4.5). Schist area with the highest weight value is located at the top center of the map where Pos Selim big landslide and other slope failures occurred.

### 4.1.3 Weight Values and Thematic Map of Elevation

The division of elevation classes referred to elevation ranges from the attributes of the landslide map. The height of landslide sites ranges from 540.96 m to 1864.97 m. This range of elevation was classified into 5 classes using natural break approach in ArcGIS environment (shown in Table 4.1) to determine the intervals of elevation. The elevation range in the study area is spanning from 80 m to 2100 m, exceeding the elevation range of the landslide map. To accommodate this, two more elevation classes were added namely 80 m – 540.96 m and 1864.97 m -2100 m.

Overlaying landslide and elevation maps produced important information on typical landslide occurrences against elevation (Fig. 4.6). Elevations from 1394.33 m to 1585.69 m contain the highest number of landslide occurrences, 100. Meanwhile, LSI values indicate a different elevation range, 1130.56 – 1249.51 m that prone to landslide. This elevation range contains 92 landslide occurrences number which was close to that of the first elevation range. Between elevations 1249.51 m and 1394.33 m, about 75 landslide occurrences were identified. From this information, it can be concluded that landslides mostly took place at high land areas ranging from elevation of 1130.56 to 1585.69 m. Beyond this elevation range, the number of landslides decreased, below 75. Previous study on LHZ at the same study area carried out by Omar, et al. [9] showed that the most prone area to landslide was located between elevations 400 and 500 m. This elevation range was derived from the equation of height risk developed by Gao and Lao [81]. From the work of Gahgah, et al. [43] on LHZ in Cameron Highlands and Gua Musang, elevation interval of 250 to 500 m was occupied by the highest number of landslide occurrences. The different results between this work and the current work may come from the utilization of different training areas. The first work included landslide data from Gua Musang while the latter only used landslide data mainly from Cameron Highlands.

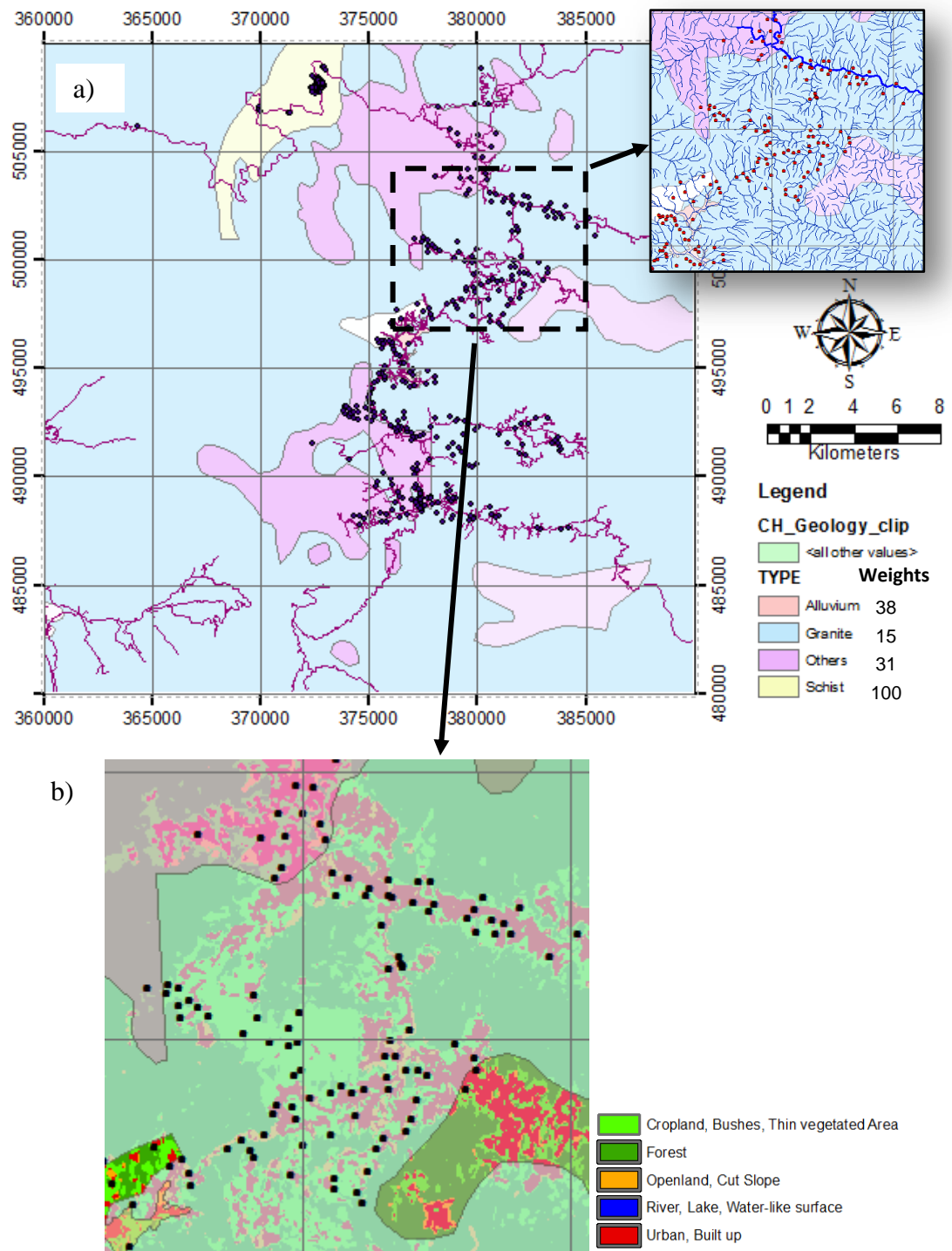


Fig. 4.5 a) Thematic map of lithology, b) Overlay of lithology, land use and landslide maps

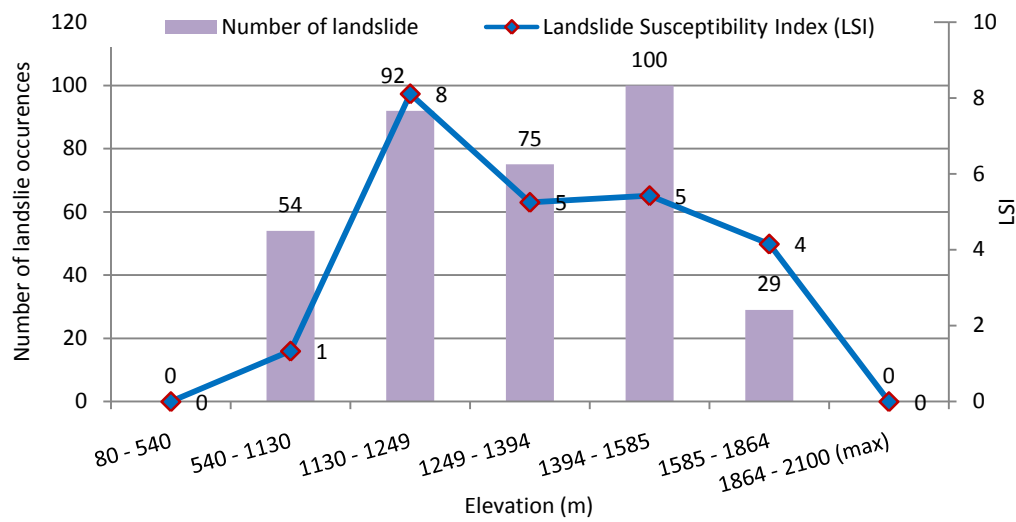


Fig. 4.6 Landslide occurrences number and Landslide Susceptibility Index of lithology

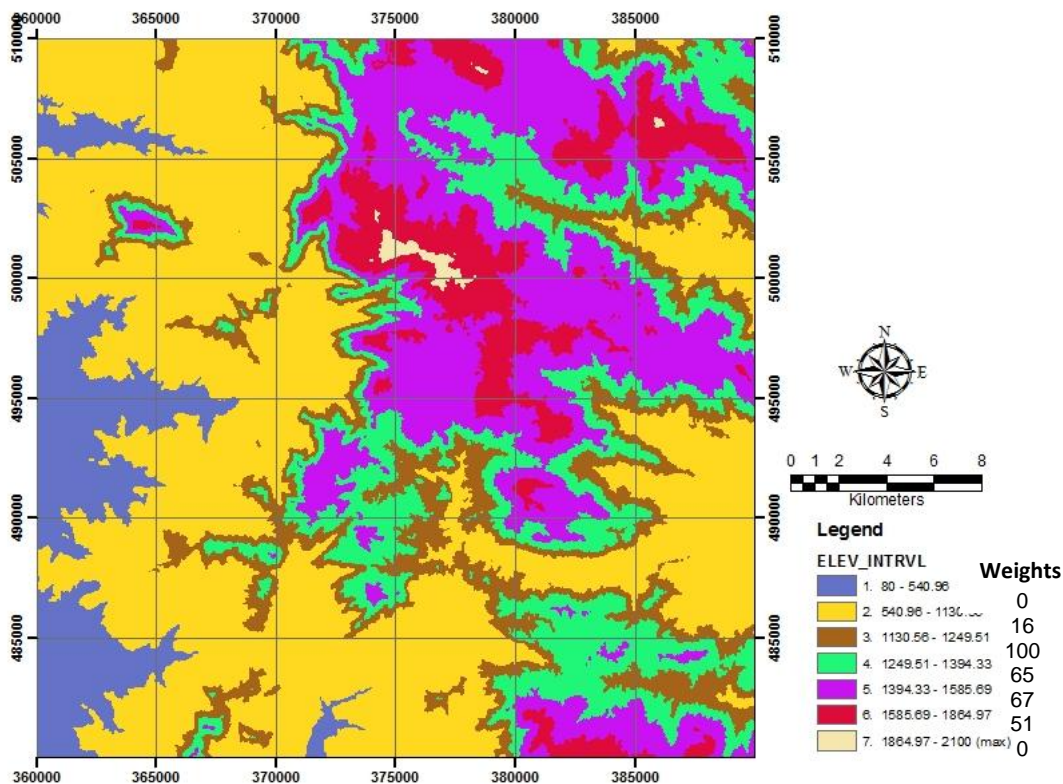


Fig. 4.7 Thematic map of elevation

For use in GIS analysis, a thematic map of elevation showing weight values of each elevation range were constructed (Fig. 4.7). LSI values were used to derive

rating weight values using the procedure mentioned earlier. Elevation range of 1130.56 to 1249.51 m was assigned a maximum weight value of 100. The other weight values were computed proportional to their respective LSI values and were shown in Table 4.1 at column 10 of elevation factor.

#### 4.1.4 Weight Values and Thematic Map of Slope Gradient

Overlaying slope map with landslide map revealed that landslides took place on slopes having gradients ranging from  $0^{\circ} - 51^{\circ}$ . Beyond this range,  $51^{\circ}$  to  $89.6^{\circ}$  (the maximum slope gradient), there is no landslide exists. The first slope range was divided into 5 classes for determining the slope intervals. The latter slope range was set as an additional slope range. All slope intervals are shown in Table 4.1.

Among five slope intervals, the interval of  $19.3^{\circ} - 27.3^{\circ}$  contains the largest number of landslide occurrences, 90 (see Fig. 4.8). The remaining slope intervals, except slope interval of  $36.3^{\circ} - 51^{\circ}$ , contain a fairly large amount of landslide occurrences. Meanwhile, LSI values show that the first slope interval namely  $0^{\circ} - 7.8^{\circ}$  has the highest LSI (6.26), meaning that this slope interval is the most likely to fail. Slope interval of  $19.3^{\circ} - 27.3^{\circ}$  has a lower LSI value compared to the first slope interval even though it contains landslide occurrences at most. The same conditions happen to the second and fourth slope intervals. The large coverage of these slopes causes the small values of LSI. A fairly steep slope,  $36.3^{\circ} - 51^{\circ}$ , has the high value of LSI due to its small coverage area. Slope range of  $0^{\circ} - 7.8^{\circ}$  that has the highest landslide occurrences seems to be contradictive from geotechnical point of view. This research does not employ geotechnical approach as described in section 4.1 for identification of areas susceptible to landslide. Otherwise, this research employs bivariate statistical approach for evaluating landslide distribution that relies on crossing between landslide inventory map and a particular landslide factor map. Hence, the accuracy of both maps determines the distribution of landslide occurrences into classes.

Previous discussion highlighted two slope intervals,  $19.3^{\circ} - 27.3^{\circ}$  and  $0^{\circ} - 7.8^{\circ}$ , categorized as the most hazard slope intervals according to either the number of

landslide occurrences took place within this interval or LSI value. Previous works in the same field carried out by local investigators showed different dangerous slope intervals. Slope interval of  $20^{\circ} - 34^{\circ}$  is the most dangerous slope as reported by Omar, et al. [9] who worked on landslide zonation using GIS and remote sensing in Pos Selim - Cameron Highlands areas. This slope interval is almost similar or close to that found in this recent work. This author described that landslide densities increase up to slope angle of  $28^{\circ}$ . The author added that at slope angel of  $35^{\circ}$ , the granular unconsolidated materials usually repose. Gahgah, et al. [43] found similar result to the previous works that slope interval of  $20^{\circ} - 35^{\circ}$  contains landslide occurrences at most. These two works did not use any objective measures of landslide occurrence relative to different classes in a landslide causative factor over the entire of the study area such as LSI, and LFI.

LSI values of slope were then used to derive weight values. All weight values are directly proportional to the values of LSI. Hence, the first slope interval has the maximum weight value accordingly due to the highest LSI value it has. All weigh values of elevation are shown in Table 4.1 at column 10. The weight values were used as the map attribute to construct a thematic map of elevation (Fig. 4.9).

#### **4.1.5 Weight Values and Thematic Map of Slope Aspect**

The overlay between slope aspect map and landslide shows that there is no dominant slope aspect that contains the largest number of landslide occurrences (Table 4.1). Landslide events were almost evenly distributed for all slope aspects except flat slope and north/south facing slopes. The percentage of landslide occurrences that spans from 10% to 15% for all classes confirmed this situation. This can be an indirect indicator that slope aspect may not be an important landslide influencing factor. However, slopes that facing towards southeast, southwest, northeast and northwest tend to have more landslide occurrences compared to the other slope directions. This result suits the assumption made by DeGraff and Romesburg [62] and Omar, et al. [9] that slopes facing sun, especially afternoon sun, tend to have higher soil temperature, lower soil moisture and hence are easier to erode. Caiyan, et al. [70] found almost a similar result to the previously mentioned work in his investigation on the growth of

landslides in Yunyang to Wushan segment in the Three Gorges Reservoir area in China that slopes facing towards south, southwest and southeast contribute moderately to landslide events.

Fig. 4.10 shows graphical overlay of the number of landslide occurrences and LSI values. Both graphs show a similar trend. Slopes facing four wind directions or morning and afternoon sun have higher LSI values compared to the others. A weight value of 100 goes to northeast and northwest facing slopes. Both slopes have similar number of landslides. Thus, they have the same LSI and rating weight values accordingly. The next places go to southwest and southeast facing slopes with their respective weight values of 94 and 85. The remaining slope aspects have lower LSI values although the values are not very low that is above 50.

The thematic map of slope aspect showing weight values of each aspect was constructed based on LSI values. Thus, slope facing northeast, northwest, southeast and southwest directions have higher rating weight values than the other slope aspects. The map of slope aspect is shown in Fig. 4.11 with road and landslide maps overlaid on top of the map. Example of slopes facing northwest is indicated by circle on Figure 4.11. This is the location of massive slope failure near the border of Perak and Pahang States, Malaysia (shown as inset pictures in Fig. 4.11).

#### **4.1.6 Weight Valued and Thematic Map of Curvature**

Table 4.2 also shows the result of crossing between curvature and landslide sites maps. As mentioned before, negative value of curvature means that the curvature is concave and vice versa is convex. Based on the result, most of landslides (44%) are concentrated within the transition interval from concave to convex, from -1.8 to 1.81. Landslides occurred at both concave and convex slopes.

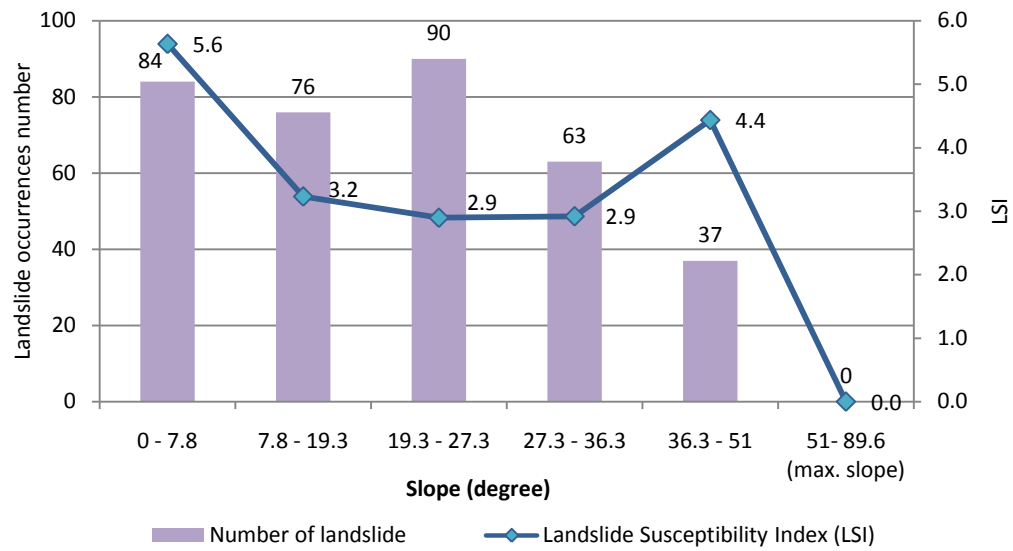


Fig. 4.8 Landslide occurrences number and LSI of elevation

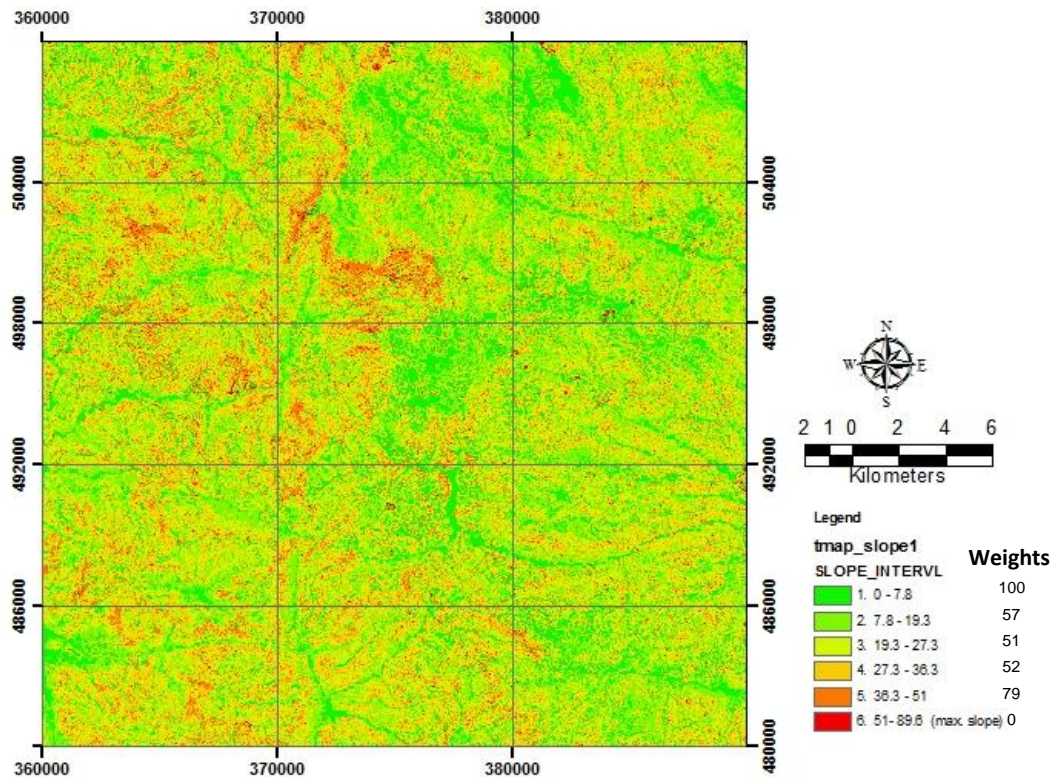


Fig. 4.9 Thematic map of slope



Table 4.2 Landslide attributes from slope aspect, curvature, distance from road maps, and weighting systems

Landslide factors	Sub-Categories	Landslide number, (%)	Landslide areas (m2)	Number of Pixel of each category	Area of each sub category (m2)	Landslide Susceptibility Index (LSI)	Landslide Freq Index	LSI-based Weight Values
Slope aspect	Flat (-1)	0, (0)	0	23461	21114900	0.00	0.00	0
	North (0-22.5)	16, (4)	14400	61898	55708200	2.58	2.87	59
	Northeast (22.5-67.5)	53, (15)	47700	121995	109795500	4.34	4.83	100
	East (67.5-112.5)	39, (11)	35100	122927	110634300	3.17	3.53	73
	Southeast (112.5-157.5)	44, (12)	39600	119454	107508600	3.68	4.09	85
	South (157.5-202.5)	42, (12)	37800	124042	111637800	3.39	3.76	78
	Southwest (202.5-247.5)	50, (14)	45000	122246	110021400	4.09	4.54	94
	West (247.5-292.5)	37, (10)	33300	123276	110948400	3.00	3.33	69
	Northwest (292.5-337.5)	52, (15)	46800	119757	107781300	4.34	4.82	100
	North (337.5-360)	17, (5)	15300	60936	54842400	2.79	3.10	64
Curvature	-28.24 - -14.7	0, (0)	0	473	425700	0.00	0.00	0
	-14.7 - -6.45	30, (8)	27000	35155	31639500	8.53	9.48	100
	-6.45 - -1.89	64, (18)	57600	274263	246836700	2.33	2.59	27
	-1.89 - 1.81	159, (44)	143100	459415	413473500	3.46	3.85	41
	1.81 - 6.61	74, (21)	66600	196218	176596200	3.77	4.19	44
	6.61 - 16.84	23, (6)	20700	33906	30515400	6.78	7.54	79
	16.84 - 33.59	0, (0)	0	561	504900	0.00	0.00	0
Distance from road	0 - 145.50	156, (44)	140400	53290	47961000	29.27	32.53	100
	145.50 - 424.37	111, (31)	99900	88870	79983000	12.49	13.88	43
	424.37 - 860.86	49, (14)	44100	113883	102494700	4.30	4.78	15
	860.86 - 1430.73	29, (8)	26100	127672	114904800	2.27	2.52	8
	1430.73 - 3103.95	13, (4)	11700	277494	249744600	0.47	0.52	2
	3103.95 - 14606.09	0, (0)	0	401751	361575900	0.00	0.00	0

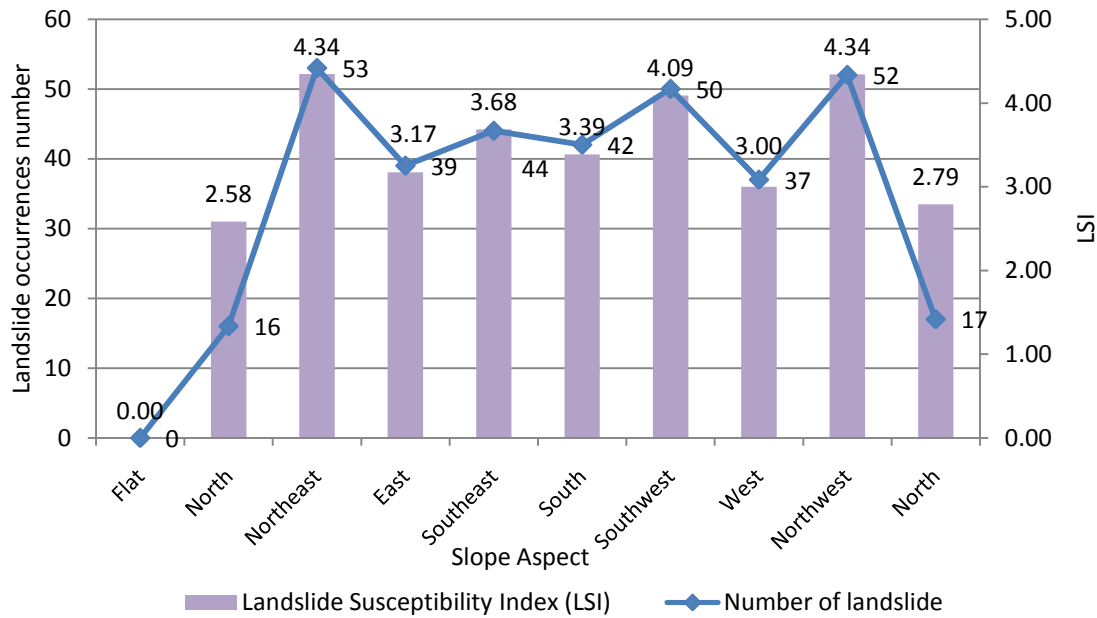


Fig. 4.10 Landslide occurrences number and LSI values of slope aspects

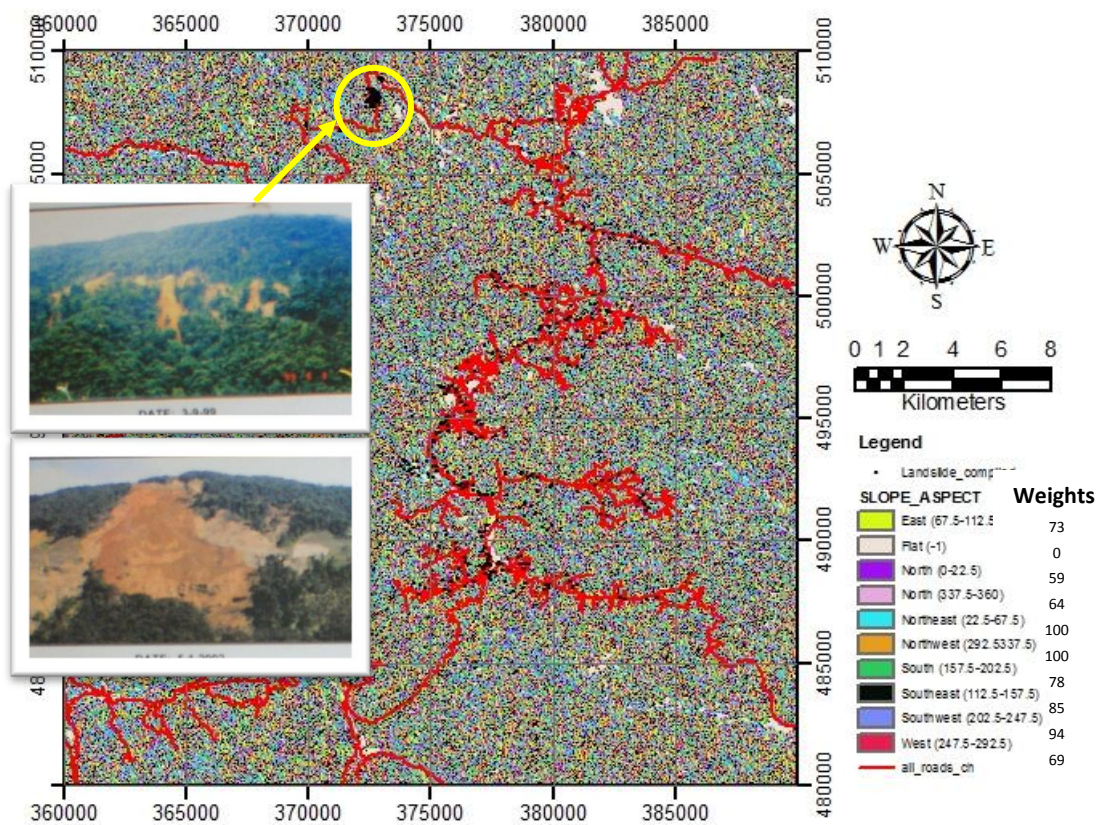


Fig. 4.11 Thematic map of slope aspect

LSI values describe different things about the areas susceptible to landslide compared to interval based-landslide occurrences. Based on LSI values, the curvature interval that has the highest susceptibility to landslide is the interval of -14.7 to -6.45, the concave curvature, followed by the interval of 6.61 to 16.84, the convex curvature. These intervals have fewer number of landslide occurrence compared to the first interval (Fig. 4.12). This situation is similar to that of other causative factors such as land use land cover and lithology when LSI is used as the measure of areas susceptible to landslides. This is the nature of LSI that measures the proportion of landslide areas and considers the size of failure.

Fig. 4.13 shows the thematic map of curvature of the study area showing rating weight values derived from LSI values. Visual interpretation of spatial distribution of curvature is rather difficult to perform due to the size of the pixels that is 30 meter. The important thing is that the landslide concentrations are located either on concave or convex areas, or even on transitional areas from concave-planar-convex. However, LSI based-thematic map of curvature shows that the areas having the highest susceptibility to landslide are those with concave curvatures (with weight value of 100) followed by convex areas (with weight value of 79). This fact complements the findings of previous researchers that the landslides were likely to occur in the concave areas such as works of Ahmad and McCalpin [73], Lee and Evangelista [74], Kumar, et al. [64] and Oh, et al. [77]; in the convex areas such as works of Lee and Talib [55], Lee and Pradhan [7] and Oh, et al. [76]; in planar curvature such as work of Ohlmacher [75]. Based on the variety of curvature conditions that lead to landslide, the curvature data itself cannot be guaranteed to use as a direct indicator to assess landslide hazard zones. Other causative factors may play importance roles in causing areas susceptible to landslide in conjunction with curvature data.

#### **4.1.7 Weight Values and Thematic Map of Proximity to Road**

The spatial distribution of landslides with respect to the road network in term of the distance to/from the road is shown in Table 4.2. The intervals of the distance from road were generated from the landslide attributes resulted from crossing between

distance from road and landslide sites maps. The farthest landslide site from the road is 3103.95 m.

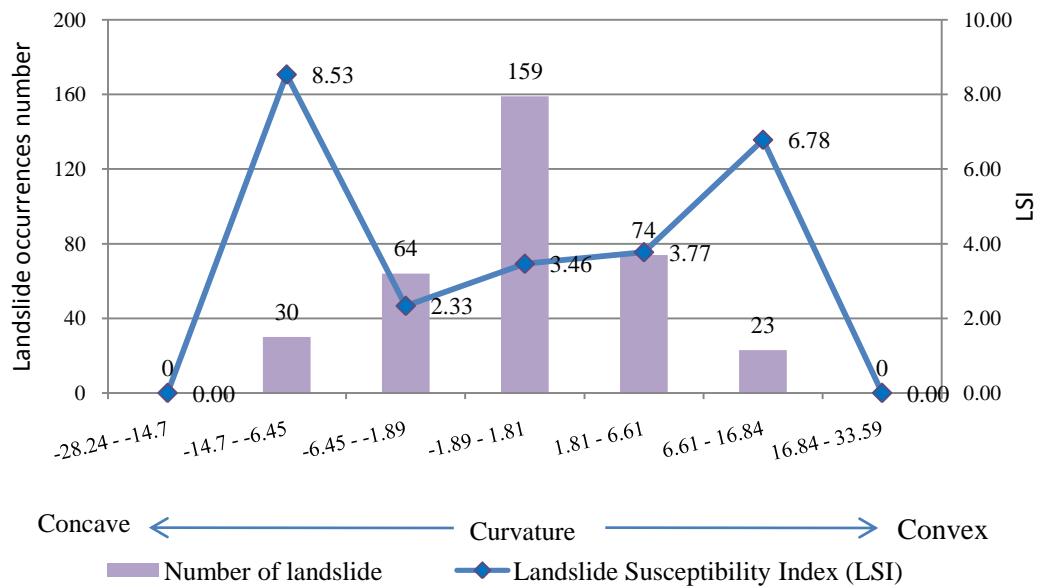


Fig. 4.12 Landslide occurrences number and LSI values of curvature

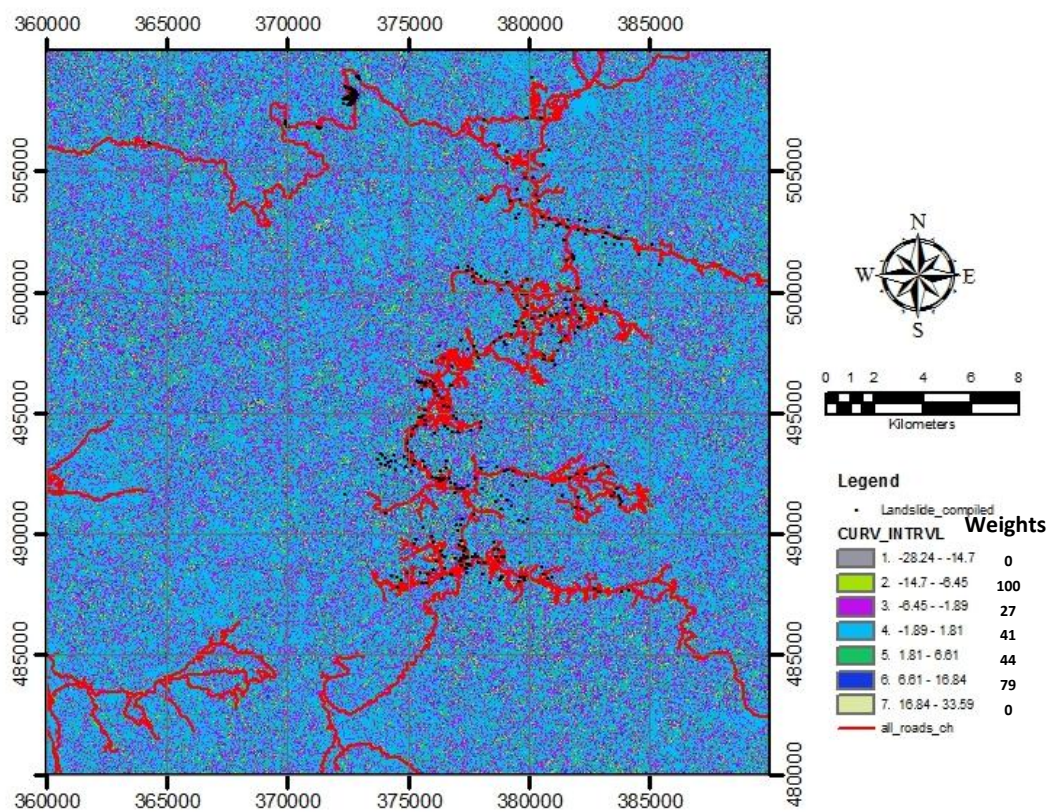


Fig. 4.13 Thematic map of slope aspect

The distance from road was then reclassified into 5 intervals. These intervals are shown in Fig. 4.14. This figure shows the overlay of landslide distributions and respective LSI values of distance from road. It is clearly shown that both values have a similar trend. Simply speaking, the closer the distance from road, the higher the number of landslide occurrences and the larger the LSI values and vice versa. Some researchers who arrived at this conclusion such as Jadda, et al. [58] who worked on landslide susceptibility evaluation in central Alborz of the north of Iran; Kelarestaghi and Ahmadi [91] who worked on mapping landslide susceptibility in Kingston Metropolitan area, Jamaica; and Sharma and Kumar [101] who work on LHZ in Parwanoo area, Himalaya.

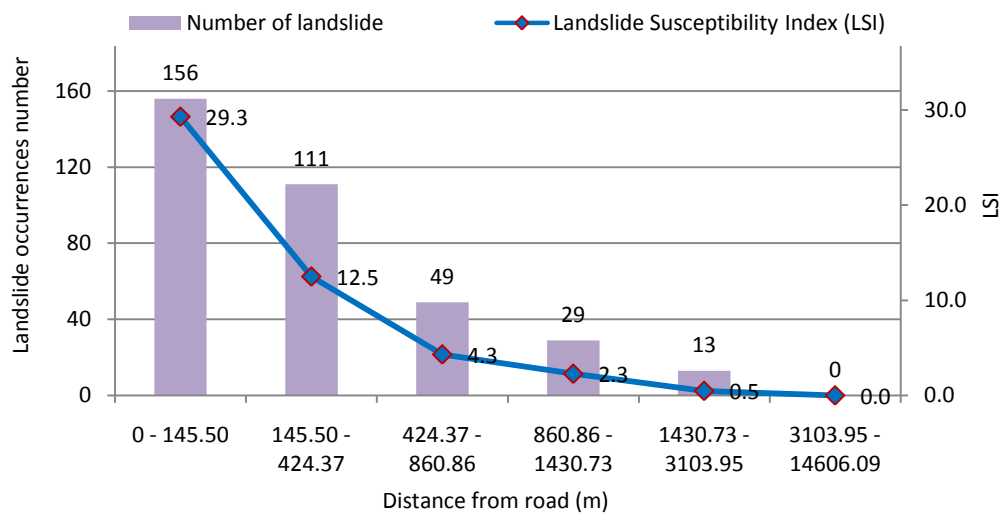


Fig. 4.14 LSI values and landslide occurrences number of distance from road

The distance from road as a landslide causative factor does not mean that the road itself causes landslides. However, a road network crossing hilly areas is usually developed by means of cutting and clearing vegetated slopes prior to road construction. The natural slopes that are disturbed or modified for road development purposes are then vulnerable to fail. The undisturbed slopes surrounding the cut/modified slopes can be landslide feeder zones or in other words they are vulnerable to fail too. The term “feeder zones” is associated with the upper slope areas, the locations of the source of mass movement. Coppola, et al. [232] divided the parts of a slope into three areas: feeder zones (upper slope), accumulation zones and stream erosion zones.



Thematic map of distance from road, shown in Fig. 4.15, was constructed using weight values derived from LSI values. The map shows buffered zones with the road lines as the origin. The farthest areas from the road are the forest areas that are considered as the most secure areas with the lowest rating weight values, 0. Lanes of 145 widths on each side of the road indicate the most dangerous areas and are assigned a maximum weight value, 100. The areas in between these two intervals are given weight values proportional to the distance from road.

#### 4.1.8 Rating Weight and Thematic Map of Lineament

The Landslide attribute related to the distance from lineament (geology fault) is shown in Table 4.3. The intervals of the distance from lineaments were determined based on the landslide attributes resulted from crossing distance from lineament and landslide maps. About 82% of landslide sites are located within the distance of 2.5 km from the lineaments. The farthest landslide sites (3% of landslide data) from the lineaments are about 9.6 km. The number of landslides tends to decrease as the distance from the lineaments increase (Fig. 4.16). The spatial distribution of LSI values expressed the same graphical tendency as the spatial distribution of landslides against the lineaments. From Fig. 4.16, it can be inferred that lineaments affect the spatial distribution of landslides. Researchers such as Carrara, et al. [59], Pachauri and Pant [53], and Prentice [233] have found that a large number of landslides exist near the geology faults.

Thematic map of the distance from lineament was constructed using the corresponding rating weight values derived from LSI values (Fig. 4.17). The map shows buffer zones for each interval of the distance from lineament. Besides showing distance from lineament, this map also shows lineaments and river/lake layers. There are three locations that may represent the contribution of lineaments to landslide occurrences. Zone 1 on Figure 4.17 shows that a number of landslides are located alongside a geology lineament denoted by arrow with a letter 'a'. This lineament coincides with *Sungai Terla* (Terla River). Zone 2 is the location of massive landslide at Pos Selim. It is located near the far end of lineament 'a'. Jamaluddin [219] reported that discontinues existed in this area especially in bedding planes of rock mass of

granite and metamorphic bedrock. Zone 3 is located at Tanah Rata. Ramli, et al. [93] reported that a large number of short lineaments exist in Tanah Rata area. According to landslide map from ARSM, many landslides were found in this area.

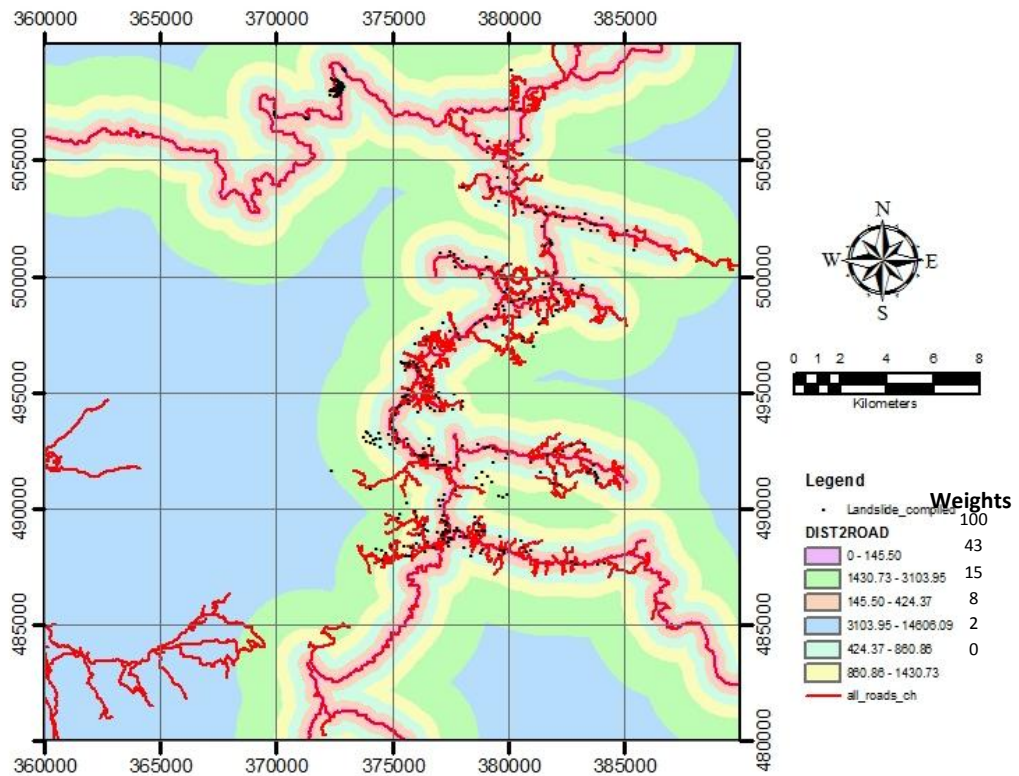


Fig. 4.15 Thematic map of distance from road

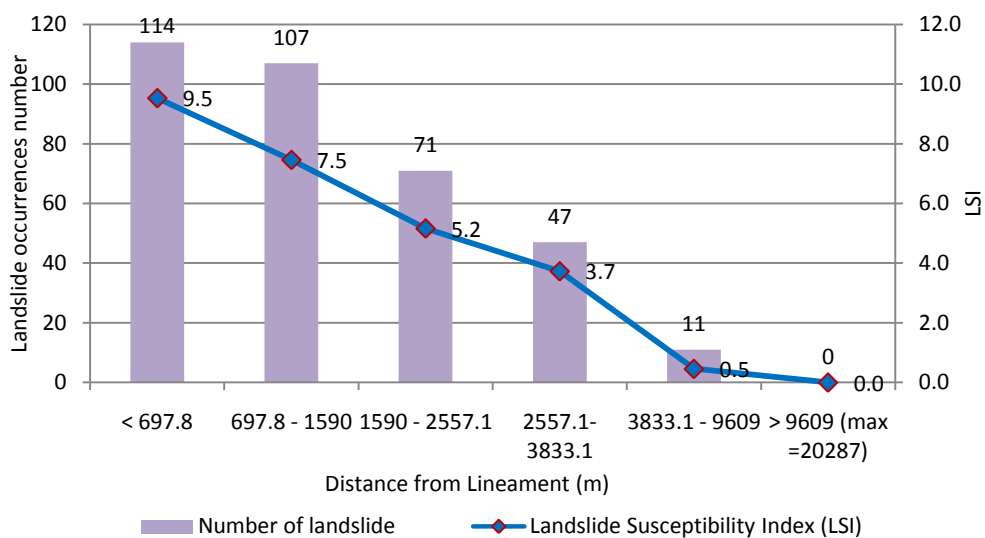


Fig. 4.16 LSI values and landslide occurrences number of distance from lineaments

#### 4.1.9 Weight Values and Thematic Map of River and Lake

River and lake as a causative factor appears to have a significant contribution to landslides as geology fault. Fig. 4.18 shows the spatial distribution of landslide occurrences with respect to the distance from river and lake. The classification of the distance from river/lake was derived from landslide attributes resulted from crossing between distance from river and lake and landslide maps. About 136 (38 %) of landslides took place within the distance up to 548.9 m from rivers/lakes. The number of landslides decreases as the distance increases until about 1.7 km away from river/lake. Areas close to a river are potential to experience slope failures. Investigation carried out by Shimazu and Oguchi [234] and Újvári, et al. [235] found this relation. At intervals of 1732.46 - 2521.5 m and 2521.5 – 4391.2 m, the number of landslides tends to increase. This seems to be unreasonable considering that the effect of river/lake, in term of the distance, has diminished or exhausted. A reasonable explanation would be the existence of other landslide influencing factors.

Fig. 4.19 shows the thematic map of distance from river/lake layer and the corresponding map legend that contains weight values. It was constructed from LSI-based rating weight values. Considerable weight values were assigned to areas close to rivers/lakes. *Sungai Bertam* and *Terla* are the rivers surrounded by landslide sites. Three rivers were identified during image processing. The big one is called *Empangan* (Lake) *Sultan Abu Bakar* (denoted by arrow). The two other lakes are the small ones and located near the junction of *Kampung Raja* (denoted by 'a' in Figure 4.19) and southwest of *Sungai Mesun* (denoted by 'b'). As discussed earlier, this layer appears to have an important relation with landslides due the concentration of many landslide sites near the river/lake. There are two river surrounded by landslides: *Sungai Terla* (zone 1 shown in Figure 4.19) and *Sungai Bertam* (zone 2 shown in Figure 4.19). At zone 1, the pattern of *Sungai Terla* coincides with the lineament 'a' as depicted in Figure 4.17. Thus, the influence of lineament on causing slope failure is amplified by the existence of the river. At zone 2, landslides are clustered at north part/headwater of *Sungai Bertam*, *Empangan* (Lake) *Sultan Abu Bakar*, and continue eastward.



Table 4.3 Landslide attributes from distance from lineament, distance from river/lake, soil maps, and weighting systems

Landslide factors	Sub-Categories	Landslide number, (%)	Landslide areas (m2)	Number of Pixel of each category	Area of each sub category (m2)	Landslide Susceptibility Index (LSI)	Landslide Freq Index	LSI-based Weight Values
Distance from lineament	< 697.8	114, (32)	102600	119689	107720100	9.52	10.58	100
	697.8 - 1590	107, (30)	96300	143505	129154500	7.46	8.28	78
	1590 - 2557.1	71, (20)	63900	137604	123843600	5.16	5.73	54
	2557.1- 3833.1	47, (13)	42300	126145	113530500	3.73	4.14	39
	3833.1 - 9609	11, (3)	9900	241156	217040400	0.46	0.51	5
	> 9609 (max =20287)	0, (0)	0	231901	208710900	0.00	0.00	0
Distance from river/lake	0 - 548.90	136, (38)	122400	201107	180996300	6.76	7.51	100
	548.90 – 1200.71	66, (18)	59400	209939	188945100	3.14	3.49	46
	1200.71 - 1732.46	40, (11)	36000	156682	141013800	2.55	2.84	38
	1732.46 - 2521.50	48, (13)	43200	194864	175377600	2.46	2.74	36
	2521.50 - 4391.18	68, (19)	61200	241884	217695600	2.81	3.12	42
	4391.18 - 9037.37	0, (0)	0	32524	29271600	0.00	0.00	0
Soil	Podzols and Lithosols soil	60, (17)	54000	123781	111402900	4.85	5.39	100
	Red-Yellow Podzolic soil with Lithosol	298, (83)	268200	862379	776141100	3.46	3.84	71
	Red-Yellow Podzolic soil with Reddish Lateritic	0, (0)	0	13840	12456000	0.00	0.00	0

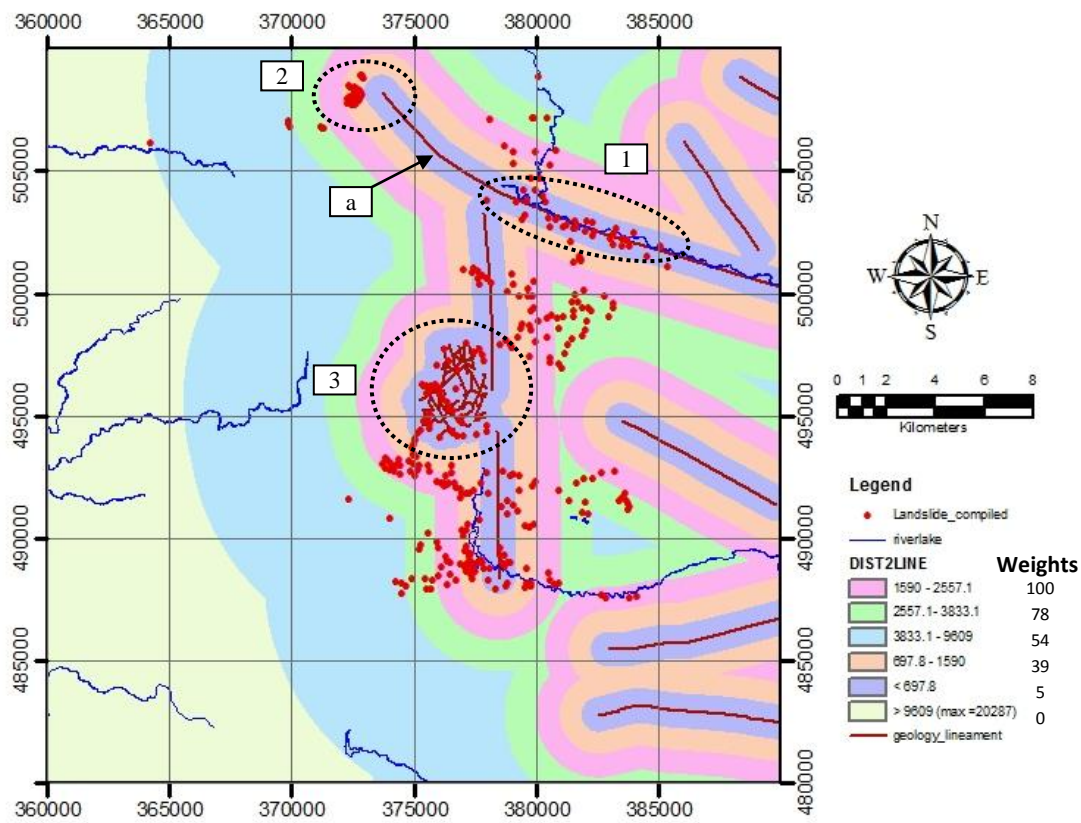


Fig. 4.17 Thematic map of distance from lineaments

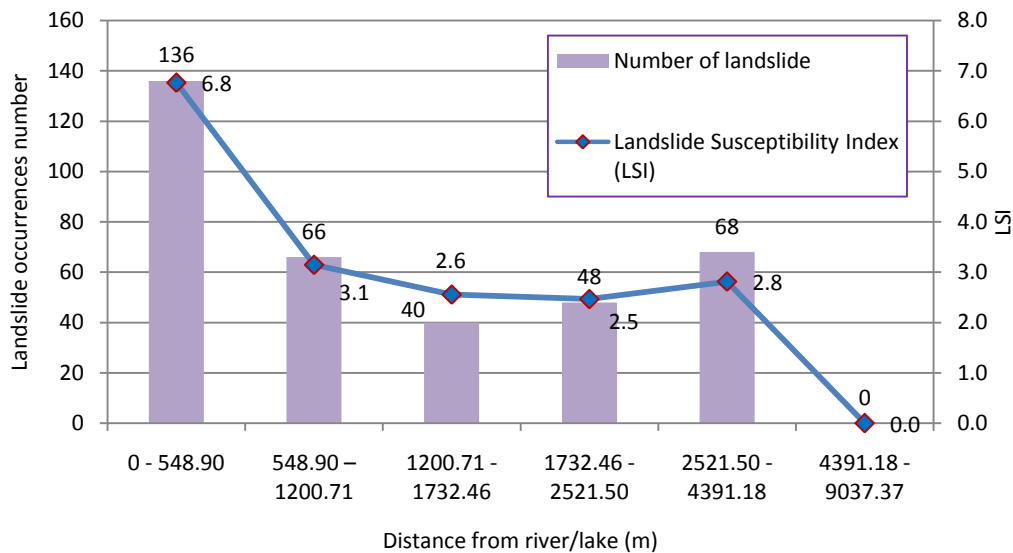


Fig. 4.18 Thematic map of distance from river/lake

#### **4.1.10 Weight Values and Thematic Map of Soil**

The study area is dominated by soil type of Red-Yellow Podzolic soils with Lithosols on acid to intermediate igneous rocks as shown in Table 4.3. Crossing the soil map with the landslide map shows that 83 % of landslides are located at the areas with this dominating soil type area. About 17% of landslides are located at areas covered by soil type of Podzols and Lithosols (on acid igneous rocks). There is no landslide at the remaining soil type. The highest LSI value, 5.39, is assigned to the dominating soil type. The second place goes to soil type of Podzols and Lithosols with the LSI value of 3.84.

The thematic map of soil showing the spatial distribution of the respective weight values is portrayed in . The characteristic of the dominating soil is sandy soil mixed with peat as reported by Fortuin [150]. The color of the weathered overlying soil varies from deep red, light yellow and pink. These colors can be seen on logging track and cut slope for road development. From visual interpretation of the soil map, it appears that there is no typical soil type occupied by most landslides occurrences even though LSI values say different thing.

#### **4.1.11 Weight Values and Thematic Maps of NDVI**

NDVI maps of different seasons derived from 4 Landsat images. The images were acquired on February, May, June, and September were crossed with the landslide map. The landslide attributes in relation with multi temporal NDVI conditions are shown in Table 4.4. NDVI values have been scaled into the range of -1 to 1 into 0 to 255. The selection of NDVI intervals was based on the landslide attributes obtained from crossing between NDVI maps and landslide map. The number of landslide sites used for deriving landslide attributes was reduced from the original landslide number, 358, to provide only landslide data that are free from cloud and shadow effect. After applying clouds and associated shadows masks to multi temporal data (i.e. NDVI, soil wetness, and LST), the remaining landslide data available for further processing (e.g. deriving landslide attributes, validation) are 298, 267, 350, and 339 for February, May, June and September.

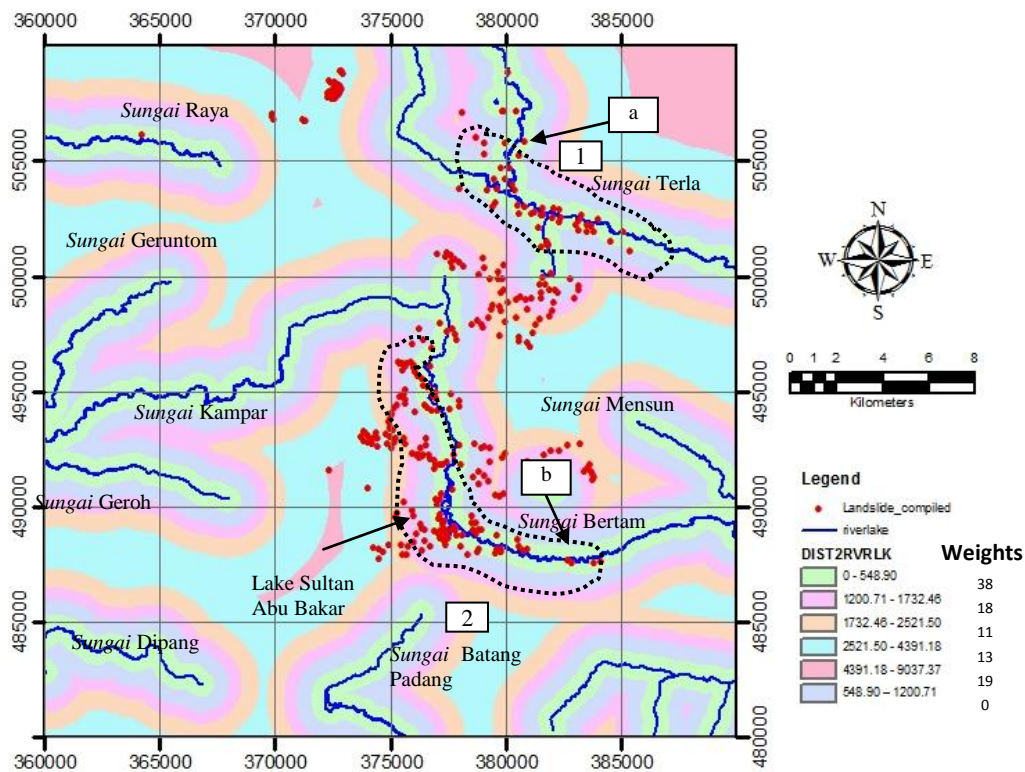


Fig. 4.19 Thematic map of distance from river/lake

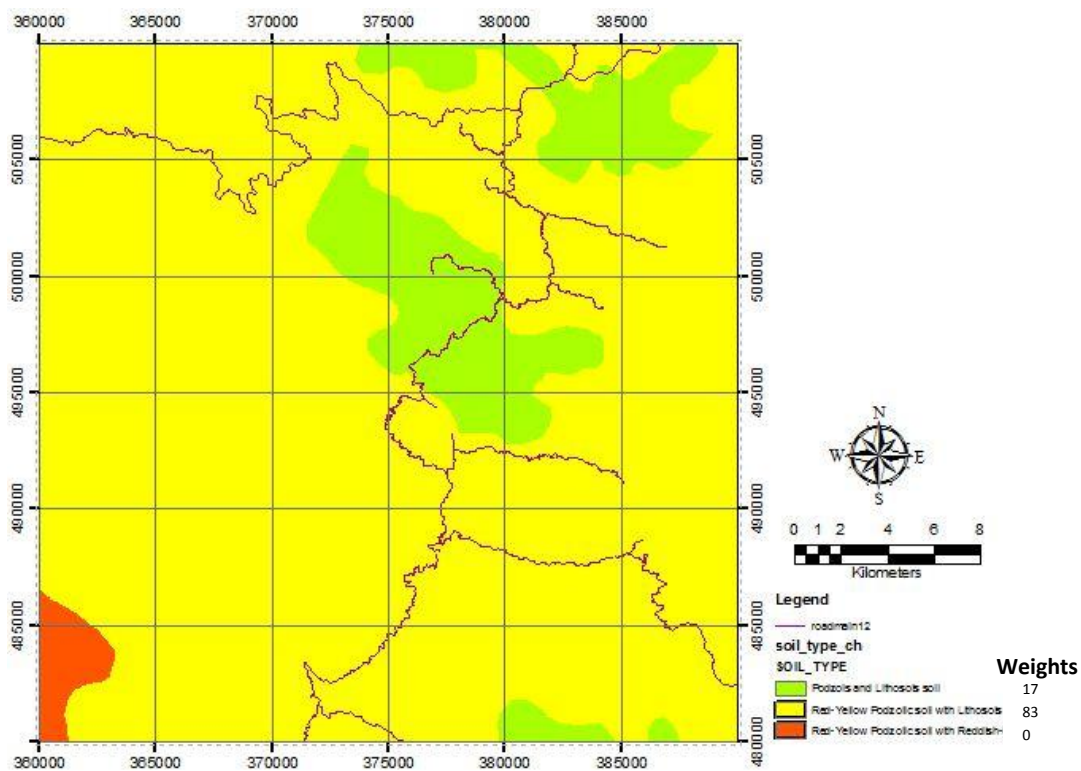


Fig. 4.20 Thematic map of soil

Table 4.4 Landslide attributes of NDVI and weighting system

Landslide factors	Sub-Categories	The number of Landslides, (%)	Landslide areas (m2)	Number of Pixel of each category	Area of each sub category (m2)	LSI	LSI-based weight Values
NDVI Feb	0 - 47	30, (10)	6750	36593	8233425	8.20	100
	47 - 115	41, (14)	9225	106218	23899050	3.86	47
	115 - 182	51, (17)	11475	112102	25222950	4.55	55
	182 - 231	53, (18)	11925	122607	27586575	4.32	53
	231 - 255	123, (41)	27675	262631	59091975	4.68	57
NDVI May	0 - 57	28, (10)	6300	50433	11347425	5.55	100
	57 - 135	34, (13)	7650	120435	27097875	2.82	51
	135 - 190	29, (11)	6525	75082	16893450	3.86	70
	190 - 228	28, (11)	6300	66636	14993100	4.20	76
	228 - 255	148, (55)	33300	271803	61155675	5.45	98
NDVI Jun	0 - 47	30, (9)	6750	18941	4261725	15.84	100
	47 - 98	52, (15)	11700	119468	26880300	4.35	27
	98 - 135	72, (20)	16200	180314	40570650	3.99	25
	135 - 165	89, (25)	20025	565886	127324350	1.57	10
	165 - 199	107, (31)	24075	291792	65653200	3.67	23
	199 - 218	0, (0)	0	19958	4490550	0.00	0
NDVI Sep	0 - 23	0, (0)	0	2194	493650	0.00	0
	23 - 59	18, (5)	4050	14602	3285450	12.33	100
	59 - 91	54, (15)	12150	153349	34503525	3.52	29
	91 - 115	53, (15)	11925	116550	26223750	4.55	37
	115 - 137	97, (27)	21825	222725	50113125	4.36	35
	137 - 167	117, (33)	26325	244027	54906075	4.79	39
	167 - 188	0, (0)	0	623831	140361975	0.00	0

The range of NDVI values of landslide sites vary month by month. NDVI of February and May have a full range of 0 to 255. Meanwhile, NDVI values of June and September range from 0 to 190 and 23 to 167. The difference of these values may be related to the quality of the corresponding Landsat images. Atmospheric effects might be different for each image. In addition, only standard atmospheric correction was applied to remove the atmospheric effects. Five intervals of each NDVI map were determined based on the respective available NDVI values range.

Based on rainfall data (Figure 1.2), February is dry season; May is the month after the peak of rainy season; June is the month before the peak of second dry season, July; and September is the month before the peak of second rainy season. On February, the dry season, about 34% of landslide data shows high NDVI values from

231-255, indicating a good vegetation health. The remaining values are distributed almost evenly to all classes. Areas with low vegetation index are relatively small. The same trends happen to NDVI of other months. The most likely cause of this case is the existence of a fairly long period (1981-2001) between the acquisition date of remote sensing data used for landslide identification and for deriving NDVI images. During this period, landslide scarp areas may be overgrown by bushes. Another possible cause is that a fairly number of landslide sites was reported by Pradhan and Lee [229] as scarps located in crop land and at cut slopes identified during field investigation. The dimension of the scarps might be so small that Landsat 7 ETM+ image (with resolution of 30 m) could not differentiate this object from the adjacent objects such as agricultural plants and bushes.

For GIS analysis purpose, NDVI thematic maps representing the rating weight values were constructed. The rating weight values were derived from LSI values. The respective LSI values indicate that areas with low NDVI have the highest LSI values, meaning that these areas are prone to landslide. Areas with low NDVI values can be associated with landslide locations. The works done by Vohora and Donoghue [97] confirmed that low NDVI values were related to landslides which were recognized as denuded areas or disturbed vegetation as the landslide case studied by Lin, et al. [98]. The multi temporal thematic maps of NDVI are shown in Appendix E. This appendix shows thematic maps of NDVI before and after removing covered areas by cloud and shadow.

Response of vegetation condition to rainfall has been discussed in section 2.2.7.1. Normally, vegetation index will increase during rainy seasons and vice versa. Fig. 4.21 represents different NDVI conditions of part of Tanah Rata area, (indicated by boxes in figures of Appendix E), and the corresponding Landsat image (dated 20 September 2001) and topographic map. The figure shows the different coverage of areas with high weight values. On February and May, the coverage of areas prone to landslide indicated by the lowest NDVI values is wider than that of June and September. However, Liu, et al. [236] suggested that NDVI values cannot be solely used to identify landslide prone areas because landslides areas, river valley,

residential areas, building, exposed areas/barren land are indicated by low vegetation index values.

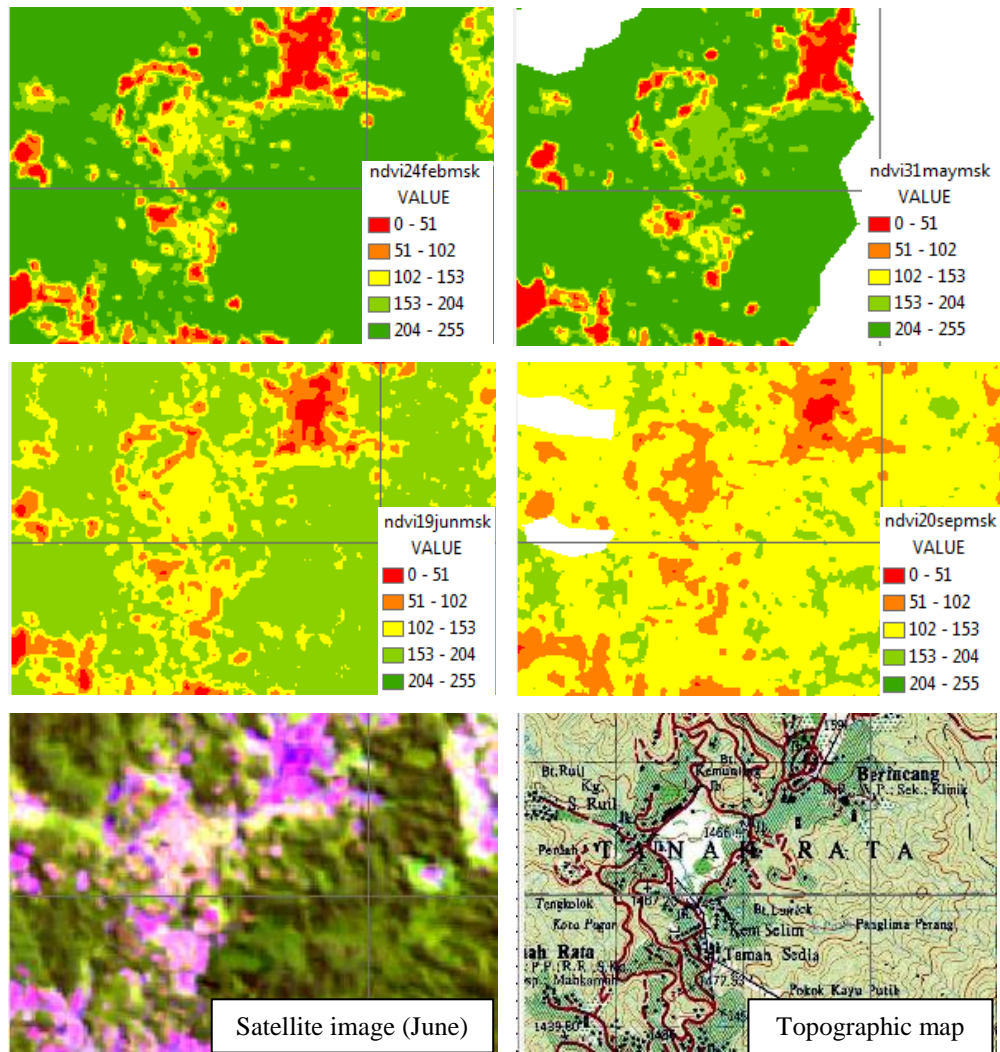


Fig. 4.21 Different NDVI conditions in Tanah Rata

#### 4.1.12 Weight Values and Thematic Maps of Soil Wetness

Weight values of multi temporal soil wetness/moisture maps were obtained by crossing these maps with the landslide map. Further discussion is solely based on crossing result without accommodating geotechnical point of view as mentioned in section 4.1. These maps were resulted from the application of Tasseled Cap Transformation (TCT) that optimizes viewing Landsat data for vegetation studies e.g. wetness of soil. Soil wetness reflectance obtained from TCT ranges from -0.5 to 1.4. For further GIS analysis, this range was normalized to extent from 0 to 255. The



landslide attributes related to multi temporal of soil wetness conditions are shown in Table 4.5. The number of landslide data used to derive the landslide attributes was reduced to accommodate the areas with no data due to the influence of clouds and associated shadows. The determination of soil wetness intervals was done by using the same manner as the determination of NDVI intervals.

Table 4.5 Landslide attributes of Soil Wetness and weighting system

Landslide factors	Sub-Categories	The number of Landslides, (%)	Landslide areas (m2)	Number of Pixel of each category	Area of each sub category (m2)	LSI	LSI-based weight Values
TCWet Feb	0 - 27	126, (41)	28350	358510	80664750	3.51	100
	27 - 68	50, (16)	11250	312242	70254450	1.60	46
	68 - 115	49, (16)	11025	664007	149401575	0.74	21
	115 - 166	38, (12)	8550	934494	210261150	0.41	12
	166 - 233	42, (14)	9450	707097	159096825	0.59	17
	233 - 254	0, (0)	0	27480	6183000	0.00	0
TCWet May	0 - 23	95, (35)	21375	329093	74045925	2.89	64
	23 - 60	49, (18)	11025	355599	80009775	1.38	31
	60 - 97	43, (16)	9675	686124	154377900	0.63	14
	97 - 143	47, (17)	10575	104224	23450400	4.51	100
	143 - 213	41, (15)	9225	582341	131026725	0.70	16
	213 - 254	0, (0)	0	35219	7924275	0.00	0
TCWet Jun	0 - 29	125, (36)	28125	363202	81720450	3.44	87
	29 - 70	73, (21)	16425	421429	94821525	1.73	44
	70 - 110	55, (16)	12375	936694	210756150	0.59	15
	110 - 161	57, (16)	12825	143894	32376150	3.96	100
	161 - 232	40, (11)	9000	629135	141555375	0.64	16
	232 - 255	0, (0)	0	33081	7443225	0.00	0
TCWet Sep	0 - 22	261, (77)	58725	220293	49565925	11.85	100
	22 - 74	40, (12)	9000	460761	103671225	0.87	7
	74 - 134	15, (4)	3375	390496	87861600	0.38	3
	134 - 193	6, (2)	1350	274529	61769025	0.22	2
	193 - 245	17, (5)	3825	210062	47263950	0.81	7
	245 - 254	0, (0)	0	34749	7818525	0.00	0

Table 4.5 shows the variation of the range of soil wetness values on column 2. The number of interval classes for each soil wetness map was set to five classes based on soil wetness values of landslide data. None of the landslide data has the values suitable for the sixth interval class. Most of landslide data has low soil wetness values: 41% of landslide data on February, 35 % on May, 36% on June, and 77% on September. The remaining landslide data was distributed almost evenly to other class



intervals. This condition is reasonable knowing that most of landslide sites were recognized at crop land and at cut slopes identified during field investigation. These typical of land uses have low soil moisture.

The thematic maps of multi temporal soil wetness are presented in Appendixes F. This appendix presents the multi temporal soil wetness maps before and after applying cloud and shadow map. The latter maps shows soil maps in form of rating weight values based on LSI values. According to Ray and Jacobs [84], Xu, et al. [86] and Jotisankasa and Vathananukij [85], slopes with high level of soil wetness are more prone to landslide occurrences. On the contrary, Table 4.5 shows that most landslides are located in low moisture areas for all months. This can be understood since areas with low moisture refer to barren land/open land/cut slope while those with high moisture refer to for example vegetated areas.

Meanwhile, LSI-based rating weight values describes that on May and June, the areas prone to landslides are located at more moist parts, indicated by weight values of 100. The other months, the most prone areas to landslide occurrences are at the driest parts.

#### **4.1.13 Weight Values and Thematic Maps of LST**

Table 4.6 shows the typical LST of landslide site. The landslide characteristics were obtained from crossing multi temporal LST maps with landslide map. The number of landslide data used for deriving the landslide characteristics varies month by month that is 305, 275, 358, and 346 respectively for February, May, June, and September. The five intervals of each LST map were defined and derived from LST values of landslide sites. The final temperature was reduced to the local temperature monitored at Tanah Rata weather station.

Table 4.6 shows that a large number of landslide occurrences are concentrated at different LST intervals for each month. The LST ranges and the corresponding percentage of landslide occurrences are 17.0<sup>0</sup>C-17.9<sup>0</sup>C (42% of landslide data), 17.5<sup>0</sup>C-18.2<sup>0</sup>C (41%), 18.1<sup>0</sup>C-18.9<sup>0</sup>C (51%), and 18.6<sup>0</sup>C -19.3<sup>0</sup>C (36%) respectively

for February, May, June, and September. It is difficult to relate the variation of LST and monsoonal rainfall. However, the monthly average value of LST shows the same

Table 4.6 Landslide attributes of LST and weighting system

Landslide factors	Sub-Categories	Number of Landslides, (%)	Landslide areas (m2)	Number of Pixel	Area (m2)	LSI	LSI-based weight Values
LST Feb	< 15.5	0, (0)	0	22521	20268900	0.00	0
	15.5 - 16.3	5, (2)	4500	395725	356152500	0.13	1
	16.3 - 17.0	43, (14)	38700	345927	311334300	1.24	12
	17.0 - 17.9	127, (42)	114300	206278	185650200	6.16	58
	17.9 - 18.5	90, (30)	81000	84310	75879000	10.67	100
	18.5 - 19.3	40, (13)	36000	88320	79488000	4.53	42
	> 19.3	0, (0)	0	4243	3818700	0	0
LST May	<16.2	0, (0)	0	36230	32607000	0.00	0
	16.2 - 16.8	9, (3)	8100	24630	22167000	3.65	52
	16.8 - 17.5	59, (21)	53100	962540	866286000	0.61	9
	17.5 - 18.2	112, (41)	100800	160559	144503100	6.98	100
	18.2 - 18.9	86, (31)	77400	364692	328222800	2.36	34
	18.9 - 19.6	9, (3)	8100	31367	28230300	2.87	41
	>19.6	0, (0)	0	5567	5010300	0.00	0
LST Jun	<16.3	0, (0)	0	54408	48967200	0.00	0
	16.3 - 17.2	8, (2)	7200	74139	66725100	1.08	12
	17.2 - 18.1	71, (20)	63900	807902	727111800	0.88	10
	18.1 - 18.9	181, (51)	162900	249521	224568900	7.25	81
	18.9 - 19.8	70, (20)	63000	352210	316989000	1.99	22
	19.8 - 20.6	28, (8)	25200	31131	28017900	8.99	100
	> 20.6	0, (0)	0	7488	6739200	0.00	0
LST Sep	<16.6	0, (0)	0	30158	27142200	0.00	0
	16.6 - 17.3	9, (3)	8100	98238	88414200	0.92	10
	17.3 - 17.9	92, (27)	82800	841024	756921600	1.09	12
	17.9 - 18.6	104, (30)	93600	110199	99179100	9.44	100
	18.6 - 19.3	125, (36)	112500	131827	118644300	9.48	100
	19.3 - 19.9	16, (5)	14400	147954	133158600	1.08	11
	> 19.9	0, (0)	0	22550	20295000	0.00	0

trend as the ground truth of temperature data issued by Worldclimate [217] which was obtained from a monitoring weather station at Tanah Rata. Fig. 4.22 shows the graphical overlay of rainfall, temperature, and LST data. From January to August, temperature and rainfall show the same graphical trend. As the rainfall amount increases, the temperature does so, reaching to the peak of rainfall on April and temperature on May. The temperature does not increase as significant as the rainfall.

In other words, rainfall amount is not sufficient to reduce the temperature. The effects from environmental factors other than rainfall may apply. Meanwhile, the average LST value of each month is close to the corresponding temperature value except that of May which does not increase significantly.

For further data processing using GIS, LSI was computed to derive weight values purpose. Table 4.6 shows that LST intervals with the highest number of landslide occurrences do not always have the highest rating weight values as the case of February and June. Using the rating weight values, multi temporal thematic maps of LST were constructed. The maps are portrayed in Appendix G. The average LST of landslide data is 17.5<sup>0</sup>C, 17.96<sup>0</sup>C, 18.57<sup>0</sup>C, and 18.39<sup>0</sup>C respectively for each month that represents different climate conditions. Meanwhile, the average LST for the entire study area is a bit lower than that of the landslide data that are 16.45<sup>0</sup>C, 16.72<sup>0</sup>C, 17.96<sup>0</sup>C, and 17.44<sup>0</sup>C respectively for February, May, June, and September.

Visual interpretation of multi temporal LST maps reveals that, in general, there is no specific pattern of LST at landslide sites compared to that of their surroundings. Of the reasonable reason is that the landslide data is in the form of point data, not the area, with the pixel size of 30 m x 30m. At the location of past massive landslide at Pos Selim, the LST values are higher than the surroundings, indicated by circles in Figure 4.23. Landslide locations can be identified based on their LST values that are distinguishable from the surroundings as explained by Shikada, et al. [237], Mondini, et al. [83], and Vohora and Donoghue [97]. Shikada, et al. [237] found that LST at landslide areas is higher than at non-landslide areas in Hokuriku district, Japan. On the contrary, preliminary results of the investigation carried out by Mondini, et al. [238] showed that the distribution of surface temperature in landslide sites are lower than in the stable areas due to different soil moisture.

#### **4.1.14 Anbalagan's LHEF Weighting System**

In order to compare landslide hazard maps resulted using LSI-based weighting system, another weighting system namely LHEF rating system developed by Anbalagan [2] was adopted. LHEF rating system has been discussed in section

2.4.1.2. The assignment of weight values to landslide causative factors can be found in Table 2.1 and Table 2.2. This rating system involves seven causative factors: rock type, soil, depth of soil, slope gradient, relative relief, land use land cover, water condition. Some modifications were made to adapt available causative factors from the current study to involve in LHEF rating system. Modifications include reducing the number of classes of rock type and soil into 4 and 3 types respectively; replacing depth of soil with distance from river and lake, relative relief with distance from geology lineament (following Pachauri and Pant [53]), water conditions with soil moisture/wetness; and multiplying the LHEF rating by 10 to facilitate overlay process. As mentioned in Table 2.1, some causative factors can have maximum LHEF weight values either 10 or 20. The higher the LHEF rating value the greater the

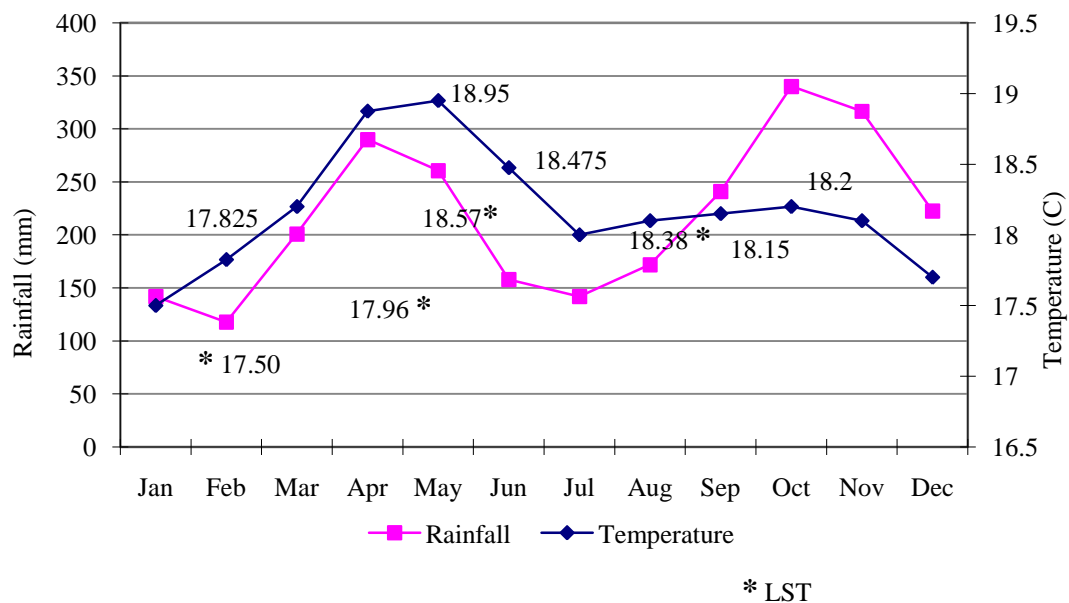


Fig. 4.22 Monthly average rainfall and temperature in Cameron Highlands

Sources: Worldclimate [217]

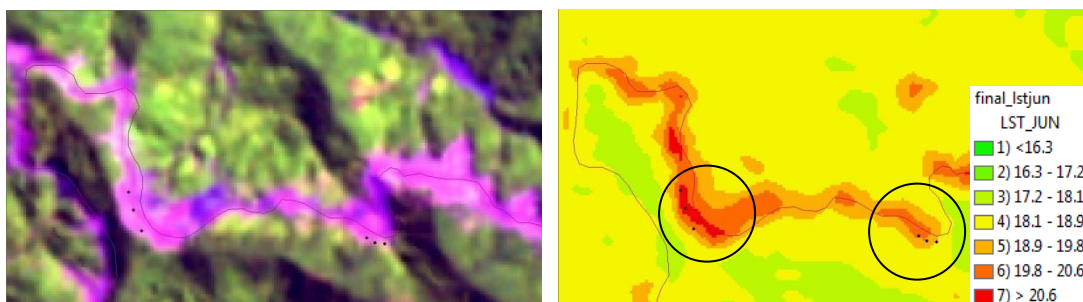


Fig. 4.23 LST at Pos Selim landslide sites

Table 4.7 Adaption of LHEF rating system for the current case study

No	Factor	Subcategories/Classes	Rating
1	Lithology: rock type	Acid and undifferentiated Granitoids	3
		Others (sedimentary rock with associated lava and tuff)	10
		Alluvium	18
		Schist	13
2	Lithology: soil	Podzols and Lithosols on acid igneous rocks at elevation above 5000 feet. (Type I)	14
		Red-Yellow Podzolic soil with Lithosols on acid to intermediate igneous rocks. (Type II)	12
		Red-Yellow Podzolic soil with Reddish-Brown	10
		Lateritic soil on residual materials from acid to intermediate igneous rocks. (Type III)	
3	Distance from geology lineament	0 – 2 km	20
		2 – 4 km	17
		4 – 6 km	12
		6 – 8 km	8
		> 8 km	5
4	Slope gradient	>45	20
		36-45	17
		26-35	12
		16-25	8
		<15	5
5	Distance from river/lake	0 – 200 m	20
		200 – 400 m	17
		400 – 600 m	12
		600 – 800 m	8
		> 800 m	5
6	Land use land cover	Cropland, bushes, thin vegetated area	6
		River, lake	0
		Forest	8
		Urban, built up	15
		Open land, cut slope	20
7	Soil wetness	Drier (0-29)	0
		Dry (29-82)	2
		Medium (82-134)	5
		Wet (134-193)	8
		Wetter (193-254)	10

contribution to landslide occurrences. Depending on the significant contribution among classes of a causative factor, they were assigned rating value from 0 to 10 or 0 to 20. The rating assignment for all classes of all factors is presented in Table 4.7.

Detailed explanation on the modification of landslide causative factors of the current study to apply in LHEF weighting system is as follows. Lithology consists of 4 rock types. Acid and undifferentiated granitoids, simply called as granite and schist are clearly stated in LHEF rating system and assigned a weight value of 3 and 13 (after multiplied by 10). Granite is the hardest rock among the other types so that it is less likely to slide and assigned a low weight value of 3. Alluvium is made up of a variety of material such as silt and clay. Hence, it is assigned a considerable rating value of 15. Other types, sedimentary rock with associated lava and tuff type, are put between granite and schist, the sedimentary rock type too. It is assigned a weight value of 8, indicating that this rock is harder than schist due to the presence of lava and tuff within the rock.

Soil data consists of three types and assigned a weight value of 14, 12 and 10 respectively. According to Anonymous [239], a glossary soil published by The University of Sidney, podzolic is sandy soil type with no concretion in the profile while lateritic contains many concretions in the profile. In addition, a mixture of clayey iron and aluminum hydroxide existed in lateristic soil. Anthoni [240] added that lithosol is stony soil with shallow profiles as found on steep mountains. It is thin soil with poorly defined layers horizons that consists mainly of partially weathered rock fragments as defined in Encarta Word English Dictionary Anonymous [241]. All soil types are sandy due to the present of podzolic soil. Due to the existence of lateristic soil, soil type III is given the lowest weight value of 10. It means that this soil type is less likely to slide. This value is based on that in LHEF rating system. Soil type II is put behind soil type III in term of the stability to slide due to the presence of thin weathered-fragmented rock and is assigned a rating of 12. The last soil type is the co-existence of sandy podzolic and weathered-fragmented soils and is assigned a rating value of 14; meaning that it is more likely to slide.

The classification of distance from geology fault was adopted from Pachauri and Pant [53] while the weight value was adopted from LHEF rating system. It simply

says that the closer the distance from a geology lineament the more prone to landslide the areas. This also applies to distance from river/lake although this factor was absence in LHEF weighting system. The interval of distance from river/lake is set as shown in Table 4.7 considering the working pixel size, that is 30 meter. There is no consensus about classifying the distance from river/lake in term of its influence to landslide. Different distance classification has been applied by various researches such as Lee and Sambath [46], Oh, et al. [77], Sharma and Kumar [101], and Sarkar, et al. [109]. Slope classification was set the same as that of LHEF weighting system. There was a little modification on land use land cover factor made due to the presence of river/lake, urban and built up, and by the absence of moderately vegetated forest area features. Barren land was replaced by open land; sparsely vegetated forest area replaced by cropland. Thick vegetated forest area is simply set as forest. The rating of river/lake was set to 0 since there is no landslide within these areas. The remaining LULC types were assigned weight values based on LHEF system.

Water condition factor puts flowing condition as having the highest weight value in LHEF weighting system that is 10. Adapting this condition, the areas with the highest soil wetness condition was given the maximum weight value of 10. The remaining classes were assigned weight values based on LHEF weighting system with the following constraint, the lower the soil wetness the lower the rating values.

Landslide susceptibility map was constructed by summing up all LHEF weight values of causative factors on the basis of pixel. The total summation of LHEF weight values is also called as The Total Estimated Hazard (TEHD). Based on TEHD, five categories of landslide hazard/susceptible zones were determined and shown on the map as very low hazard, low hazard, medium hazard, high hazard, and very high hazard.

## **4.2 Final Landslide Susceptibility Maps (LSMs) and Maps Validation**

Final LSMs that represents the total susceptibility to landslide occurrences were constructed by overlaying all landslide causative factors on the basis of pixel by pixel

summation. Prior to summation, each pixel of each layer has been assigned a weight value, either using LSI or LHEF rating scheme

The LSMs consist of the following maps:

1. LSMs produced from scenario 1. These maps were produced using static causative factors. Scenario 1 applied different weighting systems, i.e. LSI and LHEF, to allow the evaluation between statistical and non-statistical approaches. This scenario also allows the evaluation of the significance of different number of landslide causatives involved in constructing LSMs on the accuracy of the maps.
2. LSMs produced from scenario 2. These maps were constructed by using the combination of all static causative factors and multi temporal NDVI data. The effect of additional multi temporal NDVI can be evaluated through these maps.
3. LSMs produced from scenario 3. Multi temporal soil wetness data were added to data set containing all causative factors to produce multi temporal LSMs. The effect of additional this multi temporal factor can be evaluated through these maps.
4. LSMs produced from scenario 4. LST of four different climatic conditions were added to static data set to produce multi temporal LSMs. The effect of additional this multi temporal factor can be evaluated through these maps.

The final LSMs indicate five categories of susceptibility zones to landslide. Since the number of landslide causative factors is different between static and multi temporal data set, the maximum of susceptibility level, as the summation of all rating values, may be different. On the basis of the maximum susceptibility level, five categories of landslide susceptibility zones were defined. The maps were reclassified into 5 zones/criteria using equal interval method expressing different susceptibility levels. The five categories are Very Low Susceptibility (VLS), Low Susceptibility (LS), Moderate Susceptibility (MS), High Susceptibility (HS), and Very High Susceptibility (VHS).

To measure the accuracy of LSMs, these maps were validated by means of crossing these maps with landslide/slope failure locations and evaluating the



susceptibility status of these locations. Evaluation of the accuracy of the LSMs was carried out on the basis of an assumption that all landslide sites should fall on the category of HS and VHS. The number or percentage of landslide points falling in these categories determined the accuracy of the LSMs. This measure was also used to facilitate comparisons between the LSMs derived from different scenarios.

#### **4.2.1 Final LSMs of Scenario 1 and Validation of the Maps**

The final LSMs resulted from scenario 1 consist of:

1. LSM derived using LHEF weighting system involving 6 landslide causative factors, factor 1 to 6 as shown in Table 4.7. The factors are rock type, soil, distance from geology lineament, slope gradient, distance from river/lake and land use land cover
2. LSM derived using LHEF rating system involving 6 landslide causative factors and additional soil wetness data, factor 7 (see Table 4.7).
3. LSM derived using LSI-based rating system involving the same 6 landslide causative factors as procedure No. 1.
4. LSM derived using LSI-based rating system involving all (10) static causative factors as shown in on Table 4.1, Table 4.2, and Table 4.3.

Fig. 4.24 a) shows LSM constructed using 6 causative factors based on LHEF rating system. As per visual interpretation, areas having HS and VHS status are concentrated around the roads and cropland. Besides these areas, the map also showed areas with moderate into high susceptibility status as indicated by arrows in Fig. 4.24 a). This may be caused by the contribution of superposition of river/lake and geology lineament layers for location 1 and 2, and the contribution of river/lake layer for location 3 and 4. Safe areas with VLS status are mainly located at forest areas, the left side of the map. Meanwhile, forest areas at the right side of the map mostly indicate low and moderate susceptibility status. Fig. 4.24 b) shows LSM constructed using the same causative factors as the previous result with soil wetness as additional layer. This layer was derived from the transformation of Landsat 7 band acquired on 20 September 2001 into soil wetness using Tasseled Cap Transformation.

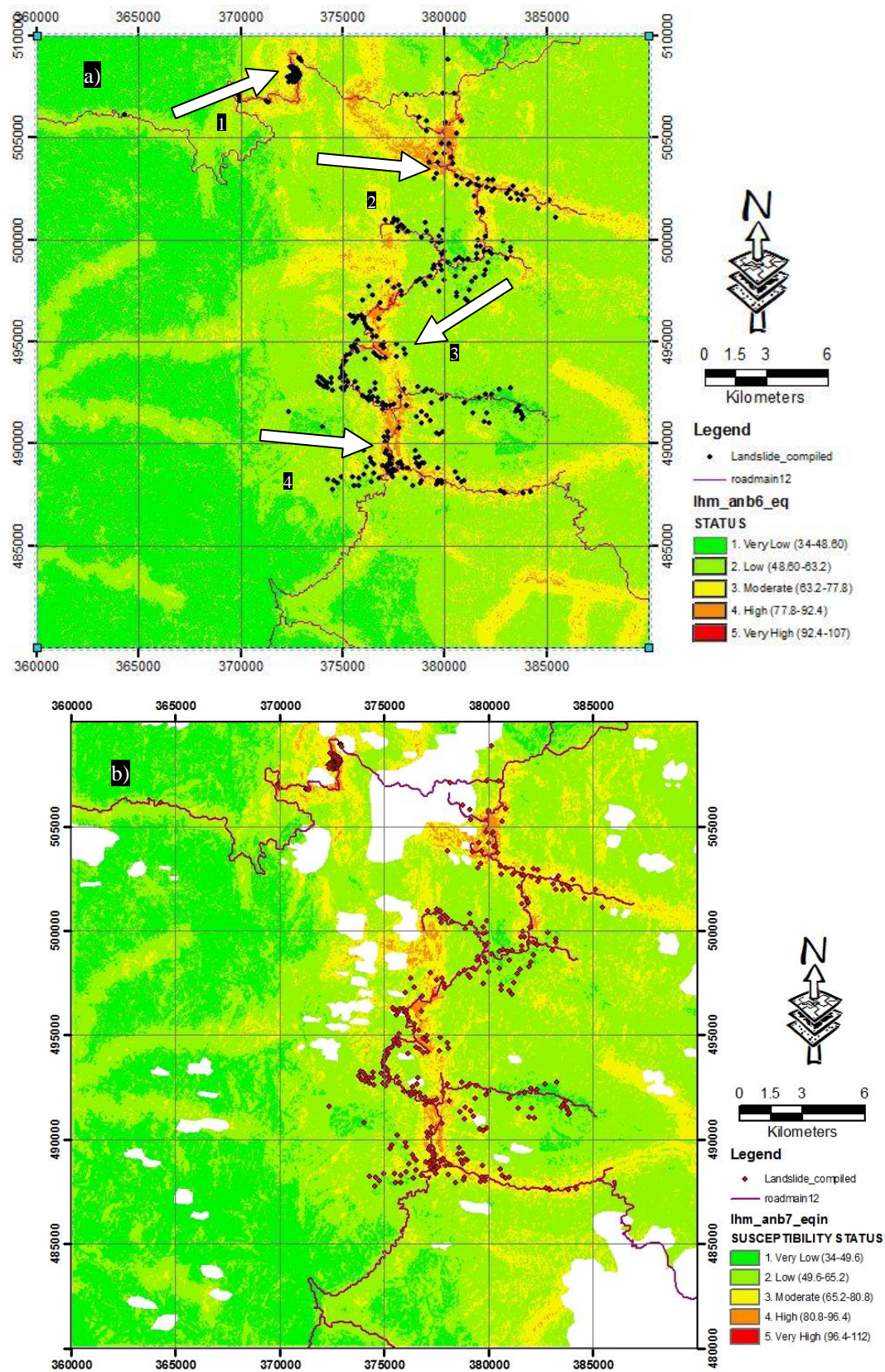


Fig. 4.24 LHEF rating system-based LSM derived using: a) 6, and b) 7 factors.



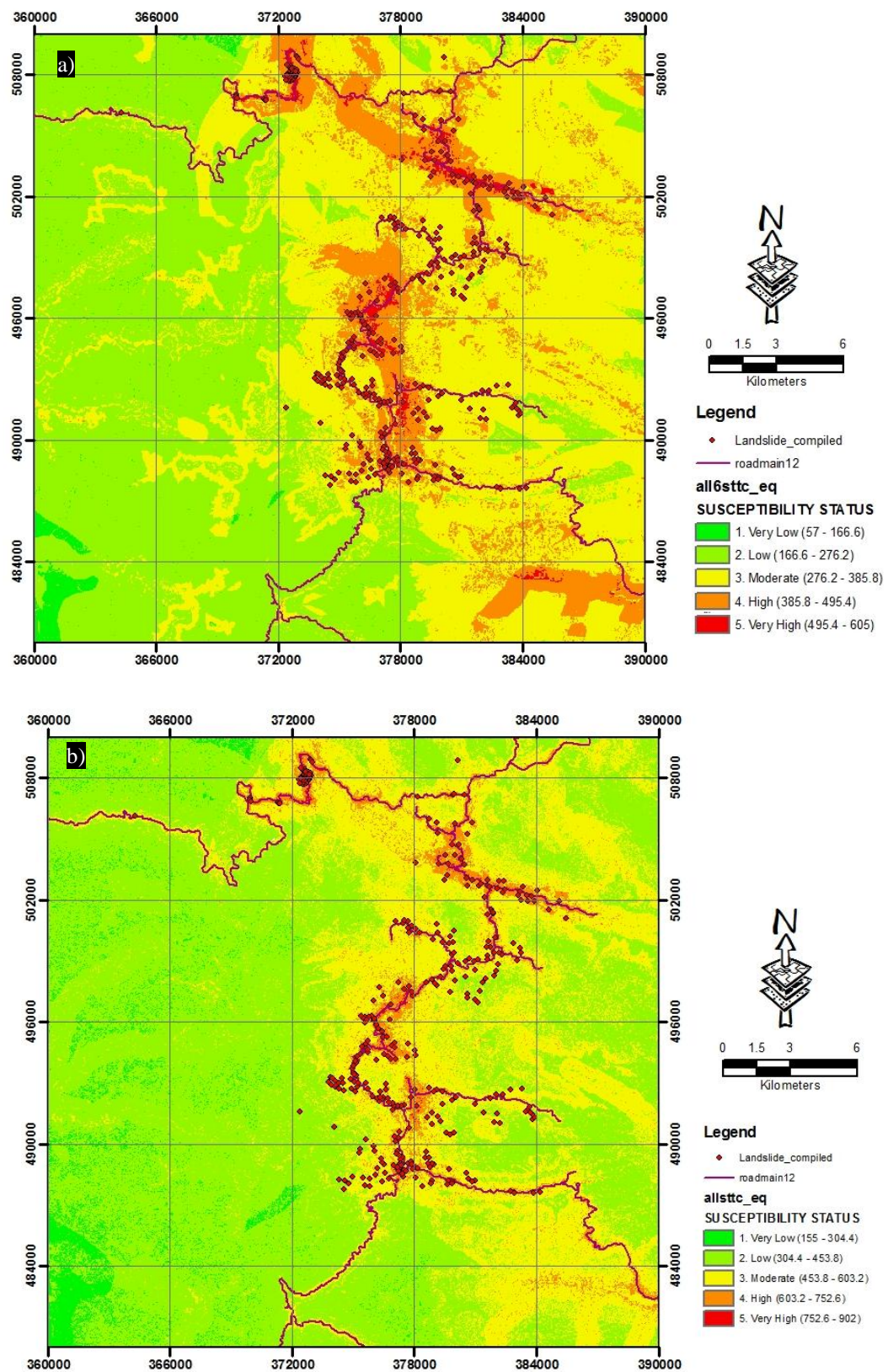


Fig. 4.25 LSI-based LSM derived using: a) 6, and b) all static factors.

The distribution of susceptibility areas on this map is almost similar to the previous map except it contains removed/blank areas caused by coverage of clouds and the associated shadows.

Fig. 4.25 a) shows LSM constructed using 6 causative factors based on LSI weighting system. Compared to the previous maps, this map shows more areas having HS status. The HS areas as indicated by arrows in Fig. 4.24 a) become more clearly apparent on this map. This may be caused by the effect of the application of LSI weighting system which assigns weight values based on landslide attributes extracted from the study area. Fig. 4.24 b) show LSM constructed by using all static causative factors, ten factors. The factors consist of the same 6 factors as those used to derive either LHEF- or LSI-based LSM. The four additional causative factors are shown in Table 4.8. Unlike the previous map, addition of more causative factors seems not to produce more areas categorized as HS and VHS as seen on the map.

Table 4.8 Statistics of LSM of scenario 1

	Landslide causative factors						Susceptibility status and the corresponding coverage (in %)				
	Rock type Soil Dist. from lineament Slope gradient Dist. from river/lake Land use land cover	Elevation	Slope aspect	Curvature	Dist. from road	Soil wetness of September	Very Low	Low	Moderate	High	Very High
LHEF 6		-	-	-	-	-	28.7	53.1	16.4	1.8	0
LHEF 7		-	-	-	-		25.7	55.9	16.8	1.5	0
LSI 6		-	-	-	-	-	1.0	40.5	45.2	12.2	1.1
LSI 10 (all factors)						-	4.1	58.2	33.4	4.1	0.2

Table 4.8 shows the percentage of the predicted areas with the corresponding susceptibility status from VLS to VHS. The total coverage of the study area is about 30 km x 30 km or 900 km<sup>2</sup> and the pixel size of all landslide causative factors is set to 30 m. Special attention is given to areas with HS and VHS status. According to the table, the percentage of both areas predicted by LHEF 6 and 7 is lesser than that predicted by LSI. Due to small values of percentage of VHS areas predicted by LHEF

weighting system, their values appear as zero. Again, addition of soil wetness layer was unable to increase the areas of HS and VHS. Moreover, addition of more static landslide causative factors (up to ten factors) appears to reduce the percentage of both types of area in case of LSI-based LSM. Six static causative factors are reasonable/sufficient number of landslide causative factor for constructing LSM. This dataset produces the largest coverage of areas of both types

As mentioned earlier, the LSMs or predicted landslide susceptibility zones were validated by using existing landslide/slope failure data. The capability of each landslide susceptibility model to predict back the existing landslide sites as HS and VHS status determines the accuracy of the model. Table 4.9 shows the validation results.

Table 4.9 Validation for GIS-based LSM of scenario 1

	Landslide causative factors						The number of validated landslide points (in %) and the corresponding susceptibility status					
	Rock type Soil Dist. from lineament Slope Dist. from river/lake Land use land cover	Elevation	Slope aspect	Curvature	Dist. from road	Soil wetness of September	Very Low	Low	Moderate	High	Very High	High + Very High
LHEF 6		-	-	-	-	-	2.5	37.4	39.7	20.4	0.0	20.4
LHEF 7		-	-	-	-		3.2	42.4	36.3	16.6	1.5	18.0
LSI 6		-	-	-	-	-	0	0.8	41.3	43.9	14	57.8
LSI 10 (all factors)						-	0	5	53.4	39.4	2.2	41.6

Table 4.9 shows that among LHEF-based LSMs, LHEF that involves 6 static landslide causative factors, simply written as LHEF 6, produced a better LSM compared to that involving 7 causative factors, LHEF 7, in term of the number of predicted landslide sites falling within HS and VHS status. It means that addition of soil wetness map reduced the accuracy of the previous map. LHEF 6 managed 20.4% (73 points) of the total of 358 landslide points while LHEF 7 managed only 62 points (about 18% of the total of landslide points). Among LSI-based LSMs, inclusion of all

static causative factors, (10 factors), did not necessarily improve the accuracy of the landslide susceptibility model. The accuracy of LSI-based LSM constructed using 6 static causative factors are superior to that using all static factors. The first confirmed about 57.8% (207 points) while the latter confirmed about 41.6% (149 points) of the total number of landslide points. This result left a question on why involvement of more causative factors cannot automatically improve the accuracy of the LSM. There must be causative factors that may have insignificant contribution to improve the accuracy of LSM or even tend to reduce the accuracy of the LSM if combined with other factors. The investigation regarding this problem is discussed sub chapter 4.3 .

On the overall, six static landslide causative factors seems to be sufficient number to model landslide susceptibility either using statistical (LSI) or non statistical (LHEF) approaches in scenario 1. In addition, statistical approach produces better results of LSM than LHEF approach, the non statistical approach. Even after removing areas due to clouds and shadows coverage to conform to the thematic map of soil wetness acquired on September 1991, LSI-based LSMs remain superior over LHEF-based LSMs. After removing areas blocked by clouds and the associated shadows, LSI 6 and LSI all static factors are still able to predict back 57.6% (198 points) and 41.8% (143 points) of the total number of existing landslide data respectively as having HS and VHS status.

#### **4.2.2 Final LSMs of Scenario 2 and Validation of the Maps**

Scenario 2 combined all static causative factors and multi temporal NDVI maps and produced 4 LSMs. Each map represents the influence of different conditions of NDVI as response to monsoonal rainy seasons in determining the susceptibility of the study area to slide. The NDVI maps were derived from Landsat images acquired on February (first dry season), May (first rainy season), June (second dry season), and September (second rainy season). Fig. 4.26 and Fig. 4.27 show LSMs with the influence of different NDVI conditions. The susceptibility values ranges for each season vary. For the first rainy season (February), the range is 202-1002. The ranges of next seasons are 225-1000 (May), 178-985 (June), 174-985 (September). The higher the susceptibility values the more susceptible to landslide the corresponding

areas. On the basis of the susceptibility values, five categories of landslide susceptibility zones have been determined. Using equal interval approach, these ranges of values were divided into five statuses: VLS, LS, MS, HS, and VHS.

The LSMs produced from scenario 2 as shown in Fig. 4.26 and 4.27 cannot be presented as full maps because they contain blank areas caused by clouds and the associated shadows. This is the common problem when deriving any spatial data from any passive remote sensing sensors such as the ones used by Landsat 7 that detect the reflected or emitted electromagnetic radiation from natural sources such as the sun. Unlike an active sensor such as radar, the passive sensor cannot record the reflectance or emission of objects under coverage of clouds. In addition, cloud shadows cause a problem, that is, producing reflectance numbers that may have similarity/closeness with those of water body features such as lakes. Besides this drawback, these LSMs are able to indicate the spatial distribution of zones HS and VHS zones as indicated by arrows and the corresponding numbers in Fig. 4.26 and Fig. 4.27. The description of the numbered areas is as follows:

1. Slopes at road sides starting from Pos Selim where the massive landslide occurred until Ringlet.
2. Urban areas at Kampong Raja and Kampong Kuala Terla.
3. Urban areas at Tanah Rata.
4. Urban areas at Ringlet.

The spatial distribution of susceptibility statuses of the study area varies from map to map. Table 4.10 shows the statistic of susceptibility zonation. Most of the area of study falls in LS status followed by MS and VLS status. Fewer areas fall in HS status. Areas with very HS status occupy the smallest part of the study area. Even, the combination of areas with HS and VHS status still occupies the smallest part of the study area. Regardless the capability of the GIS-based landslide susceptibility model in determining the level of susceptibility of the study area, model validation needs to be carried out to measure the accuracy of the susceptibility status of predicted zones.



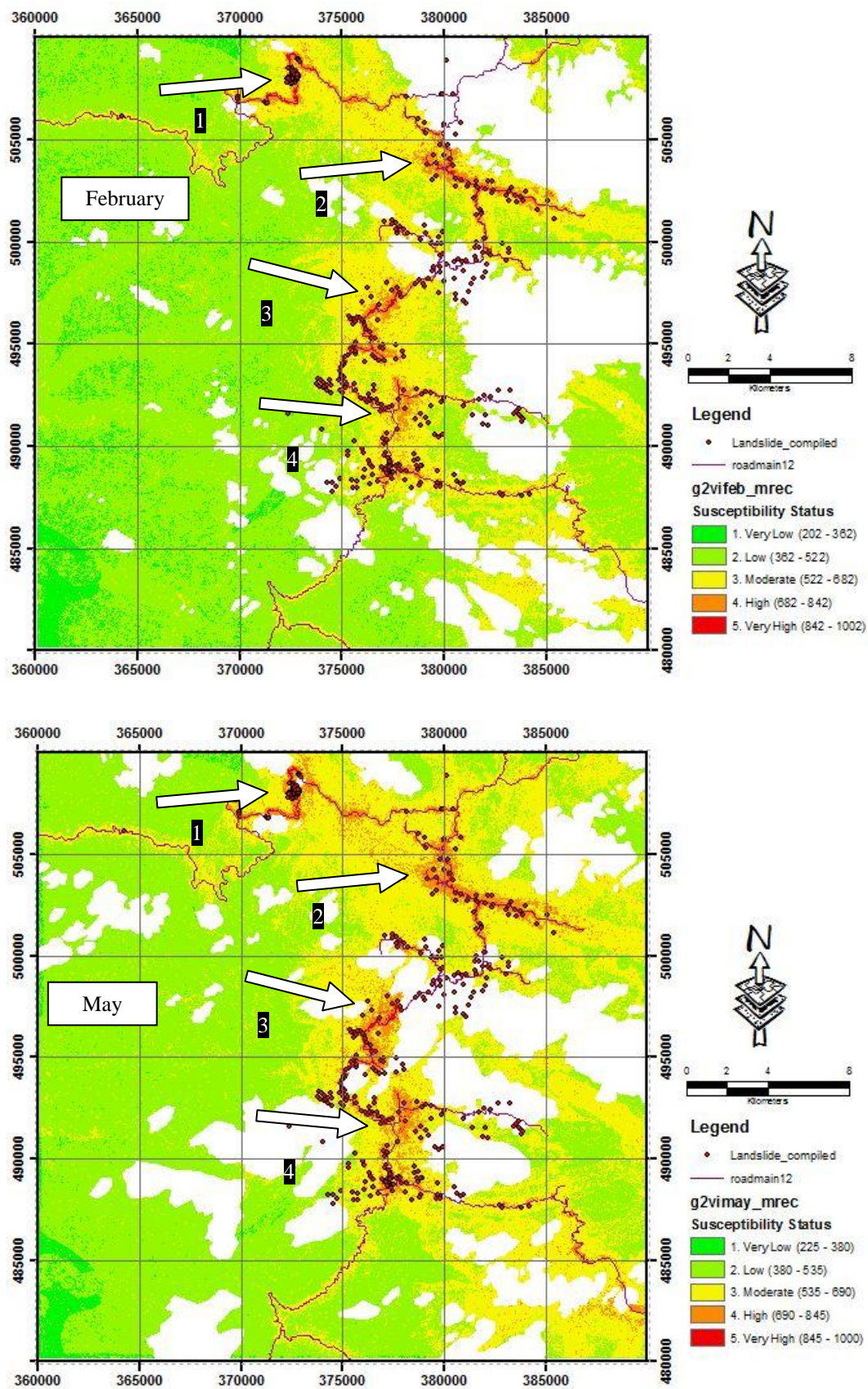


Fig. 4.26 LSMs of Scenario 2: all static factors and NDVI February and May



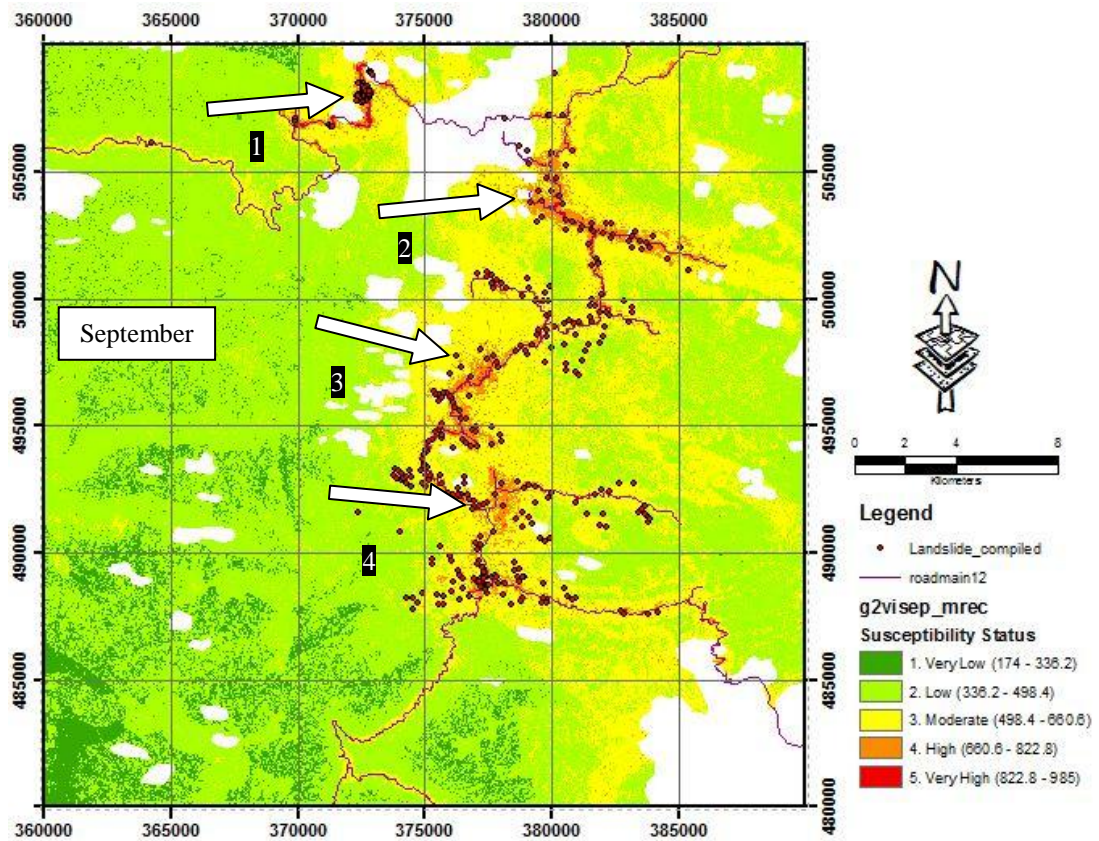
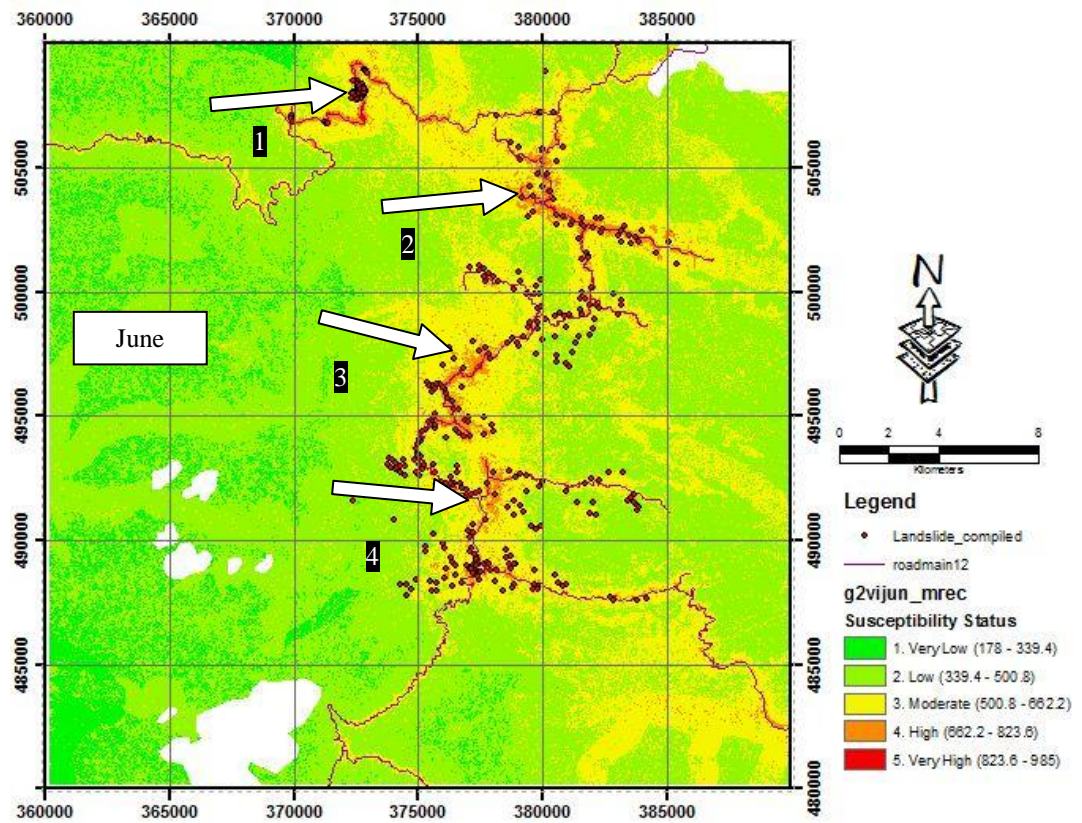


Fig. 4.27 LSMs of Scenario 2: all static factors and NDVI June and September

Another thing that needs to take a note is that each map has different removed areas caused by clouds and the associated shadows coverage. The removed areas are 24.2%, 23.7%, 3.4%, and 10.4% of the study area respectively represents cloud and shadow conditions for February, May, June, and September. Hence, comparing susceptibility conditions map by map is not logical. A common area available on all maps should be defined to allow map by map comparison. Polygons called as training areas were defined by delineating areas which are free of clouds and shadows. The training are should be applicable for all LSMs. The delineation of polygons were attempted, as much as possible, to cover all landslide locations. Fig. 4.28 shows the required training areas for map by map evaluation which are shown in dark blue.

Table 4.10 Statistic of LSMs of scenario 2

Susceptibility statuses	Areas in km2				Areas in %			
	Feb	May	Jun	Sep	Feb	May	Jun	Sep
Very Low	37.6	12.2	75.4	62.1	5.6	1.8	8.8	7.7
Low	434.6	380.4	541.8	493.2	64.5	55.9	63.1	61.4
Moderate	178.2	253.1	220.8	224.7	26.4	37.2	25.7	28.0
High	22.5	33.4	20.4	22.1	3.3	4.9	2.4	2.8
Very High	0.9	1.2	0.7	0.9	0.1	0.2	0.1	0.1
Area	673.8	680.4	859.2	803.1	74.9	75.6	95.5	89.2
High + Very High	23.4	34.6	21.9	23.5	3.4	5.1	2.5	2.9
Clouds and shadows coverage	217.6	213.7	304.7	93.3	24.2	23.7	3.4	10.4
Total area (≈)	900	900	900	900	100	100	100	100

The coverage of the training area is about 49.5 km<sup>2</sup>. Each LSM was cropped by using this training area. The statistic of susceptibility status of extracted map is presented in Table 4.11. The spatial variation of each susceptibility status can be identified. Special attention is focused on the areas with HS and VHS status. The possibility of both statuses to expand or collapse caused by change in vegetation index, i.e. NDVI, as its response to monsoonal rainfall system can be identified. Both categories show that during rainy seasons (May and September), the coverage of these areas increases (Fig. 4.29). On the contrary, during dry seasons (February and June), their coverage relatively decreases. The other susceptibility statuses, e.g. MS, LS and VLS, are not of the main concern to discuss in this work. According to Liao

[47], very LS and VLS areas are considered as safe areas for development. Meanwhile, MS areas may contain some locally vulnerable zones of instability. In the training areas, there are no areas with VLS status.

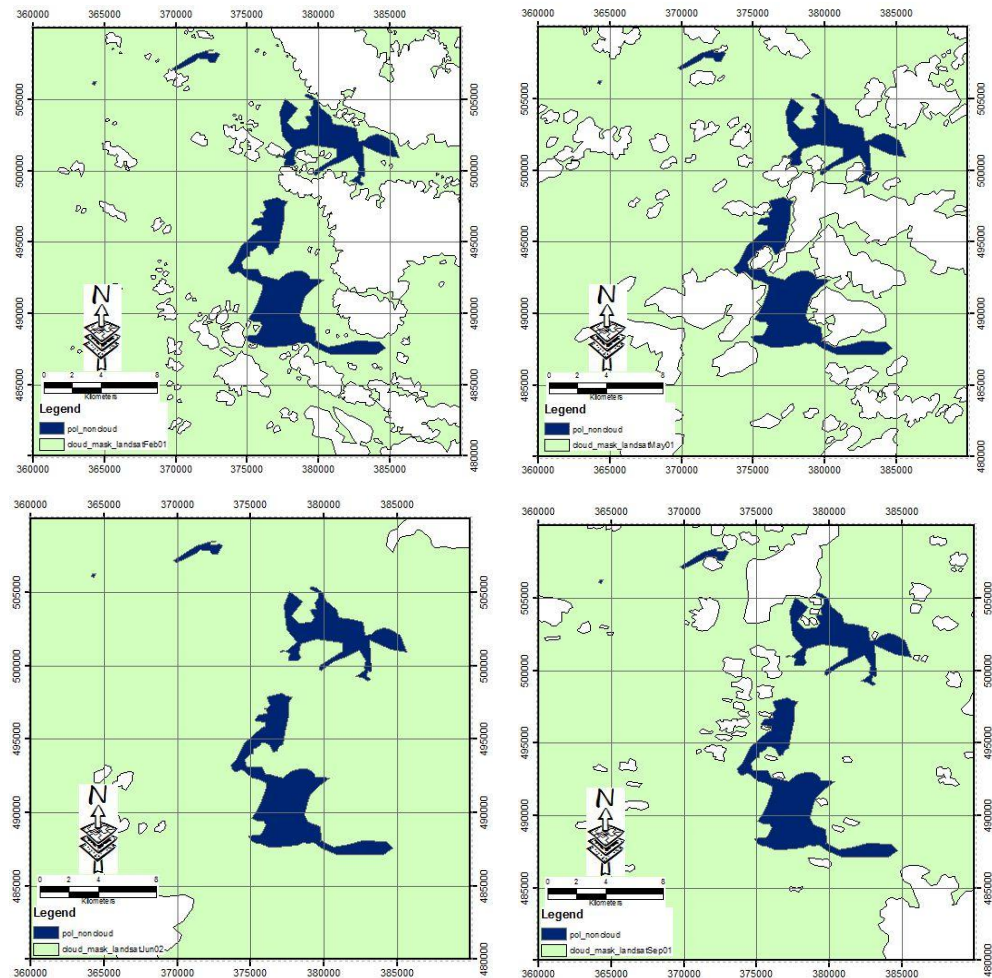


Fig. 4.28 Polygons used as training areas shown as dark areas

Table 4.11 Statistic of the training area for scenario 2

Susceptibility Statuses	Areas in km2			
	February	May	June	September
Very Low	0	0	0	0
Low	4.9	1.9	7.6	4.2
Moderate	32.4	31.6	31.8	32.8
High	11.7	15.3	9.7	12.0
Very High	0.5	0.8	0.4	0.5
High and Very High	12.2	16.1	10.1	12.5
Total of area	49.5	49.5	49.5	49.5



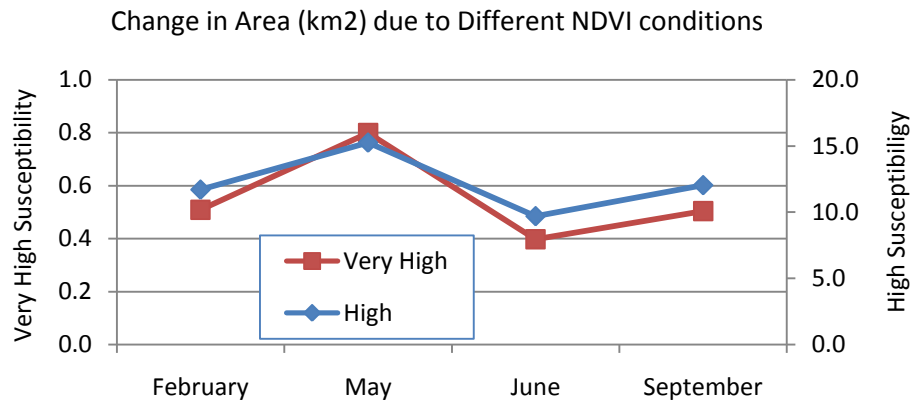


Fig. 4.29 The increase and decrease of areas fall in very high and high susceptibility status due to change of NDVI

The most importance procedure to conduct when one would produce a GIS-based landslide susceptibility or hazard map is to validate that map. The number of landslide points used for validation is not 358 (the total number) but reduced to 230 (64.2% of the total number of landslide data) to conform to the training areas. Hence, only landslide data within the training areas were used. The unused landslide data is 128 points (35.8% of the total number of landslide data). The 230 points were used to extract the susceptibility values from each LSM that represents different NDVI conditions. These values were reclassified using the same interval classes as those of SMs of scenario 2. The result is shown in Table 4.12. None of the landslide data within the training areas fall in very low susceptibility category, the safest zones. The combination of landslide points having HS and VHS status shows a graphical pattern that may relate to rainfall variation (Fig. 4.30). During two rainy seasons on May and September, NDVI maps of these seasons contribute the increase of the number of validated landslide points with both statuses which is relatively greater than that of two dry seasons. The number/percentage of validated landslide points is 119 point (42.6% of used landslide data) and 102 points (44.3%) for May and September; 98 points (42.6%) and 85 points (37.0%) for February and June respectively. NDVI of rainy seasons tends to increase the susceptibility zones to landslide with HS and VHS status. Hence, it can be said that besides being used as a measure of the accuracy of the GIS-based LSMs, the different number of validated landslide points of each

month may also be used to represent the relation of spatial variation of possible dangerous areas (with HS and VHS status) and rainfall pattern.

Table 4.12 Validation for GIS-based LSM of scenario 2

Susceptibility status	Number of validated points				Percentage of validated points			
	Feb	May	Jun	Sep	Feb	May	Jun	Sep
Very Low	0	0	0	0	0.0	0.0	0.0	0.0
Low	13	6	17	13	5.7	2.6	7.4	5.7
Moderate	119	105	128	115	51.7	45.7	55.7	50.0
High	93	105	75	97	40.4	45.7	32.6	42.2
Very High	5	14	10	5	2.2	6.1	4.3	2.2
High and Very High	98	119	85	102	42.6	51.7	37.0	44.3

Up to this step, the final landslide susceptibility maps involving one of environmental change factors, multi temporal NDVI maps, have been constructed. Hence, one of the objectives of the research has been fulfilled. However, the significance role of involvement of multi temporal NDVI maps in determining the accuracy of the LSMs has not been determined. The evaluation of the accuracy of these maps requires a reference map resulted from scenario 1 that employed only static causative factors. By comparing these two LSMs, the significant role of NDVI maps in GIS-based landslide susceptibility model can be determined. The discussion about this can be found in subsection 4.2.5.

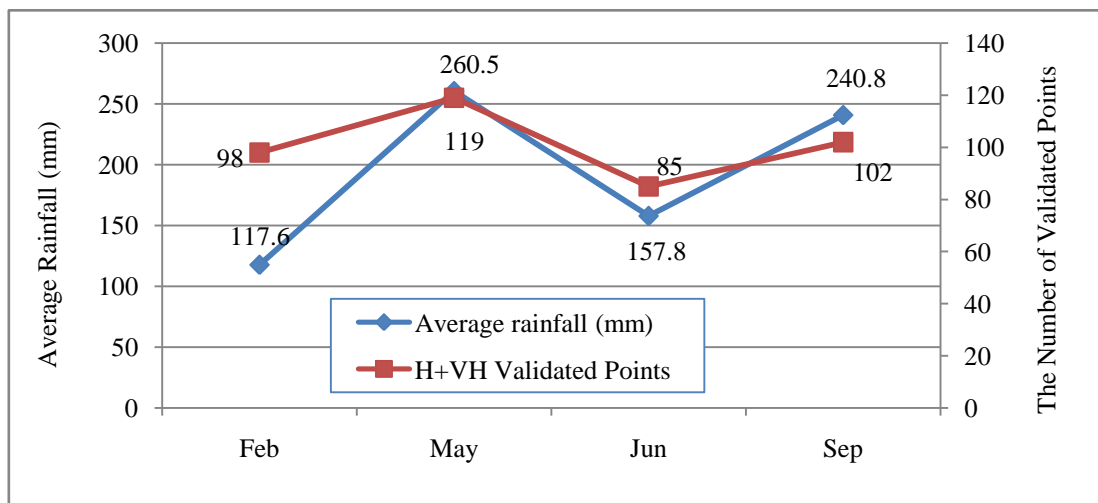


Fig. 4.30 Average rainfall and the number of predicted landslide points falls in very high and high susceptibility status due to change of NDVI

### 4.2.3 Final LSMs of Scenario 3 and Validation of the Maps

Final LSMs of scenario 3 accommodate the influence of 4 seasonal conditions of soil wetness besides the main data, all static causative factors as used in scenario 1. The soil wetness maps were derived from Landsat images acquired during 2 rainy seasons (May and September) and 2 dry seasons (May and June). The final LSMs of scenario 3 are shown in Fig. 4.31 and Fig. 4.32.

The range of susceptibility values vary for each seasons: 182-996 (dry season of February), 170-991 (rainy season of May), 170-991 (dry season of June), and 162-1005 (rainy season of September). The higher the susceptibility values the more susceptible to landslide the corresponding areas. The range of susceptibility values was divided into five susceptibility zones namely VLS, LS, MS, HS and VHS.

The LSMs produced from scenario 3 as shown in Fig. 4.31 and Fig. 4.32 contain blank areas caused by clouds and their respective shadows as the case of scenario 2. These maps show the spatial distribution of landslide susceptibility zones. The possibly dangerous zones (with high and very high susceptibility statuses) for slope to fail are the same as those of LSMs of scenario 2. The zones are indicated by circles and the corresponding numbers. The first zone is the location around the post landslide site at Pos Selim. The second zone covers urban areas at Kampung Raja and Kuala Terla, and agriculture area around Terla River. The third and the last zones cover urban areas at Tanah Rata and Ringlet respectively.

The area of each susceptibility status varies from season to season. The variation of susceptibility areas of all statuses is shown in Table 4.13. LS and VLS are considered as safe areas. The latter dominates the study area followed by moderate status. The possibly danger areas categorized as having high and very high susceptibility occupy small part of the study area. As the case of LSMs of scenario 1, map by map comparison cannot be carried out due to different size of blank areas caused by coverage of clouds and the corresponding shadows (see Table 4.13). The coverage of these two objects is the same for all scenarios that are 24.2%, 23.7%, 3.4% and 10.4% of 900 km<sup>2</sup>, the total area of the study area. Moreover, the quality of the map should be accessed by means of map validation.

Table 4.13 Statistic of LSMs of scenario 3

Susceptibility statuses	Areas in km2				Areas in %			
	Feb	May	Jun	Sep	Feb	May	June	Sep
Very Low	101.1	74.5	40.2	43.4	15.0	11.0	4.7	5.4
Low	396.8	372.1	437.6	419.0	58.9	54.7	50.9	52.2
Moderate	147.0	203.6	331.9	299.4	21.8	29.9	38.6	37.3
High	27.3	29.3	47.8	39.9	4.0	4.3	5.6	5.0
Very High	1.6	0.9	1.7	1.5	0.2	0.1	0.2	0.2
Area	673.8	680.4	859.2	803.1	74.9	75.6	95.5	89.2
High + Very High	28.9	30.2	49.5	41.3	4.3	4.4	5.8	5.1
Clouds and shadows coverage	217.6	213.7	304.7	93.3	24.2	23.7	3.4	10.4

The area of each susceptibility status varies from season to season. The variation of susceptibility areas of all statuses is shown in Table 4.13. LS and VLS are considered as safe areas. The latter dominates the study area followed by moderate status. The possibly danger areas categorized as having high and very high susceptibility occupy small part of the study area. As the case of LSMs of scenario 1, map by map comparison cannot be carried out due to different size of blank areas caused by coverage of clouds and the corresponding shadows (see Table 4.13). The coverage of these two objects is the same for all scenarios that are 24.2%, 23.7%, 3.4% and 10.4% of 900 km<sup>2</sup>, the total area of the study area. Moreover, the quality of the map should be accessed by means of map validation.

The training area is needed to perform map by map comparison. The same training area used in scenario 2 was applied to scenario 3. Comparing map by map would result in knowledge about the increase/expansion or decrease of areas with a particular susceptibility status. The next benefit is that the effect of rainy cycle in changing the conditions of soil wetness to GIS-based LSMs can be evaluated. Each landslide susceptibility map was cropped using the training area that cover the area of 49.5 km<sup>2</sup>. Recapitulation of spatial variation of susceptibility areas is presented in Table 4.14.

Areas with different susceptibility statuses in the training area vary season by season. Referring to Table 4.14, the areas with HS and VHS status start to decrease

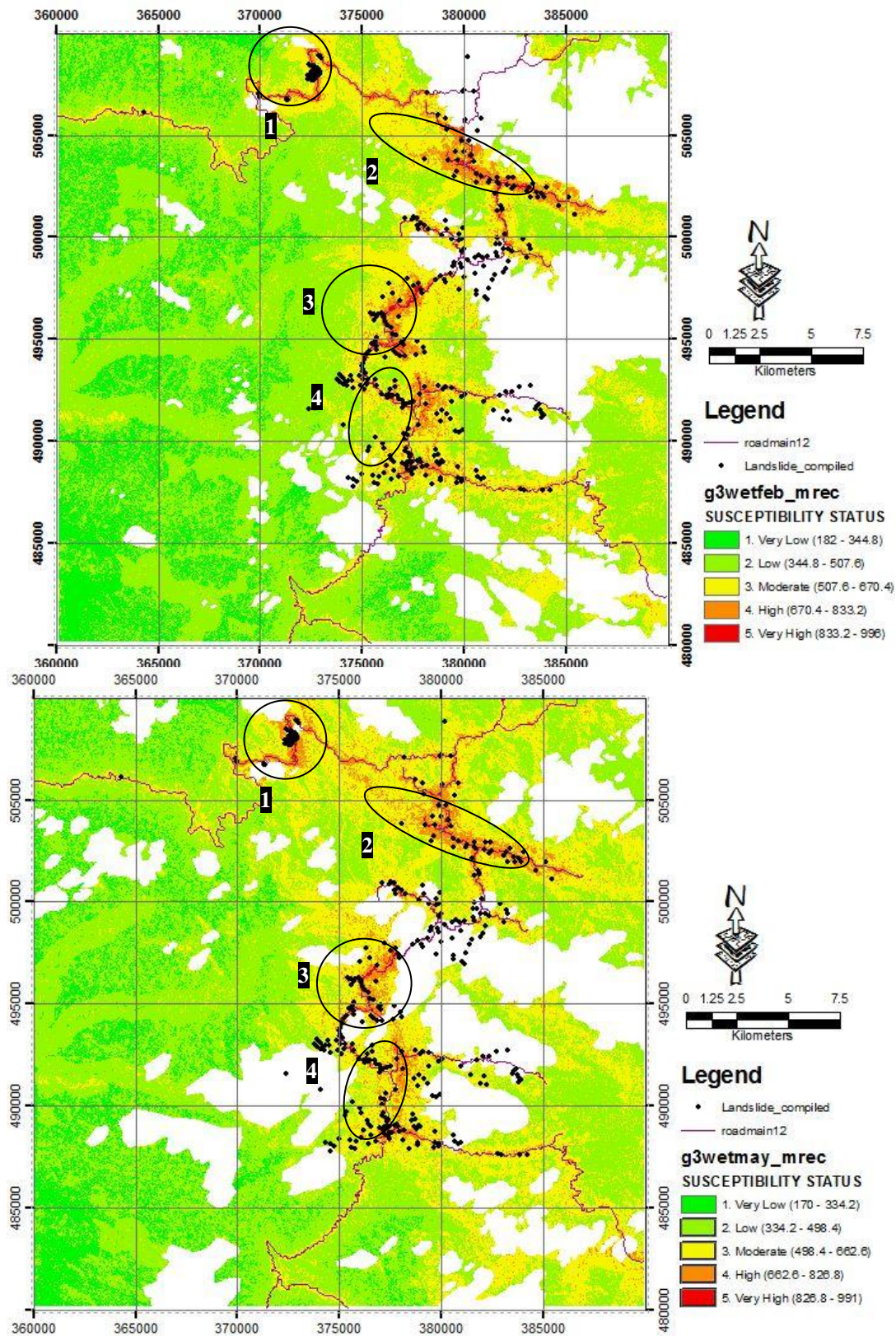


Fig. 4.31 LSMs of Scenario 3: all static factors and soil wetness of February and May



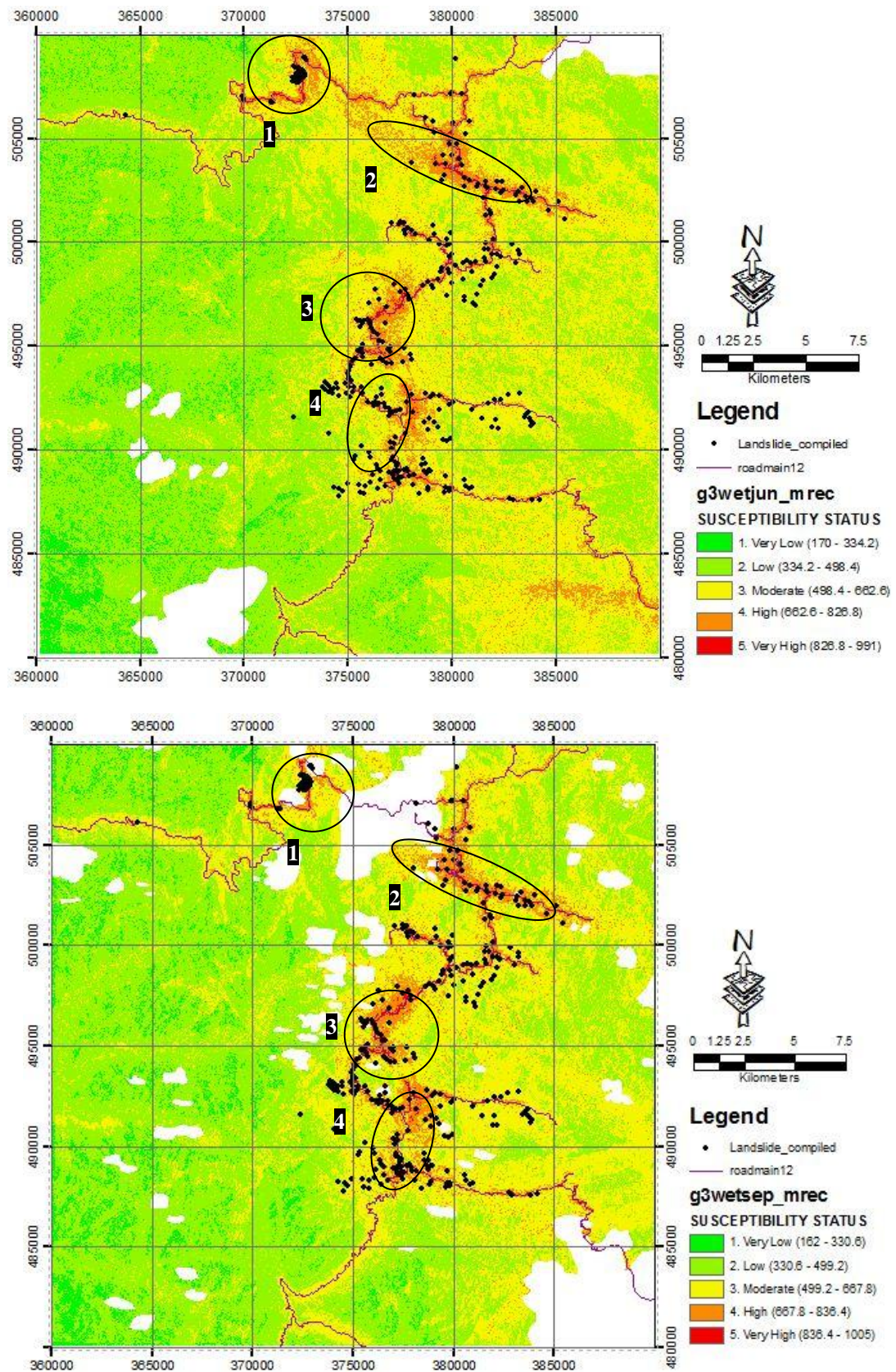


Fig. 4.32 LSMs of Scenario 3: all static factors and soil wetness of June and September

from February (31 km<sup>2</sup>) to May (28.2 km<sup>2</sup>) by 10%; increase from May to June (52.6 km<sup>2</sup>) by 25.9%; and increase from June to September (39.9 km<sup>2</sup>) by 12.5%. Unlike the case of LSMs with additional NDVI maps, there is no significant increase of possibly dangerous areas on May, the rainy season. Otherwise, these two areas relatively decrease compared to those of February, the dry season. However, on June and September, the possibly dangerous areas have the same characteristics as the case of scenario 2, decreasing during dry season and increasing during rainy season. This pattern resembles the rainfall data pattern. Fig. 4.33 may give a comprehensive view about: 1) average rainfall, 2) the number of validated landslide points, and 3) change in areas with high and very high susceptibility status within the training area. It shows that graph 2 and 3 have a similar trend. When compared to the graph of rainfall data of Tanah Rata, only soil wetness of May that does not show the same trend as that of the rainfall data. This contradiction may originate from the selected Landsat image, dated 31 May 2001, which was not the peak time of rainy season. The peak time of rainy season was supposed to fall in April. Unfortunately, the required image was unavailable as discussed in section 3.3.3. This result is somewhat contradictory from geotechnical point of view. This is the weak point of bivariate statistical approach that does not consider geotechnical point of view. This approach is solely based on the characteristic of used data. In other words, it is commonly known as data driven approach as described by Suzen [57]. In addition, whether or not the addition of soil wetness contributes significant improvement of the GIS-based landslide susceptibility model, discussion about this can be found in section 4.2.5.

Validation result of LSMs of scenario 3 is shown in Table 4.15. LSMs constructed from scenario 3 were validated by using a set of landslide locations within training area. About 230 of 358 landslide data located within the training area were used for validation. The result shows that none of the landslide data has VLS status. Most of them were predicted as having MS, followed by HS status. VLS and VHS areas take minor part of the training area. The percentage of landslide locations predicted as having HS and VHS status is constant at 47.4% either for LSMs of February and May. The accuracy becomes greater on June and September by 52.6% and 63.5 respectively. This means that LSMs of September has the highest accuracy followed by those of June, May and February.

Table 4.14 Statistic of the training area for scenario 3

Susceptibility Statuses	Areas in km2			
	February	May	June	September
Very Low	0.0	0.0	0.0	0.0
Low	13.1	11.5	6.7	6.2
Moderate	55.9	60.2	57.8	53.8
High	28.8	27.1	33.3	37.7
Very High	2.2	1.1	2.2	2.2
High and Very High	31.0	28.2	35.5	39.9

Table 4.15 Validation of LSMs of scenario 3

Susceptibility Status	Number of validated points				Percentage of validated points			
	Feb	May	Jun	Sep	Feb	May	Jun	Sep
Very Low	0	0	0	0	0.0	0.0	0.0	0.0
Low	7	10	8	1	3.0	4.3	3.5	0.4
Moderate	114	111	101	83	49.6	48.3	43.9	36.1
High	103	96	110	134	44.8	41.7	47.8	58.3
Very High	6	13	11	12	2.6	5.7	4.8	5.2
High + Very High	109	109	121	146	47.4	47.4	52.6	63.5

The final landslide susceptibility maps that incorporate multi temporal soil wetness maps have been constructed, complementing the previous results for fulfilling one of the objectives of the research. Evaluation on the importance role of multi temporal soil wetness in determining the accuracy of GIS-based LSMs still needs to be carried out by comparing these maps with the LSMs of scenario 1. This matter is discussed in section 4.2.5.

#### 4.2.4 Final LSMs of Scenario 4 and Validation of the Maps

Final LSMs of scenario 4 were constructed using all static landslide causative factors and multi temporal LST as additional data. The LST maps were derived from Landsat images acquired on different seasons: February (dry) May (rainy), June (dry), and September (rainy). The final LSMs of scenario 4 consist of 4 maps. The maps accommodate 4 seasonal conditions of LST are shown in Fig. 4.34 and Fig. 4.35. The range of susceptibility values is different for each map. The ranges are 196-965 for

February (first dry season), 189-1002 for May (first rainy season), 177-983 for June (second dry season), and 155-1002 for September (second rainy season). Areas with high susceptibility values are possibly the dangerous areas in term of the possibility of the respective slopes to fail. Each map was divided into five zones with equal interval representing areas with VLS, LS, MS, HS, and VLS status.

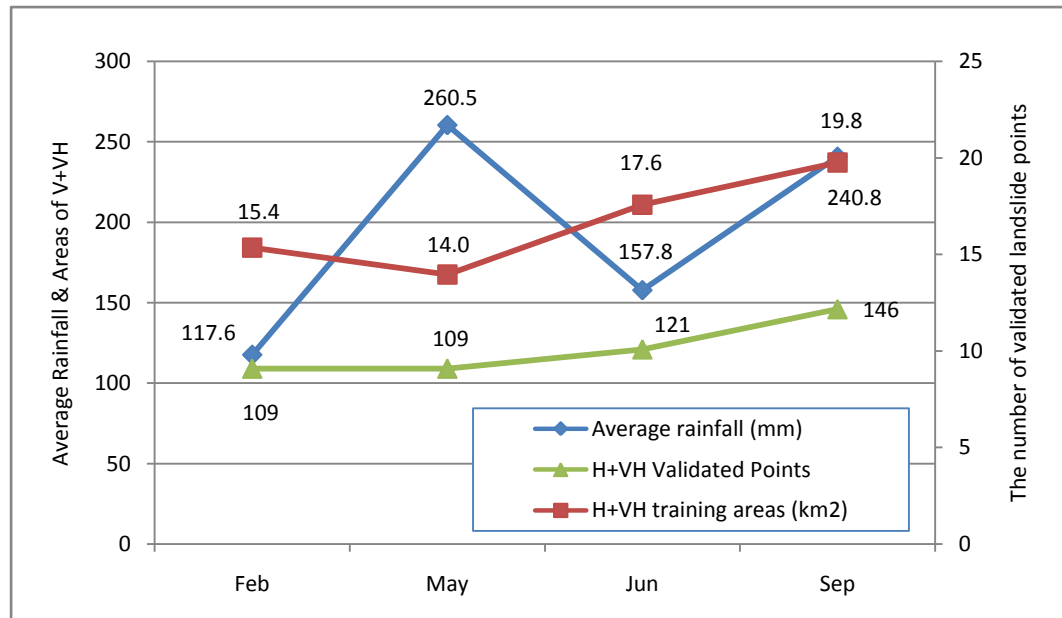


Fig. 4.33 Average rainfall, areas of very high and high susceptibility statuses, and the number of validated points due to change of soil wetness

Clouds and their shadows are inherent natural factors for highlands areas such as Cameron Highlands, the study area. Since the LSMs produced from scenario 4 utilized LST derived from Landsat 7 satellite image, the existence of blank areas are unavoidable (Fig. 4.31 and Fig. 4.32). This problem happens to all final LSMs. In spite of this defect, the maps are able to locate the possibly dangerous areas with HS and VHS status as indicated by circles and the corresponding numbers. The possibly dangerous areas include: 1) areas around post landslide site at Pos Selim, 2) urban areas at Kampung Raja and Kuala Terla, and agriculture area around Terla River, 3) urban areas at Tanah Rata, and 4) urban areas at Ringlet. The statistic of LSMs of scenario 4 is shown in Table 4.16.

Most of areas on each map are categorized as save (LS and VLS status). Moderate susceptibility status is the second dominating areas. Small part of the study area is considered as possibly dangerous areas with HS and VHS status. These particular areas spatially change with time, namely during two dry and rainy seasons. However, these changes mean nothing since each map is not comparable one to another due to different size, shape, and position of blank areas caused by clouds and the associated shadows. A fair comparison can only be done by using the training area as discussed earlier in subsection 4.2.2. The areas extracted from each LSM by using the training areas are ready for evaluation. The statistic of the training area of each map is presented in Table 4.17.

Table 4.16 Statistic of LSMs of scenario 4

Susceptibility statuses	Areas in km2				Areas in %			
	Feb	May	Jun	Sep	Feb	May	June	Sep
Very Low	30.4	48.7	22.9	14.4	4.5	7.2	2.7	1.8
Low	440.0	395.3	469.3	413.9	65.3	58.1	54.6	51.8
Moderate	171.6	207.0	324.9	328.7	25.5	30.4	37.8	41.1
High	30.3	28.6	40.7	40.7	4.5	4.2	4.7	5.1
Very High	1.4	0.8	1.4	1.9	0.2	0.1	0.2	0.2
Area	673.8	680.4	859.2	803.1	74.9	75.6	95.5	89.2
High + Very High	31.7	29.4	42.0	42.5	4.7	4.3	4.9	5.3
Clouds and shadows coverage	217.6	213.7	304.7	93.3	24.2	23.7	3.4	10.4

Table 4.17 Statistic of the training area for scenario 4

Susceptibility Statuses	Areas in km2			
	February	May	June	September
Very Low	0	0	0	0
Low	9.1	11.9	8.1	8.2
Moderate	57.9	59.6	59.6	51.4
High	31.0	27.4	30.6	37.7
Very High	2.0	1.1	1.7	2.8
High and Very High	33.0	28.5	32.3	40.5
Total of area	49.5	49.5	49.5	49.5



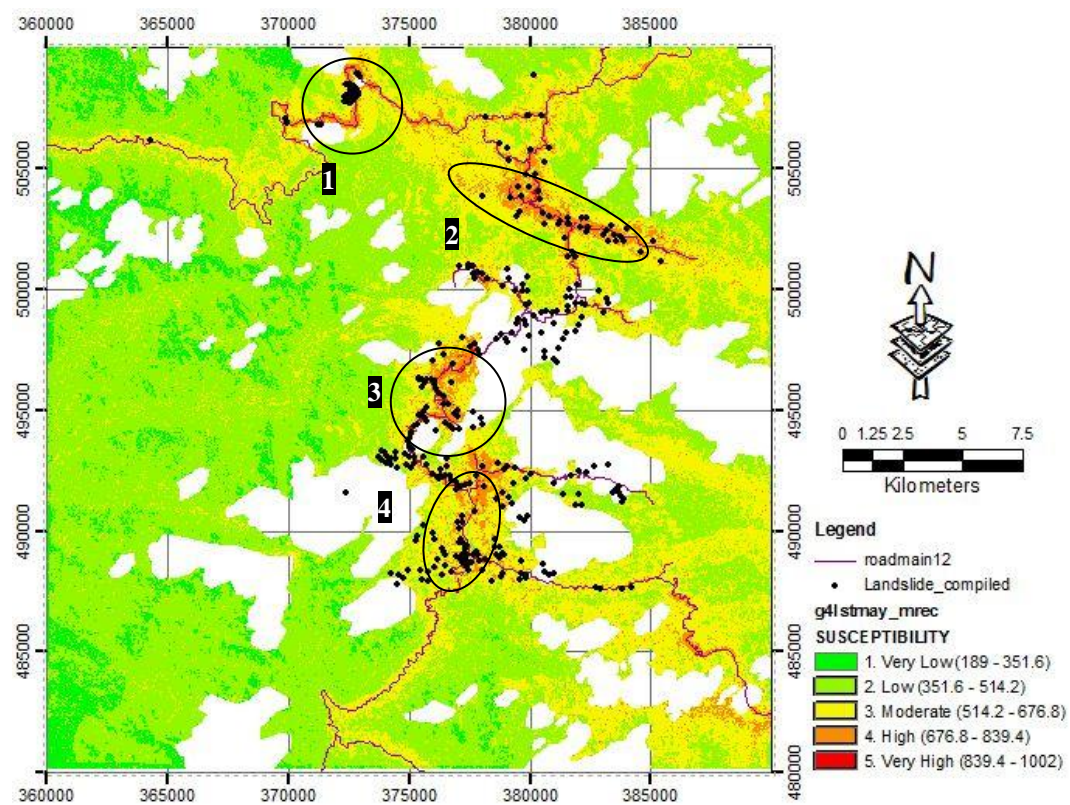
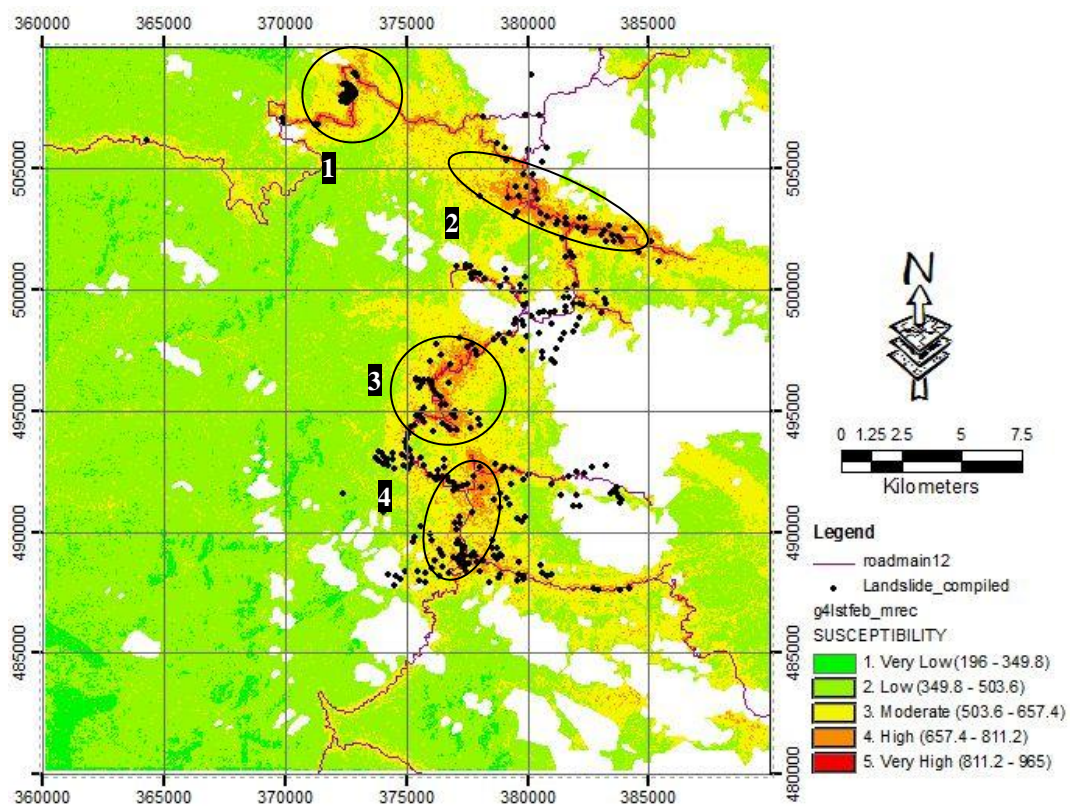


Fig. 4.34 LSMs of Scenario 4: all static factors and LST of February and June



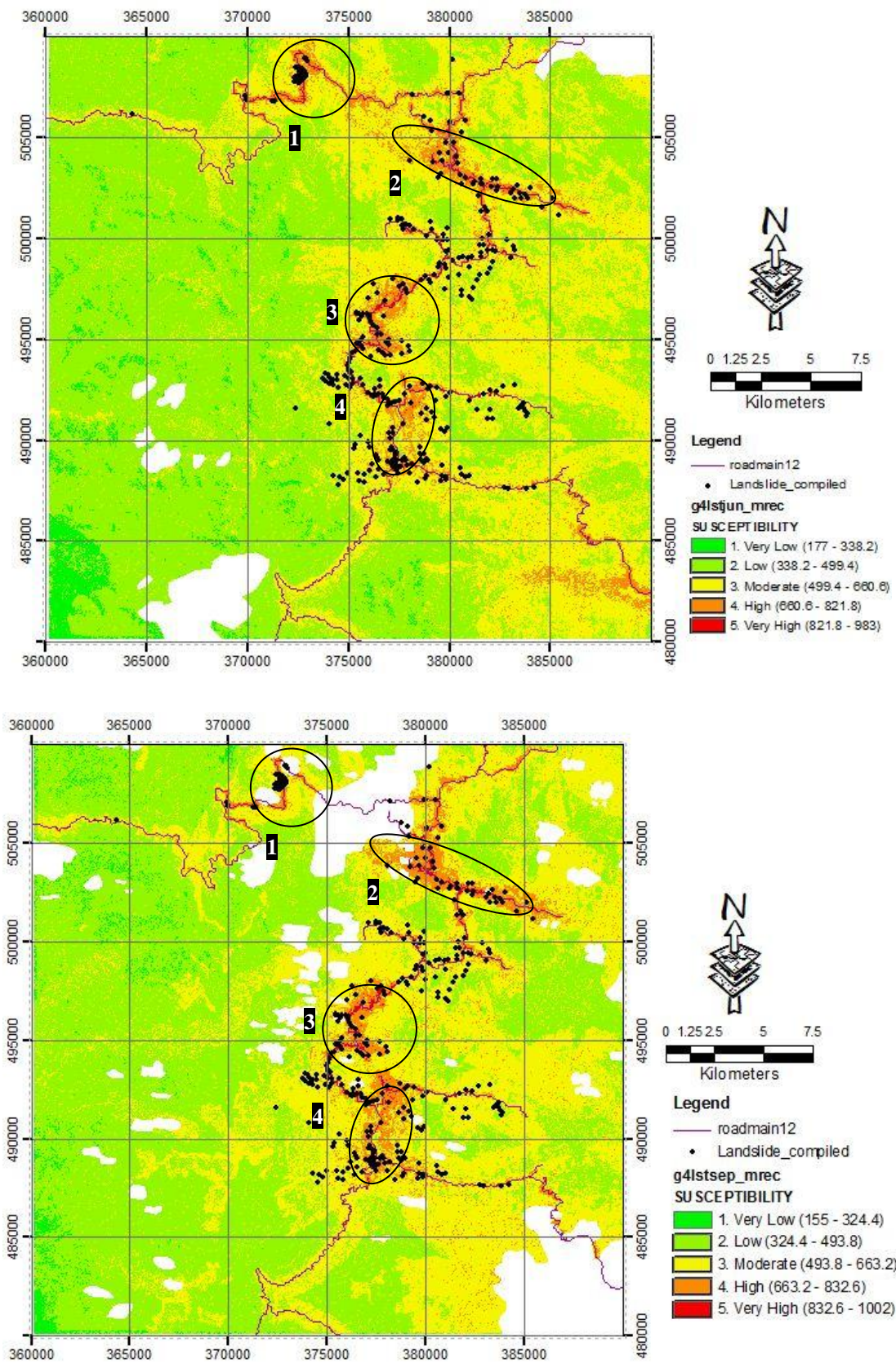


Fig. 4.35 LSMs of Scenario 4: all static factors and LST of June and September

Extraction of the size of a particular area from each map allows evaluation on possibly expansion or shrinkage of particular areas. Special attention was focused on extracted areas with HS and VHS status. The remaining areas are not discussed assuming that these areas are considered as safe locations. Table 4.17 shows that there is change in areas of HS and VHS status from 33 km<sup>2</sup>, 28.5 km<sup>2</sup>, 32.3 km<sup>2</sup>, and 40.5 km<sup>2</sup> respectively on February, May, June, and September. Areas of both status from February to May somehow drop by 15.8% (from 33 km<sup>2</sup> to 28.5 km<sup>2</sup>) although it is considered as rainy season when most landslides usually occurs. Meanwhile, on September, the rainy season, these areas increase significantly by 42.1% when compared to those of May, the rainy season, from 28.5 km<sup>2</sup> to 40.5 km<sup>2</sup>. Fig. 4.36 shows graphs of rainfall at Tanah Rata weather station, the number of validated points, and change in areas with high and very high susceptibility status. It can be said that the first two graphs have similar trend except on May where the area with HS and VHS statuses. Apart of small dissimilarity of the graph, the statistical result of the training areas on Table 4.17 comes from LSMs that have not been measured their accuracies. Map validation is needed to ensure the accuracy of LSMs. Whether or not the change in both areas is due to the introduction of LST in GIS-based LSMs constructed using all static causative factors, this question can only be answered after performing comparison between LSMs produced from scenario 4 and 1. The result is discussed in sub chapter 4.2.5

Table 4.18 Validation of LSMs of scenario 4

Susceptibility Status	Number of validated points				Percentage of validated points			
	Feb	May	Jun	Sep	Feb	May	Jun	Sep
Very Low	0	0	0	0	0.0	0.0	0.0	0.0
Low	9	10	10	0	3.9	4.3	4.3	0.0
Moderate	104	116	107	85	45.2	50.4	46.5	37.0
High	106	99	101	129	46.1	43.0	43.9	56.1
Very High	11	5	12	16	4.8	2.2	5.2	7.0
High + Very High	117	104	113	145	50.9	45.2	49.1	63.0



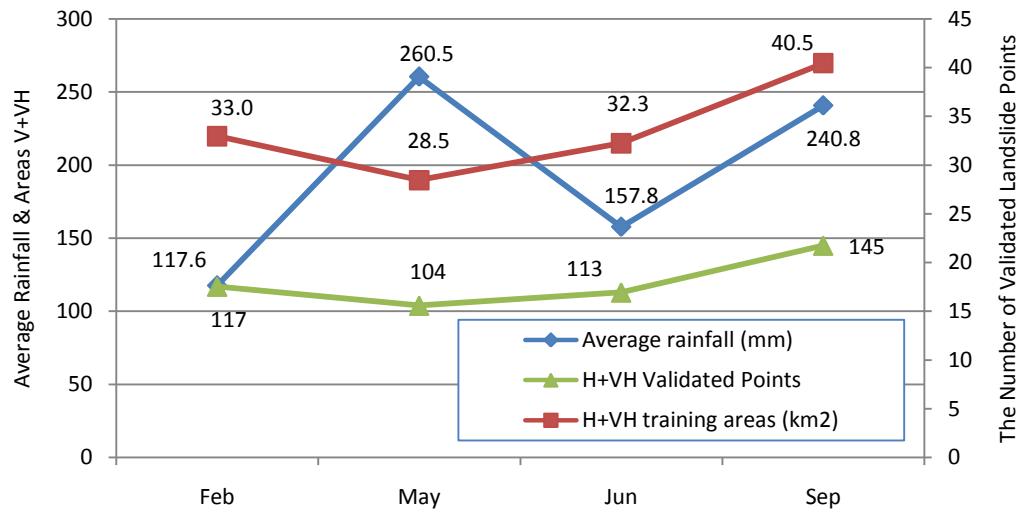


Fig. 4.36 Average rainfall, areas of very high and high susceptibility statuses, and the number of validated points due to change of soil wetness

Similar to previous scenarios, about 230 of landslide locations was used for map validation. Maps validation result is shown in Table 4.18. The LSMs of scenario 4 can predict back landslide locations as having status either HS or VHS as many as 50.9%, 45.2%, 49.1%, and 63.0% respectively for LSM of February, May, June, and September. On the overall, the LSMs can predict back half and slightly above half of the total used landslide locations. Overlay of rainfall graph and validated points shows the similarity of both graphs except data on May (Fig. 4.36). Meanwhile, graphs of validated points and training areas with high and very high susceptibility statuses show a similar trend. Seeing these facts, it is difficult to draw a conclusion in regard to the correlation of rainfall and the number of validated points and areas falling in HS and VHS categories especially the results of May. As the case of scenario 3, this contradictory may originate from utilization of Landsat image dated 31 May 2001 which was not the peak time of rainy season.

The final landslide susceptibility maps of scenario 4 that incorporate multi temporal LST maps have been constructed. Hence, GIS-based landslide susceptibility modeling using scenario 1 to 4 has fulfilled one of the objectives of this research. Evaluation on the importance role of multi temporal LST and other environmental

factors, i.e. NDVI and soil wetness, is another objective to achieve. It is discussed in the following sub chapter.

#### **4.2.5 Static versus Multi Temporal Causative Factors-Based LSMs**

The most important objective of this research is to evaluate whether additional multi temporal environmental factors i.e. NDVI, soil wetness, and LST contribute significant improvement to the accuracy of GIS-based ‘static’ landslide susceptibility model. Improvement means the capability of the models of scenario 2, 3, and 4, to predict back existing landslide locations, as much as possible, as having status of HS and VHS. Prior to do that, LSI-based LSMs of scenario 1, i.e. using 6 and all static factors, should be cropped by using the training areas applied to LSMs of scenarios 2, 3, and 4. Map validation for the cropped areas should also be carried out using the same number of landslide points that is 230 points.

The statistical recapitulation of the training area of LSMs of scenario 1 and maps validation result are shown in Table 4.19. The range and classes interval of each susceptibility status are different. The first reason regarding this problem is due to utilization of ‘weighted sum’ overlay method. Therefore, the more number of landslide causative factors include the higher the value of susceptibility index. The second reason is due to the application of equal interval approach in dividing susceptibility zones. The predicted areas with HS and VHS status of LSI 6 are higher (29.8 of 49.5 km<sup>2</sup>) than those of LSI all factors (15.9 of 49.5 km<sup>2</sup>). HS status dominates the LSM of LSI 6 while MS dominates the LSM of LSI all factors. As proven earlier, the accuracy of LSM of LSI 6 is, again, superior over LSM of LSI all factors in term of the number of validated landslides points as having HS and VHS status. The first model can predict 159 points (69.1 % of the total points) while the latter can only predict 111 points (48.3 % of the total points). These numerical results are very useful for evaluating all LSMs with additional multi temporal environmental factors (NDVI, soil wetness, and LST).

Table 4.19 Statistic of training areas and validated points of LSMs of scenario 1

Susceptibility Status	Training Areas in km2				The Number of Validated Points	
	Range	6 factors	Range	All factors	6 factors	All factors
Very Low	-	0	-	0	0	0
Low	166.6 - 276.2	0.2	304.4 - 453.8	2.9	1	9
Moderate	276.2 - 385.8	19.5	453.8 - 603.2	30.7	70	110
High	385.8 - 495.4	24.3	603.2 - 752.6	15.0	118	103
Very High	495.4 - 605	5.5	752.6 - 902	1.0	41	8
High + Very High		29.8		15.9	159	111

Having all required parameters made available, evaluation of the contribution of additional multi temporal factors can be carried out. The thing to evaluate is the number of HS and VHS points the model can predict. Fig. 4.37 shows the graphical representation of the number of validated points of all scenarios. From the graph, it can be concluded that none of the landslide models produced better accurate LSMs than LSI 6 landslide model. GIS-based LSMs with additional multi temporal environmental factors i.e. NDVI (scenario 2), soil wetness (scenario 3), and LST (scenario 4), are only comparable with LSM of LSI all factors. The discussion regarding this is given below.

Comparison among these graphs shows that it is difficult to directly draw conclusions regarding the contribution of multi temporal factors in to the accuracy of LSMs. On the overall, there are improvements and degradations as well in the accuracy of LSMs as the results of addition of multi temporal NDVI, soil wetness, and LST (see Fig. 4.37). Addition of multi temporal NDVI maps in scenario 1, on the overall, produced the lowest accuracy of LSMs, namely 42.6% (NDVI of February), 37.0% (NDVI of June), and 44.3% (NDVI of September). The accuracy of all these LSMs is below the accuracy of LSI all factors (48.3%). NDVI of May is the exception because it contributes the improvement of the accuracy of the corresponding LSM up to 51.7%. Addition of multi temporal soil wetness maps in scenario 3 produced better accuracy of LSMs than that of scenario 2. It managed comparable accuracies on February and May by 47.4% even though these accuracies are still below that of LSI all factors. Better accuracies of 53.6% and 63.5% were obtained when soil wetness of June and September were added to landslide model of

LSI all factors. On the overall, addition of multi temporal LST factors in scenario 4 produced a better accuracy of LSMs than those of scenario 3 and LSI all factors. LST of February, June, and September increased the accuracy up to 50.9%, 49.1%, and 63.0% respectively. The exception occurred on May when the corresponding LST reduced the accuracy to 45.2 %. Among additional environmental factors, LST appeared to be the most influencing factor to improve the accuracy of LSMs. Soil wetness and NDVI are in the second and third position as landslide influencing factors.

Earlier discussion stated that selection of multi temporal NDVI, soil wetness, and LST was referred to the time of monsoonal rainfall cycle. These data were intended as the replacement of the unavailable high resolution rainfall data. By involving environmental data acquired during rainy and dry seasons, the resulted LSMs are expected to reflect rainfall cycle. Among all additional environmental factors, only addition of NDVI maps can result in various accuracies that resemble the graph of rainfall (Figure 4.29 and Figure 4.34). LSMs of scenario 2 described that during rainy seasons, the possible dangerous areas increase (areas with HS and VHS status), and during dry season, these areas decrease.

#### **4.3 Evaluation on Significance of Landslide Causative Factors**

Knowing that inclusion of more causative factors cannot guarantee the accuracy of the resulted landslide susceptibility maps, investigation on the significant role of each causative factor was carried out in order to sort out the significant factors from the insignificant factors. The investigations were carried out in two ways as follows:

1. Step by step inclusion of causative factors.
2. Accumulative inclusion of causative factors.

The detail of these approaches is discussed in their corresponding part. All causative factors including static or multi temporal causative factors were evaluated. The evaluation was limited for the data acquired on September, the second rainy season. As discussed earlier, this season was proven to be superior in producing the accurate LSMs. For this purpose, a training area delineating areas free of clouds and the

associated shadows was created. The training area of September is a bit wider than the one used for evaluating multi temporal factors for all seasons (Fig. 4.38). A total number of 345 landslide points that are not covered by clouds/shadows was used for the assessment of landslide causative factors. All landslide causative factors were cropped to conform to the training area to allow map by map comparison. Evaluation was based on the number of validated existing landslide points that falls in HS and VHS status the models can predict.

#### **4.3.1 One by One Inclusion of Causative Factors**

Slope, land use and geology (lithology) maps are landslide causative factors commonly used for constructing landslide susceptibility/hazard map. These three factors were used as basic factors/maps for evaluating the remaining factors. The order of causative factors added to three basic maps for constructing GIS-based landslide susceptibility map is show in Fig. 4.39. It begins with the addition of soil, distance from road (d2rd), distance from lineament (d2ln), distance from riverl/lake (d2rvlk), curvature (curv), elevation (elev), slope aspect (sasp), soil wetness (wet), Normalized Different Vegetation Index (NDVI), and Land Surface Temperature (LST). The additional environmental factors, i.e. NDVI, soil wetness, and LST, are only data of September. The order of inclusion of a particular factor does not reflect the significant role of the corresponding factor. The significant role remains unknown until the number of validated point the additional factor can predict determines the order of its significance. LSI was used for weighting system while weighted sum was used for overlay method. The final LSM was constructed by summing up pixel-based LSI values of all used factors. The number of validated existing landslide points that fall in HS and VHS status due to the addition of a particular causative factor is assumed to be the indicator of its significant contribution to LSM.

The variation of the number of validated points from one by one inclusion of causative factors is shown in Fig. 4.39. This figure also contains the percentage of increase or decrease when a particular causative factor is added to the basic factors. For example, addition of soil map into the landslide susceptibility model using the basic factors increases the number of validated points by 40% (from 98 to 137

points). Meanwhile, addition of slope aspect map decreases the number of validated points by -3% (from 98 to 95 points). The same case happens when distance from lineament map is added to basic maps. The complete result is presented in Table 4.20.

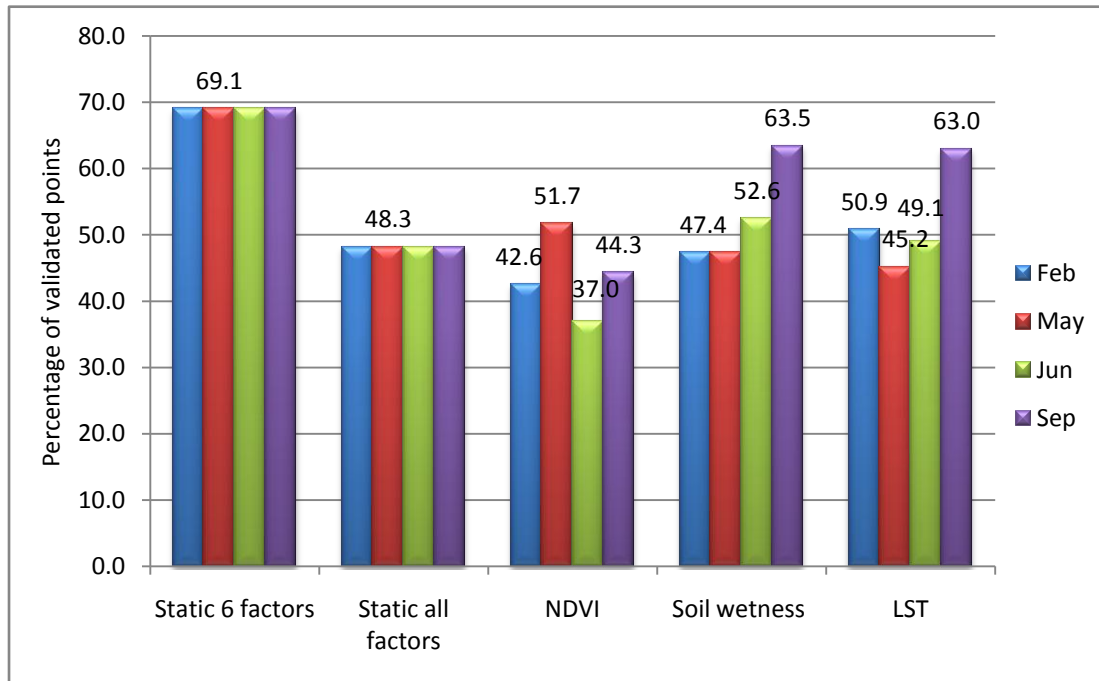


Fig. 4.37 Comparison of the percentage of validated points from LSMs of all scenarios

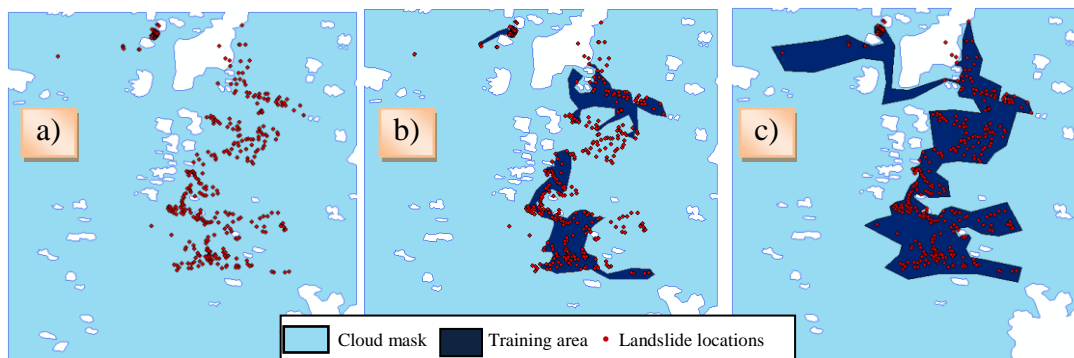


Fig.4. 38 a) clouds/shadows coverage on September and landslide sites distribution, b) the training area for all seasons, and c) the training area for September

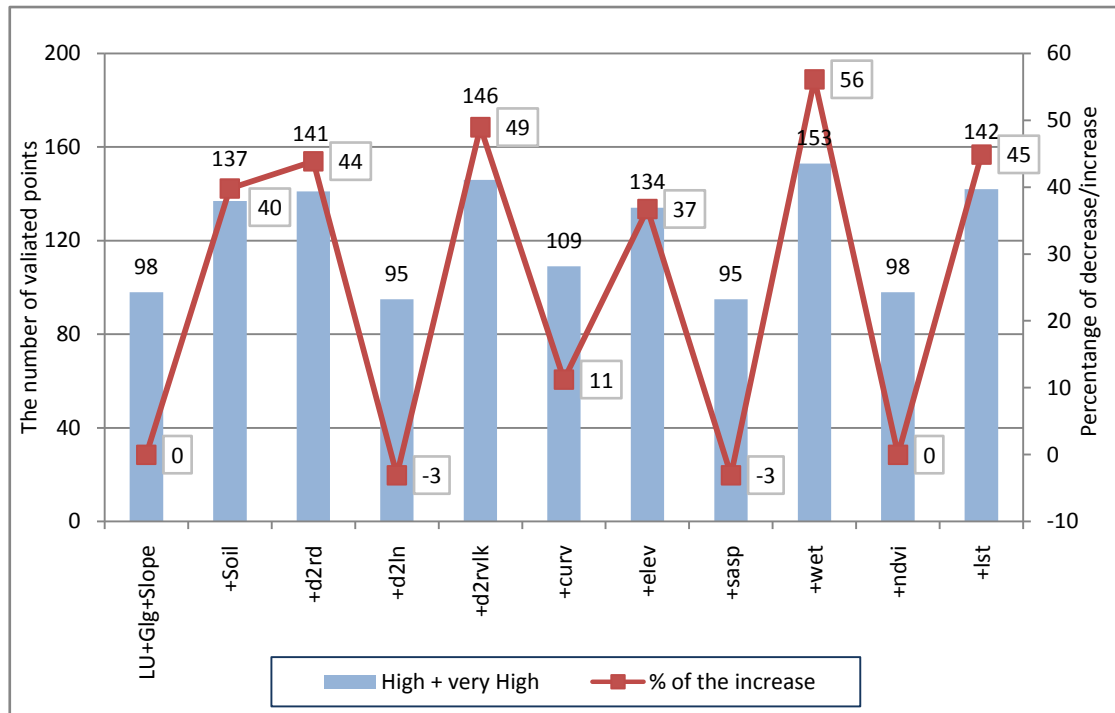


Fig. 4.39 The number of validated points from one by one inclusion of causative factors and the percentage of increase/decrease

Based on the number of validated landslide sites, all involved causative factors are sort out (Table 4.20). Since land use, slope, and geology factors are set as the main factors, they are assumed to be the most significant factors. The order of causative factors, from very significant to less significant statuses, are soil wetness, distance from river/lake, LST, distance from road, soil, elevation, and curvature. There are three insignificant factors identified from this process. Addition of these factors either results in the same number of validated points as the case of NDVI or decreases it as the cases of distance from lineament and slope aspect. The decrease of the accuracy of LSMs due to the inclusion of NDVI has been discussed in previous sub chapter. Slope aspect has been suspected to be insignificant factor as discussed in section 4.1.5. The distribution of landslide/slope failure locations are almost evenly distributed to slopes facing all wind directions.

Table 4.20 The order of significance of causative factors

No.	Order of Significant Causative Factors	Percentage of Increase	The order of significance
0	Land use, slope, geology	Not available	1,2,3
1	Soil wetness	56	4
2	Distance from river/lake	49	5
3	LST	45	6
4	Distance from road	44	7
5	Soil	40	8
6	Elevation	37	9
7	Curvature	11	10
8	Normalize Different Vegetation Index	0	11
9	Distance to lineament	-3	11
10	Slope Aspect	-3	12

### 4.3.2 Accumulative Inclusion of Causative Factors

In this approach, GIS-based landslide susceptibility map was first constructed using the same basic maps as the previous approach namely, land use, slope, and geology maps. The latter was then replaced by soil map. The method for constructing the final LSM is the same as the previous approach. The first data set (with geology map) resulted in 98 validated points while the second dataset (with soil map) resulted in 177 validated points which are higher than the previous result (Table 4.21). It suggests that soil is more significant than geology. The next process employed soil map as the replacement of geology. Table 4.21 shows the overall scenarios of dataset and results of accumulative inclusion of causative factors. Accumulative inclusion as presented on Table 4.21 is explained as follows, dataset 3 consists of dataset 2 with additional geology factor for constructing LSM; dataset 4 consists of data 3; dataset 5 consists of dataset 4, and so on. Addition of geology factor to dataset 2 decreases the number of validated points by 40 points. Meanwhile, addition of distance from river/lake map to dataset 3 increase the accuracy of the model by 35 points. The overall increase or decrease indicators are presented on Table 4.21. Landslide causative factors that tend to decrease the accuracy of resulted LSMs are slope aspect, curvature, LST, and geology. Slope aspect is again identified as insignificant factor. Investigator s disagreed about the significant role of curvature as discussed in 4.1.6



as well as the significant role of LST as discussed in sub chapter 4.1.13 This experiment identified geology as an insignificant factor (Table 4.21).

Table 4.21 Accumulative inclusions of causative factors and the order of significance factors

Dataset	Causative Factors	The number of validated points	Increase / Decrease		The order of significance
Dataset 1	LU, slope, geology	98	-	-	-
Dataset 2	LU, slope, soil	177	79	↑	1,2,3
Dataset 3	Dataset 2 + geology	137	-40	↓	13
Dataset 4	Dataset 3 + distance from river/lake	172	35	↑	6
Dataset 5	Dataset 4 + distance from road	196	24	↑	8
Dataset 6	Dataset 5 + elevation	252	56	↑	4
Dataset 7	Dataset 6 + distance from lineament	284	32	↑	7
Dataset 8	Dataset 7 + slope aspect	283	-1	↓	10
Dataset 9	Dataset 8 + curvature	278	-5	↓	11
Dataset 10	Dataset 9 + NDVI	292	14	↑	9
Dataset 11	Dataset 10 + soil wetness	340	48	↑	5
Dataset 12	Dataset 11 + land surface temperature	303	-37	↓	12

The order of significant landslide causative factors is sort out based on significant increase or decrease of the number of validated points. Since land use, slope, and soil are selected as the basic factors, their significant role is assumed to stand as the first, second, and third place. Following these factors are elevation, soil wetness, distance from river/lake, distance from lineament, distance from road, and NDVI. Slope aspect, curvature, LST, and geology are considered as insignificant factors.

#### 4.4 GIS-Based LSM Constructed Using Selected Causative Factors

As discussed earlier, the number of causative factors included in constructing LSM does not guarantee the accuracy of the produced LSM. In addition, two attempts have been made to sort out significance causative factors from the available factors. Using these significant factors, GIS-based LSMs were constructed. For comparison purpose,

LSM of LSI 6 was set as the reference map. In addition, two dataset containing selected significant factors were prepared. Each dataset contains 6 factors to allow a fair comparison with the reference map. Six significant factors of dataset from one by one inclusion of causative factors are land use, slope, geology, soil wetness, distance from river/lake, and LST. Six factors of dataset from accumulative inclusion of causative factors are land use, slope, soil wetness, distance to river/lake, soil, and elevation. Both dataset have the same 4 significant factors in common namely, land use land cover, slope, distance from river/lake, and soil wetness.

The final LSMs of selected significant factors were constructed using weighted sum overlay method. The number of validated existing landslide points that fall in HS and VHS status is compared to those of other scenarios (Fig. 4.40). The accuracy of LSM of both dataset is still below that of LSI 6 that is able to validate 159 points (69.1%). One by one inclusion approach validated 124 landslide points (53.9%) while accumulative inclusion approach validated 145 points (63.0%). Significant factors of accumulative inclusion approach produced better validation result than those of one by one inclusion approach. Apart from these results, dataset of both approaches produce more accurate LSMs than that resulted from LSI all factors (48.3%). Again, it suggests that inclusion of all (or more) factors in constructing GIS-based LSM does not guarantee the accuracy of the produced LSMs. Otherwise, inclusion of limited number of selected significant factors may produce more accurate LSMs. Comparison between the accuracy of both approaches and that of GIS-based LSMs that involves multi temporal environmental factors, i.e. NDVI, soil wetness, and LST, reveals that the first maps are better than the latter maps in term of the number of validated points. Only additional soil wetness and LST of November into LSM of scenario1 with 6 static factors can balance the accuracy of LSMs of both approaches.

The different between both approaches in the number of validated data may be due to simplicity of the approaches in evaluating the significance of each factor. Of advanced methods for establishing the relationship between causative factors and landslide locations are linear regression as described in Zhou, et al. [51] and logistic regression as applied by Lee and Sambath [46]. Such methods require ArcGRID workstation with special extension of multivariate toolbox that is regression analysis.

The software was unavailable during the research work. In addition, assumption that three basic layers automatically have significant roles may not be entirely correct even though they are commonly used by investigators in constructing LSM.

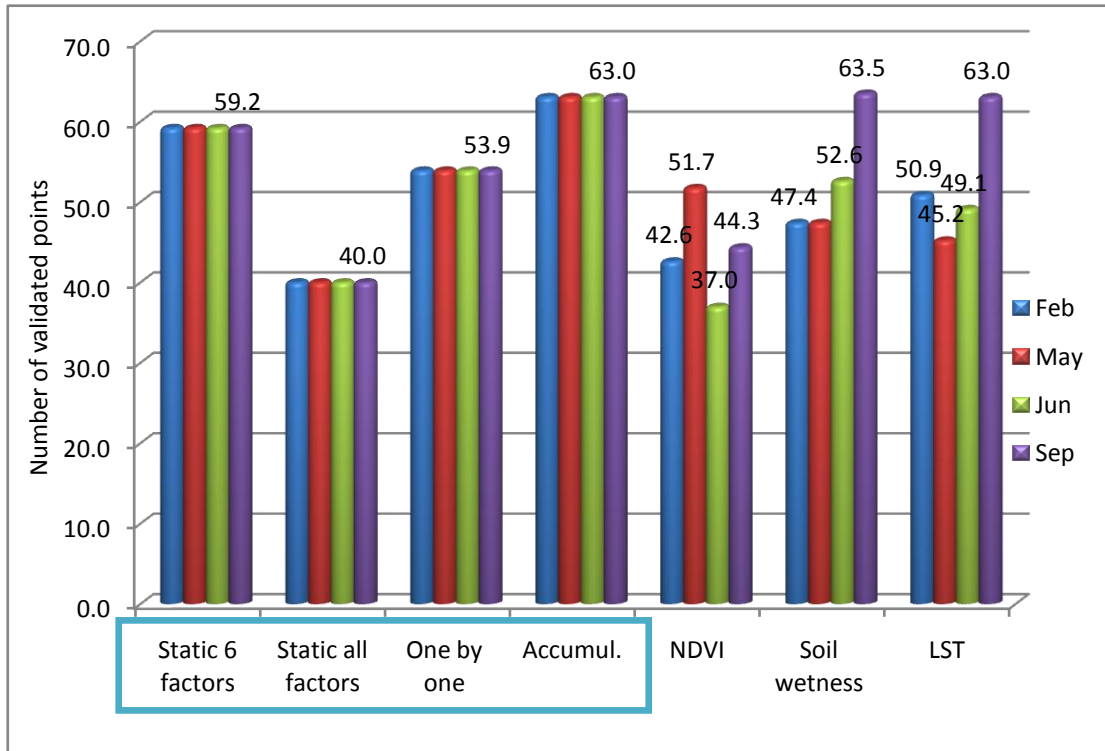


Fig. 4.40 Comparison of GIS-based LSMs using selected significant factors with those of all scenarios

Evaluation on the significance of each causative factor, at least, can show that some factors are significant and the others are insignificant. A group of selected causative factors has been proven to be superior in producing more accurate LSM than that resulted from a group of non-selected or all causative factors. For future construction of LSM, one is suggested to involve either a set of 6 static causative factors used in scenario 1 or a set of 6 factors used in accumulative inclusion method.

#### 4.5 Test of Applicability of The developed Landslide Model

The landslide model developed from the study area has shown a good agreement with landslide occurrences data especially the model involving 6 factors (LSI 6). To test

the applicability of the developed model, Penang Island was selected as the test site because this place is considered as landslide prone area and has required data for modeling landslide susceptibility. This experiment is intended to investigate whether a landslide susceptibility model developed from a particular area can be applied to another area and to investigate the applicability of bivariate statistical based-weighting system to the test site.

Application of the landslide susceptibility model of Cameron Highlands to Penang Island requires several following procedures to carry out:

1. Selecting causative factors of Penang that are considered as significant factors identified in Cameron Highlands and applying necessary modifications on classes of causative factors,
2. Assigning weight values to classes of selected factors,
3. Constructing the final LSM of Penang Island using Cameron Highlands landslide model,
4. Constructing a final LSM of Penang Island landslide susceptibility model developed from landslide attributes of Penang Island. This is intended for comparing the accuracy of both LSMs of Penang,
5. Evaluating the applicability of the landslide susceptibility model.

For testing the applicability of the model, six significant landslide causative factors were selected either from the result of one by one or accumulative inclusion processes. The selected factors are land use land cover, slope, distance from river/lake and soil wetness. LST was not selected due to their less significant issues. Soil map of Penang Island was not included because it contains wider variety of soil types, 5 types, than that of Cameron Highlands, 3 types, causing difficulties in judging the soil strength. Elevation and geology were added in the landslide susceptibility model.

Before sending all factors into overlay operation, all classes of every causative factor were assigned the same LSI-based weight values as suggested by Liao [47]. This is the meaning of test of applicability of the developed model into different area. Some modifications of dataset of Penang Island are required to suit dataset of Cameron Highlands. Paddy field coverage was grouped as crop land for land use

factor. Wetland was grouped as river/lake. The lithology type of both places is almost similar except that there is no schist type in Penang Island. Elevation range of Cameron Highlands is 80 – 2100 m while that of Penang Island is 0 – 820 meter. The latter was reclassified into two classes, 0 – 540.96 m and 540.96 – 820 m, to suit elevation intervals of Cameron Highlands. The other factors, soil wetness, slope, and distance from river, have almost similar intervals to those of Cameron Highlands. Therefore, there are no more modifications required. Summary of all causative factors along with LSI-based weight values for their corresponding classes are presented Table 4.22. The final LSM of Penang Island was constructed using these weight values of Cameron Highlands.

Table 4.22 LSI of Cameron Highlands applied to dataset of Penang Island

Landslide Factors	Sub-Categories	Weight Values (CH)	Landslide Factors	Sub-Categories	Weight Values (CH)
<b>Land Use</b>	Crop land	11	<b>Soil wetness</b>	0 - 22	100
	Forest	6		22 - 74	7
	Urban, Built up	60		74 - 134	3
	River/lake	0		134 - 193	2
<b>Geology</b>	Granite	15		193 - 245	7
	sedimentary rocks	31		245 - 254	0
	Alluvium	38	<b>Distance from river/lake</b>	0 - 548.9	100
<b>Slope</b>	0 - 7.8	100		548.9 - 1200.7	46
	7.8 - 19.3	57		1200.7 - 1732.5	38
	19.3 - 27.3	51		1732.5 - 2521.5	36
	27.3 - 36.3	52		2521.5 - 4391.2	42
	36.3 - 51	79		4391.2 - 9037.4	0
	51- 89.6	0	<b>Elevation (m)</b>	0 - 540.9	0
				540.9 - 820	16

In order to provide a comparison LSM of Penang Island, another LSM was constructed using LSI derived from landslide attributes of available causative factors. A number of 434 landslide/slope failure locations have been recorded by ARSM through interpretation of aerial photograph and field investigation as reported by Lee and Talib [55]. Crossing between landslide map of Penang Island and all causative factors was carried out in order to compute LSI and LSI-based weight values (Table 4.23). Unlike the previous dataset, elevation factor now have 5 classes. The weight

values of Cameron Highland landslide susceptibility and Penang Island assigned to all classes are totally different. Using these weight values, another final LSM of Penang Island was constructed.

Table 4.23 Rating weight system of Penang Island

Landslide Factors	Sub-Categories	Number of Landslide	Landslide Areas (m2)	Area of Each Sub Category (m2)	LSI	Weight Values
Land Use	Crop land	233	209700	125142300	16.8	100.0
	Forest	92	82800	76944600	10.8	64.2
	Urban, Built up	102	91800	87307200	10.5	62.7
	River/lake	5	4500	6096600	7.4	44.0
Geology	Granite	352	316800	33001200	96.0	93.6
	sedimentary rocks	11	9900	964800	102.6	100.0
	Alluvium	71	63900	12708900	50.3	49.0
Elevation	0 - 122.1	236	212400	180128700	11.8	48.2
	122.1 - 246.5	128	115200	47133000	24.4	100.0
	246.5 - 370.9	48	43200	29649600	14.6	59.6
	370.9 - 495.4	13	11700	18463500	6.3	25.9
	495.4 - 619.8	7	6300	12980700	4.9	19.9
	619.8 - 820	0	0	7118100	0.0	0.0
Slope	0 - 7.5	0	0	146165400	0.0	0.0
	7.5 - 15.3	101	90900	20234700	44.9	100.0
	15.3 - 23.2	95	85500	54296100	15.7	35.1
	23.2 - 31.1	143	128700	47116800	27.3	60.8
	31.1 - 39.0	81	72900	19908900	36.6	81.5
	39.0 - 46.9	12	10800	5764500	18.7	41.7
	46.9 - 88.9	0	0	1987200	0.0	0.0
Soil Wetness	0 - 51	60	54000	50058000	10.8	75.9
	51 - 102	22	19800	15537600	12.7	89.7
	102 - 153	26	23400	19741500	11.9	83.4
	153 - 204	91	81900	62583300	13.1	92.1
	204 - 255	233	209700	147570300	14.2	100.0
Distance from River/Lake (m)	0 - 721.5	123	110700	104470200	10.6	39.2
	721.5 - 1335.5	130	117000	76409100	15.3	56.6
	1335.5 - 2251.8	107	96300	72552600	13.3	49.1
	2251.8 - 3804.1	48	43200	33401700	12.9	47.8
	3804.1 - 5596.8	26	23400	8657100	27.0	100.0

The final LSMs of Penang Island constructed from both CH model and Penang model are shown in Fig. 4.38. Visually interpreted, LSM of Penang Island constructed by using Cameron Highlands model shows that the distribution of areas

of HS and VHS concentrated mostly at urban areas, the low land or flat areas. These distributions are out of the distribution of landslide/slope failure locations. Meanwhile, LSM of Penang Island developed using Penang model shows agreements in term of distribution of HS and VHS areas and location of landslide/slope failures. LSM developed using native landslide attributes is better than using those of different area. Statistical measures of the accuracy of both maps are presented in Fig. 4.38. The first model can predict only 10.1% of recorded landslide/slope failures (434 locations) to fall in HS and VHS statuses. The second model provides better prediction in which 54.4% fell into categories of HS and VHS.

The final LSMs of Penang Island constructed from both CH model and Penang models are shown in Figure 4.38. Visually interpreted, LSM of Penang Island constructed by using Cameron Highlands model shows that the distribution of areas of HS and VHS concentrated mostly at urban areas, the low land or flat areas. These distributions are out of the distribution of landslide/slope failure locations. Meanwhile, LSM of Penang Island developed using Penang model shows agreements in term of distribution of HS and VHS areas and location of landslide/slope failures. LSM developed using native landslide attributes is better than using those of different area. Statistical measures of the accuracy of both maps are presented in Table 4.38. The first model can predict only 10.1% (44 locations) of recorded landslide/slope failures (434 locations) to fall in HS and VHS statuses. The second model provides better prediction in which 54.4% (236 locations) fell into categories of HS and VHS.

The failure of applicability test may be caused by several factors. The geographical setting is mostly different. Penang Island is not highlands areas as Cameron Highlands. It is an island surrounded by sea water so that the elevation range starts from 0 m until 820 m. Therefore, it may not be appropriate to call Penang Island as 'highlands areas' as Cameron Highlands. The consequences are NDVI, soil wetness, and LST may be different. Other factors such as soil types and slope ranges are different. These factors could contribute the failure of applicability of Cameron Highland landslide susceptibility model to Penang Island landslide case.

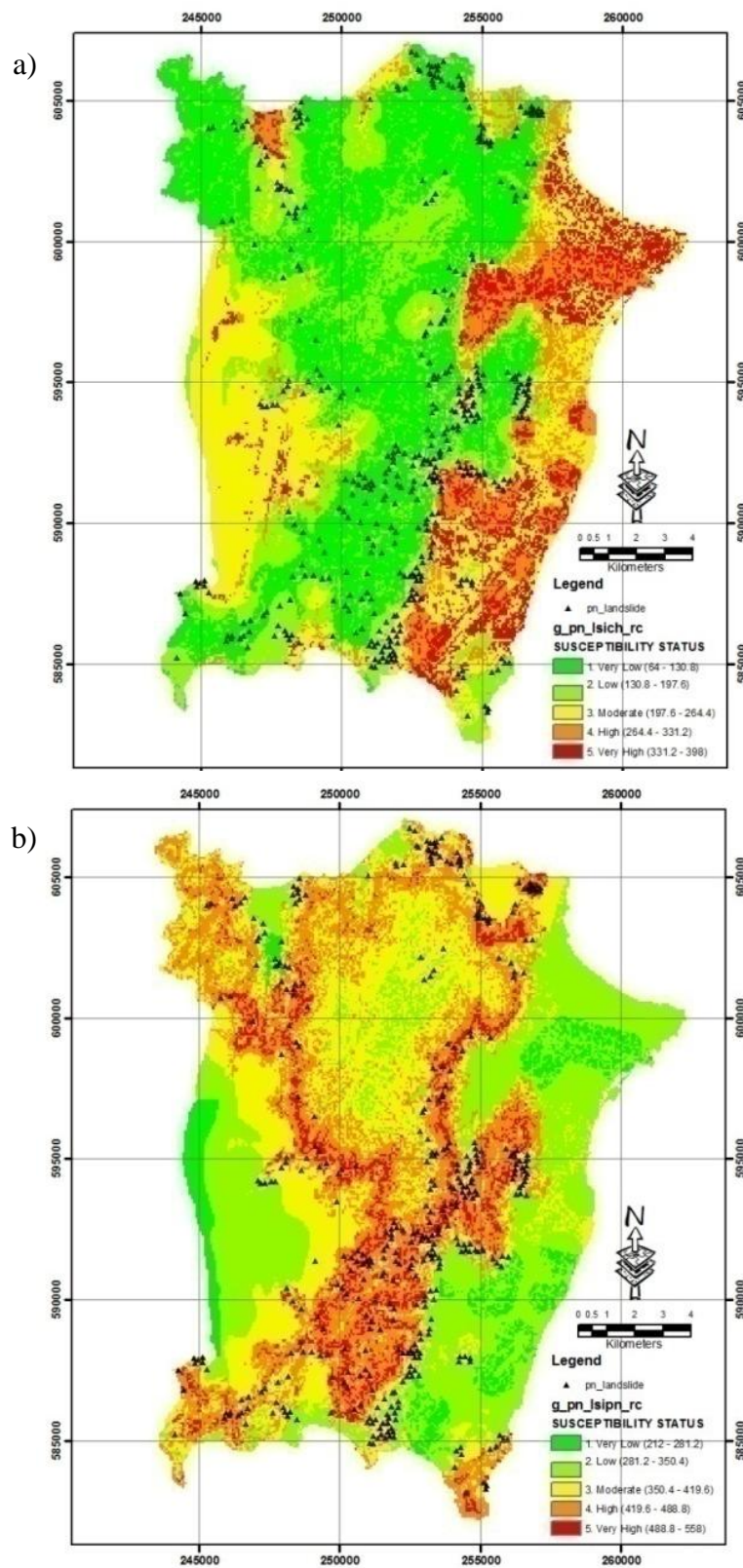


Fig. 4.41 Final LSM of Penang Island using: a) CH model, and b) Penang model



This result confirms the drawback of statistical method as explained by Carrara, et al. [50]. Since statistical method is considered as data-driven method, a landslide susceptibility model built up for one region cannot readily be extrapolated/applied to the neighboring areas. Slope assessment developed from place cannot be applied to other places as stated by local landslide expert, Jamaluddin, et al. [227].

Table 4.24 Results of test of applicability of the landslide susceptibility model

GIS Penang with LSI of Cameron Highlands					
Susceptibility Status	Map Statistic			Validation	
	Range	Pixels	Areas	Range	Pixels
Very Low	64 - 130.8	17606	15845400	50.8 - 130.8	188
Low	130.8 - 197.6	12386	11147400	130.8 - 197.6	131
Moderate	197.6 - 264.4	12226	11003400	197.6 - 264.4	70
High	264.4 - 331.2	5036	4532400	264.4 - 331.2	35
Very High	331.2 - 398	4533	4079700	331.2 - 375	9
				HS & VHS	44
GIS Penang with LSI of Penang					
Susceptibility Status	Map Statistic			Validation	
	Range	Pixels	Areas	Range	Pixels
Very Low	212 - 281.2	2655	2389500	-	-
Low	281.2 - 350.4	15943	14348700	269.3 - 350.4	52
Moderate	350.4 - 419.6	16203	14582700	350.4 - 419.6	145
High	419.6 - 488.8	13536	12182400	419.6 - 488.8	166
Very High	488.8 - 558	3450	3105000	488.8 - 558	70
				HS & VHS	236

## 4.6 Discussion

There are some important results obtained from this research. Bivariate statistical-based weighting system produced more accurate LSMs than LHEF/non-statistical-based weighting one. The research shows that selected significant factors were proven to produce better accurate LSMs. Expansion and contraction of areas susceptible to landslide due to rainfall cycle can be identified using developed landslide susceptibility model. Addition of multi temporal NDVI best described this phenomenon. On the overall, addition of multi temporal factors cannot automatically increase the accuracy of LSMs especially those maps of rainy seasons. This research also shows LSI values developed from Cameron Highlands cannot be extrapolated to

the test site, Penang Island. However, application of bivariate statistical-based weighting system resulted in a good agreement between landslide map of Penang Island and the corresponding developed model. Although the developed models cannot be applied elsewhere, the average accuracy of LSMs produced by the developed models with inclusion of multi temporal factors is 49.1%. This accuracy can be improved if only selected significant factors are involved and each factor is assigned different weight value. In addition, LSI 6 model has predicted the area of the latest landslide event in Sungai Ruil Orang Asli village, Brinchang, Tanah Rata, Cameron Highlands, August 7th, 2011, as having status of HS to VHS as shown in Fig. 4.42. The remaining models have predicted this location as having MS to HS.

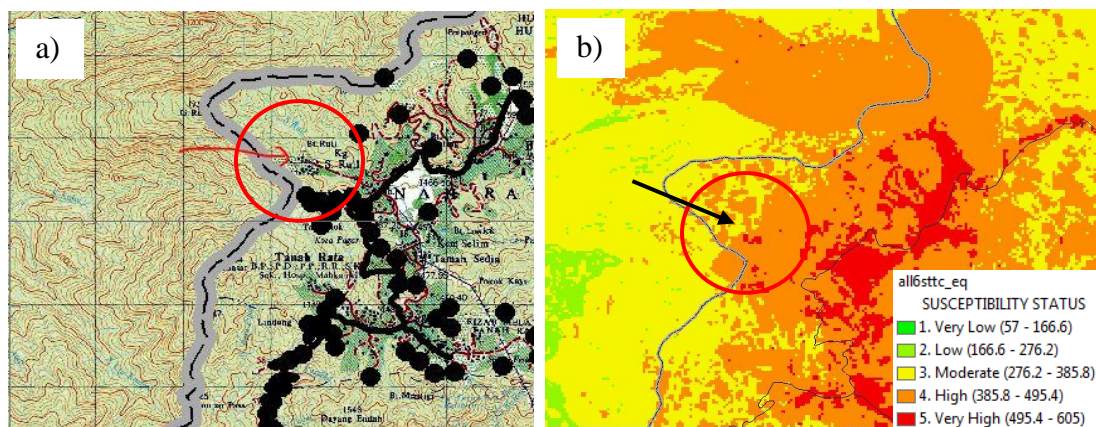


Fig. 4.42 a) Latest landslide location on topographic map, b) the corresponding LSM

A part of achievements obtained from this research as mentioned previously, this research also introduced some limitations. The spatial relationship between landslide map and landslide causative factors derived from bivariate statistical approach was somewhat contradictive with geotechnical point of view. For example, a slope class of  $0-7.8^0$  is considered as a secure slope according to geotechnical perspective. Using bivariate statistical method, this slope is categorized as having the highest LSI value meaning that this is the most dangerous slope (section 4.1.4). The same situation exists in spatial relationship between soil wetness maps and landslide occurrences. This is the first limitation of this research. A combination of bivariate statistical and geotechnical methods in assigning weight values may increase the accuracy of LSMs.

Inclusion of multi temporal factors cannot guarantee to increase the accuracy of LSMs. There are increase and decrease in accuracy of LMSs. There are factors that may be responsible to this problem. Firstly, the selected Landsat images that did not exactly coincide with required peak periods of the rainy and dry seasons may express different condition of NDVI, soil wetness and LST. Secondly, temporal factors were derived from Equation s 2.16-2.19 for LST, Equation 2.27 for NDVI and Equation 2.28 for soil wetness. These equations resulted in NDVI, soil wetness and LST maps. These maps were included in producing LSMs without passing any ground truthing procedures. This procedure was not conducted in this research due to fund and time limitations. By conducting ground truthing or calibration of temporal factors, appropriate weight values can be assigned to these factors, more accurate LSMs can be expected, and credibility of research findings can be strengthened. The third, there may be insignificant factors involved in developing landslide susceptibility model. c

#### **4.7 Chapter Summary**

Modeling landslide susceptibility of Cameron Highlands areas which includes different conditions of environmental factors has been finalized through several comprehensive steps. Several LSM have been produced as the outcome of landslide susceptibility modeling. The summary of the steps is presented in the following passages.

The modeling landslide susceptibility was begun with deriving various rating weight systems. Three rating weight systems were evaluated namely Anbalagan LHEF, LFI, and LSI weighting system. LHEF, a non statistical approach, and LSI, a statistical approach, were used for generating weighting values. The modeling involved 10 ‘static’ causative factors, i.e. land use land cover, lithology, elevation, slope, slope aspect, curvature, distance from road, distance from lineament, distance from river/lake, and soil. The modeling also involved multi temporal factors called ‘dynamic’ factors that are NDVI, soil wetness and LST of February, May, June, and September. Four scenarios for constructing GIS-based LSMs were established.

Scenario 1 showed that statistical weighting system provided more accurate LSM than non statistical one. The results also showed that inclusion more causative factors could not guarantee to produce an accurate LSM. On the contrary, six static factors produced more accurate LSM. Places identified as dangerous zones, i.e. having HS and VHS statuses, are post landslide site at Pos Selim, Kampung Raja and urban areas at Kampong Kuala Terla, urban areas at Tanah Rata and Ringlet. Scenario 2 produced LSMs representing the influence of different conditions of NDVI maps. Scenario 3 produced LSMs representing the influence of different conditions of soil wetness maps. Scenario 4 produced LSMs representing the influence of different conditions of LST maps. Accuracy of LSMs of these three scenarios was below the one of LSI 6 static factors of scenario 1. Only addition environmental data acquired on September contributed comparable accuracy of LSMs to that of scenario 1. Expected expansion or depreciation of dangerous zones appeared only on LSMs of scenario 2 as the contribution of monsoonal NDVI conditions. The trend of expansion and depreciation resembles rainfall trend.

Investigation on the significant of landslide causative factors showed that land use land cover, slope, soil wetness, and distance from river are among the significant factors. Following these are soil, elevation, geology, and LST. These factors were identified during the processes namely one by one and accumulative inclusion of causative factors. Among the less significant of insignificant factors are slope aspect, NDVI, and distance from lineament. LSM derived using selected causative factors produced a fairly comparable accuracy but its accuracy is still below the accuracy of LSI 6 static factors.

Landslide model developed from Cameron Highlands is not applicable to the test site, Penang Island. The failure of applicability test is not caused by the low accuracy of the developed model. This is due to the nature of bivariate statistical method which is data-driven method. Therefore, the developed model cannot be extrapolated to other places. Meanwhile, the way weight values derived using bivariate statistical approach can be applied to Penang Island.

## CHAPTER 5

### CONCLUSIONS AND RECOMMENDATIONS

#### **5.0 Overview**

The study has investigated the effect of different conditions of environmental factors in landslide susceptibility model developed for Cameron Highlands, Malaysia. This is the main objective of this research. The study selected the appropriate weighting system, evaluated the landslide susceptibility models and maps, assessed the role of multi temporal factors, investigated the significant role of landslide causative factors, and tested the applicability of the developed landslide model. The followings are the concluding remarks.

#### **5.1 Conclusions**

Based on the results/findings during this study, it is now possible to draw the following conclusions:

1. Based on the result of scenario 1 landslide susceptibility modeling, statistical based-weighting system (LSI) was proven to be a better one than that of non-statistical approach (LHEF) in term of producing more accurate LSM. LSI 6 managed 69.1% of the total number of landslide/slope failure locations, 358. Meanwhile, LHEF 6 managed only 20.4% of the total number of landslide/slope failure locations.
2. The final LSMs have been produced from scenario 1, 2, 3, and 4 with various accuracies. Various accuracies of LSMs were resulted from validation process and summarized in Table 5.1. The accuracy is presented in percentage (%) representing the capability of the developed model in predicting back existing

landslide locations as having HS and VHS. The overall accuracy of LSMs as result of addition of multi temporal factors is 49.1%. However, this accuracy is still below the accuracy of LSM resulted from six selected static factors (LSI 6).

3. On the overall, addition of multi temporal environmental factors cannot automatically increase the accuracy of LSMs especially those LSMs produced using additional multi temporal factors acquired during rainy seasons. Addition of these factors caused increase and decrease in accuracy of LSMs. In general, multi temporal LST contributes more accurate LSMs, followed by multi temporal soil wetness, and then NDVI. Addition of multi temporal NDVI tends to reduce the accuracy of LSMs. Multi temporal soil wetness resulted in better accuracy of LSMs than NDVI.

Table 5.1 Summary of accuracy of LSMs (in %)

	February (Dry)	May (Rainy)	June (Dry)	September (Rainy)
Scenario 1- 6 factors	69.1			
Scenario 1-10 factors	48.3			
Scenario 2 (NDVI)	42.6	51.7	37.0	44.3
Scenario 3 (soil wet.)	47.4	47.4	52.6	63.5
Scenario 4 (LST)	50.9	45.2	49.1	63.0

4. Rise and fall of the accuracy of LSMs due to inclusion of multi temporal environmental factors allows identification of expansions or contraction of areas susceptible to landslide (HS and VHS categories) as shown in Table 5.2. The phenomenon was apparent especially when multi temporal NDVI maps were added to the static dataset. Both accuracy of LSMs and change in areas due to addition of multi temporal NDVI are consistent with the trend of landslide occurrences and rainfall intensity in year. Addition of remaining temporal factors, i.e., soil wetness and LST, do not show the consistency as NDVI does.

Table 5.2 Expansion and contraction of areas susceptible to landslide (in km<sup>2</sup>)

	February (Dry)	May (Rainy)	June (Dry)	September (Rainy)
Scenario 2	12.2	16.1	10.1	12.5
Scenario 3	31.0	28.2	35.5	39.9
Scenario 4	33.0	28.5	32.3	40.5

5. There are possible factors so that the accuracy of LSMs of scenario 2, 3 and 4 is lower than that of LSI 6 of scenario 1. The first is that the selected Landsat images may not represent actual peak periods of rainy and dry seasons. The second is that ground truthing to calibrate NDVI, soil wetness, and LST, has not been conducted. The third, geotechnical perspective was not involved in assigning weight values. The last is the existence of insignificant factors involved in developing landslide susceptibility model that reduces the accuracy of LSMs. Dropping insignificant factors can increase the accuracy of LSMs.
6. Experiments of one by one inclusion and accumulative inclusion of landslide causative factors resulted in an explanation on how inclusion of more number of landslide causative factors, as the case of LSI all factors, could not guarantee to get better accurate LSMs than that of LSI 6. Both experiments highlighted slope aspect and curvature as the insignificant factors in dataset of LSI all factors. Running landslide susceptibility models employing selected significant factors has proven efficient in increasing the accuracy of the final LSMs.
7. Test of the applicability of the developed landslide susceptibility model of Cameron Highlands applied in the test site, Penang Island, revealed that the model is not applicable to the test site. This is not due to low accuracy of the model. This is the nature of bivariate statistical approach, the data driven method, using which a model developed from a particular area cannot be extrapolate other regions. The developed model has proven to be sufficient in producing accurate LSMs. A place with the same characteristics as Cameron Highlands is required to test the model.
8. Two recommendations on landslide susceptibility modeling over areas under monsoonal rainfall system with the lack of sufficient resolution of rainfall data can be drawn as follows:
  - a. For those who want to involve multi temporal factors.

Landslide susceptibility modeling begins with selection of significant static causative factors. Bivariate statistical analysis should be selected for deriving weighting system. Multi temporal NDVI factors are recommended to select rather than two other multi temporal factors. Inclusion of these factors provides insight of possible expansion or contraction of possible dangerous areas to landsliding.

- b. For those who do not want to involve multi temporal factors.

The same recommendation as above is applied except inclusion of multi temporal NDVI factors.

These recommendations are optional depending on the purpose of study and the availability of required spatial data

## **5.2 Recommendations for Future Works**

Although all of research objectives have been achieved, there are limitations and difficulties encountered during research works. To overcome these shortages, the following works are recommended for future research:

1. To improve accuracy of LSMs with inclusion of multi temporal factors, the following manners are suggested:
  - a. Besides assigning weight values to classes of causative factors, each causative factor is required to be assigned different weight values following the results of one by one and cumulative inclusion process.
  - b. Ground truthing for temporal factors i.e. NDVI, soil wetness and LST should be conducted in order to calibrate these data, to ensure characteristics of landslide since indicated by these factors and to get appropriate weight values for classes of these factors.
  - c. Geotechnical point of view should be involved in assigning weight values along with bivariate statistical.
2. Spatial and temporal correlation of causative factors should be investigated in order to improve the model.
3. It is suggested to use satellite data from other satellite mission such as ALOS, Envisat, Terrasat, SPOT, etc. to fulfill the unavailability of Landsat images acquired at periods of interest, i.e. peak periods of rainy and dry seasons.
4. Highlands areas such as Genting Highlands and other highlands areas in Pahang may be used to test the developed model due to similarity of topographical characteristics.



## REFERENCES

- [1] D. M. Cruden, "A simple definition of a landslide," *Bulletin of the International Association of Engineering Geology* vol. 43, pp. 27-29, 1991.
- [2] R. Anbalagan, "Landslide hazard evaluation and zonation mapping in mountainous terrain," *Engineering Geology*, vol. Vol. 32, pp. 269-277, 1992.
- [3] A. K. Saha, R. P. Gupta, I. Sarkar, M. K. Arora, and E. Csaplovics, "An approach for GIS-based statistical landslide susceptibility zonation-with a case study in the Himalayas," *Landslides*, vol. 2, 2005.
- [4] S. Peloquin and Q. H. J. Gwyn, "Using Remote Sensing, GIS and Artificial Intelligence to Evaluate Landslide Susceptibility Levels: Application in the Bolivian Andes," *4th International Conference on Integrating GIS and Environmental Modelling*, 2000.
- [5] L. Ayalew and H. Yamagishi, "The application of GIS-based logistic regression for landslide susceptibility mapping in the Kakuda-Yahiko Mountains, Central Japan.," *Geomorphology*, vol. Vol. 65, pp. 15-31, 2005.
- [6] J. Hervas, J. I. Barredo, P. L. Rosin, A. Pasuto, F. Mantovani, and S. Silvano, "Monitoring Landslide from Optical Remotely Sensed Imagery: The Case History of Tessina Landslide, Italy," *Geomorphology*, vol. 54, pp. 63-75, 2003.
- [7] S. Lee and B. Pradhan, "Landslide hazard mapping at Selangor, Malaysia, using frequency ratio and logistic regression models," *Landslides*, vol. 4, pp. 33-41, 2007.
- [8] J. A. Talib, "Slope Instability and Hazard Zonation Mapping using Remote Sensing and GIS Techniques in the Area of Cameron Highlands, Malaysia," in *The 18th Asian Conf. Remote Sensing*, Malaysia 1997.
- [9] S. N. S. Omar, F. k. M. Jeber, and S. Mansor, "GIS/RS for landslides zonation in Pos Slim-Cameron Highlands district, Peninsula Malaysia," *Disaster Prevention and Management*, vol. 13, pp. 24 - 32, 2004.
- [10] S. Lee and B. Pradhan, "Landslide hazard assessment at Cameron Highland Malaysia using frequency ratio and logistic regression models," *Geophysical Research Abstract, European Geosciences Union*, vol. 8, 2006.

- [11] B. Pradhan and S. Lee, "Remote sensing and GIS based landslide hazard mapping at Cameron Highland, Malaysia using frequency ratio and logistic regression models," 2006.
- [12] B. Pradhan and S. Lee, "Regional Landslide Susceptibility Analysis using Back-propagation Neural Network Model at Cameron Highlands, Malaysia," *Landslides, Springer Berlin / Heidelberg*, 2009.
- [13] JKR, "National Slope Master plan 2009-2023,"Kuala Lumpur: Cawangan Kejuruteraan Cerun, 2009
- [14] J. Suhaila and A. A. Jemain, "Fitting the Statistical Distribution for Daily Rainfall in Peninsular Malaysia Based on AIC Criterion," *Journal of Applied Sciences Research*, vol. 4, pp. 1846-1857, 2008.
- [15] M. L. Davenport and S. E. Nicholson, "On the relation between rainfall and the Normalized Difference Vegetation Index for diverse vegetation types in East Africa," *International Journal of Remote Sensing*, vol. 14, pp. 2369-2389, 1993.
- [16] H. Xia, J.-j. Wu, and J.-l. Fan, "Study on rainfall effect on vegetation change in the north piedmont of Yin mountain," in *IEEE Int. Geoscience and Remote Sensing Symp. (IGARSS) '07*, 2007, pp. 3474-3477.
- [17] W. Korres, C. N. Koyama, P. Fiener, and K. Schneider, "Analysis of surface soil moisture patterns in agricultural landscapes using empirical orthogonal functions " *Hydrology and Earth System Sciences*, vol. 6, pp. 5565-5601, 2009.
- [18] M. Zribi, C. Andre, and B. Decharme, "A Method for Soil Moisture Estimation in Western Africa Based on the ERS Scatterometer," *Geoscience and Remote Sensing, IEEE Transactions on*, vol. 46, pp. 438-448, 2008.
- [19] J. Kyoung-Wook, E. Njoku, and S. Chan, "Impact of Rainfall on the Retrieval of Soil Moisture using AMSR-E Data," in *IEEE Int. Conf. Geoscience and Remote Sensing Symp. (IGARSS) '06.* , 2006, pp. 1740-1743.
- [20] M. S. Nash, P. J. Wierenga, and A. Gutjahr, "Time Series Analysis of Soil Moisture and Rainfall Along A Line Transect in Arid Rangeland," *Soil Science*, vol. 152, pp. 189-198, 1991.

- [21] K. L. Findell and E. A. B. Eltahir, "An analysis of the soil moisture-rainfall feedback, based on direct observations from Illinois," *Water Resources Research*, vol. 33, pp. 725–735, 1997.
- [22] Y. Iijima, A. N. Fedorov, H. Park, K. Suzuki, and H. Yabuki, "Abrupt Increases in Soil Temperatures following Increased Precipitation in a Permafrost Region, Central Lena River Basin, Russia," *Permafrost and Periglacial Processes*, vol. 21, pp. 30-41, 2009.
- [23] P. Berg, J. O. Haerter, P. Thejll, C. Piani, S. Hagemann, and J. H. Christensen, "The relationship between precipitation and surface temperature in the European domain," *Geophysical Research Abstracts*, vol. 11, 2009.
- [24] R. W. Kulawardhana, "Determination of Spatio-Temporal Variations of Vegetation Cover, Land Surface Temperature and Rainfall and Their Relationships over Sri Lanka Using NOAA AVHRR DATA," M.S. Thesis, Dep. Agricultural Eng., Fac. Agriculture Univ. Peradeniya Peradeniya, Sri Lanka, 2010.
- [25] Q. Hu and S. Feng, "How have soil temperatures been affected by the surface temperature and precipitation in the Eurasian continent?," *Geophysical Research Letters*, vol. 32, p. 14711, 2005.
- [26] M. T. J. Terlien, "Modeling Spatial and Temporal Variations in Rainfall-Triggered Landslides," PhD Dissertation, ITC, Enschede, The Netherlands, 1996.
- [27] T. W. J. Van Asch, J. Buma, and L. P. H. Van Beek, "A View of Some Hydrological Triggering System in Landslides," *Geomorphology*, vol. 30, pp. 25-32, 1999.
- [28] S. Agostoni, M. Cardinali, A. Carrara, G. Crosta, D. Fossati, P. Frantini, F. Guzzetti, R. Laffi, and P. Reichenbach, "Assessment of landslide hazard of the Staffora Basin (Northern Italy) by Integrating Geomorphological and Historical Data Within a Multivariate Model," presented at the XXV EGS General Assembly, Nice, France, 2000.
- [29] F. Guzzetti, "Landslide Hazard Assessment and Risk Evaluation: Limit and Perspectives," in *The 4th EGS Plinius Conf. on Mediterranean Storms*, Mallorca, Spain, 2002.

- [30] F. Guzzetti, G. Crosta, R. Detti, and F. Agliardi, "STONE: A Computer Program for the Three-Dimensional Simulation of Rock-falls," *Computer & Geosciences*, vol. 28, pp. 1079-1093, 2002.
- [31] T. W. J. Van Asch and H. Van Steijn, "Temporal Patterns of Mass Movements in the French Alps," *Catena*, vol. 18, pp. 515-527, 1991.
- [32] L. P. H. Van Beek and T. W. J. Van Asch, "Regional Assessment of the Effects of Land-Use Change on Landslide Hazard by Means of Physically Based Modelling," *Natural Hazards*, vol. 31, pp. 289-304, 2004.
- [33] MMD, "Rainfall Intensity and Rainfall Days at Cameron Highlands," Malaysia Meteorological Department, 2009.
- [34] L. M. Highland and P. Bobrowsky, *The Landslide Handbook—A Guide to Understanding Landslides* vol. 1325. Reston, Virginia: United States Geological Survey Geological Survey of Canada, 2008.
- [35] J. F. Gilbert, W. E. Dietrich, J. M. Duncan, P. E. Lamoreaux, G. G. Mader, W. F. Marcuson, P. J. May, N. R. Morgenstern, J. Preuss, A. K. Turner, and T. L. Youd, "Partnerships for Reducing Landslide Risk: Assessment of the National Landslide Hazards Mitigation Strategy," *Committee on the Review of the National Landslide Hazards Mitigation Strategy, National Research Council*, vol. THE NATIONAL ACADEMIES PRESS, 2004.
- [36] F. Guzzetti, "Landslide Hazard and Risk Assessment," Ph.D Dissertation, Mathematic-Naturwissenschaftlichen Fakultät der Rheinischen Friedrich-Wilhelms, Univ. of Bonn, Bonn, Germany, 2005.
- [37] K. Sassa, "Progress in Landslide Science," vol. XVII, K. Sassa, *et al.*, Eds., ed. Germany: Springer, 2007, p. 378
- [38] D. J. Varnes, "Landslide Hazard Zonation: A Review of Principles and Practice," *Commission on Landslides of the IAEG, UNESCO, Natural Hazard*, vol. No. 3, p. 61 pp, 1984.
- [39] AGS, "Landslide Risk Management Concepts and Guidelines. Australian Geomechanics," *Australian Geomechanics (Australian Geomechanics Society)*, vol. 35, pp. 49-92, 2000.
- [40] UN, *Living with Risk. A global review of disaster reduction initiatives*. Geneva, Switzerland, 2002.

- [41] S. Ahmad, M. I. Seeni, and M. Hashim, "Application of Remote Sensing Techniques for Prediction of Landslide Hazard Areas in Malaysia," presented at the Fourteenth UN/IAF Workshop on Capacity Building in Space Technology for Benefits of Developing Countries, with Emphasis on Natural Disaster Management, Vancouver, Canada, , 2004.
- [42] Z. Chuanhua and W. Xueping, "Landslide Susceptibility Mapping: A Comparison of Information and Weights-of-Evidence Methods in Three Gorges Area," in *Environmental Science and Information Application Technology, 2009. ESIAT 2009. International Conference on*, 2009, pp. 342-346.
- [43] M. M. Gahgah, J. M. Akhir, A. G. M. Rafek, and I. Abdullah, "GIS Based Assessment on Landslide Hazard Zonation: Case Study of Cameron Highlands - Gua Musang Road Kelantan, Malaysia," *Sains Malaysiana*, vol. 38, pp. 827-833, 2009.
- [44] Y. Hong, R. Alder, and G. Huffman, "Use of Satellite Remote Sensing Data in the Mapping of Global Landslide Susceptibility," *Natural Hazards*, 2006.
- [45] M. Komac, "A landslide susceptibility model using the Analytical Hierarchy Process method and multivariate statistics in perialpine Slovenia," *Geomorphology*, vol. 74, pp. pages 17-28, 2006.
- [46] S. Lee and T. Sambath, "Landslide susceptibility mapping in the Damrei Romel area, Cambodia using frequency ratio and logistic regression models," *Environmental Geology*, vol. 50, pp. pages 847-855, 2006.
- [47] Q. Liao, "GIS-Based Landslide Hazard Zonation Mapping using Statistical Approaches," PhD Dissertation, Dep. Civil Eng., Univ. Arkansas, Arkansas, 2004.
- [48] E. E. Brabb, "IV Innovative Approaches to Landslide Hazard and Risk Mapping," in *Int. Symp. Landslides*, Toronto, 1984, pp. 307-323.
- [49] C. J. Van Westen, T. W. J. Van Asch, and R. Soeters, "Landslide hazard and risk zonation - why is it so difficult?," *Bulletin Engineering Geology Environment*, vol. 65, 2006.
- [50] A. Carrara, M. Cardinali, F. Guzzetti, and P. Reichenbach, "GIS-Based Techniques for Mapping Landslide Hazard," in *Geographical Information*

- Systems in Assessing Natural Hazards*, A. Carrara and F. Guzzetti, Eds., Dordrecht, The Netherlands: Kluwer Publications, 1995, pp. 135–176.
- [51] C. H. Zhou, C. F. Lee, J. Li, and Z. W. Xu, "On the Spatial Relationship Between Landslides and Causative Factors on Lantau Island, Hong Kong," *Geomorphology*, vol. 43, pp. 197-207, 2002.
  - [52] J. N. Hutchinson, "Landslide Hazard Assessment," presented at the 6th Int. Symp. Landslides, Christchurch, New Zealand, 1995.
  - [53] A. K. Pachauri and M. Pant, "Landslide Hazard Mapping based on Geological Attribute," *Engineering Geology*, vol. 32, pp. 81-100, 1992.
  - [54] J. Chaco'n, C. Irigaray, T. Fern'andez, and R. E. Hamdouni, "Engineering Geology Maps: Landslides and Geographical Information Systems," *Bulletin Engineering Geology Environment*, vol. 65, pp. 341-411, 2006.
  - [55] S. Lee and J. A. Talib, "Probabilistic landslide susceptibility and factor effect analysis," *Environmental Geology*, vol. 47, pp. 982-990, 2005.
  - [56] R. Fell, J. Corominas, C. Bonnard, L. Cascini, E. Leroi, and W. Z. Savage, "Guidelines for Landslide Susceptibility, Hazard and Risk Zoning for Land Use Planning," *Engineering Geology*, vol. 102, pp. 85–98, 2008.
  - [57] M. L. Suzen, "Data Driven Landslide Hazard Assessment using Geographical Informations Systems and Remote Sensing," Ph.D Dissertation, Geological Eng., Middle East Univ., Turkey, 2002.
  - [58] M. Jadda, H. Z. M. Shafri, S. B. Mansor, M. Sharifikia, and S. Pirasteh, "Landslide Susceptibility Evaluation and Factor Effect Analysis Using Probabilistic-Frequency Ratio Model," *European Journal of Scientific Research*, vol. 33 pp. 654-668, 2009.
  - [59] A. Carrara, F. Guzzetti, M. Cardinali, and P. Reichenbach, "Use of GIS Technology in the Prediction and Monitoring of Landslide Hazard," *Natural Hazards*, vol. 20, pp. 117-135, 1999.
  - [60] R. K. Pande, D. Burman, and R. Singh, "Landslide hazard zonation in Hanuman Chatti area of Uttarakhand, India," *Disaster Prevention and Management*, vol. 18, pp. 410-417, 2009.
  - [61] A. Carrara, E. Catalano, M. S. Valvo, C. Reali, and I. Osso, "Digital Terrain Analysis for Landslide Evaluation," *Geologia Applicata e Idrogeologia*, vol. 13, pp. 69-127, 1978.

- [62] J. V. DeGraff and H. C. Romesburg, "Regional Landslide-Susceptibility Assessment for Wildland Managemet: ," in *A Matrix approach. Chapter 19 In: Thresholds in Geomorphology*, C. R. Coats and J. Vitek, Eds., London: Allen and Unwin, 1980, pp. 401-414.
- [63] ESRI. ArcGIS Desktop Help [Online]. Available: [www.esri.com](http://www.esri.com)
- [64] S. V. Kumar, N. Raja, and G. P. Babu, "Extraction of Topographic and Morphometric Features for Landslide Zonation-A Case Study for Ooty Mettupalayam Highway," presented at the Map Word Forum, Hyderabad, India, 2005.
- [65] H.-B. Havenith, A. Strom, F. Caceres, and E. Pirard, "Analysis of landslide susceptibility in the Suusamyr region, Tien Shan: statistical and geotechnical approach," *Landslides*, vol. 00, pp. 371-383, 2005.
- [66] S. Jäger and G. F. Wieczorek, "Landslide Susceptibility in the Tully Valley Area, Finger Lakes Region, New York," United State Geological Survey (USGS) 2001.
- [67] D. Greenbaum, M. Tutton, M. Bowker, T. Browne, J. Buleka, K. Greally, G. Kuna, A. McDonald, S. Marsh, E. O'Connor, and D. Tragheim, "Rapid Methods of Landslide Hazard Mapping: Papua New Guinea Case Study," 1995
- [68] C. J. Van Westen, N. Rengers, M. T. J. Terlien, and R. Soeters, "Prediction of the occurrence of slope instability phenomenal through GIS-based hazard zonation," *Geologische Rundschau*, vol. 86, pp. 404-414, 1997.
- [69] F. C. Dai and C. F. Lee, "Landslide characteristics and slope instability modeling using GIS, Lantau Island, Hong Kong," *Geomorphology*, vol. 42, pp. 213-228, 2002.
- [70] W. Caiyan, Q. Jianping, and W. Meng, "Landslides and slope aspect in the Three Gorges Reservoir area based on GIS and information value model," *Wuhan Universiti Journal of Natural Sciences*, vol. 11, pp. 773-779, 2006.
- [71] G. M. Lineback, W. A. Marcus, R. Aspinall, and S. G. Custer, "Assessing landslide potential using GIS, soil wetness modeling and topographic attributes, Payette River, Idaho," *Geomorphology*, vol. 37, pp. 149-165, 2001.

- [72] R. A. Marston, M. M. Miller, and L. P. Devkota, "Geoecology and mass movement in the Manaslu-Ganesh and Langtang-Jugal Himals, Nepal," *Geomorphology*, vol. 26, pp. 139-150, 1998.
- [73] R. Ahmad and J. P. McCalpin, "Landslide Susceptibility Maps for the Kingston Metropolitan Area, Jamaica with Notes on Their Use," USAID-OAS Caribbean Disaster Mitigation Project, Mona, Kingston, Jamaica 1999.
- [74] S. Lee and D. G. Evangelista, "Landslide Susceptibility Mapping using Probability and Statistics Models in Baguio City," presented at the 31st Int. Symp. Remote Sensing of Environment, Saint Petersburg, Russia, 2005.
- [75] G. C. Ohlmacher, "Plan Curvature and Landslide Probability in Regions Dominated by Earth Flows and Earth Slides," *Engineering Geology*, vol. 91, pp. 117-134, 2007.
- [76] H.-J. Oh, S. Lee, and G. M. Soedradjat, "Quantitative landslide susceptibility mapping at Pemalang area, Indonesia," *Environmental Earth Science*, vol. 60, pp. 1317-1328, 2010.
- [77] H.-J. Oh, S. Lee, W. Chotikasathien, C. H. Kim, and J. H. Kwon, "Predictive landslide susceptibility mapping using spatial information in the Pechabun area of Thailand," *Environmental Geology*, vol. 57, pp. 641-651, 2009.
- [78] Y. E. Asfaw, "Landslide Assessment in Blue Nile Gorge, Central Ethiopia," Physical Land Resources, Universiteit Gent, Vrije Universiteit Brussel, Brussel, 2010.
- [79] K. Chau and J. Chan, "Regional bias of landslide data in generating susceptibility maps using logistic regression: Case of Hong Kong Island," *Landslides*, vol. 2, pp. 280-290, 2005.
- [80] H. Gómez and T. Kavzoglu, "Assessment of shallow landslide susceptibility using artificial neural networks in Jabonosa River Basin, Venezuela," *Engineering Geology*, vol. 78, pp. 11-27, 2005.
- [81] J. Gao and C. P. Lao, "Micro-scale Modeling of Terrain Susceptibility from a DEM: a GIS approach," *Journal of Geocarto International*, vol. 10, pp. 615-627, 1995.
- [82] D. Z. Seker, M. O. Altan, Z. Duran, M. B. Shrestha, A. Yuasa, and K. Kawamura, "Producing landslide risk map of Sebinkarahisar by means of



- remote sensing and GIS techniques," presented at the XXIst ISPRS Congr., Beijing, CHINA, 2008.
- [83] A. Mondini, R. Carlà, P. Reichenbach, M. Cardinali, and F. Guzzetti, "Use of a remote sensing approach to detect landslide thermal behaviour," *Geophysical Research*, vol. 11, pp. 7790-7798, 2009.
  - [84] R. L. Ray and J. M. Jacobs, "Landslide Susceptibility Mapping Using Remotely Sensed Soil Moisture. ," presented at the 2008 IEEE Int. Geoscience & Remote Sensing Symp., Boston, Massachusetts, U.S.A., 2008.
  - [85] A. Jotisankasa and H. Vathananukij, "Investigation of soil moisture characteristics of landslide-prone slopes in Thailand " presented at the Int. Conf. Management Landslide Hazard in the Asia-Pacific Region, Sendai, Japan, 2008.
  - [86] L. Xu, R. Niu, X. Wang, L. Peng, T. Wu, and S. Wu, "Landslide Hazard Assessment in the Three Gorges of the Yangtze River with TRMM Data," presented at the 2008 IEEE Int. Geoscience & Remote Sensing Symp., Boston, Massachusetts, U.S.A., 2008.
  - [87] R. Ray and J. Jacobs, "Relationships among remotely sensed soil moisture, precipitation and landslide events," *Natural Hazards*, vol. 43, pp. 211-222, 2007.
  - [88] D. Kallen, W. Xiang, D. Ehret, and J. Rohn, "Landslides at Qingjiang River in the Downstream Area of Shuibuya Dam Site, China," *Journal of China University of Geosciences*, vol. 17, pp. 158-162, 2006.
  - [89] J. G. Liu, P. J. Mason, N. Clerici, S. Chen, A. Davis, F. Miao, H. Deng, and L. Liang, "Landslide hazard assessment in the Three Gorges area of the Yangtze river using ASTER imagery: Zigui-Badong," *Geomorphology*, vol. 61, pp. 171-187, 2004.
  - [90] H. Shimazu and T. Oguchi, "River process after rapid valley-filling due to large landslides," *GeoJournal*, vol. 38, pp. 339-344, 1996.
  - [91] A. Kelarestaghi and H. Ahmadi, "Landslide susceptibility analysis with a bivariate approach and GIS in Northern Iran," *Arabian Journal of Geosciences*, vol. 2, pp. 95-101, 2009.

- [92] I. 1. Yilmaz, "The effect of the sampling strategies on the landslide susceptibility mapping by conditional probability and artificial neural networks," *Environmental Earth Science*, vol. 60, pp. 505–519, 2010.
- [93] M. F. Ramli, W. N. A. Sulaiman, M. K. Yusoff, Y. Y. Low, and M. A. Manap, "Open source geographical resources analysis support system (GRASS) for landslide hazard assessment," *Disaster Prevention and Management*, vol. 14, pp. 522-532, 2005.
- [94] P. J. Gibson and C. H. Power, *Introductory Remote Sensing: Digital Image Processing and Applications*. London, United Kingdom: Routledge, 2000.
- [95] H. L. Perotto-Baldiviezo, T. L. Thurow, C. T. Smith, R. F. Fisher, and X. B. Wu, "GIS-based spatial analysis and modeling for landslide hazard assessment in steeplands, southern Honduras," *Agriculture, Ecosystems and Environment*, vol. 30, 2004.
- [96] S. Jayaseelan and S. Sanjeevi, "Visible and NIR reflectance spectra of the components of a landslide zone in the Nilgiris, South India," presented at the Asian Conf. Remote Sensing, India, 2002.
- [97] V. K. Vohora and S. L. Donoghue, "Application of Remote Sensing Data to Landslide Mapping in Hongkong," in *ISPRS XXXVII Congr.*, Istanbul, 2004.
- [98] W.-T. Lin, C.-Y. Lin, and W.-C. Chou, "Assessment of vegetation recovery and soil erosion at landslides caused by a catastrophic earthquake: A case study in Central Taiwan," *Ecological Engineering*, vol. 28, pp. 79-89, 2006.
- [99] D. Alexander, "On the causes of landslides: Human activities, perception, and natural processes," *Environmental Geology*, vol. 20, pp. 165-179, 1992.
- [100] T. Glade, "Landslide occurrence as a response to land use change: a review of evidence from New Zealand," *Elsevier Science*, vol. 51, pp. 297-314, 2003.
- [101] M. Sharma and R. Kumar, "GIS-based landslide hazard zonation: a case study from the Parwanoo area, Lesser and Outer Himalaya, H.P., India," *Bulletin of Engineering Geology and the Environment*, vol. 67, pp. 129-137, 2008.
- [102] N. W. Chan, "Environmental hazards associated with hill land development in Penang Island, Malaysia: some recommendations on effective management," *Emerald-Disaster Prevention and Management*, vol. 7, pp. 305–318, 1998.
- [103] S. Lee and B. Pradhan, "Probabilistic landslide hazards and risk mapping on Penang Island, Malaysia," *Journal of Earth System Science*, vol. 115, 2006.

- [104] P. Jordan, "Regional incidence of landslides.," in *Watershed assessment in the Southern Interior of British Columbia*, British Columbia, Canada, 2000.
- [105] A. Malone, A. Hansen, S. Hencher, and C. Fletcher, "Post-failure movements of a large slow rock slide in schist near Pos Selim, Malaysia," in *Landslides and Engineered Slopes. From the Past to the Future*: CRC Press, 2008, pp. 457-461.
- [106] A. Yalcin, "GIS-based landslide susceptibility mapping using analytical hierarchy process and bivariate statistics in Ardesen (Turkey): Comparisons of results and confirmations," *Catena*, vol. 72, pp. 1-12, 2008.
- [107] C.-J. F. Chung and Y. Leclerc, "A Quantitative Technique for Zoning Landslide Hazard," presented at the Int. Association of Mathematical Geology Conference, Mount Tremblant, Quebec, Canada, 1994.
- [108] C. J. Van Westen, "Geoinformation Tools for Landslide Risk Assessment. An Overview of Recent Development," [www.itc.nl/library/Papers\\_2004/n\\_p\\_conf/vanwesten.pdf](http://www.itc.nl/library/Papers_2004/n_p_conf/vanwesten.pdf), 2004.
- [109] S. Sarkar, D. P. Kanungo, A. K. Patra, and P. Kumar, "GIS Based Spatial Data Analysis for Landslide Susceptibility Mapping," *Journal of Mountain Science*, vol. 5, pp. 52-62, 2008.
- [110] R. K. Dahal, S. Hasegawa, A. Nonomura, M. Yamanaka, T. Masuda, and K. Nishino, "GIS-based weights-of-evidence modelling of rainfall-induced landslides in small catchments for landslide susceptibility mapping," *Environmental Geology*, vol. 54, pp. 311-324, 2007.
- [111] C. J. Van Westen, "The Modelling of Landslide Hazards Using GIS," *Surveys in Geophysics*, vol. 21, pp. 241-255, 2000.
- [112] C.-J. F. Chung and A. G. Fabbri, "Probabilistic Prediction Models for Landslide Hazard Mapping," *Photogrammetric Engineering & Remote Sensing*, vol. 65, pp. 1389-1399, 1999.
- [113] R. Anbalagan, D. Chakraborty, and A. Kohli, "Landslide hazard zonation (LHZ) mapping on meso-scale for systematic town planning in mountainous terrain," *Journal of Scientific & Industrial Research*, vol. 67, pp. 486-497, 2008.

- [114] K. M. Neaupane and M. Piantanakulchai, "Analytic Network Process Model for Landslide Hazard Zonation," *Engineering Geology-Elsevier*, vol. 85, pp. 281-294, 2 May 2006 2006.
- [115] M. Süzen and V. Doyuran, "A comparison of the GIS based landslide susceptibility assessment methods: multivariate versus bivariate," *Environmental Geology*, vol. 45, pp. 665-679, 2004.
- [116] P. Aleotti and R. Chowdhury, "Landslide hazard assessment: summary review and perspective," *Bulletin Engineering Geology Environment*, vol. 58, pp. 21-44, 1999.
- [117] S. Ayele, "Slope Instability and Hazard Zonation Mapping using Remote Sensing and GIS Technique in Abay Gorge (Gohatsion Dejen), Central Ethiopia," Master of Science, Faculty of Science, Addis Ababa University, Addis Ababa, 2009.
- [118] S. M. J. Baban and K. J. Sant, "Mapping landslide susceptibility for the Caribbean island of Tobago using GIS, multi-criteria evaluation techniques with a varied weighted approach," *Caribbean Journal of Earth Science*, vol. 38, pp. 11-20, 2005.
- [119] G. F. Wieczorek, "Preparing a detailed landslide-inventory map for hazard evaluation and reduction," *Bulletin Association Engineering Geologists*, vol. 21, pp. 337–342, 1984.
- [120] F. Mantovani, F. Gracia, P. de Cosmo, and A. Suma, "A new approach to landslide geomorphological mapping using the Open Source software in the Olvera area (Cadiz, Spain)," *Landslides*, vol. 7, pp. 69-74, 2010.
- [121] T. Hiramatsu, Y. Yamano, Y. Suzuki, K. Nohara, M. Hamada, and F. Anada, "Geomorphological analysis associated with the 2007 Noto Hanto earthquake by LiDAR DEM " presented at the MAPASIA 2009, Singapore, 2009.
- [122] G. J. Hearn, "Landslide and erosion hazard mapping at Ok Tedi copper mine, Papua New Guinea," *Quarterly Journal of Engineering Geology and Hydrogeology*, vol. 28, pp. 47-60, February 1, 1995 1995.
- [123] P. Canuti, F. Frascati, C. A. Garzonio, and G. Rodolfi, "Dinamica morfologica di un ambiente soggetto a fenomeni franosi e ad intensa attività agricola," *C.N.R. publication*, vol. 142 pp. 81–102 1979.

- [124] F. Mantovani, R. Soeters, and C. J. Van Westen, "Remote sensing techniques for landslide studies and hazard zonation in Europe," *Geomorphology*, vol. 15, pp. 213-225, 1996.
- [125] R. Soeters and C. J. van Westen, "Slope instability recognition, analysis, and zonation," in *Landslides, investigation and mitigation*. vol. 247, A. K. Turner and R. L. Schuster, Eds., Washington, D.C: National Academy Press, 1996, pp. 129 - 177.
- [126] R. Anbalagan and B. Singh, "Landslide hazard and risk assessment mapping of mountainous terrains- a case study from Kumaun Himalaya, India," *Engineering Geology*, vol. 43, pp. 237-246, 1996.
- [127] N. Abu-Zeid, E. Mazzini, P. Semenza, and M. C. Turrini, "Applicazione di un metodo cartografico-numerico al bacino dell'Alpago (Bl) per la zonazione della pericolosità potenziale da frana," *Geologia tecnica e ambientale*, vol. 3, pp. 45-55, 1994.
- [128] M. C. Turrini and P. Visintainer, "Proposal of a method to define areas of landslide hazard and application to an area of the Dolomites, Italy," *Engineering Geology*, vol. 50, pp. 255-265, 1998.
- [129] Z. Chuanhua and W. Xueping, "Landslide Susceptibility Mapping: A Comparison of Information and Weights-of-Evidence Methods in Three Gorges Area," in *Int. Conf. on Environmental Science and Information Application Technology (ESIAT)*, 2009, pp. 342-346.
- [130] T. Glade, "Landslide Occurrence as a Response to Land Use Change: A Review of Evidence from New Zealand " *CATENA*, vol. 51, pp. 297-314, 2003.
- [131] A. Carrara, "Multivariate models for landslide hazard evaluation," *Mathematical Geology*, vol. 15, pp. 403-426, 1983.
- [132] J.-J. Dong, Y.-H. Tung, C.-C. Chen, J.-J. Liao, and Y.-W. Pan, "Discriminant analysis of the geomorphic characteristics and stability of landslide dams," *Geomorphology*, vol. 110, pp. 162-171, 2009.
- [133] G. C. Ohlmacher and J. C. Davis, "Using multiple logistic regression and GIS technology to predict landslide hazard in northeast Kansas, USA," *Engineering Geology*, vol. 69, pp. 331-343, 2003.

- [134] B. Pradhan, "Landslide susceptibility mapping of a catchment area using frequency ratio, fuzzy logic and multivariate logistic regression approaches," *JOURNAL OF THE INDIAN SOCIETY OF REMOTE SENSING*, vol. 38, pp. 301-320, 2010.
- [135] R. Jelínek and P. Wagner, "Landslide hazard zonation by deterministic analysis (Veľká Čausa landslide area, Slovakia)," *Landslides*, vol. 4, pp. 339-350, 2007.
- [136] M. T. J. Terlien, T. W. J. V. Asch, and C. J. V. Westen, *Deterministic Modeling in GIS-Based Landslide Hazard Assessment*. The Netherlands: Kluwer Academic Publishing, 1995.
- [137] I. Yilmaz, "Landslide susceptibility mapping using frequency ratio, logistic regression, artificial neural networks and their comparison: A case study from Kat landslides (Tokat--Turkey)," *Computers & Geosciences*, vol. 35, pp. 1125-1138, 2009.
- [138] B. Pradhan and S. Lee, "Delineation of Landslide Hazard Areas of Penang Island, Malaysia, by using Frequency Ratio, Logistic Regression, and Artificial Neural Network," *Environmental Earth Science*, 2009.
- [139] C. J. Van Westen, "Application of Geographic Information Systems to Landslide Hazard Zonation," PhD Dissertation, Technical University Delft, Enschede, 1993.
- [140] C. J. Van Westen, "Application of geographic information systems to landslide hazard zonation," PhD Dissertation, ITC-Publication Number 15, ITC, Technical Univ. Delft, Enschede, The Netherlands, 1993.
- [141] N. T. Long, "Landslide Susceptibility Mapping of the Mountainous Area in a Loui District, Thua Thien Hue Province, Vietnam," Dep. Hydrology and Hydraulic Eng., Fac. Eng., Vrije Univ. Brussel, Brussel, 2008.
- [142] F. Vergari, M. Della Seta, M. Del Monte, P. Fredi, and E. Lupia Palmieri, "Landslide susceptibility assessment in the Upper Orcia Valley (Southern Tuscany, Italy) through conditional analysis: a contribution to the unbiased selection of causal factors," *Nat. Hazards Earth Syst. Sci.*, vol. 11, pp. 1475-1497, 2011.

- [143] K. Yin, L. and T. Z. Yan, "Statistical prediction model for slope instability of metamorphosed rocks," in *5th Int. Symp. Landslides*, Lausanne, Switzerland, 1988, pp. 1269 – 1272.
- [144] L. Ayalew, H. Yamagishi, H. Marui, and T. Kanno, "Landslides in Sado Island of Japan: Part II. GIS-based susceptibility mapping with comparisons of results from two methods and verifications," *Engineering Geology*, vol. 81, pp. 432-445, 2005.
- [145] K.-c. Gao, P. Cui, F.-q. Wei, Y. Li, and Q.-y. Zhang, "GIS-based assessment of landslide hazards of Wanzhou in Three Gorges region," in *IEEE Int. Geoscience and Remote Sensing Symp. (IGARSS) '05*, , 2005, pp. 5227-5230.
- [146] D. G. Sapir, R. Below, A. Diaz, F. Vos, and J. Rodriguez. (2009, Oct. 7). *Emergency Events Database EM-DAT* [Online]. Available: <http://www.emdat.be>
- [147] ADRC, "Malaysia Country Report 2008," <http://www.adrc.asia/countryreport/MYS/2008/malaysia2008.pdf>, 2009.
- [148] N. W. Chan, "Responding to Landslide Hazards in rapidly developing Malaysia: a Case of Economics versus Environmental Protection," *Disaster Prevention and Management*, vol. 7, pp. 14-27, 1998.
- [149] A. Guha, *Environmental Constraints to Agriculture in Malaysia. Country Report: Malaysia: Agricultural Research & Advisory Bureau [ARAB]*, Malaysia, 1995.
- [150] R. Fortuin, "Soil Erosion in Cameron Highlands: an Erosion Rate Study of Highland Area," Saxion Hogeschool Deventer, The Netherlands, Faculty of Spatial Planning and Built Environment, Study on Environmental Technology, Brinchang, Cameron Highlands 2006.
- [151] B. Y. Aminuddin, M. H. Ghulam, W. Y. W. Abdullah, M. Zulkifli, and R. B. Salama, "Sustainability of Current Agricultural Practices in The Cameron Highlands, Malaysia," *Water, Air, and Soil Pollution: Focus*, vol. 5, pp. 89–101, 2005.
- [152] TNBHidro-Sdn.Bhd., "Reservoir Sedimentation: Cameron Highlands Hydroelectric Scheme, Malaysia," presented at the IEA Hydropower Implementing Agreement Annex VIII - Hydropower Good Practices: Environmental Mitigation Measures and Benefits Case Study, Japan, 2000.

- [153] M. S. Yusof, E. John, and S. Sayuthi, "Some of Camerons Forest Reserve to Go," in *New Strait Times*, 15 April 2005, ed. Kuala Lumpur, 2005.
- [154] A. N. Matori, A. Basith, and I. Harahap, "Study of regional monsoonal effects on landslide hazard zonation in Cameron Highlands, Malaysia," *Arabian Journal of Geosciences*, pp. 1-16, 2011.
- [155] B. Pradhan, S. Manshor, S. Lee, and M. F. Buchroithner, "Application of Data Mining Model for Landslide Hazard Mapping," presented at the ISPRS Congr. Beijing, Beijing, 2008.
- [156] T. M. Lillesand and R. W. Kiefer, *Remote Sensing and Image Interpretation*. New York, NY: John Wiley & Sons, 1994.
- [157] S. C. Liew. (1997, 6 June ). *Infrared Remote Sensing* [Online]. Available: <http://www.crisp.nus.edu.sg/~research/tutorial/rsmain.htm>
- [158] CSIRO. (2009, Jun. 4). *An introduction to remote sensing* [Online]. Available: <http://www.cmis.csiro.au/rsm/intro/>
- [159] J. R. Irons. (2011, 6 June). *The Landsat Program* [Online]. Available: <http://landsat.gsfc.nasa.gov/>
- [160] N. M. Short. (2010, Jun. 5). *NASA Remote Sensing Tutorial* [Online]. Available: <http://rst.gsfc.nasa.gov/>
- [161] Geocommunity. (2010, Sep. 16). *A Primer on Landsat 7* [Online]. Available: <http://imaging.geocomm.com/features/sensor/landsat7/>
- [162] NASA. (2011, 6 June). *Landsat 7 Science Data Users Handbook* [Online]. Available: <http://landsathandbook.gsfc.nasa.gov>
- [163] Geoscience-Australia. (2010, sep. 15). *Remote Sensing* [Online]. Available: <http://www.ga.gov.au/remote-sensing>
- [164] S. Riazanoff. (2002, Aug. 7). *SPOT Satellite Geometri Handbook* [Online document]. Available: <http://www.spotimage.fr>
- [165] J. Gao, *Digital Analysis of Remotely Sensed Imagery*. New York, United State: McGraw-Hill, 2009.
- [166] T. M. Lillesand, R. W. Kiefer, and J. W. Chipman, *Remote Sensing and Image Interpretation*, 6th ed. New Jersey, United States: John Wiley & Sons, Inc., 2007.



- [167] T. S. Unger Holtz, "Introductory Digital Image Processing: A Remote Sensing Perspective, Third Edition," *Environmental Engineering Geoscience*, vol. 13, pp. 89-90, 2007.
- [168] J. R. Jensen, *Introductory Digital Image Processing: a remote sensing perspective*, 2nd ed. Upper Saddle River, NJ: Prentice Hall, 1996.
- [169] D. G. Hadjimitsis, G. Papadavid, A. Agapiou, K. Themistocleous, M. G. Hadjimitsis, A. Retalis, S. Michaelides, N. Chrysoulakis, L. Toullos, and C. R. I. Clayton, "Atmospheric correction for satellite remotely sensed data intended for agricultural applications: impact on vegetation indices," *Nat. Hazards Earth Syst. Sci.*, vol. 10, pp. 89-95, 2010.
- [170] S. Yuzhong and S. K. Jakkula, "Aerial Image Enhancement Based on Estimation of Atmospheric Effects," in *IEEE Int. Conf. Image Processing (ICIP)*, 2007, pp. III - 529-III - 532.
- [171] L. S. Bernstein, S. M. Adler-Golden, R. L. Sundberg, R. Y. Levine, T. C. Perkins, A. Berk, A. J. Ratkowski, G. Felde, and M. L. Hoke, "A new method for atmospheric correction and aerosol optical property retrieval for VIS-SWIR multi- and hyperspectral imaging sensors: QUAC (QUick atmospheric correction)," in *Geoscience and Remote Sensing Symp., 2005. IGARSS '05*, 2005, pp. 3549-3552.
- [172] Y. Jinguo and N. Zheng, "Evaluation of atmospheric correction using FLAASH," in *Int. Workshop on Earth Observation and Remote Sensing Applications (EORSA)*, 2008, pp. 1-6.
- [173] A. Hall, "ERMMapper Tutorial: Change Detection," unpublished.
- [174] S. H. Sanaeinejad, A. Astaraei, P. Mirhoseini.Mousavi, and M. Ghaemi, "Selection of Best Band Combination for Soil Salinity Studies using ETM+ Satellite Images (A Case study: Nyshaboore Region,Iran)," *World Academy of Science, Engineering and Technology* vol. 54, pp. 519-521, 2009.
- [175] M. F. Ramli and D. N. Petley, "Best band combination for landslide studies in temperate environments," *International Journal of Remote Sensing*, vol. 27, pp. 1219 - 1231, 2006.
- [176] J. W. Quinn. (2001, Mar. 30). *Band Combinations* [Online]. Available: <http://web.pdx.edu/~emch/ip1/bandcombinations.html>

- [177] GDSC. (2011, Jan. 3). *Band Combinations* [Online]. Available: [http://gdsc.nlr.nl/gdsc/en/information/earth\\_observation/band\\_combinations](http://gdsc.nlr.nl/gdsc/en/information/earth_observation/band_combinations)
- [178] CCRS. (2008, Jun. 9). *Tutorial: Fundamentals of Remote Sensing* [Online]. Available: [http://www.ccrs.nrcan.gc.ca/resource/tutor/fundam/chapter4/05\\_e.php](http://www.ccrs.nrcan.gc.ca/resource/tutor/fundam/chapter4/05_e.php)
- [179] J. R. Anderson, E. E. Hardy, J. T. Roach, and R. E. Witmer, "A Land Use And Land Cover Classification System For Use With Remote Sensor Data," *Geological Survey Professional Paper 964*, p. 16, 1976.
- [180] Z. Qin, A. Karnieli, and P. Berliner, "A Mono-Window Algorithm for Retrieving Land Surface Temperature from Landsat TM Data and Its Application to Israel-Egypt Border Region," *International Journal of Remote Sensing*, vol. 22, pp. 3719-3746, 2001.
- [181] J. C. Jimenez-Munoz, J. Cristobal, J. A. Sobrino, G. Soria, M. Ninyerola, and X. Pons, "Revision of the Single-Channel Algorithm for Land Surface Temperature Retrieval From Landsat Thermal-Infrared Data," *Geoscience and Remote Sensing, IEEE Transactions on*, vol. 47, pp. 339-349, 2009.
- [182] L. Hua, L. Qinhuo, Z. Bo, D. Yongming, W. Heshun, and W. Qiao, "A single-channel algorithm for land surface temperature retrieval from HJ-1B/IRS data based on a parametric model," in *IEEE Int. Geoscience and Remote Sensing Symp. IGARSS '10*, 2010, pp. 2448-2451.
- [183] J. A. Sobrino, J. C. Jiménez-Muñoz, and L. Paolini, "Land surface temperature retrieval from LANDSAT TM 5," *Remote Sensing of Environment*, vol. 90, pp. 434-440, 2004.
- [184] H. Chudong, S. Yun, L. Jing, C. Jinsong, and L. Jinghui, "Temporal Analysis of Land Surface Temperature in Beijing Utilizing Remote Sensing Imagery," in *IEEE Int. Geoscience and Remote Sensing Symp. (IGARSS)*, 2008, pp. III - 1304-III - 1307.
- [185] S. Cheng, W. Zhifeng, L. Zhiqiang, and W. Jianbing, "Spatial-Temporal Analysis of Land Surface Temperature and Its Interplay with Land Use Change," in *2nd Inter. Conf. on Information Engineering and Computer Science (ICIECS)*, 2010, pp. 1-4.
- [186] L. Chuansheng, Z. Wanchang, Z. Dengzhong, and G. Yongnian, "Remotely-sensed evapotranspiration of typical oasis in the southern edge of tarim basin

- and its relationship to land cover changes," in *IEEE Int. Geoscience and Remote Sensing Symp. IGARSS*, 2007, pp. 3237-3240.
- [187] J. S. Yang and Y. Q. Wang. (2006, Aug. 7). *Estimation of Land Surface Temperature Using Landsat-7 ETM+ Thermal Infrared and Weather Station Data* [Online]. Available: [www.ltrs.uri.edu/research/LST\\_page/paper4.doc](http://www.ltrs.uri.edu/research/LST_page/paper4.doc)
  - [188] J. Zhang, Y. Wang, and Y. Li, "A C++ program for retrieving land surface temperature from the data of Landsat TM/ETM+ band6," *Computers & Geosciences*, vol. 32, pp. 1796-1805, 2006.
  - [189] B. L. Markham and J. L. Barker, "Landsat MSS and TM post-calibration dynamic rangers, exoatmospheric reflectance and at-satellite temperatures," *EOSAT Landsat Technical Notes*, vol. Aug, 1986.
  - [190] J. R. Schott and W. J. Volchok, "Thematic mapper thermal infrared calibration," *Photogrammetric Engineering and Remote Sensing*, vol. 51, pp. 1351-1357, 1985.
  - [191] J. S. Yang, Y. Q. Wang, and P. V. August, "Estimation of Land Surface Temperature Using Spatial Interpolation and Satellite-Derived Surface Emissivity," *Journal of Environmental Informatics*, vol. 4, pp. 37-44, 2004.
  - [192] R. J. Kauth and G. S. Thomas, "The tasseled cap --a graphic description of the spectral-temporal development of agricultural crops as seen in Landsat," in *Symp. Machine Processing of Remotely Sensed Data*, 1976, pp. 41-51.
  - [193] J. B. Campbell, *Introduction to Remote Sensing*. London: Taylor and Francis, 1996.
  - [194] C. Huang, B. Wylie, L. Yang, C. Homer, and G. Zylstra, "Derivation of a tasselled cap transformation based on Landsat 7 at-satellite reflectance," *International Journal of Remote Sensing, Taylor & Francis*, vol. 23, pp. 1741-1748, 2002.
  - [195] E. Stylianidis, P. Patias, V. Tsioukas, L. Sechidis, and C. Georgiadis, "A Digital Close-Range Photogrammetric Technique for Monitoring Slope Displacements," in *11 th FIG Symp. on Deformation Measurements*, Santorini, Greece, 2003.
  - [196] G. Bitelli, M. Dubbini, and A. Zanutta, "Terrestrial Laser Scanning and Digital Photogrammetry Techniques to monitor Landslide Bodies," in *XXth ISPRS Congr.*, Istanbul, Turkey, 2004.

- [197] O. Monserrat and M. Crosetto, "Deformation measurement using terrestrial laser scanning data and least squares 3D surface matching," *ISPRS Journal of Photogrammetry and Remote Sensing*, vol. 63, pp. 142-154, 2008.
- [198] J. Walstra, J. H. Chandler, N. Dixon, and T. A. Dijkstra, "Aerial photography and digital photogrammetry for landslide monitoring," *Geological Society*, vol. 283, pp. 53-63, 2007.
- [199] Y. Hong, R. Adler, and G. Huffman, "Use of satellite remote sensing data in the mapping of global landslide susceptibility," *Natural Hazards*, vol. 43, pp. 245-256, 2007.
- [200] M. Shikada, N. Muramatu, T. Kusaka, and S. Goto, "Extraction of landslide areas using satellite remote sensing and GIS technology," presented at the IEEE Geoscience and Remote Sensing Symp. 1995 (IGARSS '95). 'Quantitative Remote Sensing for Science and Applications', Florence, Italy, 1995.
- [201] M. Shikada, T. Kusaka, Y. Kawata, and K. Miyakita, "Extraction of characteristic properties in landslide areas using thematic map data and surface temperature," *IEEE*, pp. 103-105, 2003.
- [202] C. Chi, Z. Liu, and J. Zhang, "Interpretation of Landslide from SPOT-5 Imageries in the Three Gorges Reservoir Area," presented at the 2008 Int. Workshop on Earth Observation and Remote Sensing Applications, Beijing, China, 2008.
- [203] K. G. Nikolakopoulos, D. A. Vaiopoulos, G. A. Skianis, P. Sarantinos, and A. Tsitsikas, "Combined Use of Remote Sensing, GIS and GPS Data for Landslide Mapping," *IEEE*, pp. 5196-5199, 2005.
- [204] J. Nichol and M. S. Wong, "Satellite remote sensing for detailed landslide inventories using change detection and image fusion," *International Journal of Remote Sensing*, vol. 26, pp. 1913-1926, 2005.
- [205] V. H. Singhroy, J. E. Loehr, and A. C. Correa, "Landslide risk assessment with high spatial resolution remote sensing satellite data," in *IEEE Int. Geoscience and Remote Sensing Symposium (IGARSS) '00* 2000, pp. 2501-2503 vol.6.

- [206] T. Han, Y. Li, H. Han, Y. Zhang, and Y. Wang, "Land cover classification in Western Loess Plateau of China with MODIS imagery," in *IEEE Int. Geoscience and Remote Sensing Symp. IGARSS '05*, 2005, p. 4 pp.
- [207] D. Li, C. Li, F. Hao, and Z. Lingfang, "Complex vegetation cover classification study of the Yellow River Basin based on NDVI data," in *Proc. IEEE International Geoscience and Remote Sensing Symposium (IGARSS) '04* 2004, pp. 3360-3363 vol.5.
- [208] S. Khorram, J. A. Brockhaus, and H. M. Cheshire, "Comparison of Landsat MSS and TM Data for Urban Land-Use Classification," *Geoscience and Remote Sensing, IEEE Transactions on*, vol. GE-25, pp. 238-243, 1987.
- [209] X. Yaowen, Z. Xiaojiong, L. Linlin, and W. Haoyu, "Calculating NDVI for Landsat7-ETM data after atmospheric correction using 6S model: A case study in Zhangye city, China," in *18th Int. Conf. Geoinformatics*, 2010, pp. 1-4.
- [210] J. Jiabin, J. Hong, W. Yueqi, and Z. Xiuying, "Temporal and spatial variations of NDVI in Lake Baikal," in *18th Int. Conf. Geoinformatics*, 2010, pp. 1-4.
- [211] C. Xuhua, G. Huili, L. Xiaojuan, and Z. Lin, "Remote sensing retrieval of soil moisture using ENVISAT-ASAR images: A case study in suburban region of Peking, China," in *18th Int. Conf. Geoinformatics*, 2010, pp. 1-4.
- [212] S. Alsultan, H.-S. Lim, M. Z. MatJafri, and K. Abdullah, "An Algorithm for Land Surface Temperature Analysis of Remote Sensing Image Coverage Over Alqassim, Saudi Arabia," presented at the FIG Working Week, Cairo, Egypt, 2005.
- [213] R. Goetzke, M. Braun, H. P. Thamm, and G. Menz, "Monitoring and Modeling Urban Land-Use Change with Multitemporal Satellite Data," in *IEEE Int. Geoscience and Remote Sensing Symp. (IGARSS)*, 2008, pp. IV - 510-IV - 513.
- [214] P. A. Burrough and R. A. McDonell, *Principal of Geographical Information System*. New York, United States: OXFORD UNIVERSITY PRESS, 1997.
- [215] R. A. Rose. (2011, Jun. 13). *GIS Tutorials and Exercises* [Online ]. Available: <http://hcl.harvard.edu/libraries/maps/gis/tutorials.cfm>

- [216] A. Van der Ent and C. Termeer, "Study on River Water Quality of The Upper Bertam Catchment," R.E.A.C.H. - Saxion University of Applied Science Deventer, 2006.
- [217] Worldclimate. (2008, Jul. 3). *Rainfall and Temperature at Cameron Highlands Malaysia* [Online]. Available: <http://www.worldclimate.com>
- [218] S. A. Bakar and A. Madun, "Geological Mapping and Stereo-net Analysis to Evaluate Cut Slope Stability at Pos Slim Lojing Highway," *6th Malaysian Road Conference*, vol. 16-18 Augustus, Sunway Pyramid Convention Centre, Kuala Lumpur, 2004.
- [219] T. A. Jamaluddin, "Engineering Geological Assessment and Slope Failures Along The Pos Selim Cameron Highland Highway," presented at the Seminar Penyelidikan Jangka Pendek (Vot F), 11 dan 12 Mac 2003, Kuala Lumpur, 2003.
- [220] JKR, "National Slope Master Plan," Kuala Lumpur, 2009.
- [221] M. A. Mulders, *Remote Sensing in Soil Science*. Amsterdam: Elsevier, 1987.
- [222] S. K. Selvaradjou, L. Montanarella, O. Spaargaren, D. Dent, N. Filippi, and S. Dominik, *European Digital Archive of Soil Maps (EuDASM) – Metadata of the Soil Maps of Asia*. Luxembourg: Office of the Official Publications of the European Communities, 2005.
- [223] L. K. Meng, "The Petroleum Geology and Resources of Malaysia," unpublished.
- [224] M. Kadir, S. Ses, K. Omar, G. Desa, A. H. Omar, K. Taib, T. C. Hua, A. Mohamed, C. L. Hua, R. Saleh, and S. Nordin, "GEOCENTRIC DATUM GDM2000 FOR MALAYSIA: IMPLEMENTATION AND IMPLICATIONS," unpublished.
- [225] E. Berset and Sangakkara. (2010, Sep. 19). *Assessing soil fertility and decomposition patterns of G. sepium green manure at three slope categories of Sri Lanka's hill country* [Online]. Available: <http://www.kfpe.ch/projects/echangesuniv/berset.php>
- [226] L. Zhu and J.-f. Huang, "GIS-based logistic regression method for landslide susceptibility mapping in regional scale," *Journal of Zhejiang University - Science A*, vol. 7, pp. 2007-2017, 2006.

- [227] S. Jamaluddin, B. B. K. Huat, and H. Omar, "Evaluation of Slope Assessment System for Predicting Landslide of Cut Slopes in Granitic and Meta-sediment Formations," *American Journal of Environmental Sciences*, vol. 2, pp. 135-141, 2006 2006.
- [228] A. Carrara, M. Cardinali, R. Detti, G. Guzzetti, V. Pasqui, and P. Reichenbach, "GIS techniques and statistical models in evaluating landslide hazard," *Earth Surface Processes and Landforms*, vol. 16, pp. 427-445, 1991.
- [229] B. Pradhan and S. Lee, "Regional landslide susceptibility analysis using back-propagation neural network model at Cameron Highland, Malaysia," *Landslides*, vol. 7, pp. 13-30, 2010.
- [230] S. Lee, J. Ryu, K. Min, and J. Won, "Development of two artificial neural network methods for landslide susceptibility analysis," in *Geoscience and Remote Sensing Symposium, 2001. IGARSS '01. IEEE 2001 International*, 2001, pp. 2364-2366 vol.5.
- [231] S. Lee, J. Ryu, K. Min, W. Choi, and J. Won, "Development and Application of Landslide Susceptibility Analysis Techniques using Geographic Information System (GIS)," *IEEE*, 2000.
- [232] L. Coppola, R. Nardone, P. Rescio, and E. Bromhead, "Reconstruction of the conditions that initiate landslide movement in weathered silty clay terrain: effects on the historic and architectural heritage of Pietrapertosa, Basilicata, Italy," *Landslides*, vol. 3, pp. 349-359, 2006.
- [233] C. S. Prentice, "Earthquake geology of the northern San Andreas fault near Point Arena, California," Ph.D Dissertation, California Inst. Tech., California, 1989.
- [234] H. Shimazu and T. Oguchi, "River processes after rapid valley-filling due to large landslides," *GeoJournal*, vol. 38, pp. 339-344, 1996.
- [235] G. Újvári, G. Mentés, L. Bányai, J. Kraft, A. Gyimóthy, and J. Kovács, "Evolution of a bank failure along the River Danube at Dunaszekcső, Hungary," *Geomorphology*, vol. 109, pp. 197-209, 2009.
- [236] J.-K. Liu, C.-C. Wong, J.-H. Huang, and M.-J. Yang, "Landslide-Enhancement Images for The Study of Torrential-Rainfall Landslides," presented at the The 23rd Asian Conf. Remote Sensing, Kathmandu, Nepal, 2002.

- [237] M. Shikada, T. Kusaka, Y. Kawata, and K. Miyakita, "Extraction of characteristic properties in landslide areas using thematic map data and surface temperature," in *Int. Geoscience and Remote Sensing Symp. (IGARSS)* '93, 1993, pp. 103-105 vol.1.
- [238] A. Mondini, R. Carlà, P. Reichenbach, M. Cardinali, and F. Guzzetti, "Use of a remote sensing approach to detect landslide thermal behaviour," *Geophysical Research Abstracts*, vol. 11, 2009.
- [239] Anonymous. (2011, April,2). *Glossary*. Available: <http://sydney.edu.au/agric/ACSS/sphysic/asis/glossary.html>
- [240] J. F. Anthoni. (2002, Apr. 1). *Seafriends - Glossary of geological terms* [Online]. Available: [www.seafriends.org.nz/books/geogloss.htm](http://www.seafriends.org.nz/books/geogloss.htm)
- [241] Anonymous. (2011, Apr, 2). *Lithosol* [Online]. Available: [http://encarta.msn.com/dictionary\\_1861699028/lithosol.html](http://encarta.msn.com/dictionary_1861699028/lithosol.html)



## APPENDIX A

### Rainfall and Raindays Data

#### A1. Rainfall Data

JABATAN METEOROLOGI MALAYSIA													
Station : Cameron Highlands Lat. : 04° 28' N Long. : 101° 22' E Ht. above M.S.L. : 1545.0 m													
<b>Records of Monthly Rainfall Amount (mm)</b>													
Year/Month	Jan	Feb	Mar	Apr	May	Jun	Jul	Aug	Sep	Oct	Nov	Dec	Annual
2000	214.4	190.2	437.6	517.4	224.5	220.8	127.9	176.6	221.8	204.2	313.5	323.1	3172.0
2001	141.5	137.2	245.4	310.7	197.2	89.7	50.2	99.2	274.8	429.2	413.7	242.9	2631.7
2002	26.0	8.9	84.9	421.5	301.6	254.5	167.0	282.4	366.2	412.3	334.0	157.3	2816.6
2003	102.0	118.0	266.6	185.7	235.4	300.7	289.0	362.0	157.0	470.4	313.5	175.5	2975.8
2004	44.2	102.4	248.9	256.4	262.2	75.6	213.8	161.9	444.9	322.9	175.3	103.1	2411.6
2005	24.5	99.3	190.4	217.9	199.8	227.2	235.0	137.1	157.4	450.4	401.2	551.6	2891.8
Average	92.1	109.3	245.6	318.3	236.8	194.8	180.5	203.2	270.4	381.6	325.2	258.9	2816.6

#### A2. Raindays data

JABATAN METEOROLOGI MALAYSIA													
Station : Cameron Highlands Lat. : 04° 28' N Long. : 101° 22' E Ht. above M.S.L. : 1545.0 m													
<b>Records of Number of Raindays</b>													
Year/Month	Jan	Feb	Mar	Apr	May	Jun	Jul	Aug	Sep	Oct	Nov	Dec	Annual
2000	17	19	24	26	21	19	14	17	21	21	22	20	241
2001	26	12	20	28	18	10	11	16	20	26	29	18	234
2002	10	2	11	22	19	14	15	16	23	27	21	23	203
2003	16	15	19	21	13	22	17	22	22	28	27	17	239
2004	11	10	23	20	18	10	17	15	27	27	26	12	216
2005	9	7	12	18	24	14	17	16	17	30	24	27	215
Average	14.8	10.8	18.2	22.5	18.8	14.8	15.2	17.0	21.7	26.5	24.8	19.5	224.7

## APPENDIX B

### RSO Projection Parameters

Parameter	Value
False_Easting	804671.299774999960000000
False_Northing	0.000000000000000000
Scale_Factor	0.999839999999999950
Azimuth	-36.974209437118013000
Longitude_Of_Center	102.250000000000000000
Latitude_Of_Center	4.000000000000000000
XY_Plane_Rotation	-36.869897645844020000

#### *Geographic Coordinate System*

Name: GCS\_Kertau  
 Angular Unit: Degree (0.017453292519943299)  
 Prime Meridian: Greenwich (0.000000000000000000)  
 Datum: D\_Kertau  
 Spheroid: Everest\_1830\_Modified  
 Semimajor Axis: 6377304.063000000100000000  
 Semiminor Axis: 6356103.038993154700000000  
 Inverse Flattening: 300.801699999999980000

	Peninsular Malaysia RSO	East Malaysia Borneo RSO	Remark
<b>Ellipsoid Parameters</b>			
Ellipsoid	GRS 80	GRS 80	
	6378137.000 Meters	6378137.000 Meters	
Flattening, 1/f	298.2572221	298.2572221	
<b>Category I – Defined Parameters.</b>			
Latitude of Origin, $\phi$	4° 00' 00" N	4° 00' 00" N	
Longitude of Origin, $\lambda_o$	102° 15' 00" E	115° 00' 00" E	
Azimuth, $\alpha$	- $\sin^{-1}$ (0.6)	- $\sin^{-1}$ (0.6)	
Scale factor, k	0.99984	0.99984	
False Origin (Easting)	804,671 Meters E	Nil	
False Origin (Northing)	Nil	Nil	
<b>Category II - Parameter that related to ellipsoid change</b>			
Parameter A	6378137.502 Meters	6378137.502 Meters	$B(\rho_o v_o)^{1/2}$
Parameter B	1.003331484644	1.003331484644	$(1+k^{-2} \cdot \cos^4 \phi_o)^{1/2}$
Parameter C	0.000003016721	0.000003013554	$\cosh^{-1}(A/\rho_o) - B\psi_o$
Basic Longitude. $\omega_o$	105° 14' 10.587"	109° 41' 08.948"	$\sin B (\omega_o - \omega) = 0.75 \sinh (B\psi + C)$

# APPENDIX C RMS of Geometric Correction of Topographic Map

# RMS error report:						
# Warp Type - Polynomial						
#		-----ACTUAL-----		---PREDICTED---		
#	Point	Cell-X	Cell-Y	Cell-X	Cell-Y	RMS
#	"1"	270.042	5061.164	269.970	5060.312	0.8559
#	"2"	429.238	5058.448	428.873	5058.133	0.4824
#	"3"	588.436	5056.151	587.728	5055.953	0.7356
#	"4"	747.060	5054.469	746.537	5053.772	0.8719
#	"5"	905.083	5052.172	905.302	5051.592	0.6204
#	"6"	1064.028	5050.103	1064.029	5049.412	0.6908
#	"7"	1222.584	5047.686	1222.719	5047.233	0.4732
#	"8"	1381.503	5045.135	1381.377	5045.056	0.1492
#	"9"	1540.033	5043.066	1540.004	5042.881	0.1875
#	"10"	1698.150	5040.582	1698.605	5040.708	0.4725
#	"11"	1857.508	5038.099	1857.183	5038.539	0.5476
#	"12"	2015.624	5036.443	2015.740	5036.374	0.1347
#	"13"	2173.741	5034.374	2174.281	5034.214	0.5631
#	"14"	2332.685	5031.890	2332.808	5032.058	0.2075
#	"15"	2491.630	5029.407	2491.324	5029.907	0.5866
#	"16"	2649.746	5027.751	2649.833	5027.763	0.0881
#	"17"	2808.691	5025.267	2808.339	5025.625	0.5019
#	"18"	2966.913	5022.834	2966.843	5023.495	0.6644
#	"19"	3125.055	5021.592	3125.350	5021.372	0.3686
#	"20"	3283.610	5018.694	3283.863	5019.257	0.6168
#	"21"	3442.166	5017.038	3442.384	5017.151	0.2451
#	"22"	3600.308	5015.796	3600.917	5015.055	0.9597
#	"23"	3759.071	5012.898	3759.466	5012.968	0.4009
#	"24"	3917.694	5010.937	3918.033	5010.891	0.3422
#	"25"	4076.183	5008.759	4076.622	5008.826	0.4445
#	"26"	4235.567	5006.689	4235.236	5006.772	0.3410
#	"27"	4393.916	5005.447	4393.879	5004.730	0.7172
#	"28"	4552.472	5003.377	4552.552	5002.701	0.6802
#	"29"	4711.028	5000.893	4711.260	5000.685	0.3117
#	"30"	4870.412	4998.823	4870.006	4998.683	0.4289
#	"31"	5028.140	4996.339	5028.793	4996.695	0.7442
#	"32"	263.753	4588.365	263.631	4588.274	0.1517
#	"33"	740.662	4582.155	740.196	4581.693	0.6560
#	"34"	1216.744	4575.117	1216.382	4575.094	0.3633
#	"35"	1692.205	4568.080	1692.273	4568.491	0.4174
#	"36"	2167.666	4560.628	2167.959	4561.900	1.3052
#	"37"	2643.748	4555.246	2643.525	4555.334	0.2392
#	"38"	3119.415	4548.208	3119.059	4548.809	0.6985
#	"39"	3594.876	4541.585	3594.647	4542.339	0.7889
#	"40"	4070.544	4535.375	4070.377	4535.940	0.5896
#	"41"	4546.626	4528.751	4546.335	4529.626	0.9220
#	"42"	5022.708	4523.783	5022.608	4523.412	0.3846
#	"43"	256.617	4116.317	257.251	4116.254	0.6364
#	"44"	734.315	4109.320	733.812	4109.646	0.5991
#	"45"	1209.925	4103.127	1209.996	4103.001	0.1445
#	"46"	1685.950	4095.643	1685.891	4096.333	0.6934
#	"47"	2161.612	4089.237	2161.584	4089.659	0.4231
#	"48"	2637.205	4082.411	2637.161	4082.991	0.5818
#	"49"	3112.783	4075.852	3112.709	4076.346	0.4993
#	"50"	3587.980	4069.164	3588.315	4069.738	0.6648

## (Appendix C cont.)

#	"51"	4063.989	4063.003	4064.067	4063.182	0.1951
#	"52"	4540.063	4056.760	4540.051	4056.692	0.0698
#	"53"	5016.848	4049.890	5016.353	4050.283	0.6324
#	"54"	250.921	3643.811	250.795	3644.221	0.4294
#	"55"	727.866	3636.980	727.349	3637.599	0.8068
#	"56"	1203.610	3631.158	1203.530	3630.922	0.2492
#	"57"	1678.906	3623.785	1679.426	3624.204	0.6673
#	"58"	2155.609	3617.663	2155.123	3617.460	0.5271
#	"59"	2630.644	3610.577	2630.707	3610.704	0.1424
#	"60"	3106.514	3604.200	3106.267	3603.953	0.3489
#	"61"	3581.913	3597.785	3581.889	3597.220	0.5660
#	"62"	4058.199	3590.699	4057.660	3590.520	0.5685
#	"63"	4533.782	3584.030	4533.666	3583.868	0.1989
#	"64"	5010.615	3577.204	5009.995	3577.279	0.6237
#	"65"	243.692	3172.119	244.233	3172.146	0.5416
#	"66"	721.359	3165.293	720.777	3165.523	0.6257
#	"67"	1196.238	3158.233	1196.952	3158.827	0.9294
#	"68"	1672.301	3151.998	1672.845	3152.072	0.5492
#	"69"	2148.236	3145.285	2148.543	3145.272	0.3074
#	"70"	2623.662	3138.199	2624.133	3138.442	0.5303
#	"71"	3099.531	3131.660	3099.702	3131.598	0.1814
#	"72"	3575.661	3124.990	3575.336	3124.753	0.4018
#	"73"	4050.983	3118.451	4051.123	3117.924	0.5459
#	"74"	4527.112	3111.652	4527.150	3111.123	0.5297
#	"75"	5003.529	3104.565	5003.503	3104.367	0.1999
#	"76"	237.439	2700.835	237.531	2699.996	0.8436
#	"77"	714.429	2693.775	714.063	2693.387	0.5333
#	"78"	1189.151	2686.662	1190.229	2686.686	1.0776
#	"79"	1665.698	2680.827	1666.117	2679.907	1.0106
#	"80"	2141.437	2673.871	2141.813	2673.065	0.8895
#	"81"	2616.706	2666.785	2617.406	2666.175	0.9279
#	"82"	3092.732	2660.115	3092.980	2659.251	0.8991
#	"83"	3568.588	2652.942	3568.624	2652.309	0.6343
#	"84"	4044.624	2645.976	4044.425	2645.363	0.6448
#	"85"	4520.814	2638.647	4520.468	2638.428	0.4097
#	"86"	4996.714	2632.017	4996.842	2631.518	0.5149
#	"87"	230.198	2227.542	230.657	2227.742	0.5004
#	"88"	707.500	2220.507	707.173	2221.160	0.7303
#	"89"	1182.777	2213.812	1183.328	2214.468	0.8562
#	"90"	1658.814	2207.481	1659.208	2207.679	0.4402
#	"91"	2135.020	2201.292	2134.900	2200.808	0.4986
#	"92"	2610.720	2193.865	2610.492	2193.871	0.2281
#	"93"	3086.279	2187.366	3086.070	2186.882	0.5273
#	"94"	3562.034	2180.416	3561.721	2179.855	0.6426
#	"95"	4037.789	2173.467	4037.532	2172.807	0.7086
#	"96"	4513.799	2166.039	4513.590	2165.751	0.3566
#	"97"	4990.146	2158.808	4989.982	2158.702	0.1953
#	"98"	222.825	1754.600	223.579	1755.352	1.0654
#	"99"	700.241	1748.438	700.077	1748.812	0.4081
#	"100"	1175.969	1741.489	1176.217	1742.141	0.6983
#	"101"	1652.174	1735.636	1652.086	1735.356	0.2938
#	"102"	2127.424	1728.996	2127.772	1728.470	0.6303
#	"103"	2603.461	1722.047	2603.360	1721.500	0.5562
#	"104"	3079.357	1714.901	3078.938	1714.459	0.6094
#	"105"	3554.634	1707.783	3554.593	1707.362	0.4232
#	"106"	4030.503	1700.215	4030.412	1700.225	0.0913
#	"107"	4506.399	1692.929	4506.482	1693.061	0.1561

(Appendix C cont.)

#	"108"	4982.577	1685.697	4982.889	1685.886	0.3646
#	"109"	216.918	1281.503	216.264	1282.797	1.4499
#	"110"	692.786	1273.976	692.741	1276.311	2.3354
#	"111"	1168.682	1269.306	1168.864	1269.676	0.4122
#	"112"	1645.366	1262.694	1644.720	1262.908	0.6810
#	"113"	2120.165	1256.012	2120.395	1256.022	0.2301
#	"114"	2596.061	1248.936	2595.977	1249.031	0.1272
#	"115"	3072.098	1241.649	3071.553	1241.952	0.6237
#	"116"	3547.348	1234.532	3547.209	1234.799	0.3009
#	"117"	4023.385	1226.808	4023.033	1227.586	0.8532
#	"118"	4499.281	1219.986	4499.112	1220.328	0.3819
#	"119"	4975.487	1212.614	4975.531	1213.041	0.4295
#	"120"	208.360	810.519	208.680	810.046	0.5714
#	"121"	685.285	803.992	685.133	803.627	0.3951
#	"122"	1161.596	797.549	1161.236	797.042	0.6218
#	"123"	1637.671	790.591	1637.075	790.305	0.6611
#	"124"	2113.088	783.808	2112.738	783.431	0.5146
#	"125"	2588.156	776.236	2588.311	776.435	0.2513
#	"126"	3064.187	768.884	3063.882	769.331	0.5414
#	"127"	3539.635	761.622	3539.537	762.134	0.5216
#	"128"	4015.373	754.560	4015.363	754.860	0.2998
#	"129"	4491.368	747.301	4491.447	747.522	0.2353
#	"130"	4967.654	739.728	4967.877	740.136	0.4653
#	"131"	200.181	337.616	200.795	337.067	0.8234
#	"132"	677.408	331.565	677.221	330.730	0.8563
#	"133"	1153.859	324.632	1153.301	324.208	0.7015
#	"134"	1629.419	318.046	1629.121	317.516	0.6089
#	"135"	2104.961	311.497	2104.768	310.668	0.8517
#	"136"	2580.286	304.129	2580.329	303.679	0.4520
#	"137"	3055.840	296.573	3055.892	296.564	0.0532
#	"138"	3531.258	288.740	3531.543	289.338	0.6622
#	"139"	4006.953	281.543	4007.368	282.016	0.6288
#	"140"	4482.970	274.079	4483.456	274.612	0.7210
#	"141"	4959.170	267.454	4959.892	267.141	0.7872
#						
#	Average RMS error : 0.546					
#	Total RMS error : 76.977					
#	End of GCP details					

# APPENDIX D RMS of Geometric Correction of SPOT 5, 19 April 2005

```

#
# GCPs for dataset      : D:\Satellite
Data\LandsatUTMCrop\SPOT5_19Apr05C.ers
#
# Total number of GCPs: 255
# Number turned on      : 254
# Warp order            : 3
# GCP CORRECTED map projection details:
#     Map Projection    : MALRSOW
#     Datum              : KERTAU
#     Rotation           : 0.000
# RMS error report:
# Warp Type - Polynomial
#
#      -----ACTUAL-----      ---PREDICTED---
#      Point      Cell-X      Cell-Y      Cell-X      Cell-Y      RMS
#      "1"        88.246    1308.275    88.247    1307.802    0.4724
#      "2"        169.179    1197.882    169.188    1197.958    0.0772
#      "3"        279.041    1167.867    278.948    1167.793    0.1194
#      "4"        1198.641    2805.387    1198.301    2805.667    0.4406
#      "5"        1720.913    2064.730    1720.813    2064.651    0.1266
#      "6"        1972.190     403.937    1972.222     403.608    0.3302
#      "7"        1990.479     605.698    1990.723     605.821    0.2731
#      "8"         292.220     392.631     292.016     392.527    0.2283
#      "9"        2020.170     176.587    2020.018     176.652    0.1653
#      "10"       2877.159     908.578    2877.229     908.137    0.4466
#      "11"       1468.088    1562.408    1468.269    1562.422    0.1816
#      "12"        922.681     134.111     922.560     134.278    0.2059
#      "13"        160.176    2619.347    160.151    2618.980    0.3674
#      "14"        372.510    2667.962     372.904    2668.119    0.4245
#      "15"        726.737    1546.679     726.944    1546.938    0.3317
#      "16"       1950.416     476.918    1950.524     476.880    0.1139
#      "17"       2101.150     787.689    2101.199     787.865    0.1827
#      "18"        209.170    1851.438     208.889    1851.375    0.2879
#      "19"        475.116    1895.392     475.235    1895.598    0.2384
#      "20"       2237.288        35.229    2237.034        35.300    0.2642
#      "21"       1707.781    1954.532    1707.786    1954.705    0.1724
#      "22"       1373.265    1673.324    1373.208    1673.596    0.2781
#      "23"       1520.100    1720.196    1520.309    1720.259    0.2180
#      "24"       1600.570    1373.677    1600.176    1373.680    0.3938
#      "25"       1857.153    1171.722    1857.288    1171.467    0.2880
#      "26"       1971.077    1100.447    1971.056    1100.861    0.4145
#      "27"       2126.496    1080.743    2126.586    1081.052    0.3214
#      "28"       2138.327     977.227    2137.916     977.000    0.4699
#      "29"       2124.330     845.591    2124.064     845.652    0.2727
#      "30"       1800.134    1201.355    1800.183    1201.120    0.2392
#      "31"       1360.240    1900.694    1360.232    1900.498    0.1966
#      "32"       1635.630    2241.754    1635.705    2242.026    0.2820
#      "33"       2613.407    2436.709    2613.343    2437.067    0.3632
#      "34"       2477.232    2127.681    2477.263    2128.033    0.3539
#      "35"        196.380     763.467     196.363     763.458    0.0185
#      "36"        726.491     866.630     726.877     866.797    0.4205
#      "37"        282.095    1534.455     281.921    1534.379    0.1902
#      "38"       1089.271     764.352    1089.104     764.581    0.2831
#      "39"         33.623     418.765         33.357     419.182    0.4939
#      "40"        674.218    2841.593     673.896    2841.852    0.4131

```

## (Appendix D cont.)

#	"41"	1948.588	2779.010	1948.404	2779.217	0.2769
#	"42"	2365.341	1252.440	2365.232	1252.541	0.1486
#	"43"	2825.673	919.280	2825.930	918.957	0.4127
#	"44"	2101.366	1896.649	2101.368	1897.118	0.4694
#	"45"	2618.560	851.872	2618.291	851.586	0.3929
#	"46"	2818.605	2116.763	2818.610	2116.802	0.0387
#	"47"	2124.344	98.499	2124.281	98.286	0.2215
#	"48"	2005.461	386.959	2005.742	386.756	0.3462
#	"49"	1349.215	1228.971	1349.023	1228.729	0.3086
#	"50"	1324.372	207.722	1324.252	207.326	0.4138
#	"51"	530.315	224.383	530.313	223.925	0.4582
#	"52"	2595.347	294.665	2595.536	294.684	0.1898
#	"53"	2916.360	1280.819	2916.590	1280.918	0.2503
#	"54"	2962.489	2636.393	2962.113	2636.556	0.4101
#	"55"	2982.763	596.392	2983.010	596.284	0.2692
#	"56"	83.230	2070.584	83.504	2070.486	0.2910
#	"57"	2700.323	2808.643	2700.499	2808.266	0.4160
#	"58"	2806.250	2564.596	2806.373	2564.732	0.1844
#	"59"	797.382	44.576	797.451	44.433	0.1587
#	"60"	120.316	137.825	120.258	137.785	0.0710
#	"61"	1286.556	64.597	1286.462	64.697	0.1367
#	"62"	497.630	18.725	497.704	18.893	0.1830
#	"63"	1734.263	6.517	1734.511	6.439	0.2599
#	"64"	2032.353	16.076	2032.221	16.004	0.1504
#	"65"	2515.075	35.792	2514.930	35.915	0.1904
#	"66"	2851.315	42.506	2851.286	42.567	0.0681
#	"67"	2901.521	96.647	2901.411	96.603	0.1179
#	"68"	744.373	339.721	744.696	339.931	0.3858
#	"69"	5.412	409.453	5.246	409.644	0.2531
#	"70"	75.382	421.073	75.716	420.881	0.3850
#	"71"	101.534	441.629	101.819	441.776	0.3201
#	"72"	139.467	430.454	139.498	430.451	0.0317
#	"73"	157.564	405.602	157.846	405.225	0.4705
#	"74"	222.440	373.309	222.344	373.340	0.1010
#	"75"	263.315	402.384	263.164	402.021	0.3931
#	"76"	926.607	341.820	926.382	342.029	0.3070
#	"77"	1026.238	305.828	1025.991	306.044	0.3283
#	"78"	1112.549	298.471	1112.694	298.144	0.3572
#	"79"	1200.509	314.480	1200.529	314.408	0.0747
#	"80"	1282.354	140.642	1282.076	140.703	0.2850
#	"81"	1364.532	215.807	1364.296	216.057	0.3428
#	"82"	1449.595	301.562	1449.673	301.320	0.2543
#	"83"	1542.421	289.455	1542.214	289.395	0.2160
#	"84"	1619.688	358.714	1619.854	358.837	0.2062
#	"85"	1700.347	348.500	1700.614	348.537	0.2695
#	"86"	1843.410	511.508	1843.408	511.259	0.2498
#	"87"	331.505	359.458	331.764	359.195	0.3692
#	"88"	390.481	390.556	390.026	390.639	0.4623
#	"89"	472.393	412.639	472.800	412.674	0.4087
#	"90"	555.514	460.642	555.663	460.951	0.3430
#	"91"	662.500	466.607	662.108	466.768	0.4245
#	"92"	690.563	511.576	690.887	511.622	0.3274
#	"93"	721.566	614.402	722.019	614.253	0.4764
#	"94"	764.261	623.678	763.948	623.906	0.3871
#	"95"	827.343	697.515	827.509	697.378	0.2158
#	"96"	872.366	720.699	872.078	720.984	0.4051
#	"97"	841.767	643.345	841.918	643.126	0.2656
#	"98"	847.551	586.342	847.322	585.925	0.4753

## (Appendix D cont.)

#	"99"	912.357	558.434	912.065	558.164	0.3984
#	"100"	984.266	585.491	984.100	585.526	0.1697
#	"101"	1024.442	507.460	1024.740	507.122	0.4503
#	"102"	1104.476	471.610	1104.424	471.453	0.1651
#	"103"	1039.457	421.584	1039.605	421.919	0.3663
#	"104"	874.486	273.510	874.405	273.405	0.1330
#	"105"	889.605	218.575	889.801	218.385	0.2725
#	"106"	962.295	318.535	962.030	318.501	0.2680
#	"107"	1082.464	302.492	1082.185	302.456	0.2812
#	"108"	1220.509	239.552	1220.785	239.236	0.4193
#	"109"	1181.416	120.431	1181.122	120.519	0.3062
#	"110"	1171.571	77.518	1171.832	77.719	0.3298
#	"111"	1241.369	134.551	1241.368	134.966	0.4153
#	"112"	1612.411	326.631	1612.524	326.935	0.3250
#	"113"	1685.359	270.410	1685.735	270.473	0.3809
#	"114"	1836.558	282.503	1836.375	282.466	0.1866
#	"115"	1959.548	269.686	1959.928	269.835	0.4085
#	"116"	1994.454	306.728	1994.567	306.974	0.2702
#	"117"	2150.402	935.697	2150.801	935.879	0.4381
#	"118"	2037.400	1085.666	2037.527	1085.606	0.1405
#	"119"	1888.358	1157.441	1888.007	1157.492	0.3545
#	"120"	1718.462	1231.597	1718.185	1231.664	0.2847
#	"121"	1611.630	1315.540	1611.876	1315.605	0.2538
#	"122"	1485.670	1533.577	1485.906	1533.358	0.3223
#	"123"	1438.490	1622.558	1438.299	1622.972	0.4558
#	"124"	1462.574	1691.522	1462.153	1691.735	0.4715
#	"125"	1580.488	1772.380	1580.352	1772.188	0.2352
#	"126"	1641.748	1804.494	1641.966	1804.765	0.3479
#	"127"	1712.584	1876.561	1712.362	1876.471	0.2399
#	"128"	1683.547	2010.602	1683.115	2010.803	0.4763
#	"129"	1678.503	2170.387	1678.706	2170.324	0.2132
#	"130"	1648.434	2229.576	1648.751	2229.713	0.3453
#	"131"	1557.642	2269.381	1557.215	2269.400	0.4274
#	"132"	1558.539	2304.334	1558.864	2304.542	0.3862
#	"133"	1577.436	2377.708	1577.010	2377.627	0.4335
#	"134"	1556.440	2457.564	1556.465	2457.849	0.2853
#	"135"	1500.502	2520.604	1500.721	2520.514	0.2364
#	"136"	1453.587	2597.336	1453.279	2597.091	0.3939
#	"137"	1373.403	2667.729	1373.663	2667.890	0.3057
#	"138"	1323.456	2691.465	1323.327	2691.372	0.1591
#	"139"	1271.423	2724.563	1271.240	2724.979	0.4550
#	"140"	1186.447	2740.372	1186.166	2740.715	0.4435
#	"141"	1115.455	2678.531	1115.273	2678.488	0.1871
#	"142"	1138.626	2720.291	1138.906	2720.278	0.2801
#	"143"	1146.551	2763.301	1146.770	2763.130	0.2777
#	"144"	1144.634	2805.499	1144.694	2805.341	0.1691
#	"145"	1169.265	2851.356	1169.499	2850.951	0.4676
#	"146"	29.424	692.556	29.495	692.945	0.3954
#	"147"	529.575	595.547	529.443	595.294	0.2853
#	"148"	501.679	751.766	501.822	751.932	0.2185
#	"149"	1393.427	466.639	1393.586	466.814	0.2362
#	"150"	1436.398	742.581	1436.600	742.543	0.2052
#	"151"	1589.372	18.558	1589.637	18.359	0.3313
#	"152"	1759.559	90.491	1759.500	90.138	0.3579
#	"153"	1711.556	586.634	1711.647	586.513	0.1518
#	"154"	2353.523	198.669	2353.138	198.772	0.3982
#	"155"	2258.484	469.607	2258.289	469.894	0.3471
#	"156"	2996.377	296.562	2996.511	296.527	0.1382



## (Appendix D cont.)

#	"157"	2652.521	531.615	2652.440	531.537	0.1121
#	"158"	2387.562	699.440	2387.391	699.614	0.2437
#	"159"	25.422	985.533	25.325	985.476	0.1129
#	"160"	393.295	995.731	392.926	995.792	0.3738
#	"161"	831.407	980.849	831.100	980.955	0.3253
#	"162"	1243.454	951.522	1243.257	951.822	0.3586
#	"163"	1621.574	916.677	1621.757	916.598	0.1995
#	"164"	1887.572	735.428	1887.489	735.554	0.1513
#	"165"	17.332	1201.335	17.431	1201.219	0.1527
#	"166"	506.488	1160.609	506.746	1161.000	0.4690
#	"167"	784.536	1161.695	784.492	1161.851	0.1617
#	"168"	1074.482	1088.625	1074.348	1088.781	0.2063
#	"169"	1738.526	1058.543	1738.773	1058.230	0.3988
#	"170"	2384.441	1068.347	2384.214	1068.265	0.2410
#	"171"	2690.450	1116.459	2690.265	1116.100	0.4042
#	"172"	304.552	1334.528	304.585	1334.710	0.1848
#	"173"	637.670	1320.516	637.782	1320.953	0.4505
#	"174"	977.419	1269.637	977.367	1269.398	0.2441
#	"175"	1482.473	1058.421	1482.654	1058.038	0.4240
#	"176"	2665.342	1297.519	2665.034	1297.365	0.3446
#	"177"	2021.410	1218.657	2021.100	1218.787	0.3365
#	"178"	20.600	1595.463	20.920	1595.432	0.3218
#	"179"	49.380	2338.469	49.016	2338.383	0.3740
#	"180"	38.478	2802.584	38.376	2802.676	0.1370
#	"181"	321.741	2412.579	321.834	2412.930	0.3640
#	"182"	397.383	2141.533	397.358	2141.351	0.1828
#	"183"	480.594	1679.413	480.544	1679.687	0.2783
#	"184"	567.404	1472.568	567.573	1472.169	0.4326
#	"185"	638.456	2662.430	638.735	2662.781	0.4477
#	"186"	557.253	2464.478	557.117	2464.254	0.2619
#	"187"	690.402	2224.366	690.168	2224.005	0.4305
#	"188"	687.661	1945.462	687.914	1945.350	0.2764
#	"189"	343.240	144.470	343.003	144.091	0.4470
#	"190"	959.464	1426.575	959.470	1426.891	0.3154
#	"191"	849.398	1683.638	848.973	1683.783	0.4493
#	"192"	851.465	1871.484	851.663	1871.273	0.2885
#	"193"	805.419	2038.411	805.580	2038.262	0.2197
#	"194"	784.284	2380.352	784.617	2380.568	0.3961
#	"195"	840.380	2514.394	840.376	2513.998	0.3966
#	"196"	830.392	2688.544	829.917	2688.577	0.4761
#	"197"	951.413	2786.547	951.888	2786.446	0.4848
#	"198"	1166.419	1350.548	1166.512	1350.382	0.1901
#	"199"	1054.195	1540.423	1053.968	1540.104	0.3917
#	"200"	1052.490	1706.487	1052.412	1706.626	0.1594
#	"201"	1057.523	1920.409	1057.505	1920.323	0.0875
#	"202"	988.342	2143.460	988.622	2143.682	0.3574
#	"203"	1045.347	2338.555	1045.483	2338.759	0.2452
#	"204"	1283.334	581.518	1283.702	581.767	0.4437
#	"205"	1126.598	2494.542	1126.657	2494.122	0.4235
#	"206"	1323.534	2484.409	1323.491	2484.093	0.3192
#	"207"	1321.482	2310.435	1321.308	2310.755	0.3646
#	"208"	1199.303	2100.458	1199.173	2100.487	0.1337
#	"209"	1448.315	2076.405	1448.008	2076.087	0.4420
#	"210"	1212.335	1766.539	1212.035	1766.367	0.3467
#	"211"	1360.382	1468.623	1360.245	1468.240	0.4058
#	"212"	276.491	582.162	276.089	582.122	0.4042
#	"213"	1940.569	893.460	1940.897	893.570	0.3460
#	"214"	1497.327	2788.612	1497.560	2788.622	0.2330

## (Appendix D cont.)

#	"215"	1747.388	2791.482	1747.436	2791.489	0.0484
#	"216"	2231.415	2772.416	2231.297	2772.200	0.2459
#	"217"	2456.414	2781.492	2456.697	2781.143	0.4491
#	"218"	2993.528	2812.615	2993.359	2812.621	0.1695
#	"219"	1680.435	2586.696	1680.746	2586.975	0.4175
#	"220"	1895.567	2583.429	1895.277	2583.191	0.3748
#	"221"	2128.553	2574.624	2128.400	2574.712	0.1764
#	"222"	2423.481	2557.594	2423.227	2557.355	0.3490
#	"223"	2602.306	2592.712	2602.014	2592.958	0.3826
#	"224"	1876.334	2367.301	1876.473	2367.143	0.2103
#	"225"	2128.601	2341.524	2128.925	2341.619	0.3375
#	"226"	2459.565	2308.442	2459.403	2308.107	0.3723
#	"227"	2894.449	2235.630	2894.822	2235.633	0.3727
#	"228"	2942.596	2340.617	2942.981	2340.757	0.4099
#	"229"	1991.547	2128.390	1991.682	2127.971	0.4399
#	"230"	2251.524	2112.599	2251.945	2112.581	0.4211
#	"231"	2312.665	1884.433	2312.672	1884.169	0.2637
#	"232"	2.519	1838.438	2.463	1838.418	0.0594
#	"233"	2537.551	1876.346	2537.199	1876.291	0.3561
#	"234"	2756.672	1879.552	2756.883	1879.265	0.3565
#	"235"	3002.435	2004.581	3002.409	2004.815	0.2356
#	"236"	2992.429	1797.549	2992.245	1797.552	0.1848
#	"237"	3002.502	1527.455	3002.822	1527.144	0.4460
#	"238"	2785.120	1559.417	2785.003	1559.787	0.3878
#	"239"	2586.463	1600.570	2586.798	1600.879	0.4563
#	"240"	2388.613	1636.496	2388.667	1636.242	0.2601
#	"241"	2170.367	1624.440	2170.370	1624.080	0.3603
#	"242"	1975.460	1735.413	1975.807	1735.109	0.4613
#	"243"	1880.461	1583.363	1880.866	1583.415	0.4091
#	"244"	1714.566	1507.419	1714.948	1507.349	0.3880
#	"245"	1877.395	1336.458	1877.339	1336.753	0.3001
#	"246"	1957.438	1439.558	1957.336	1439.594	0.1075
#	"247"	2237.444	1415.505	2237.336	1415.344	0.1941
#	"248"	2519.428	1398.604	2518.993	1398.564	0.4376
#	"249"	2791.299	690.436	2791.099	690.747	0.3698
#	"250"	2993.577	950.577	2993.399	950.566	0.1782
#	"251"	2793.452	261.506	2793.463	261.916	0.4099
#	"252"	2197.530	590.633	2197.861	590.891	0.4197
#	"253"	2637.343	2226.413	2637.368	2226.695	0.2825
#	"254"	5.579	240.445	5.782	240.844	0.4476
#	"255"	-1.000	-1.000	0.000	0.000	0.0000

# Average RMS error : 0.304

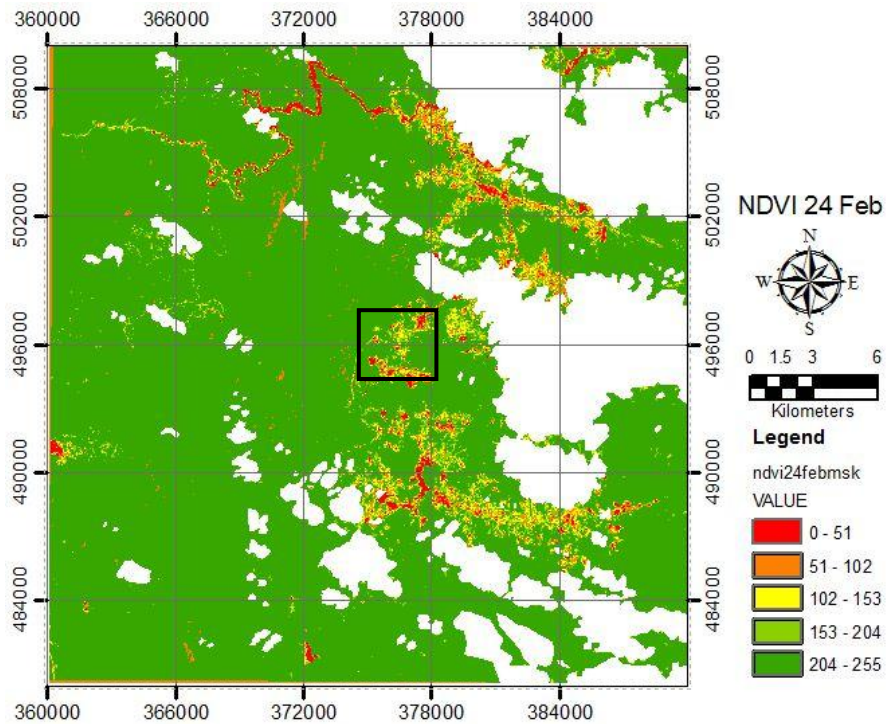
# Total RMS error : 77.204

# Note: Total and average RMS errors do not include OFF points

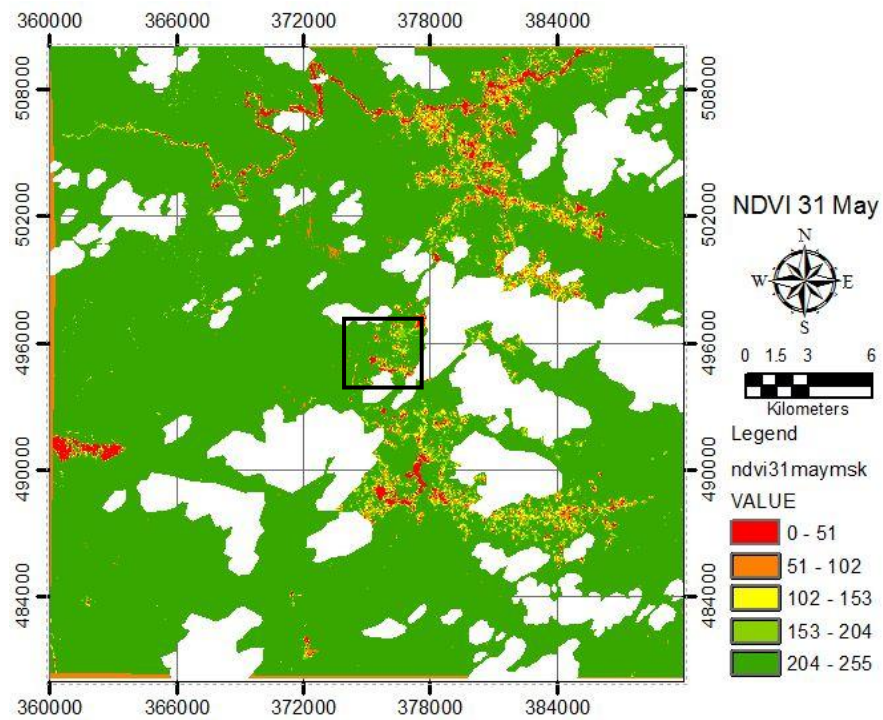
# End of GCP details

## APPENDIX E NDVI Maps

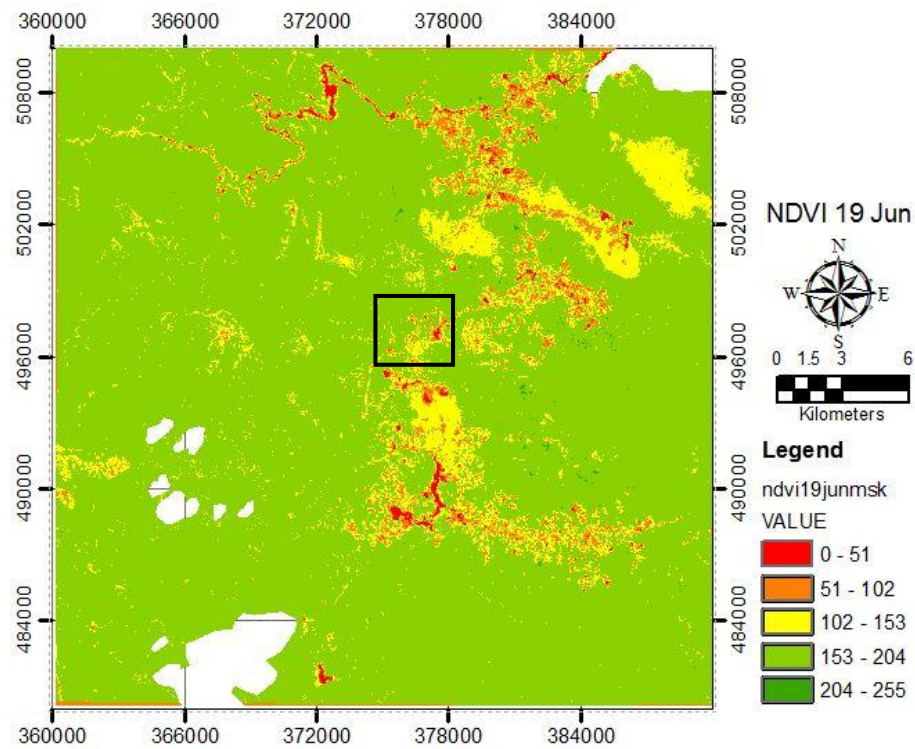
### E1. NDVI Map, 24 February 2001



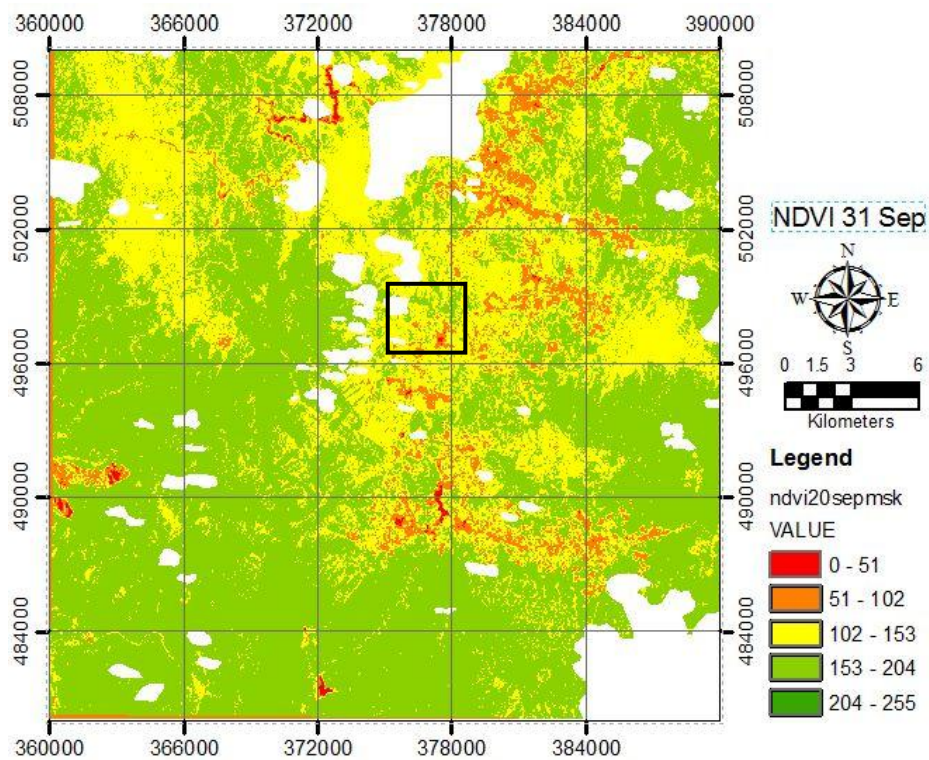
### E2. NDVI Map, 31 May 2001



### E3. NDVI Map, 19 June 2002



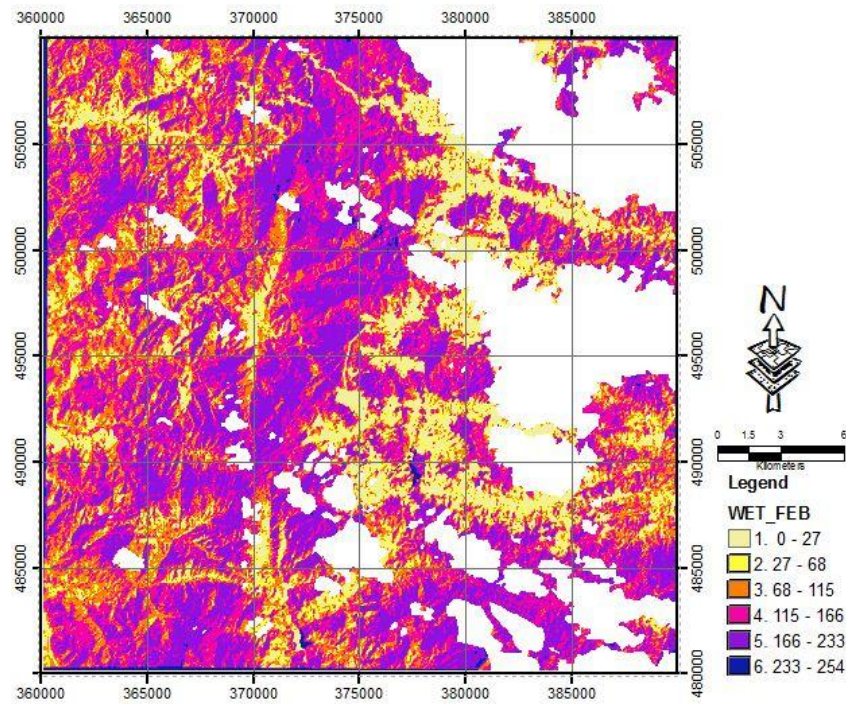
### E4. NDVI Map, 20 September 2001



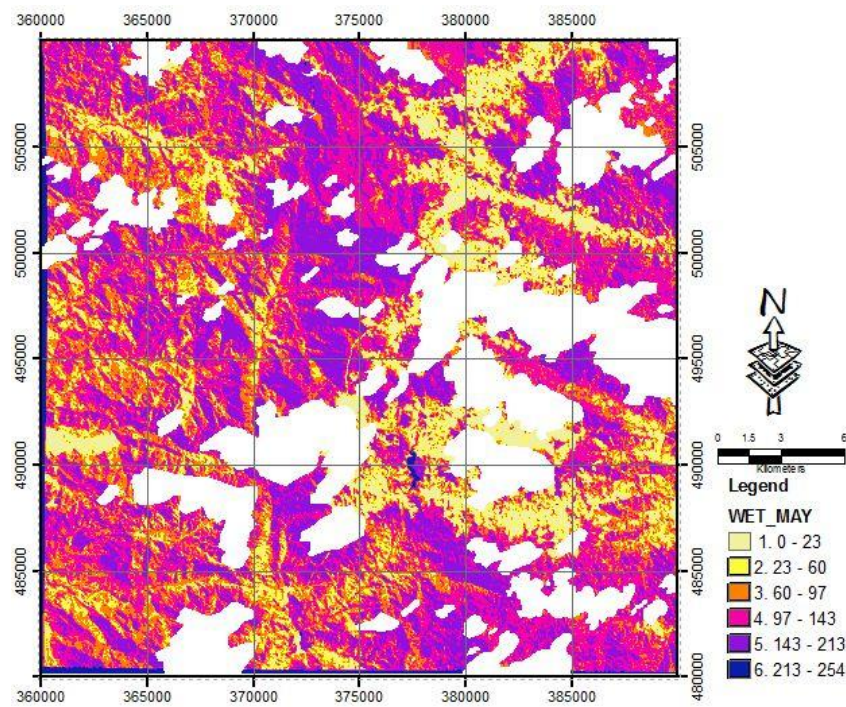


## APPENDIX F TCT Soil Wetness Maps

**F1. Soil wetness, 24 February 2001**

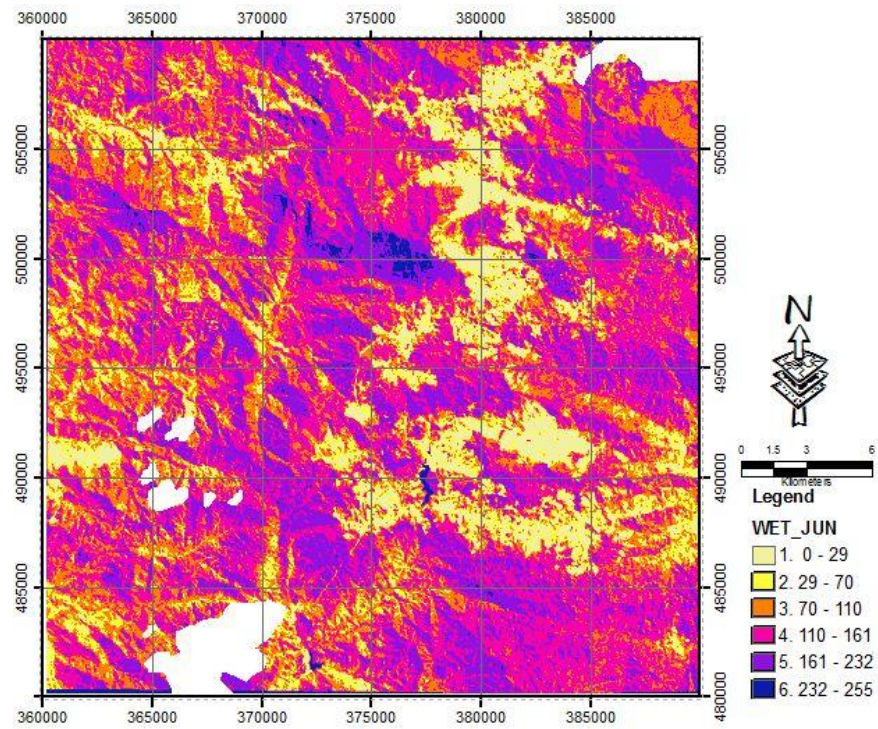


**F2. Soil wetness, 31 May 2001**

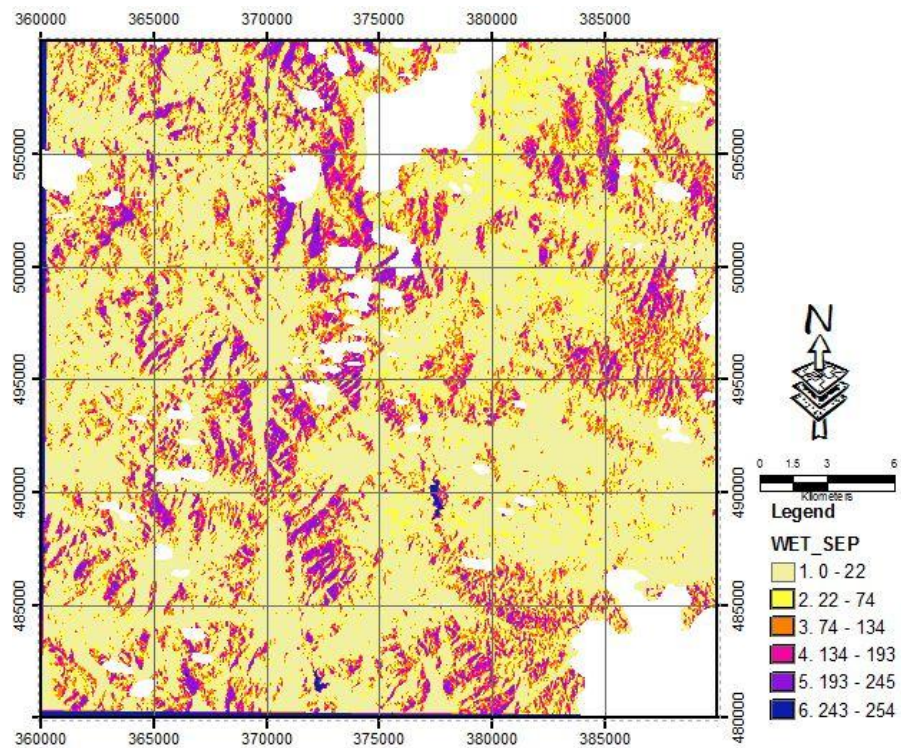




**F3. Soil wetness, 19 June 2002**



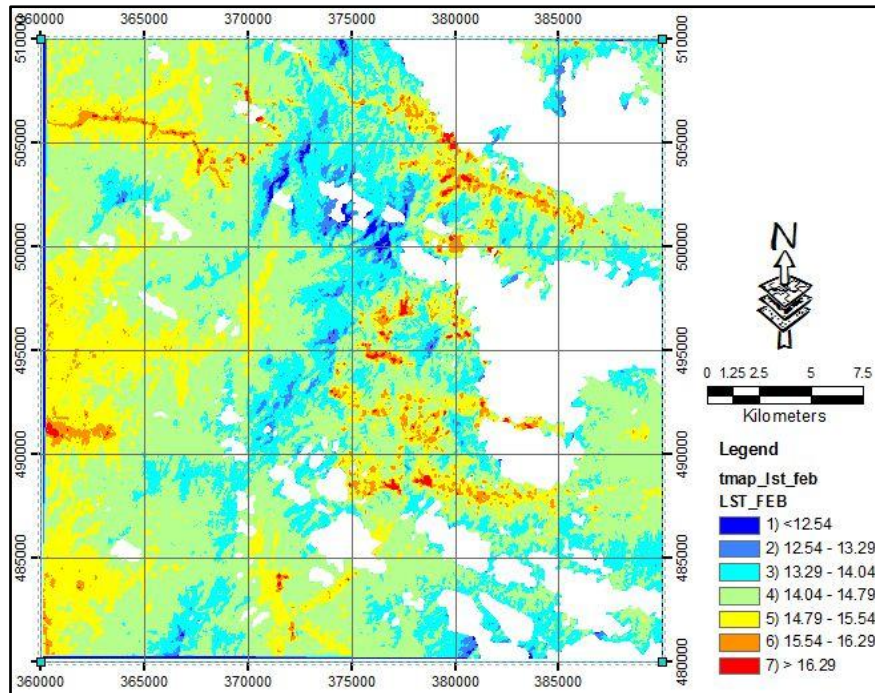
**F4. Soil wetness, 20 September 2001**



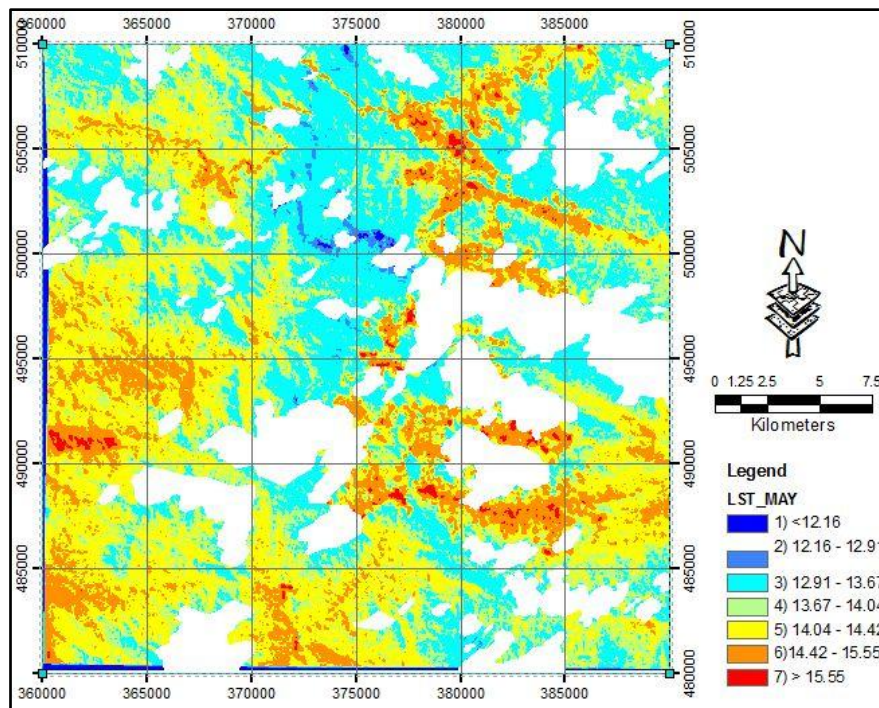
## APPENDIX G

### LST Maps

#### G1. LST 24 February 2001

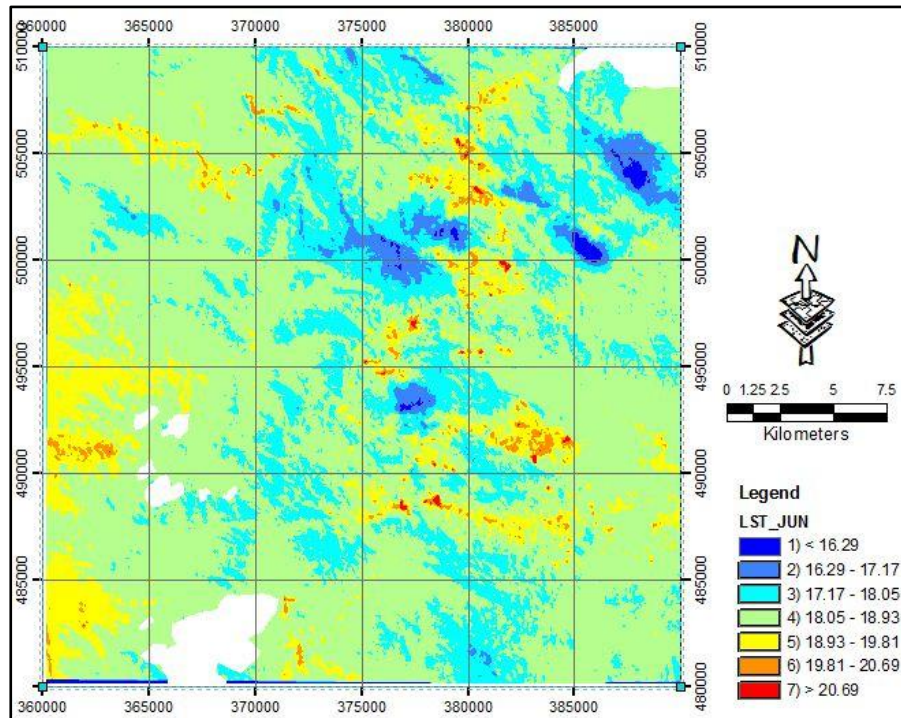


#### G2. LST 31 May 2001

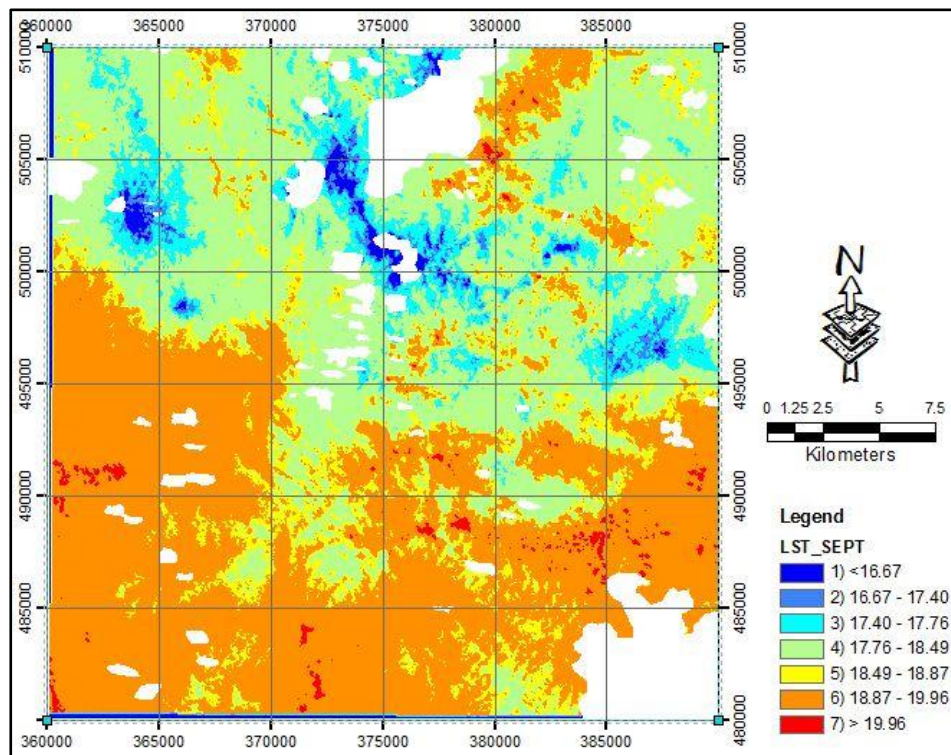




### G3. LST 19 June 2002



### G4. LST 20 September 2001

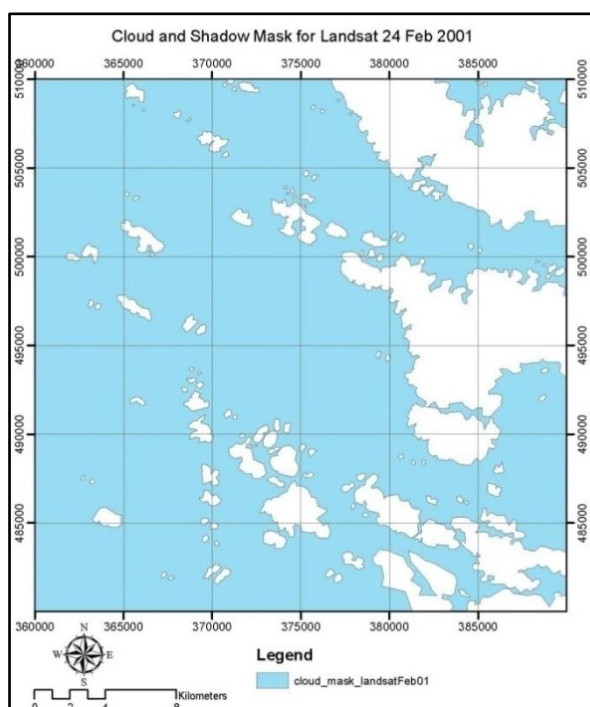




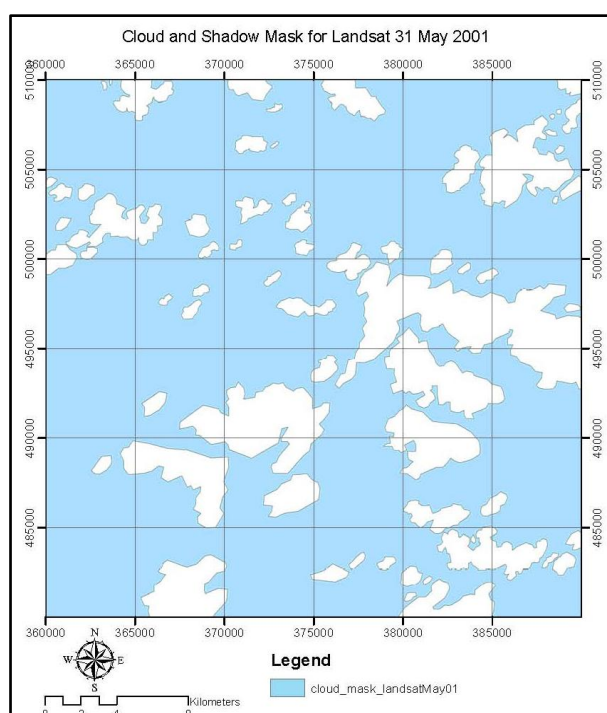
## APPENDIX H

### Cloud and shadow masks

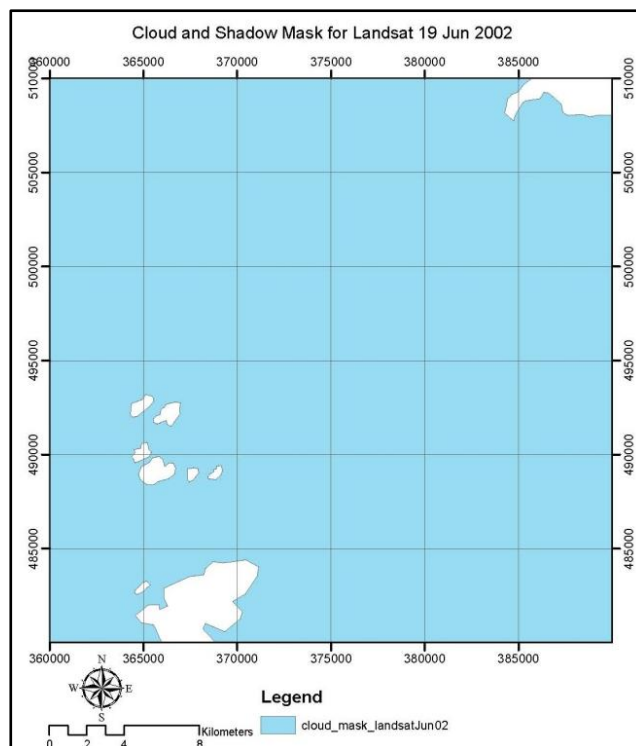
#### H1. Cloud and shadow mask for Landsat 24 February 2001



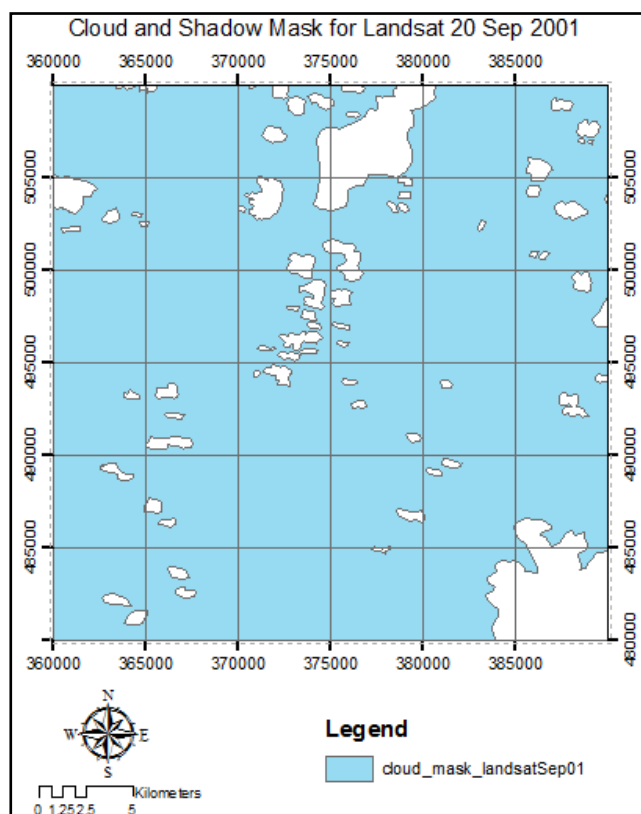
#### H2. Cloud and shadow mask for Landsat 31 May 2001



### H3. Cloud and shadow mask for Landsat 19 June 2002



### H4. Cloud and shadow mask for Landsat 20 September 2001



## LIST OF PUBLICATIONS

### **International Journal:**

1. Matori, A. N., **Basith, A.**, and Harahap, I. S. H., “Study of regional monsoonal effects on landslide hazard zonation in Cameron Highlands, Malaysia,” *Arabian Journal of Geosciences*, DOI: 10.1007/s12517-011-0309-4, 2011. Available at: <http://www.springerlink.com/content/e174p67536759487/>

### **Conference Papers:**

2. **Basith, A.** Matori, A.N and Harahap, I.S.H., 2010, “Past landslide at Post Slim: Evaluation of its causative factors using geospatial and remote sensing data.” In: *International Conference on Sustainable Building and Infrastructure (ICSBI2010)*, June 15-17, 2010, Kuala Lumpur, Malaysia.
3. **Basith, A.**, Matori, A.N., and Harahap, I.S.H. and Talib, J.A., 2010, “Application of land use changes detection for identification of landslide risk areas in Pulau Pinang using a decade of Landsat ETM+ images.” In: *MRSS (Malaysian Remote Sensing Society) 6<sup>TH</sup> International Remote Sensing & GIS Conference and Exhibition 2010*, April 28-29, 2010, Kuala Lumpur, Malaysia.
4. **Basith, A.**, Matori, A.N., and Harahap, I.S.H., 2008, “Application of SPOT 5 satellite image and GIS for updating road network map: towards building landslide spatial database.” In: *2<sup>nd</sup> International Conference on Built Environment in Developing Countries*, USM, Penang, Malaysia
5. B. K. Cahyono, A.N. Matori, Dedi Atunggal, and **A. Basith**, “Generating 3D Model of Instable Slope Area from 2D Photographs by Using Commercial Pocket Camera,” In: *International Conference on Construction and Building Technology 2008*, Kuala Lumpur, Malaysia, June 16th 2008
6. B. K. Cahyono, A.N. Matori, Dedi Atunggal, and **A. Basith**, “Correlation of Sampling Methods and Quality in Slope Modeling by Using Close-Range Photogrammetric Data,” In: *International Symposium and Exhibition on*

Geoinformation 2008, Universiti Tekonologi Malaya and Kuala Lumpur Infrastructure University College, Kuala Lumpur, Malaysia, October 13th 2008

7. Basith, A., and Abd Nasir Matori, 2008, "Assessment of Landslide Risk Zones in Cameron Highlands Using Remote Sensing and GIS," In: National Postgraduate Conference 2008, Universiti Teknologi PETRONAS, Tronoh, Perak, Malaysia.